NANYANG TECHNOLOGICAL UNIVERSITY
SINGAPORE

EXPERIMENTAL AND NUMERICAL INVESTIGATION ON SHOT PEENING OF LOW ALLOY STEEL

PHAM QUANG TRUNG

SCHOOL OF MECHANICAL AND AEROSPACE ENGINEERING

August - 2017

Experimental and Numerical Investigation on Shot Peening of Low Alloy Steel

Pham Quang Trung

SCHOOL OF MECHANICAL AND AEROSPACE ENGINEERING

A thesis submitted to the Nanyang Technological University
in partial fulfillment of the requirement for the degree of
Doctor of Philosophy (Mechanical and Aerospace Engineering)

August - 2017

Acknowledgements

First and foremost, I would like to express my deep gratitude to my supervisors, Associate Professor David Lee Butler and Associate Professor Sridhar Idapalapatiat (School of Mechanical and Aerospace Engineering, Nanyang Technological University, my thesis Thesis Advisory Committee, and Dr. Nay Win Khun (Rolls-Royce@NTU Corporate Lab) and Dr. Wang Wei (Advanced Remanufacturing and Technology Center) for the continuous support for my Ph.D. job. They not only teach me knowledge but also help me widen knowledge through supporting me attending the related workshop, training course, international conference, and working with the company.

I owe a great depth of gratitude to Nanyang Technological University and Advanced Remanufacturing and Technology Center for giving me a chance to study Ph.D. in Singapore.

I also appreciate the help from Mr. Tan, Mr. Dave, Mr. Cliff and all of the members in Abrasive Engineering Company and Advanced Remanufacturing and Technology Center. They help me a lot to train me operating the shot peening machine and allowing me using their equipment to perform my experiment research.

Finally, I would like to thank my family, my wife and my son who always support and encourage me to chase my dream.

Abstract

While shot peening is a well-established technique used in applications where compressive stresses need to be imparted to the material to improve fatigue life, there is still very little fundamental research published. To many, the process is considered to be an art rather than a science. This research aims to investigate the effects of the shot peening process parameters on the surface topography and properties of low alloy steel.

The shot peening process influences both the surface and subsurface of the target material with the latter being considered beneficial while the former detrimental. The fatigue life of the material is generally improved by inducing compressive residual stresses into the material subsurface. The process of inducing compressive stresses relies on the impact of high velocity shot onto the target material surface. The impact of these shots tends to make the surface rougher and results in the formation of local stress concentrations which can be a precursor to fatigue failure. Coverage is a major parameter of shot peening process, which is defined as the percentage of the sum of peened area over the total area on the surface of the specimen. A new method with the aid of Matlab^{TM} code to estimate the full coverage for simulation of the shot peening process is proposed in this work. Then, a three dimensional FEM model of the shot peening process was further developed using experimental results for increased accuracy. The numerical and experimental studies give a good agreement in the compared results in the topography and surface roughness of the shot peened steel. As a result, after validating the FEM model with the experimental results, the FEM model can be used to predict the results for the other shot peening conditions (same material) as well as provide the initial operating parameters to reduce the trial and error experimental process. The fatigue tests revealed that the shot peening process could significantly enhance the fatigue life of the treated components. However, a side effect of the process was an increase in surface roughness which was more prevalent under higher peening pressures and led to a

reduction in the fatigue life. Therefore, to maximize the performance of the process, the peening parameters need to be carefully selected. Microstructure analysis of the shot peened parts indicated that the nucleation cracks or initiation cracks occurred in the subsurface at depths of 10 to 20 microns in the case of as-received samples but moved up to the free surface for the shot peened parts.

Table of contents

List of tables

List of figures

List of abbreviations and symbols

A	Area of shot spread
Ar	Avrami value
C	Constant parameter of material in the Cowper-Symonds relation
$C\%$	Coverage of the shot peened sample
$C_{(t)}$	Coverage at any time t
CSP	Conventional shot peening process
d	Diameter of an indentation caused by a single shot
D	Diameter of impact region of the target material
DP	Double shot peening process
E	Dynamic energy of each shot
E	Young modulus
f	Friction coefficient
$f_{ACF}(t_x,ty)$	Autocorrelation function
l_n	Measured length (profile surface roughness)
l_t	Tracing length, tracing path of the surface probe
m	Mean mass of each shot
$\dot{m}$	Mass flow rate of shot
m_r	Areal material ratio
N	Number of shot used to simulation
σ_{max}	Maximum residual stress
$\sigma_{surface}$	Residual stress at the surface
σ_o	Initial yield stress
σ_z	Residual stress as a function of depth from the surface

p	Constant parameter of material in the Cowper-Symonds relation
ρ	Shot density
r	Average radius of shot
R	Average radius of indentation caused by a single shot
$Rand(1,1)$	Random function
R_a	Arithmetic mean roughness value
R_q	Root mean squared roughness value
R_t	Maximum peak-to-valley height over the measurement length
R_z	Average of the 5 single peak-to-valley heights (one for each cut-off length)
Re-SSP	Re-severe shot peening process
S_a	Arithmetical mean height of scale-limited surface
S_{al}	Autocorrelation length
S_{dq}	Root mean square gradient of scale-limited surface
S_{dr}	Developed interfacial area ratio of scale-limited surface
$S_{mc(mr)}$	Inverse areal material ratio of the scale-limited surface
$S_{mr(c)}$	Areal material ratio of the scale-limited surface
S_{mr1}	Peak material ratio
S_{mr2}	Dale material ratio
S_q	Root mean square height of scale-limited surface
S_k	Distance between the highest and lowest level of the core surface
S_{ku}	Kurtosis of scale-limited surface
S_p	Maximum peak height of scale-limited surface
S_{pk}	Reduced peak height parameter
S_{sk}	Skewness of scale-limited surface

S_{tr}	Texture aspect ratio
S_v	Maximum pit height of scale-limited surface
S_{vk}	Average height of the protruding dales below the core surface
S_z	Maximum height of scale-limited surface
SP	Shot peening process
SSP	Severe shot peening process
t	Exposure time
T	Shot peening cycle
v	Mean velocity of each shot
$V_{m(p)}$	Material volume
$V_{v(p)}$	Void volume

Chapter 1: Introduction

1.1 Background

Shot peening is a cold working process, which is used to enhance the properties of materials, especially the fatigue life as it induces large compressive residual stresses in the subsurface of materials [1, 2]. Nowadays, the process is widely used in industries ranging from aerospace, automotive to construction [1, 3, 4]. In the shot peening process, thousands of balls impact on the surface of the target material which causes plastic deformation of the material surface and induces compressive stresses in the bulk material. The top layers of the surface, after being shot peened will be hardened, compressed, and visually will appear rougher [5-7].

Shot peening is a complex process in which the peened surface properties depend on various parameters such as velocity, type of media, nozzle pressure, the shape of media, and properties of the target material [1]. The effectiveness of shot peening is determined by its intensity, and coverage. The intensity of shot peening, which is the measure of the direct energy of the shot stream impacted onto the surface, can be measured through the Almen strip method [1]. Coverage is the measure of the original surface covered by shot peening indentation. The degree of workpiece coverage must be determined on its surface by visual inspection. Several methods have been developed to examine the coverage parameter, i.e. visual inspection, blue-ink method, replicas, fluorescent tracer, and video method [1]. However, both intensity and coverage, are measured factors, and they are also dependent on various parameters such as ball velocity, ball shape, nozzle pressure, shot peening time, type of shot, properties of materials, etc. [1].

Recently, ultra-fine grain materials have attracted significant interest from both industry and science. They are expected to deliver superior mechanical properties when compared with the normal grain size specimens [7-10]. From the literature [5-7], surface properties have a great effect on the failure of engineering parts, for example in fatigue fracture, fretting fatigue, wear, and corrosion, etc. In many applications, it is recommended that it is not necessary to have entire components by ultra-fine grain structure. To create a ultra-fine grain material in the surface or sub-surface, a severe form of shot peening is required with much higher intensity and coverage. This process is known as severe shot peening.

1.2 Motivation

Shot peening has been widely used in the industry ranging from aerospace, automotive to construction due to its compressive residual stresses induced by shot peening process, which can prevent the formation of surface cracks and enhance the fatigue life of the mechanical part.

Recent research [1, 3, 7] including both experimental and numerical simulation approaches have explained how shot peening can improve the properties of material. However, there are some research gaps which need to be studied to obtain the fuller picture of the shot peening process and thus better control.

In recent simulation results [11-13], there are two types of model that have been employed, i.e. single shot impact and multiple-shot impacts. In the latter, multiple-shot impact model, most studies examine the effects of the shot peening process with a fixed number of shot impacts and their locations. However, the location of the shot on the surface

of the target material area is random in the reported experiments. Therefore, it is necessary to employ random functions for proper shot peening simulations.

Research into shot peening or conventional shot peening has been undertaken since the 1920's, but the severe shot peening to create the ultra-fine grain (NC) layer on the surface of material evolved in the beginning of 21st century. The ultra-fine grain layer on the surface of a material induced by severe shot peening is expected to possess superior mechanical properties different from its conventional coarse-grained interior. However, up to now, severe shot peening is still not applied to industry due to increase in shot peening time and increase in surface roughness.

In addition, another application of shot peening is to restore a material which exhibits micro cracks and extend its useful life. A crack (fatigue fracture) firstly appears on the surface of the material during operation and then propagates into the bulk [14-20]. Therefore, the presence of compressive stresses induced by the shot peening process inhibits the crack formation and its propagation thereby improving the fatigue life. It is an effective method to prevent the crack formation and enhance the fatigue life of the material.

Steel is an alloy that is most commonly used in the automotive, construction and mechanical industry. Among steels, AISI 4340, low alloy steel, is known for its high strength and great ability to plastically deform. AISI 4340 steel is widely used for power transmission gears and shafts, aircraft landing gear, automotive, machine tool applications, and other structural components. In this study, AISI 4340 low alloy steel was selected for the investigation.

1.3 Objective

The objectives of this research are to investigate experimentally and numerically the effects of the shot peening process on the properties of the target material fatigue life of a low alloy steel.

1.4 Scope

The scope is as follows:

- To perform the shot peening process under various shot peening conditions to investigate the effect of the shot peening operating parameters on the mechanical properties and tribological properties of low alloy steel.

- To investigate the generation of ultrafine grain size structures on the subsurface layer of the severe shot peened material and study a comparison of the mechanical properties and tribological properties of both conventional and severe shot peened low alloy steel.

- To develop a three-dimensional FEM shot peening model to explain the shot peening process phenomenon and to predict the effect of parameters of the shot peening process on the properties of material. Then, a new proposed process is introduced to validate the FEM shot peening results with the experimental works. The FEM model after validating can be used to optimize the shot peening operating parameters for the experiment in other case studies.

1.5 Report outline

The structure of the document is organized as follows: The literature review relating to this research is presented in Chapter 2. Chapter 3 outlines the investigation of the effects of

the shot peening parameters on the mechanical and tribological properties of the material. The comparison of the properties between the conventional and severe shot peened steel are presented in Chapter 4. A new proposed method to estimate the number of shots and their coordinates to achieve the full coverage is introduced in Chapter 5. In addition, to validate the proposed method, a FEM model to simulate the shot peening process was developed and is demonstrated in Chapter 5. A new proposed process is introduced in Chapter 6 to compare the FEM model results with the experimental results. The main purpose of the shot peening process is to improve the fatigue life of the shot peened components, therefore the effects of the shot peening process parameters on the fatigue life of the treated samples were investigated and are presented in Chapter 7. Finally, the conclusion and future work of this Ph.D. research are proposed in Chapter 8.

Chapter 2: Literature review

2.1 Introduction

2.1.1 History of shot peening process

The earliest process of shot peening started since the time of ancient artisans and blacksmiths when they used a hammer to make the shape and increase the strength of the armors. The current shot peening method was introduced in 1920's [21] by using metal, ceramic and glass shots in the same manner as that of sand blasting to obtain a thicker hardened layer on the workpiece.

In 1943, Almen created a method to measure the intensity of shot by measuring the arc height of the standard specimen (Almen strip) after it passed the shot peening process. This is a non-destructive test and the most common method to measure the intensity of the shot peening process. In 1945, the X-Ray diffraction was first applied to measure residual stresses induced by shot peening process by Milburn [21]. X-Ray diffraction and Almen test method made it possible to relate the intensity to the residual stress induced by shot peening process.

A large number of papers have been published on the effect of shot peening on the residual stress distribution and the properties of the surface target after peening [2, 3, 5, 14, 22-30]. It was shown that properties including residual stress, hardness, surface roughness, microstructure, fatigue, wear, and corrosion of the peened material all changed after using this surface treatment.

In last few decades, the ultrafine-grained materials have attracted the interest of scientists. To produce ultrafine-grained material, there are many methods, and severe plastic deformation has received the greatest attention [7, 31-35]. It is natural to think to apply shot

peening method to generate the ultrafine-grained for the target surface layer. It has been shown that the mechanical behavior of severe shot peened material has significantly changed; however, the studies of severe shot peening have not yet been fully reported.

2.1.2 Shot peening system

Figure 2-1 illustrates an air-blast shot peening machine. The media from the nozzle shoots a sample after accelerating velocity through the air compressor system. The media after peening will be collected and returned to the system for repeating the shot peening process.

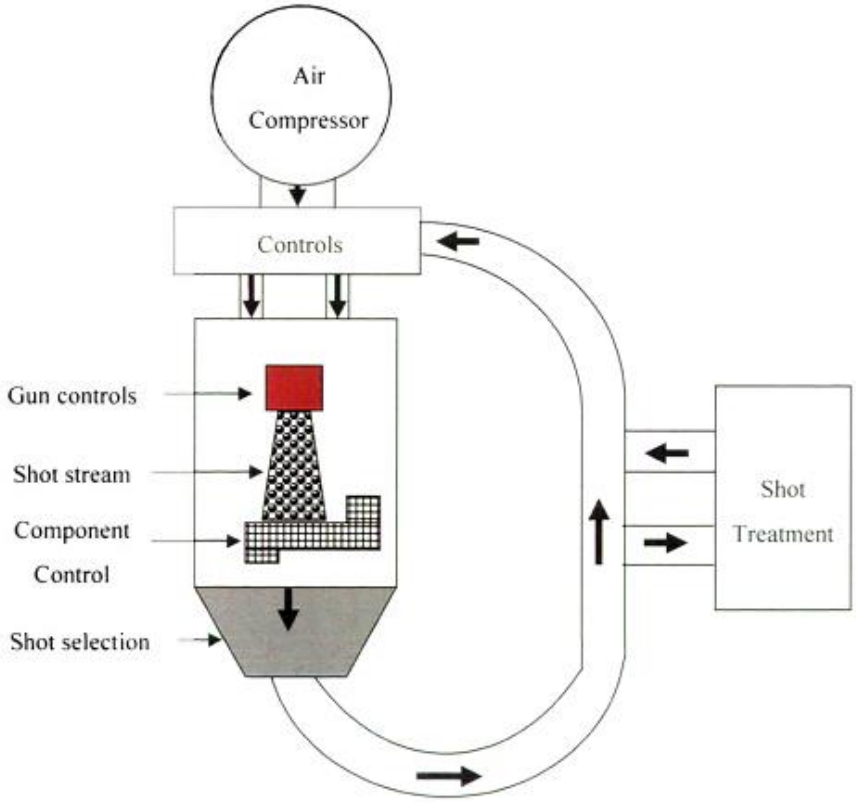

Figure 2-1. Schematic of shot peening equipment [21].

2.2 Shot peening parameters

The overview of the whole shot peening process is described in figure 2-2. There are two outputs that are used to control the operating process, e.g.intensity and coverage. Media

size, media shape, media hardness, shot flow rate, shot velocity, nozzle-workpiece distance and impact angle are parameters which directly affect the intensity. Whereas the coverage in influenced by parameters such as a system type (nozzle or wheel), nozzle geometry, shot velocity, angle of impact, mass flow rate, shot peening time, shot peening media and properties of the workpiece. Figure 2-2 also presents an overview of the measurement methods which are used to determine intensity and coverage. Finally, the properties of material, which changes due to the shot peening process, with the relevant measurement methods used to examine these properties, are also displayed in figure 2-2.

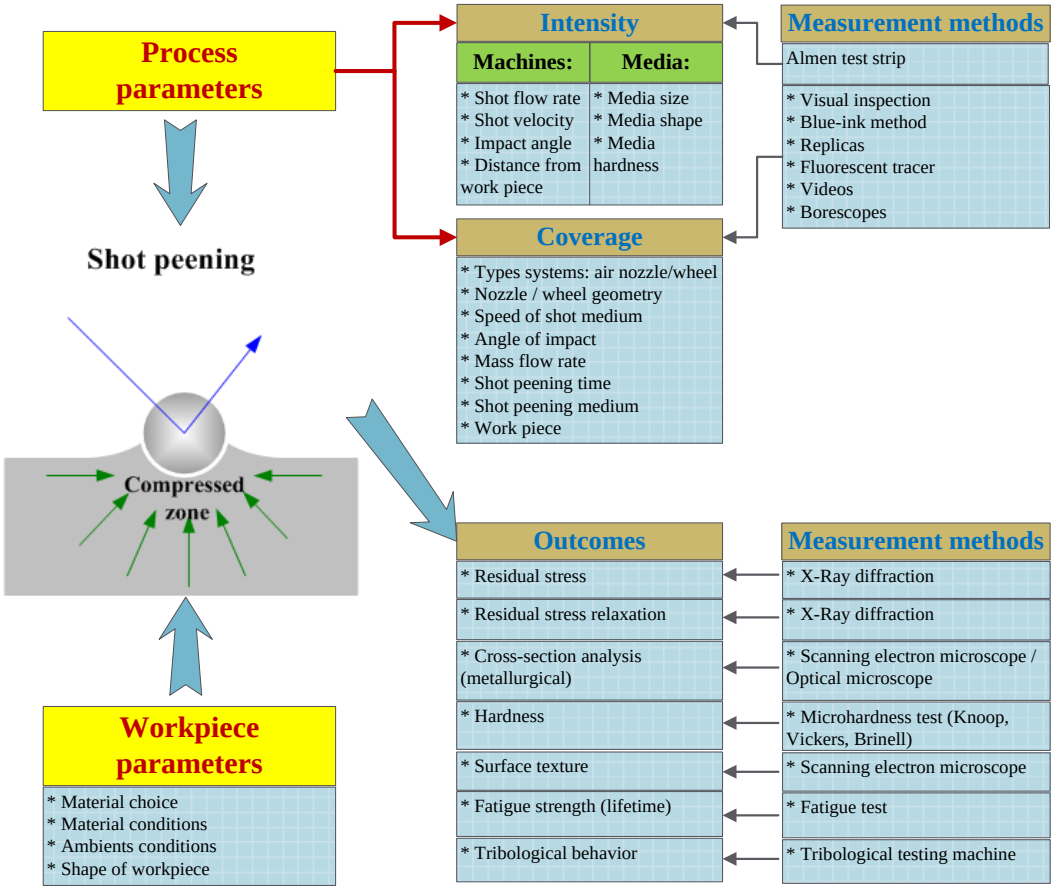

Figure 2-2. The overview of the whole shot peening process.

2.2.1 Intensity

Intensity is an indirect way of measuring the amount of energy which is transferred to the surface of a workpiece. The Almen strip and Almen gauge are used to measure intensity.

Three types of Almen strips, i.e. N, C, A, made SAE 1070 CRS (cold rolled spring steel) with a standard hardness of 44-50 HRC, are used to measure intensity. These types are the same length and width but vary in thickness.

Figure 2-3 illustrates how to obtain the arc height of single strip. The Almen strip is mounted onto the holding fixture, and it is peened under the process condition. After removing the strip from the fixture, it will bend the non-peened side again. Finally, Almen gauge the is employed to measure the height of curve and plot it with the exposure time to draw the saturation curve.

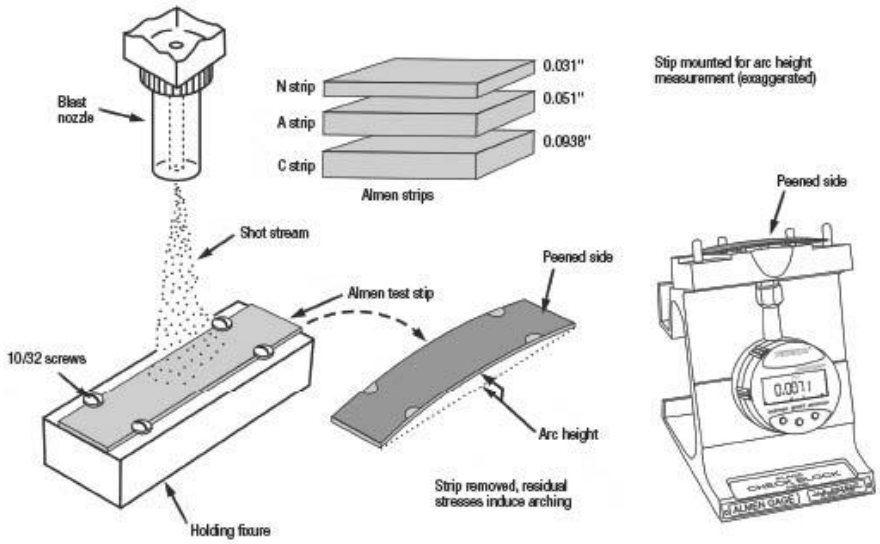

Figure 2-3. The Almen strip measurement system [36].

Saturation is defined as the earliest point of the saturation curve, in which the arc height increases by 10% or less if the peening time is double (figure 2-4). In that definition, the intensity is defined as the arc height of strip at the saturation point.

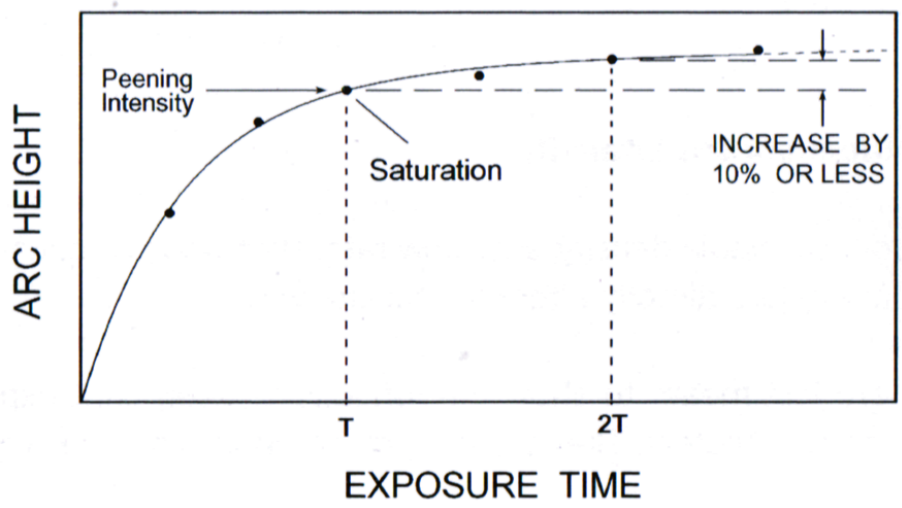

Figure 2-4. Saturation curve [36].

2.2.2 Coverage

One of the most important parameters which need to be obtained is the degree of coverage. Coverage is defined as the percentage of the sum of peened area over the total area on the surface of the specimen (figure 2.5*a*). Quality variation in coverage is not acceptable, and it causes damage leading to component failure. In many industrial applications, the range of coverage is from 100% to 200%, in which the residual stress is uniform and meet the required value and the surface is not damaged by the shot [1]. However, in some recent research, to achieve the ultrafine-grained structure layer on the top surface of the specimen, a very high degree of coverage is required, i.e. above 1000% [7].

There are some techniques to calculate the degree of coverage, i.e. visual inspection, blue-ink, replicas, fluorescent tracer, videos. Of these techniques, the most common one is visual inspection. Coverage increases with peening time but not linearly. One example of a coverage curve showing the degree of coverage as a function of the shot peening time is presented in figure 2-5*b*. The visual check works only when the degree of coverage is lower than 100%. To perform the required degree of coverage higher, e.g. 300%, the peening time is estimated as three times the required time to achieve the coverage of 98%.

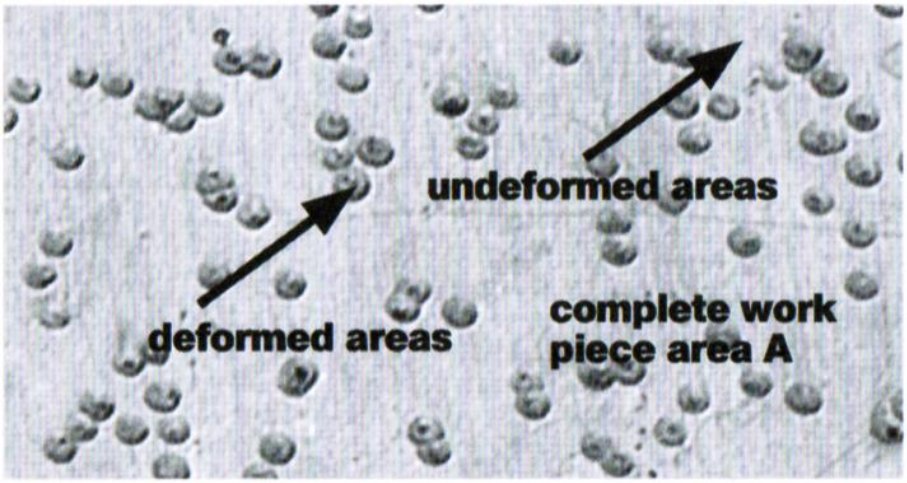

(a)

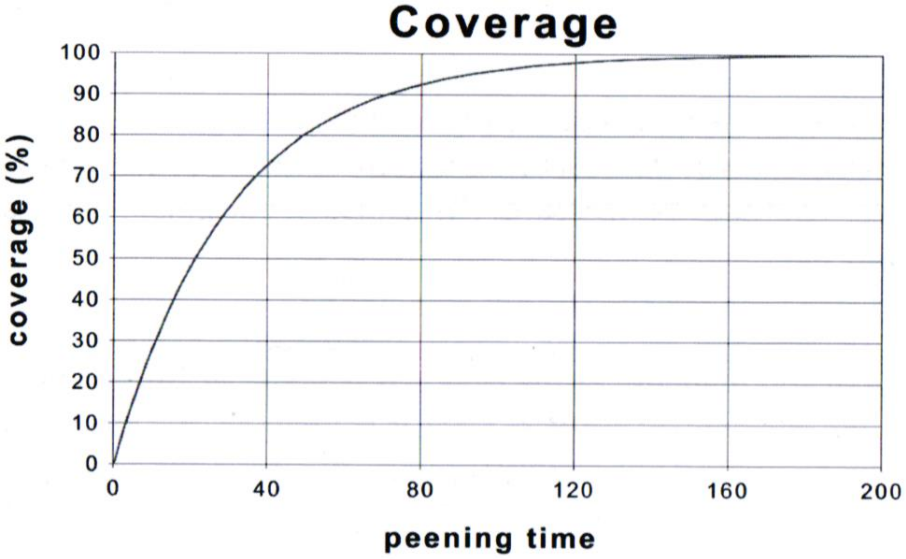

(b)

Figure 2-5. Coverage (a) definition and (b) as a function of the shot peening time [1]

In the theoretical model proposed by Kirk [37], the shot size indentation, peening rate and exposure time to predict the degree of coverage was considered based on the Avrami equation (2-1) [38].

$$C_{(t)} = 100\left[1 - exp\left(-\frac{3R^2\dot{m}t}{4Ar^3\rho}\right)\right] \quad (2\text{-}1)$$

where $C_{(t)}$ is the coverage at any particular time, R is the average radius of indentations caused by a single shot, $\dot{m}$ is mass flow rate of shot, t is exposure time, A is area of shot spread, r is the average radius of shot, ρ is the shot density.

2.3 Residual stress

2.3.1 Overview of residual stresses

The residual stresses which are presented in the mechanical parts can significantly enhance their useful life [1, 36]. It is well known that cracks do not initiate nor propagate in the compressive zone of a specimen [39]. Besides, most fatigue and stress corrosion failures originate at or near the surface. Therefore, the compressive stresses induced by shot peening can significantly increase the useful life of the mechanical parts or components [1, 40].

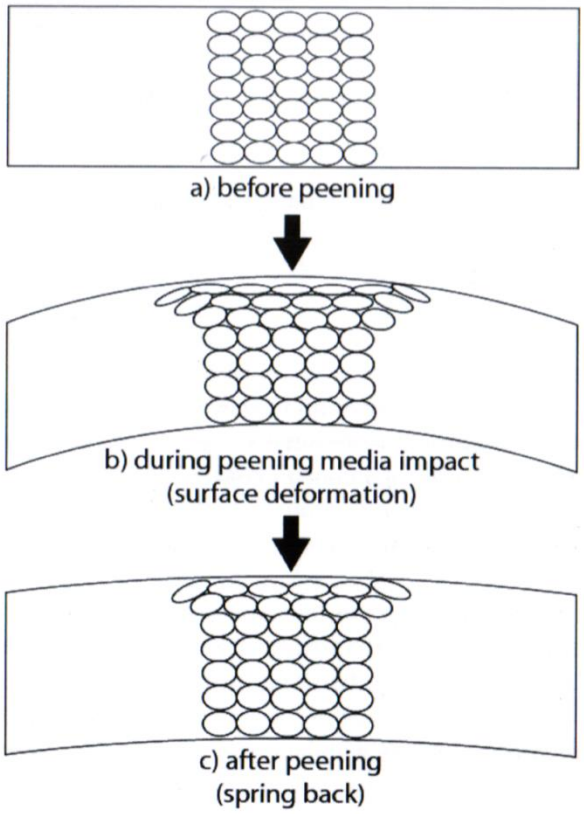

Figure 2-6. Illustration of material deformation as a result of a peening process showing: a) initial material before peening, b) surface deformation during peening media impact, and c) resultant deformation after spring back [1].

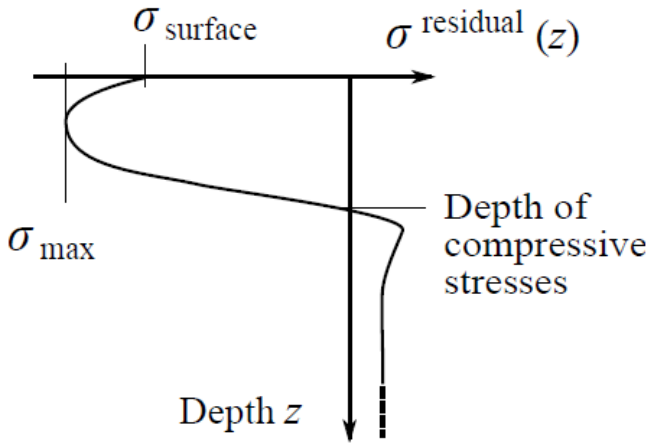

Figure 2-7. Resultant residual stress gradient after shot peening [1].

When a flat sheet is peened, it typically deforms into a convex arc shape toward the peened side. That deformation indicates that the top surface layers of the specimen are stretched plastically, which causes the permanent bend curve of the sheet. The mechanism of this process can be explained as follows.

When a flat sheet is subjected to the shot peening process, it will be compressed and bent into a convex arc around the impact area (figure 2-6*a*, and figure 2-6*b*) [1]. The resultant of this process is either elastic or plastic and is dependent on the energy of shot impact. If the energy is low, the sheet will spring back to the original stage, and there is no residual stress field generated. However, if that energy is large enough, the sheet is deformed plastically and bent. That plastic deformation is usually limited to the surface or near surface region and depends on the energy of shot impact, mechanical properties of specimen and properties of media. In the peened material, the surface and near-surface are deformed plastically or elasto-plastically, but the subsurface is deformed elastically. When the loading caused by the impact shot releases, the near surface will spring back but remains partially elongated due to the plastic deformation. Besides, the subsurface which deforms elastically also tries to spring back, but it cannot return to its original state due to plastic deformation of the surface (figure

2-6*c*) [1]. Therefore, after shot peening, the residual stresses will be introduced in subsurface of the shot peened material [1]. Figure 2-7 depicts the residual stress variatians after shot peening from the surface to the subsurface [1]. The maximum compressive residual stress normally appears at the sub-surface and the magnitude of this maximum value depends on the energy of impact and mechanical properties of peened material. Then, the magnitude of compressive stress will decrease with the increase in specimen penetration depth [1]. For equilibrium, the compressive residual stress is balanced by the tensile compressive stress. It means that the tensile stress in the subsurface will compensate completely the sub-surface compressive residual stress generated by shot peening [1].

2.3.2 Practical residual stress measurement methods

Residual stresses are defined as “lock-in” stresses which exist in components after the external loads released the material [39]. In the whole volume of components, the sum of the local regions of tensile stresses and compressive stresses are equal to zero. Figure 2-8 shows an example of a formation and a distribution of residual stresses in a material. In which, the residual stresses are created in the sub-surface of material after the releasing of externally loads.

Residual stresses are created by almost all manufacturing processes. Then, these stresses develop or relax during the service life of components. The mechanisms for creating residual stresses in the material, as shown schematically in figure 2.9, can be classified are as follows:

1. Non-uniform plastic deformation: including processes such as rolling, drawing and extrusion, forging, bending, cutting, turning, etc. These methods are employed to change the shape of the material [39].

2. Surface modification: including some techniques such as machining, grinding, plating, peening, carburizing, etc. [39]. These methods are used to improve the surface properties of the material.

3. The changes of material phase and/or density due to the presence of large thermal gradients also can create the residual stress in the material. These methods are heat treatment, casting, quenching, phase transformation in metals and ceramics, welding, etc. [39].

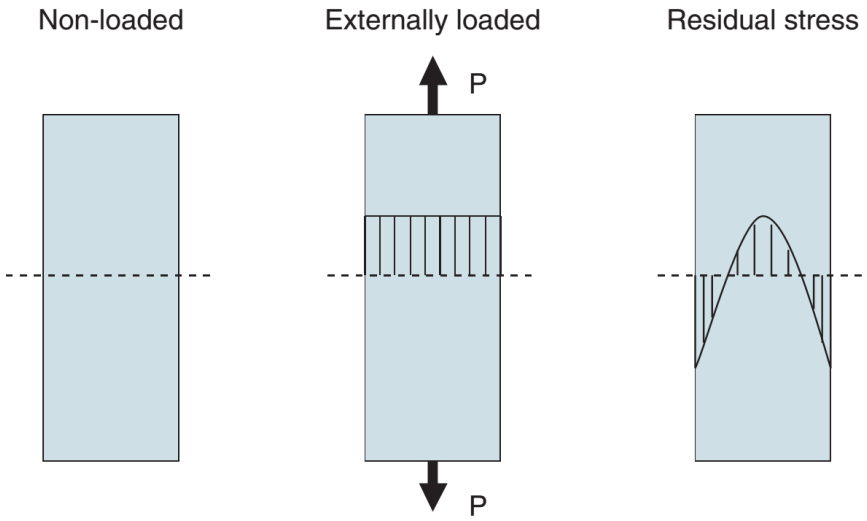

Figure 2-8. Schematic diagram of the cross-section of a material showing the formation and distribution of the residual stresses in a material [39].

It is to be noted that after finishing the manufacturing process, the tensile and compressive stresses appear simultaneously in the sub-surface of material. Take shot peening process as an example, after treatment, the compressive residual stress zones are formed close to the peened surface and the tensile stresses are created below them.

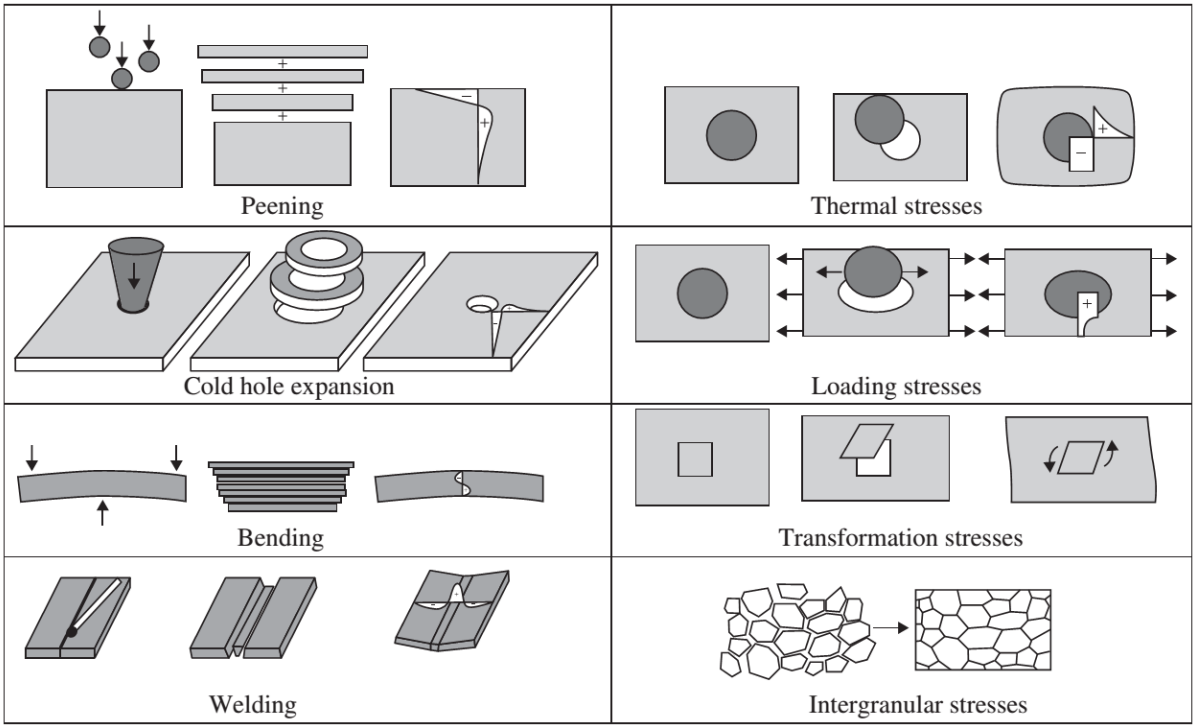

Figure 2-9. Examples of some common processes in which residual stresses are created in the material [39].

Residual stresses can be classified as either macro stress (Type I), or micro stress (Type II) or a combination of macro and micro stresses (Type III) present simultaneously in a material [39, 41]. The classification goes as follows:

+ Type I: Macro residual stress. This type stress develops in the component with the scale larger than grain size of the material [41];

+ Type II: Micro residual stress. This stress alters on on the individual grain scale [39, 41];

+ Type III: Micro residual stresses exist within a grain of material due to the presence of dislocations and crystalline defects [41].

A larger number of methods to measure the residual stresses in different types of material have been established over past decades [39, 41]. However, most of the techniques are developed to measure Type I residual stresses and they are classified into destructive, or

semi-destructive or non-detective techniques as shown in figure 2-10. The destructive and semi-destructive techniques are also named as mechanical methods or stress-relaxing methods, which evaluate the stress-relaxation formed in a component when the material is removed. These methods measure deformations of the material when residual stresses releases during the material removal. Non-destructive techniques usually measure some parameters related to the stress such as the interplanar spacing, *d*, from their stress-free value, d_o. Then, the strain could be analyzed by applying Bragg's law (in X-ray diffraction residual stress measurement). Finally, figure 2-11 and table 2-1 present the penetration and the spatial resolution and the summation of the advantages and the disadvantages of each residual stress measurement techniques, respectively.

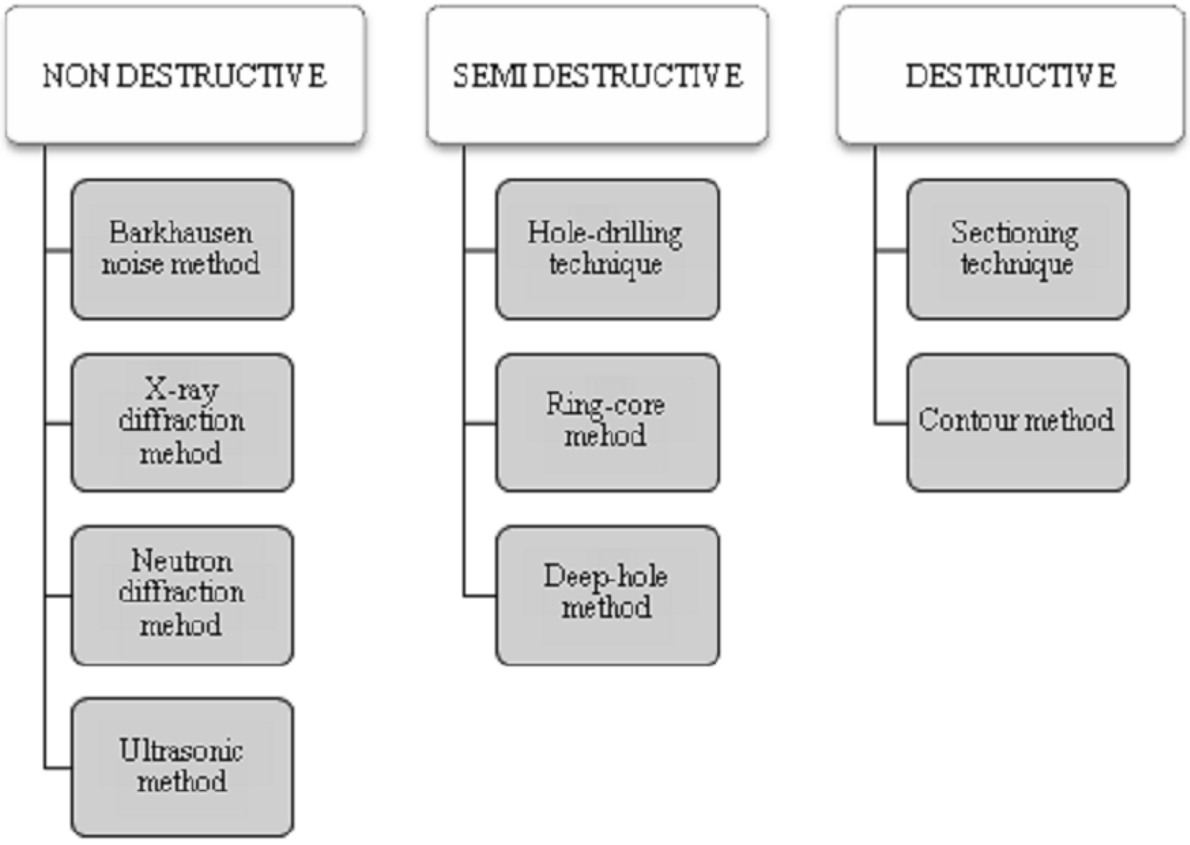

Figure 2-10. Residual stresses measuring techniques [41].

Table 2-1. Comparison of the residual stresses measurement techniques [41].

Technique	**Advantages**	**Disadvantages**
X-ray diffraction	Ductile Generally available Wide range of materials Hand-held systems Macro and Micro RS	Lab-based systems Small components Only basic measurements
Hole Drilling	Fast, Easy use Generally available Hand-held Wide range of materials	Interpretation of data Semi destructive Limited strain sensitivity and resolution
Neutron Diffraction	Macro and Micro RS Optimal penetration and resolution 3D maps	Only specialist facility Lab-based system
Barkhausen Noise	Very quick Wide sensitive to Microstructure effects especially in welds Hand-held	Only ferromagnetic materials Need to divide the microstructure signal from that due to stress
Ultrasonic	Generally available Very quick Low cost Hand-held	Limited resolution Bulk measurements over whole volume
Sectioning	Wide range of material Economy and speed Hand-held	Destructive Interpretation of data Limited strain resolution
Contour	High-resolution maps of the stress normal to the cut surface Hand-held Wide range of material Larger components	Destructive Interpretation of data Impossible to make successive slices close together
Deep hole drilling	Deep interior stresses measurement Thick section components Wide range of material	Interpretation of data Semi destructive Limited strain sensitivity and resolution
Synchrotron	Improved penetration and resolution of X-rays Depth profiling Fast Macro and micro RS	Only specialist facility Lab-based systems

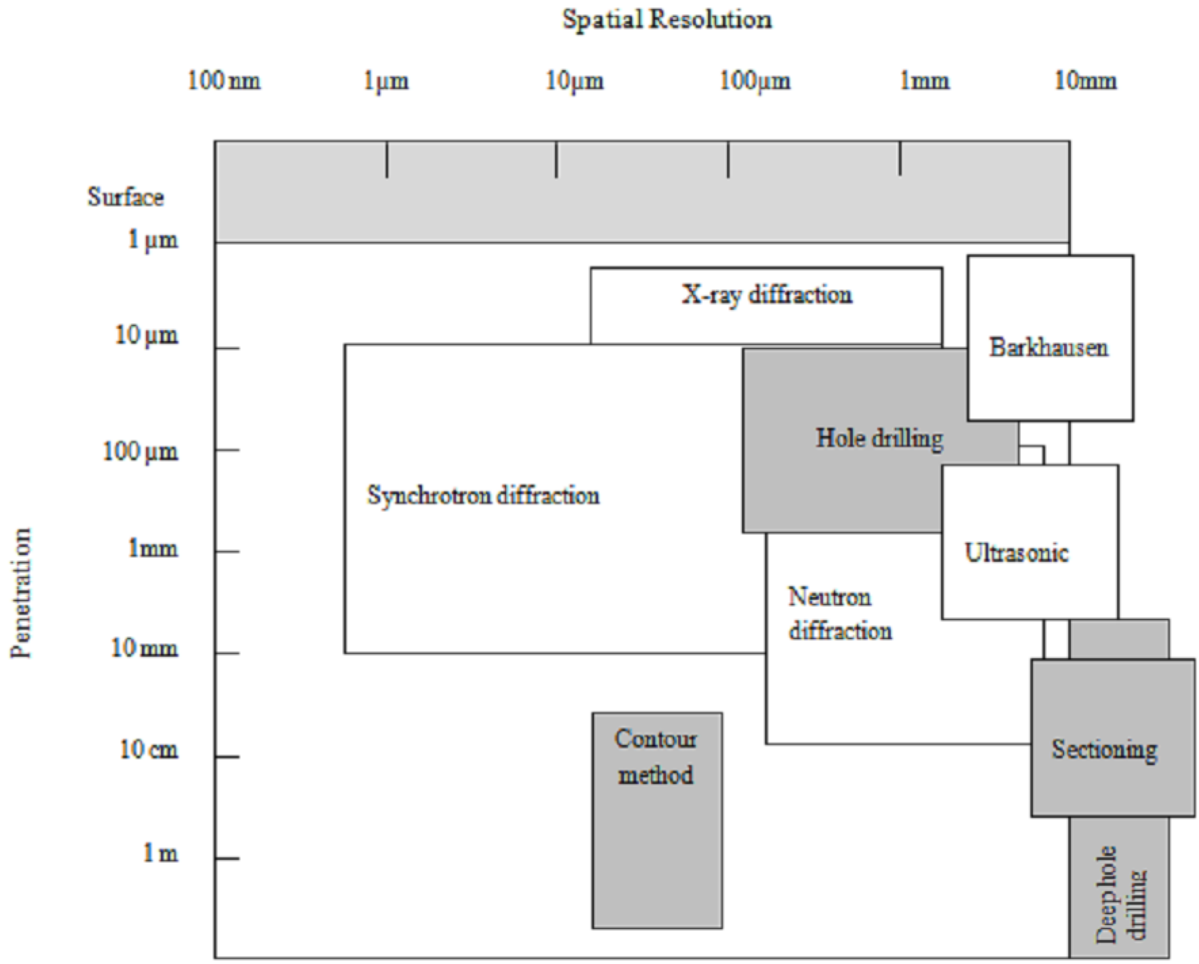

Figure 2-11. Residual stresses measuring techniques [41].

2.4 Surface texture parameters

The surface texture parameters of the shot peened material are defined according to the ISO 25178 standard [42]. The huge plurality of surface texture parameters are the field parameters. The field parameters are calculated based on every data point (the coordinates(*x*, *y*, *z*) of each point) measured on the definition area, while feature parameters only consider specific points, lines or areas. In addition, the field parameters characterize the surface heights, slopes, complexity, wavelength content, etc. of the sampling area (*A*) [43]. The surface texture parameters are classified into four general categories (figure 2.12): height (amplitude), spatial, hybrid and functional [44]. Figure 2.13 shows the typical applications for various 3D parameters, it indicates which 3D parameters needed to measure and to control

relate to the required application. The height parameters are the most frequently used in manufacturing industry because they provide simple standards to easily determine the quality of the surface finishing of specimens.

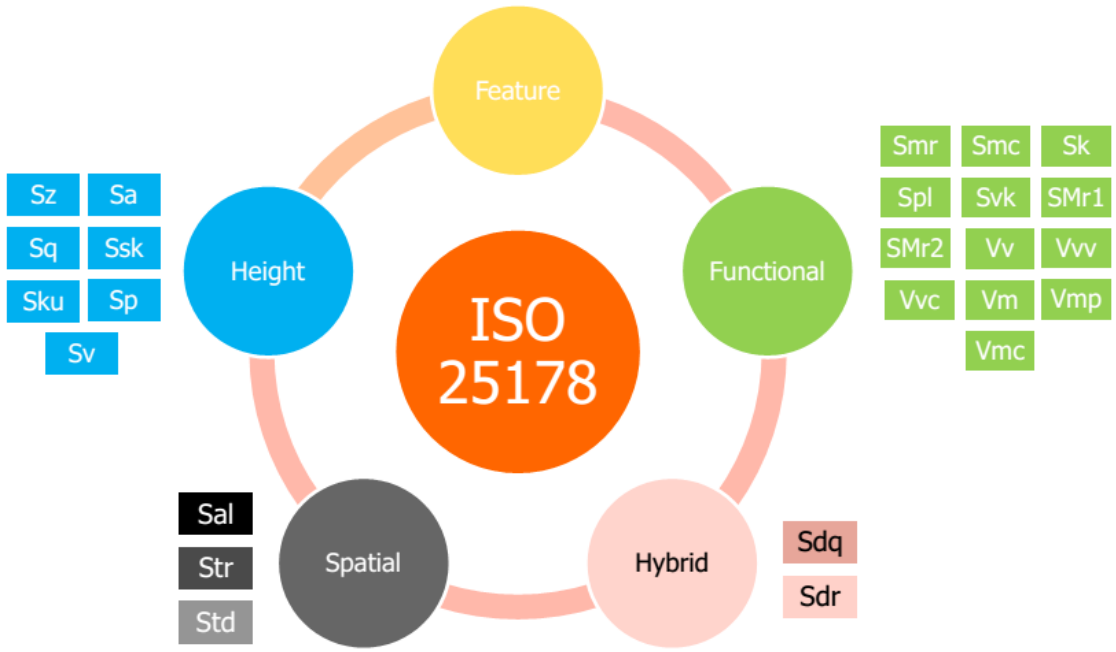

Figure 2-12. The surface texture parameters according to ISO 25178.

Function	Amplitude	Spatial	Hybrid	Functional
Bearings	▲	▲	■	▲
Seals	▲	■	▲	▲
Friction	▲	▲	▲	▲
Joint Stiffness	▲	■	■	▲
Slideways	▲	▲	■	▲
Electrical/Thermal Contacts	▲	▲	▲	▲
Wear	▲	▲	▲	▲
Galling	▲	●	▲	▲
Bonding & Adhesion	▲	●	■	▲
Painting & Plating	▲	■	■	▲
Forming & Drawing	▲	▲	■	▲
Fatigue	▲		●	▲
Stress & Fracture	▲		■	▲
Reflectivity	▲	■	▲	▲
Hygiene	▲		■	▲

▲ = Much evidence ■ = Some evidence ● = Little or circumstantial evidence

Figure 2-13. Typical applications for various 3D parameters[44].

2.5 Modeling of shot peening process

Modeling and simulation of the shot peening process are widely used as they provide a cost-effective and fast approach to understand and predict the whole process without carrying out expensive experimental trials. Besides, the simulation results can be used to improve, control and design the experiments.

2.5.1 Single shot impact

The dynamic of single shot peening model was studied by Meguid [11] (figure 2-14*a*), Hong [45] (figure 2-14*b*), Bhuvaraghan [46] (figure 2-14*c*) and Bae [21] (figure 2-14*d*). In their research, the effects of shot peening parameters i.e. shot velocity, shot size, shot shape, angle impact, etc. on residual stress distribution have been investigated.

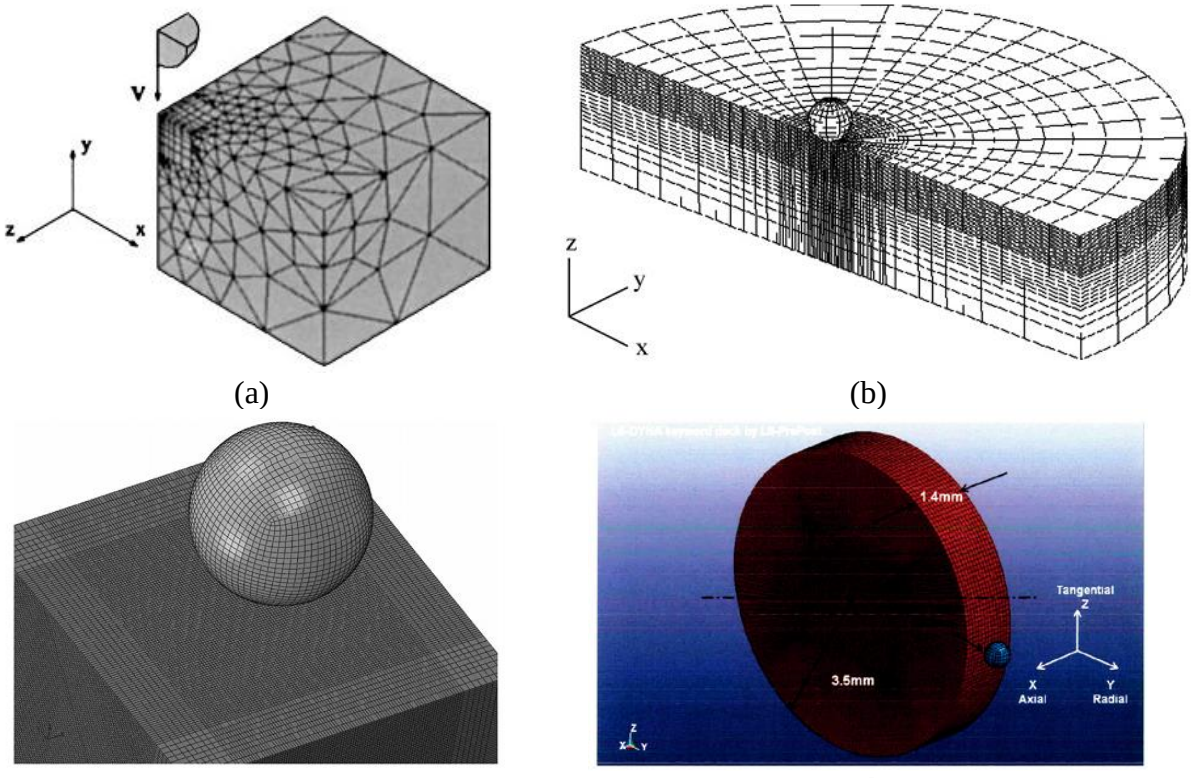

(a) (b)

(c) (d)

Figure 2-14. Single shot model: (a) Meguid [11], (b) Hong [45], (c) Bhuvaraghan [46], and (d) Bae [21].

2.5.2 Multiple-shot impacts

The dynamics of modeling of multiple-shot impacts also have been developed [12, 13, 47-50]. In research reported by Meguid [12] (figure 2-15) and Eltobgy [47], the effect of distance between the shots was conducted. Majzoobi [48] has considered the effect of the number of balls on the target material, i.e. four balls and nine balls (figure 2-16). Kim [13] studied the effect of multiple-shot impacts with various cycles and impact sequences. A random function was used to generate the location of shots in the research by Miao [49], which can predict results more reliable than the fixed and symmetrical arrangement (figure 2-17). However, from the literature review, the number of balls required to achieve 100% coverage and the coverage of the shot peening process have still not been well documented.

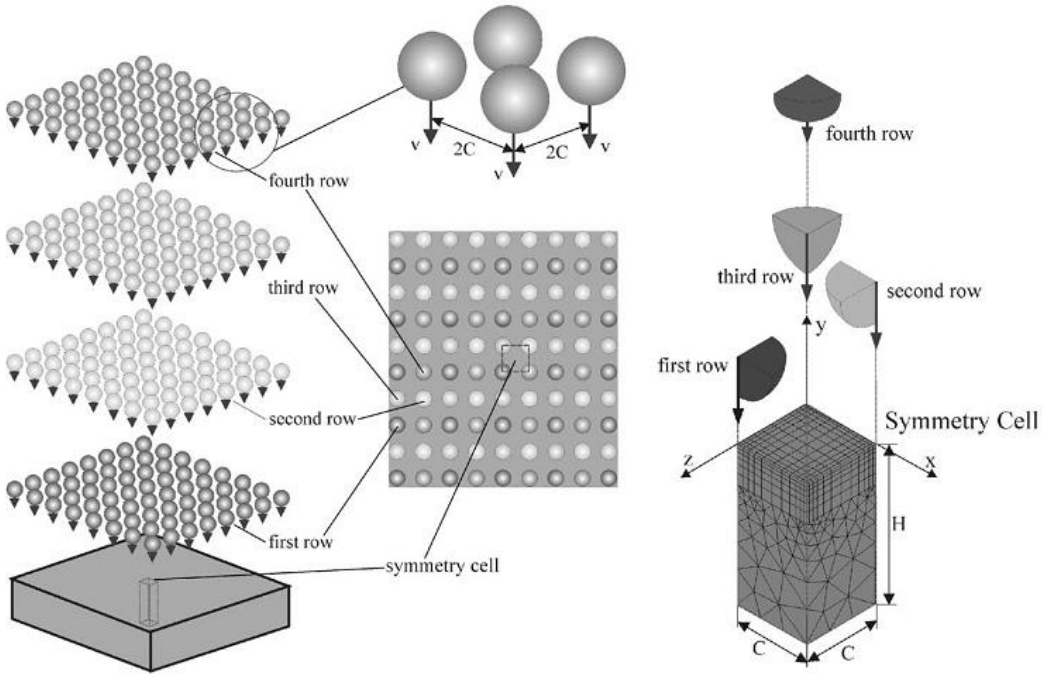

(a) (b)

Figure 2-15. FE model of multiple impingements of multiple-shot impacts: (a) full model and (b) discretized symmetry cell in Meguid research [12].

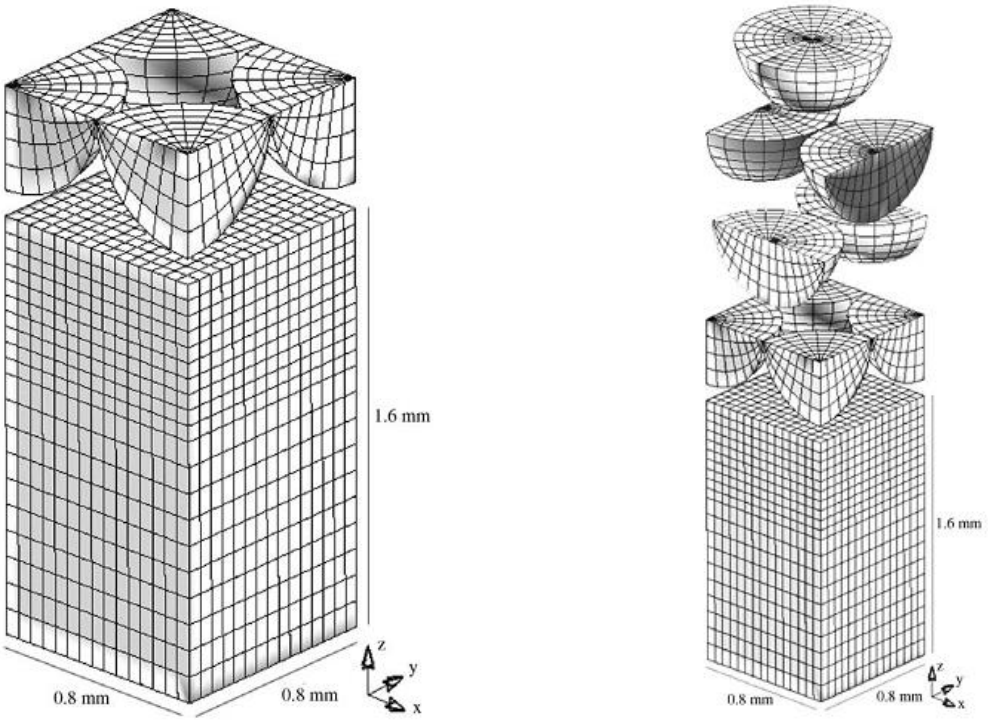

(a) (b)

Figure 2-16. Multiple-shot impact model of Majzoobi [48]: (a) four-shot model, and (b) nine-shot model.

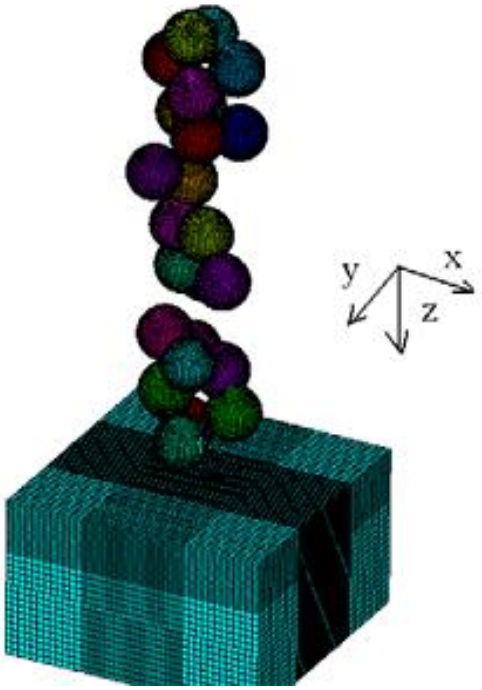

Figure 2-17. Multiple-shot impact model of Miao [49].

2.5.3 Numerical model of severe shot peening model

The research by Umemoto [33] concluded that the most important condition to produce nanocrystalline (NC) structure is a strain, with the minimum amount of strain

necessary is around 7 mm/mm. Besides, another favorable condition is repetitive or cyclic deformation. Based on that conclusion, Bagherifard [50] developed a severe shot peening model to predict the generation of a nanostructured surface layer. Comparing with the random multiple-shot impacts (used for conventional shot peening), the severe shot peening model has the same boundary conditions. However, to achieve the minimum required an amount of strain, the number of shots and their velocity are significantly high (figure 2-18*a*).

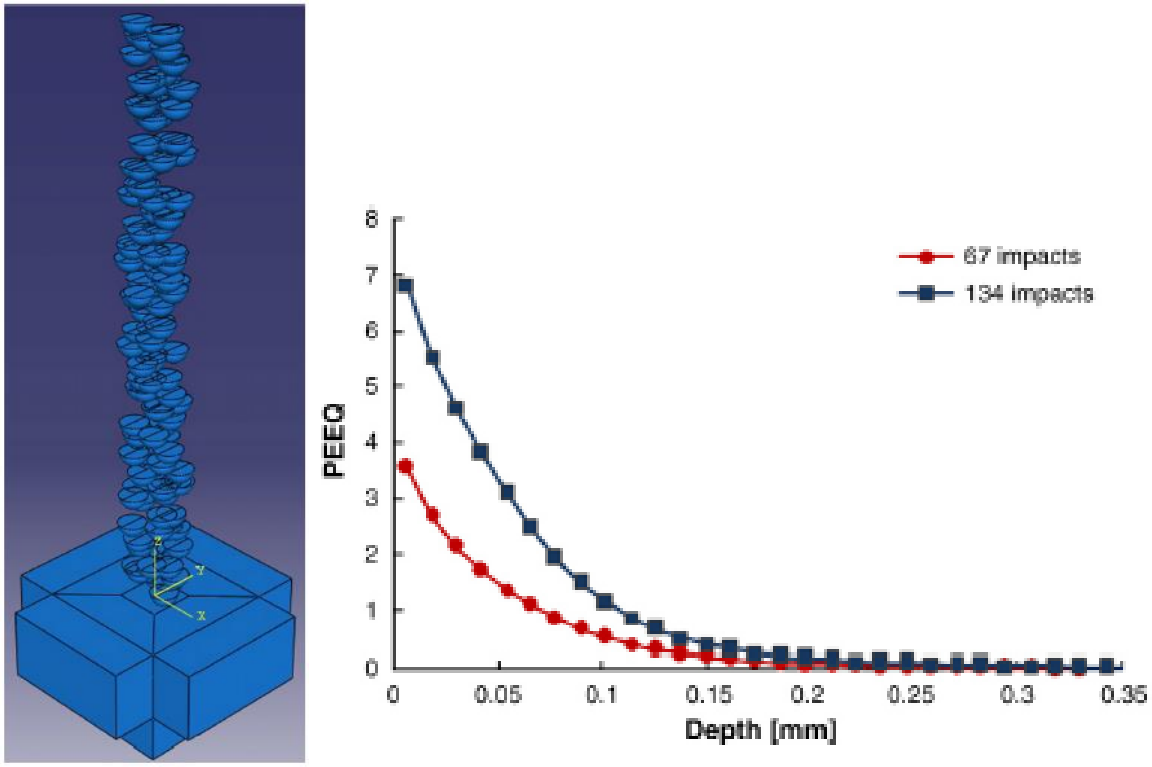

(a) (b)

Figure 2-18. (a) Severe shot peening and (b) equivalent plastic strain (PEEQ) profile within the target measured from impacted surface of Bagherifard's model [50].

Figure 2-18*b* shows the distribution of equivalent plastic strain (PEEQ) as a function of depth in the research by Bagherifard [50]. The result indicates that, under the setting condition with 134 shots, the PEEQ is larger than 7 mm/mm [50], which is the important condition to conclude that the ultrafine layer was generated on the surface of material [33].

2.5.4 An analytical model for the shot peening process: the elastic plastic with kinematic hardening model

There are numbers of material models developed for the numerical simulation. Each model has its attributes, applications. Therefore, choosing the proper material model for the numerical simulation depends on the general classes of physical materials and the physical treatment process. Shot peening is a cold working process which causes the plastic deformation on the surface and sub-surface of the material. Hence, the elastic plastic with kinematic hardening is one of the cost-effective models can be applied to calculate. This material model can be employed to study the isotropic and kinematic hardening plasticity material which can include rate effects [51].

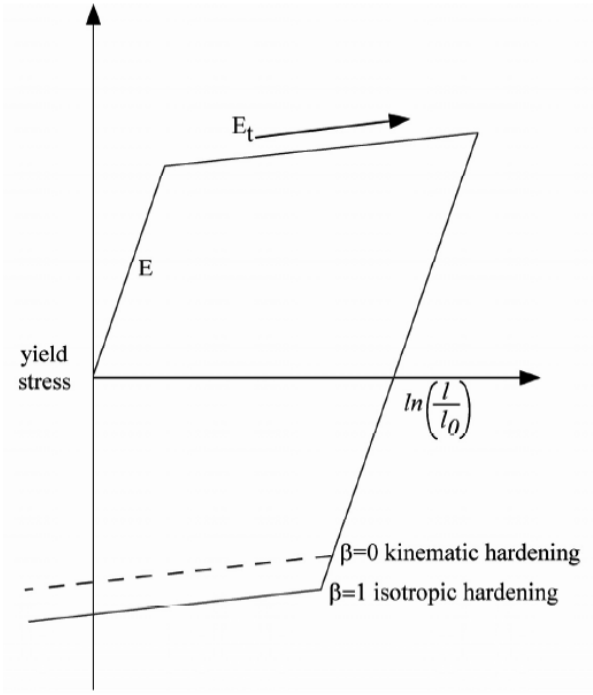

Figure 2-19. Elastic-plastic behavior with isotropic and kinematic hardening [51].

The parameter to obtain the isotropic, kinematic or a combination of isotropic and kinematic hardening is called β. It varies between 0 and 1. Figure 2.19 displays the isotropic hardening (β = 1) and kinematic hardening behavior (β = 0), where l_0 and l are the initial and

deformed length of the specimen respectively [51]. In the case of isotropic hardening, the center of yield surface is fixed but the radius is a function of the plastic strain. In a contrast, the radius of yield surface is fixed but the center translates in the direction of the plastic strain [51]. The yield condition is defined as [51]:

$$\phi = \frac{1}{2}\xi_{ij}\xi_{ij} - \frac{\sigma_y^2}{3} = 0 \tag{2-2}$$

where

$$\xi_{ij} = s_{ij} - \alpha_{ij} \tag{2-3}$$

$$\alpha_y = s_{ij} - \alpha_{ij} \tag{2-4}$$

The co-rotational rate of α_{ij} is

$$\alpha_{ij}^{\Delta} = (1-\beta)\frac{2}{3}E_p\dot{\varepsilon}_{ij}^{p} \tag{2-5}$$

So,

$$\alpha_{ij}^{n+1} = \alpha_{ij}^{n} + (\alpha_{ij}^{\nabla^{n+1/2}} + \alpha_{ik}^{n}\Omega_{kj}^{\Delta^{n+1/2}} + \alpha_{jk}^{n}\Omega_{ki}^{\Delta^{n+1/2}})\Delta t^{n+1/2} \tag{2-6}$$

Then, the Cowper Symonds model is employed to calculate the strain rate. The current radius of the yield surface, σ_y, is calculated by [51]:

$$\sigma_y = \left[1 + \left(\frac{\dot{\varepsilon}}{C}\right)^{\frac{1}{p}}\right]\left(\sigma_0 + \beta E_p \varepsilon_{eff}^{p}\right) \tag{2-7}$$

in which σ_o is static yield stress, C and p are constant parameters of material in the Cowper – Symonds relation. The strain rate ($\dot{\varepsilon}$) and plastic hardening modulus (E_p) and the effective plastic strain (ε_{eff}^{p}) are defined as [51]:

$$\dot{\varepsilon} = \sqrt{\dot{\varepsilon}_{ij}\dot{\varepsilon}_{ij}} \tag{2-8}$$

$$E_p = \frac{E_t E}{E - E_t} \tag{2-9}$$

$$\varepsilon_{eff}^{p} = \int_0^t \left(\frac{2}{3} \dot{\varepsilon}_{ij}^{p} \dot{\varepsilon}_{ij}^{p} \right)^{1/2} dt \tag{2-10}$$

The plastic strain rate is determined as [51]:

$$\dot{\varepsilon}_{ij}^{p} = \dot{\varepsilon}_{ij} - \dot{\varepsilon}_{ij}^{e} \tag{2-11}$$

where $\dot{\varepsilon}_{ij}$ and $\dot{\varepsilon}_{ij}^{e}$ are the total strain rates and the elastic strain rates respectively. In the implementation of this material model, the deviatoric stresses are uploaded elastically and repeated here for the sake of clarity [51]:

$$\dot{\sigma}_{ij} = \sigma_{ij}^{n} + C_{ijkl}\Delta\varepsilon_{kl} \tag{2-12}$$

where $\dot{\sigma}_{ij}, \sigma_{ij}^{n}, C_{ijkl},$ and $\Delta\varepsilon_{kl}$ are the trial stress tensor, stress tensor, elastic tangent modulus matrix and incremental strain tensor, respectively.

Then, the calculation is finish if the yield function is contented. In the case of it is infringed, an increase in plastic strain is calculated, and at that time the stresses are scaled back to the yield surface, as well as the yield surface center is updated. Let consider the trial elastic deviatoric stress at n+1 stage [51].

$$s_{ij}^{*} = \sigma_{ij}^{*} - \frac{1}{3}\sigma_{kk}^{*} \tag{2-13}$$

$$\xi_{ij}^{*} = s_{ij}^{*} - \alpha_{ij}^{*} \tag{2-14}$$

Define the yield function,

$$\phi = \frac{3}{2}\xi_{ij}^{*}\xi_{ij}^{*} - \sigma_y^2 = \Lambda^2 - \sigma_y^2 \begin{cases} \leq 0 \text{ for elastic or neutral loading} \\ > 0 \text{ for plastic harding} \end{cases} \tag{2-15}$$

For plastic hardening then

$$\varepsilon_{eff}^{p^{n+1}} = \varepsilon_{eff}^{p} + \frac{\Lambda - \sigma_y}{3G + E_p} = \varepsilon_{eff}^{p^{n}} + \Lambda\varepsilon_{eff}^{p} \tag{2-16}$$

Scale back the stress deviatiors

$$\sigma_{ij}^{n+1} = \sigma_{ij}^{*} - \frac{3G\Delta\varepsilon_{eff}^{p}}{\Lambda}\xi_{ij}^{*} \tag{2-17}$$

and update the center

$$\alpha_{ij}^{n+1} = \alpha_{ij}^{n} - \frac{(1-\beta)E_p\Delta\varepsilon_{eff}^{p}}{\Lambda}\xi_{ij}^{*} \tag{2-18}$$

2.6 Experimental studies

Severe shot peening (SSP) is successfully used to generate the ultrafine layer on a variety of materials, including pure materials, alloys and intermetallic compounds [7]. The majority of experiments are studied to consider the effects of ultrafine layer on the improvement of material mechanical behavior [7]. To observe the microstructure of peened material, scanning electron microscopy (SEM) and transmission electron microscopy (TEM) have been widely used [52-56]. The X-Ray diffraction (XRD) method is used to determine the residual stress and full width of the diffraction peak at half of maximum intensity (FWHM) distribution inside the components after peening [53, 54, 57]. Current severe shot peening works have compared the advantages of the properties of severe shot peened material

to the conventional shot peened material [53, 57-62]. Most studies have focused on the effect of ultrafine layer induced by severe shot peening to improve the fatigue life, distribution of residual stress, surface roughness and variation of hardness in the subsurface of low alloy steel material. However, the studies on the effects of severe shot peening on other material (like aluminium, titanium and nickel alloy) or others mechanical properties (like friction, wear, scratch resistance, corrosion, nitriding) are very limited.

2.6.1 Effect of shot peening on fatigue

It is well known that most fatigue failures initiate at the surface or subsurface close to the surface and propagate to the inside of components. The shot peening (conventional shot peening) has long been used to prevent these failures. Besides, the components of a nanostructured surface layer induced by severe shot peening are expected to significantly improve the fatigue life of components due to two main reasons: 1) The fatigue crack initiation and its propagation are very sensitive to the structure and properties of the material surface and 2) the high magnitude of compressive residual stresses can also effectively stop or retard the initiation and prevent the propagation of the fatigue cracks.

In an experiment by Bagherifard [63], a low alloy steel 39NiCrMo3 was studied in both conventional and severe shot peening conditions. The fatigue life in the case of a specimen subjected to severe shot peening is expected to be considerably higher than a conventional peened one due to the formation of an ultra-fine-grained layer on the surface of the target material. However, the surface roughness, in the severe shot peening component increases significantly, that is why on the rotating bending fatigue tests, the improvement of the fatigue life of the severe shot peened material is not notable when compared between shot peened and non-peened parts.

To reduce the negative effects of surface roughness caused by the severe shot peening process, Bagherifard [58] investigated some additional methods to reduce the surface roughness on the severe shot peening specimens. These methods include prolonging treatment time (increasing the time of shot peening process), removing a thin layer of material (a layer of almost 45 µm was removed from the surface by grinding and electropolishing by acid), and repeening (using smaller media to peen the component after severe shot peening). Table 2-2 and figure 2-20 show the effectiveness of these methods to the surface roughness and fatigue life of specimens. The results indicate that polishing is the best way to reduce the surface roughness on specimens and these methods can improve the fatigue life of severe shot peened material although it is not too much (a fatigue strength improvement of 10% in comparison with non-peened specimens).

Table 2-2. Surface roughness parameters of shot peened specimens [58].

Treatment	l_t**(mm)**	l_n**(mm)**	R_a **(µm)**	R_q**(µm)**	R_z**(µm)**	R_t**(µm)**
NP	0.8	4.0	0.57	0.79	3.45	4.95
CSP	0.8	4.0	3.53	4.34	17.41	23.21
SSP	0.8	4.0	7.53	8.98	33.90	44.34
SSP (double peening time)	0.8	4.0	8.51	9.94	37.33	50.41
SSP (electro-polishes)	0.8	4.0	3.38	4.16	15.05	20.65
SSP (abrasive wheel)	0.8	4.0	1.56	2.06	10.57	15.00
RSSP (Re-SSP)	0.8	4.0	6.92	8.72	39.24	46.70

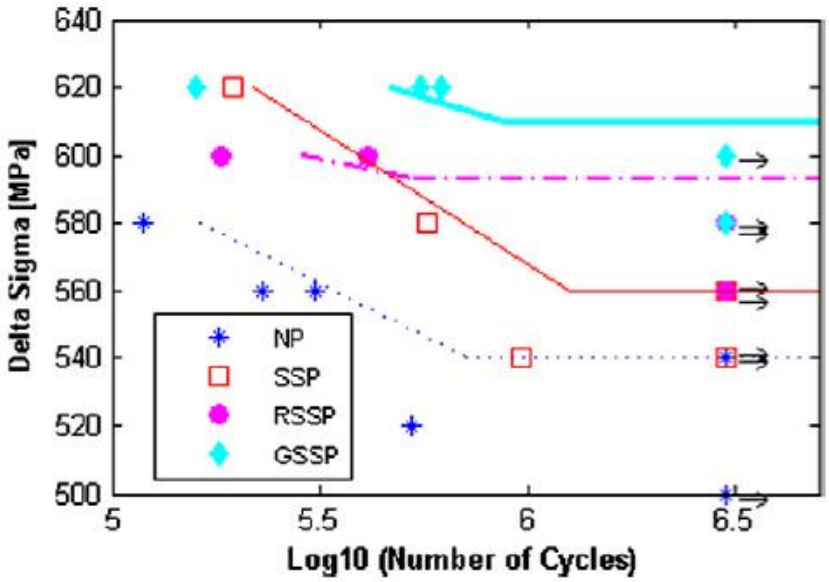

Figure 2-20. The true stress-strain curve in log-log axis (NP: not peened, SSP: severe shot peened, RSSP: re-peened, and GSSP: ground by abrasive wheel [58]).

2.6.2 Effect of shot peening on residual stress distribution

To study the state of residual stress, XRD analysis has been commonly performed. The research by Bagherifard [63] (figure 2-21*a*), [58] (figures 2-21*b*,*c*), and Miková [64] (figure 2-21*d*) show that the maximum stress values in cases of severe shot peening and conventional/typical shot peening are quite similar while the depth of compressive stress layer of severe shot peened material is double compared to the case of conventional/typical peened.

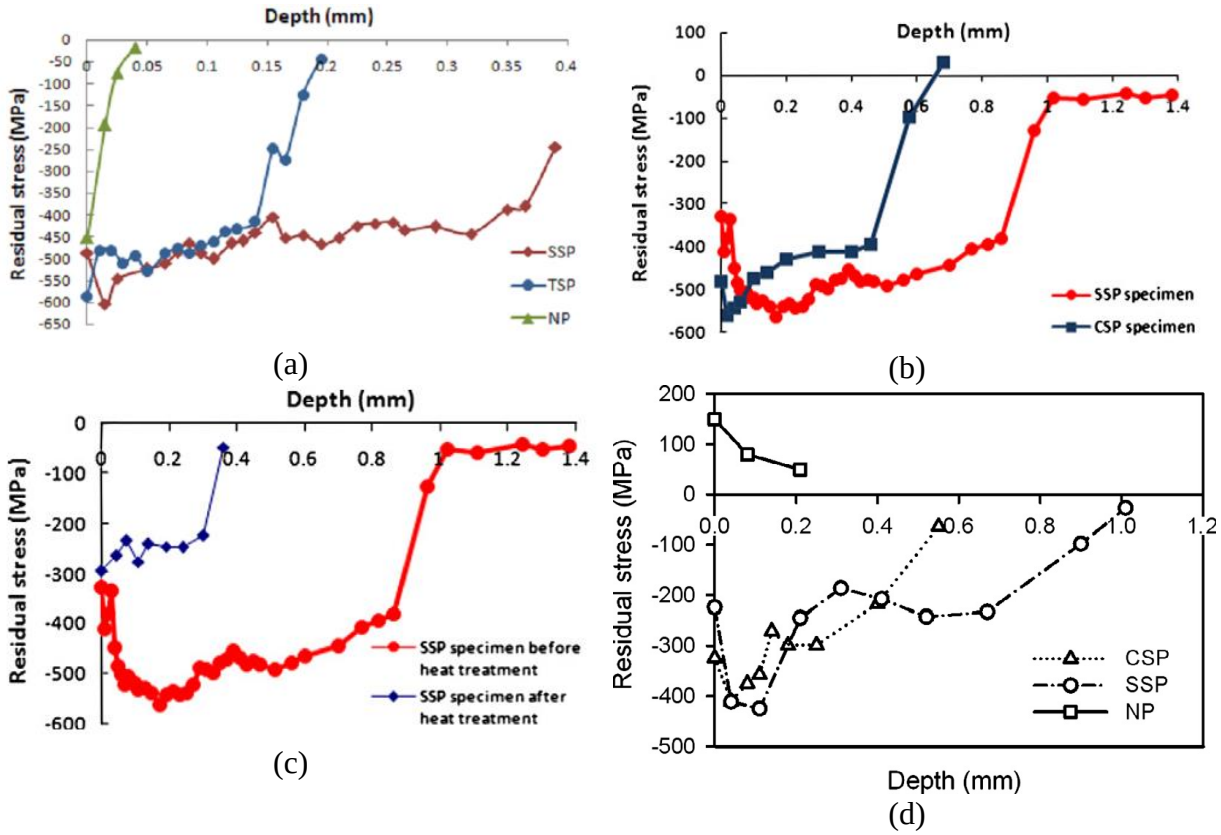

Figure 2-21. Residual stress distribution: (a) Bagherifard's report [63], (b) and (c) Bagherifard's report [58], and (d) Miková's research [64].

2.6.3 Effect of shot peening on surface hardness

To measure the micro-hardness of specimens after shot peening and severe shot peening, a cross-section of specimens were studied by using a diamond Vickers indenter with a maximum force of 25 gf [58], 200 gf [54], and 50 gf [64]. Figure 2-22 compares the microhardness value in some experiments. It can be seen that the maximum value of hardness at the surface and then gradually reduces into the inside of materials. Besides, the severe shot peened material is harder than that which was conventionally shot peened.

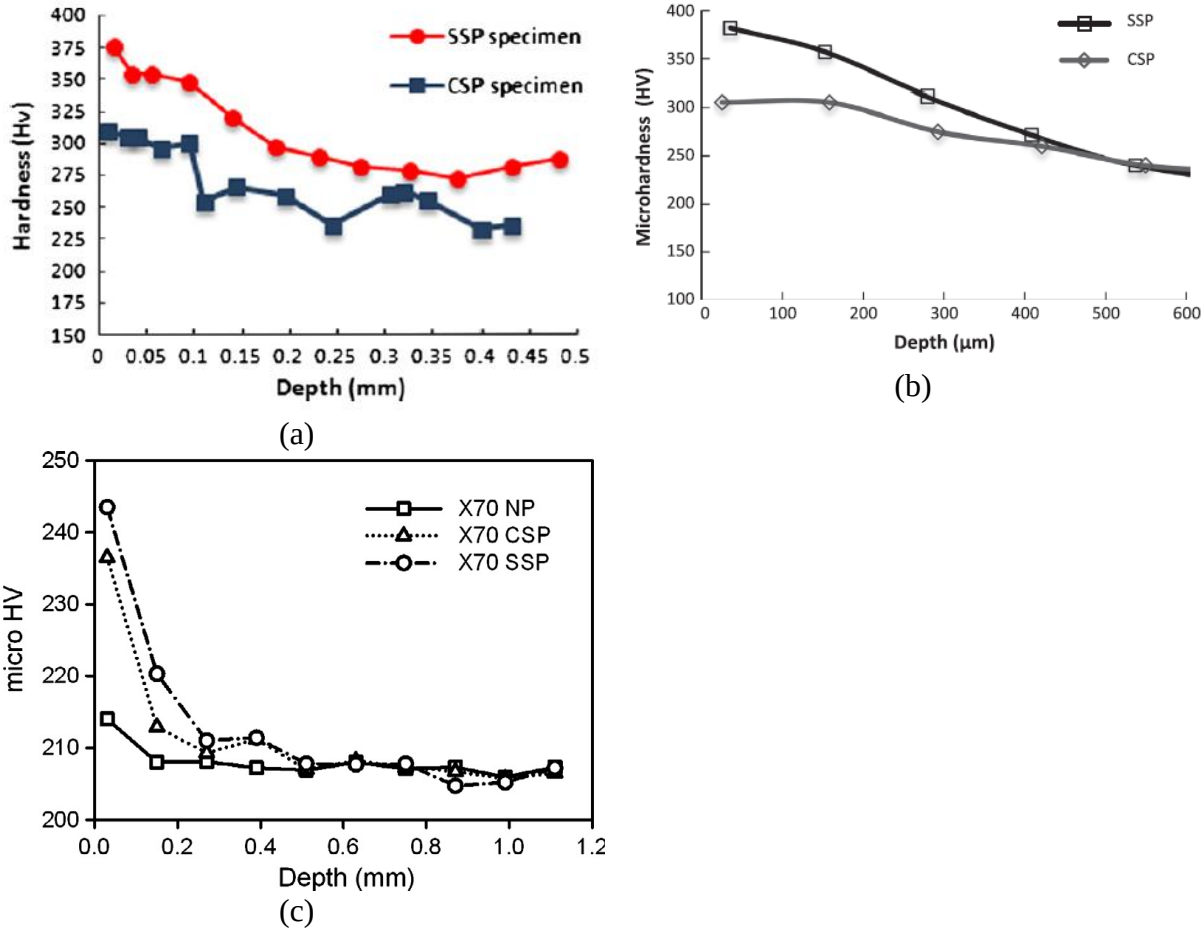

Figure 2-22. Microhardness of peened specimens: (a) Bagherifard's report [58], (b) Bagherifard's report [54], and (c) Miková's research [64].

2.7 The research gaps in the literature review

Although the shot peening process has been studied and used widely for over fifty years, data on various aspects of the process and peened material are lacking in the public domain. These include mechanical, tribological properties, distribution of residual stress in the subsurface, fatigue life of the peened component, surface quality of shot peened low alloy steel under different shot peening conditions as well as the effect of the double shot peening and severe shot peening.

With regard to the reported modeling of the shot peening process [48, 65-69], it is observed that three-dimensional multiple-shot impact models did not concentrate on the

coverage parameter. Instead, the multiple-shot impact simulations studied uniformly distributed positions and prearranged sequences. The details of these impact patterns have been discussed in a review paper by Bagherifard et al. [70]. Though the use of symmetry patterns reduces the computational costs, it cannot totally define the random nature of practical shot peening process. Therefore, these patterns often fail to simulate a full coverage condition for the actual shot peening process.

The literature review also reveals that the experimental results of the double shot peening process were reported by Vielma [71] and Scuracchio [72], but there is a lack of modeling and simulation knowledge.

In many published papers [12, 13, 49, 50, 73], the surface target material is set as a flat surface. In addition, this assumption reduces the complexity of the simulation process. However, the flat surface somehow reduces the accuracy of the numerical simulation results and cannot be applied to consider the effect of the as-received surface roughness condition on the surface topographies of the shot peened samples.

Finally, the literature review of the fatigue of the shot peened reveals that after treatment the fatigue life of samples significantly increases [7, 59, 74]. The answer for this increment was explained by the induction of the compressive residual stress in the subsurface of the material. However, it is it is necessary to find evidence to explain why the compressive stress can improve the fatigue life and why the fatigue life reduced when the samples were shot peened in the severe conditions.

2.8 Summary

This chapter began with the brief history of the shot peening process from the time of ancient artisans and blacksmiths up to modern-day shot peening technique. Shot peening

parameters and shot peening systems were also introduced in this chapter to provide an overall picture of the whole process. Besides, the mechanism of the generation of deformation zone and the resultant residual stress gradient after shot peening were explained in this section. The last part of the literature review presented the status and the limitations of the currently reported research in both simulation work and experiment work.

Chapter 3: Effects of shot peening process parameters on the microstructure, mechanical and tribological properties of low alloy steel

3.1 Introduction

The major failure mechanisms of engineering materials such as fatigue fracture, fretting fatigue, wear and corrosion, etc. are very sensitive to their surface condition and properties [7], where the typical failure originates. To improve the fatigue life of metallic components, compressive residual stresses are introduced to the surface and subsurface of mechanical components to prevent the fatigue crack initiation and growth simultaneously [7]. There are several common methods used to induce compressive residual stresses to the subsurfaces of solid materials such as shot peening [2, 75, 76], severe shot peening [55, 58, 77], laser shock peening [78, 79], deep cold rolling [6, 80] and roller burnishing [81]. Among these methods, shot peening has been widely used in industries ranging from aerospace to construction with up to 75% of the components in airplane engines being subjected to shot peening [82, 83].

Although the shot peening process has been used for over fifty years, the data on mechanical and tribological properties of shot peened components under different shot peening conditions, and double shot peening is not satisfactorily available. Among steels, AISI 4340, low alloy steel, is known for its high strength and great ability to plastically deform. AISI 4340 steel is widely used for power transmission gears and shafts, aircraft landing gear, automotive, machine tool applications, and other structural components [36, 37, 53].

In this study, AISI 4340 low alloy steel was selected as a material for investigation. Shot peening process with media S230, S110 and combining both these media (double shot peening) was performed under various pressures. The mechanical and tribological properties of as-received and shot peened AISI 4340 steel samples were systematically investigated within the context of microstructure, surface roughness, micro-hardness and ball-on-disc microtribological testing.

3.2 Experimental details

3.2.1. Material

Commercial AISI 4340 low alloy steel samples of 8 mm thickness rolled was selected for all shot peening experiments. The nominal chemical composition of the AISI 4340 steel is presented in table 3-1. Prior to the shot peening experiment, the steel samples were polished using sand papers with grit sizes of 240, 600 and 1000 to eliminate any surface oxide layer and other contaminants.

Table 3-1. The nominal chemical composition of AISI 4340 steel (weight %).

C	Si	Mn	Cr	Ni	Mo	Fe
0.34	0.25	0.50	0.90	1.55	0.25	96.21

3.2.2. Shot peening

Prior to shot peening process, to determine the intensity of the shot peening process at varying pressures of 69 to 552 kPa, the standard Almen test A strip (SAE 1070 of size 76.1 mm × 18.95 mm × 1.29 mm), Almen gauge (Almen Gages, Peening Accessories) and holding fixture were employed. At each shot peening pressure, the Almen test strip was shot with different cycle times (T) and their arc heights were measured correspondingly. A plot of

arc height with the shot peening time was drawn to obtain saturation curve and to define the shot peening intensity.

All the steel samples were shot peened for the same period (20s). In this study, three series of tests were investigated under different shot peening pressures. Two types of steel media were used, S230 and S110, which are the common media used in the industry. The details of the shot peening conditions are listed in table 3-2.

Table 3-2. Shot peening process parameters used in chapter 3.

Samples	**Media type**	**Pressure (kPa)**
S110-10	S110	68.9
S110-20	S110	137.9
S110-30	S110	206.8
S110-40	S110	275.8
S110-50	S110	344.7
S110-60	S110	413.7
S110-70	S110	482.6
S110-80	S110	551.6
S230-10	S230	68.9
S230-20	S230	137.9
S230-30	S230	206.8
S230-40	S230	275.8
S230-50	S230	344.7
S230-60	S230	413.7
S230-70	S230	482.6
S230-80	S230	551.6
DP-10-20	S230	68.9
	S110	137.9
DP-20-20	S230	137.9
	S110	137.9
DP-30-20	S230	206.8
	S110	137.9
DP-40-20	S230	275.8
	S110	137.9
DP-50-20	S230	344.7
	S110	137.9
DP-60-20	S230	413.7
	S110	137.9
DP-70-20	S230	482.6
	S110	137.9
DP-80-20	S230	551.6
	S110	137.9
As-received	NA	NA

The S230 and S110 media have the mean diameter of about 600 µm and 300 µm respectively and hardness of about 500 ± 30 Hv. To investigate the effects of combining both media on the properties of AISI 4340 steel, a series of experiments were performed where the samples were first treated by the larger media (S230) and then shot peened again by the smaller one (S110). Coverage is defined as the percentage of the sum of peened area over the total area on the surface of the specimen. The shot peened samples were analyzed, using an optical microscope at 50x magnification, to determine the level of coverage.

3.2.3. Characterization

The experimental velocities of shots were measured with a ShotMeter G3 - Particle Velocity Sensor equipment at a distance of 150 mm from the outlet of the nozzle. In this experiment, the mass flow rate was kept constant at 3 Kg/min.

Scanning electron microscopy (SEM, JEOL®, JSM-5600LV) was employed to study the surface and wear morphologies of the samples while the cross-sectional microstructures of the samples were studied using an optical microscopy (OM, Zeiss®, Axioskop 2, JVC color video camera). Prior to SEM and OM characterization, the samples were ground and polished via a chemical – mechanical polishing process with the details listed in table 3-3.

Table 3-3. Sample preparation parameters for microstructural observation.

Surface	SiC-paper 320	MD-Largo	MD-Dac	MD-Nap	MD-Chem
Suspension		Largo 9 µm	Diapro 3µm	Diapro 1µm	OPS
Lubricant	Water				
rpm	300	150	150	150	150
Force (N)	30	30	30	10	10
Time (min)	10	5	5	5	5

The surface hardness of the samples was measured using a Vickers hardness tester (Future-tech®, FM-300e) with a total applied force of 100 g, and an average hardness value was obtained from twenty indentation measurements on each sample. The cross-section hardness of the samples was measured by the nanoindenter equipment (Agilent®, G2000) (maximum depth and maximum load of indentation are 500 µm with 0.01 nm resolution and 500 mN with 50 nN resolution, respectively) using a Berkovich diamond indenter. Prior to the measurement, the sample was ground and polished to prepare a very fine surface. Continuous Stiffness Measurement (CSM) technique was applied to calculate the hardness where the contact stiffness is measured continuously during the process. Indentation load was continuously recorded during the loading and unloading cycle of indentation. To study the hardness as a function of the depth from the surface, a line indentation with 25 µm between two points was carried out. The cross-sectional hardness was calculated from five measurements at each location.

The surface roughness of the sample was measured using a surface profilometer (Taylor Hobson®, Talyscan 150) with a diamond contact stylus of 4 µm in diameter. Five areal measurements per sample were carried out to calculate the average three-dimensional surface roughness parameters such as an average areal roughness (S_a), a root mean squared (S_q), a maximum peak height (S_p), a maximum valley depth (S_v) and a maximum height of the surface (S_z). These parameters are the height parameters of the surface texture and commonly used to quickly identify the quality of surface finish of the material. These parameters defined according to ISO 25178-2: 2012 [42].

The tribological properties of the samples and wear test were investigated using a ball-on-disc micro-tribological test (CSM®, Micro-Tribometer). The samples were tested against a 100Cr6 steel ball with a diameter of 6 mm in a circular path of 1.5 mm in radius for

40000 laps at a sliding speed of 50 mm/s under a normal load of 5 N at room temperature (~ 22-24^{o}C). The wear volumes were obtained after a test duration of 40,000 laps. Five measurements on each sample were taken to obtain average tribological results.

3.3 Results and discussion

Figure 3-1*a* and *b* show the overview of the spherical shapes of media S230 and S110 with mean diameters of about 600 and 300 μm respectively. Figure 3-2 presents the velocities of S230 and S110 steel shots as a function of shot peening pressure. The measurements reveal that the rise in pressure results in the velocities of both S230 and S110 steel shots. The stream shots become less stable when the pressure increases causing an increase in variation of the measured results.The dynamic energy of each shot was calculated using: $E = ½\ mv^2$, where m and v are the mean mass and mean velocity of each shot respectively. The mean mass of each shot S230 and S110 are $8.8 \pm 0.5 \times 10^{-4}$ g and $1.1 \pm 0.1 \times 10^{-4}$ g respectively. It is clear from figure 3-2 that even the velocity of shot S230 is smaller than that of shot S110, but the dynamic energy of shot S230 is much higher than shot S110 under the same shot peening pressure condition. The difference becomes more significant with the higher shot pressures. The higher dynamic energies of shots will cause deeper and wider dimples on the shot peened materials.

The shot peening intensities measured under different shot peening pressures are depicted in figure 3-3 in which the shot peening intensities of both S230 and S110 steel shots increased linearly with increased shot peening pressure was found. To measure the intensity of the shot peening process, three types of standard Almen test strips are used, e.g. N, A and C. The N strip is employed at low intensity levels, the A strip is the most common and used in the medium range, while the C strip is used for very high intensity level only. In this experiment, the standard A strip was used to measure the intensity of the shot peening

process. Therefore, the unit of intensity is A. Besides, it is also indicated that the intensities measured in the case of S230 steel shots are higher than that for S110 steel shots, due to S230 steel shots having higher dynamic energies under the same pressure conditions.

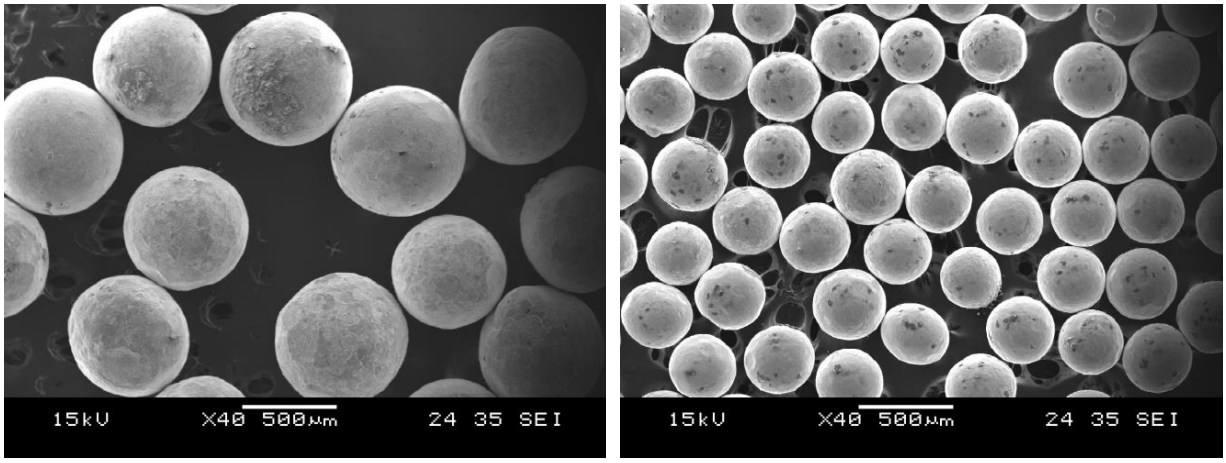

(a) (b)

Figure 3-1. SEM micrograph showing overview of media: (a) S230 and (b) S110.

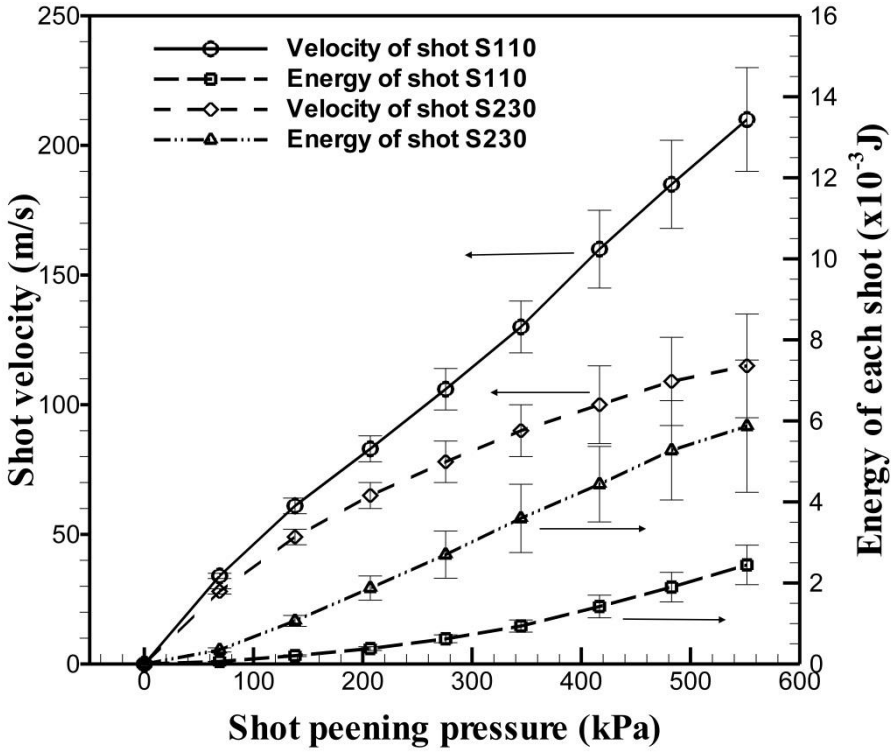

Figure 3-2. The velocity of shot and dynamic energy of each S230 and S110 steel shot measured under different shot peening pressures.

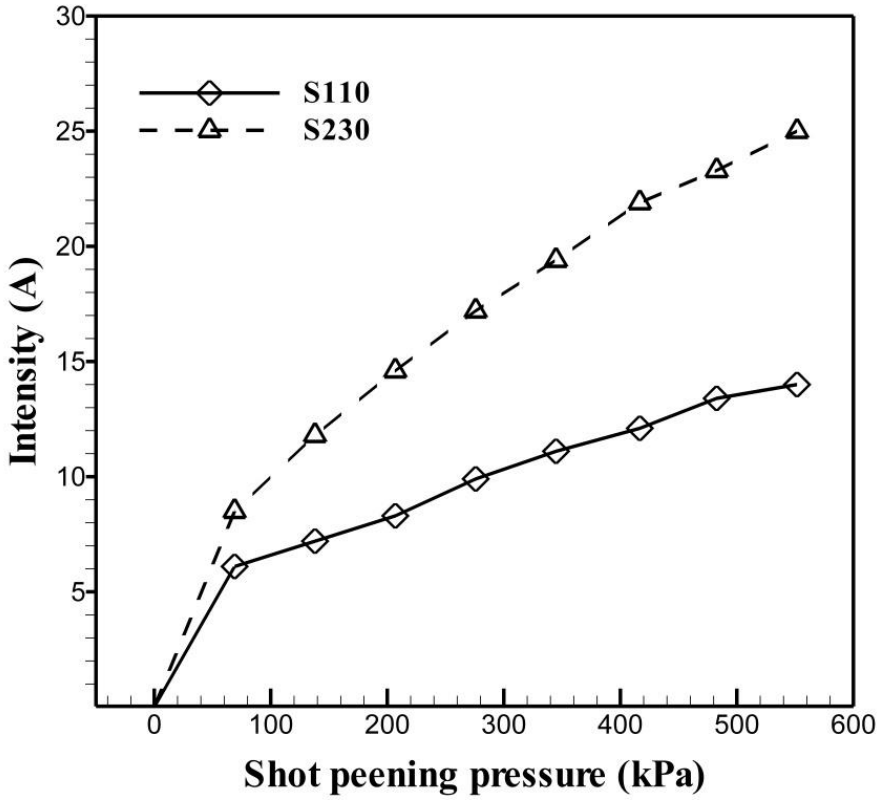

Figure 3-3. Intensities of S230 and S110 shots measured under different pressures.

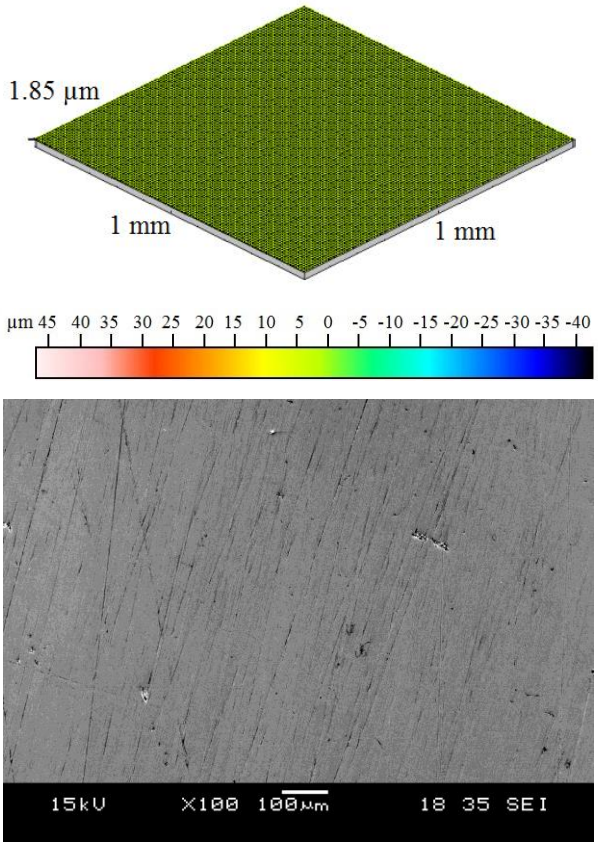

Figure 3-4. Surface topographies (above) and morphologies (below) of as-received AISI 4340 steel sample.

Figures 3-4 to 3-7 show the surface topographies and morphologies of the shot peened AISI 4340 steel under different shot peening conditions. In figure 3-4, the as-received sample reveals a relatively smooth surface. In the case of the samples treated by the S230 steel shots, at the shot peening pressure of 68.9 kPa, the level of coverage is about 60% (figure 3-5*a*), increasing to 80% at the pressure of 137.9 kPa (figure 3-5*b*) and reaching about 98% (can be considered at full coverage) at the pressure of 206.8 kPa (figure 3-5*c*).A totally full coverage is achieved at the shot peening pressure of 275.8 kPa (figure 3-5*d*). It is clearly seen that, in the case of the samples treated by the media S110, the full coverage of the shot peened sample was achieved even at the shot peening pressure of 68.9 kPa (figure 3-6*a*). On the other hand, the larger media roughens the surface of the shot peened samples by forming deeper and wider dimples on these surfaces as shown by comparison of the shot peened surface topographies after shot peening by S230 and S110 steel shots (figure 3-5 and figure 3-6). The increased surface roughness is inherent to the shot peening process. To reduce the surface roughness caused by the larger shot (S230), an additional shot peening process was performed called double shot peening in which the shot peened samples were shot peened again by a smaller shot size (S110). However, the comparison between figure 3-5 and figure 3-7 displays that only the double shot peening process can improve the surface finish of the shot peened material from the shot peening pressure of 206.8 kPa, which is the lowest pressure required to achieve full coverage by the first treatment with media S230.

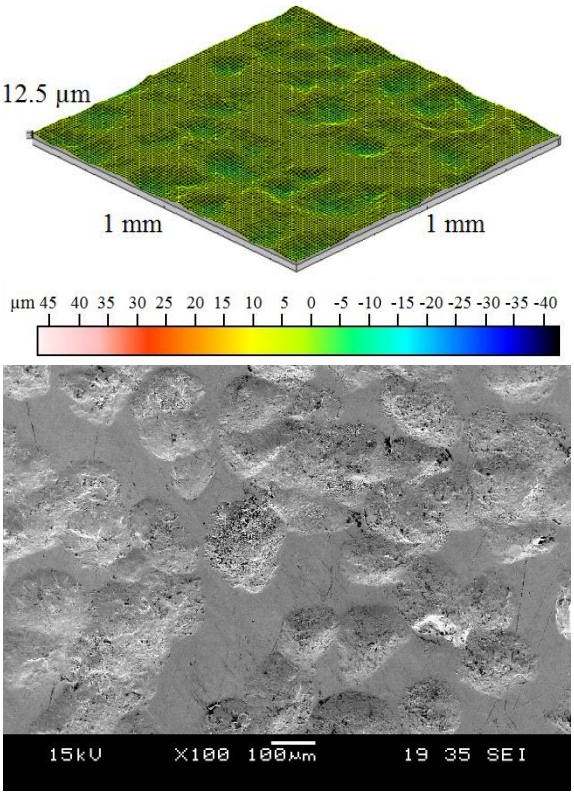

(a) S230-10

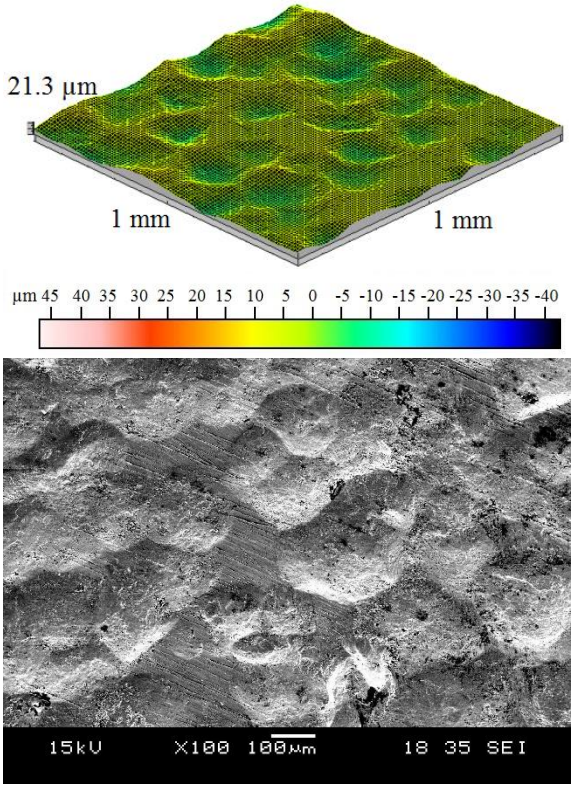

(b) S230-20

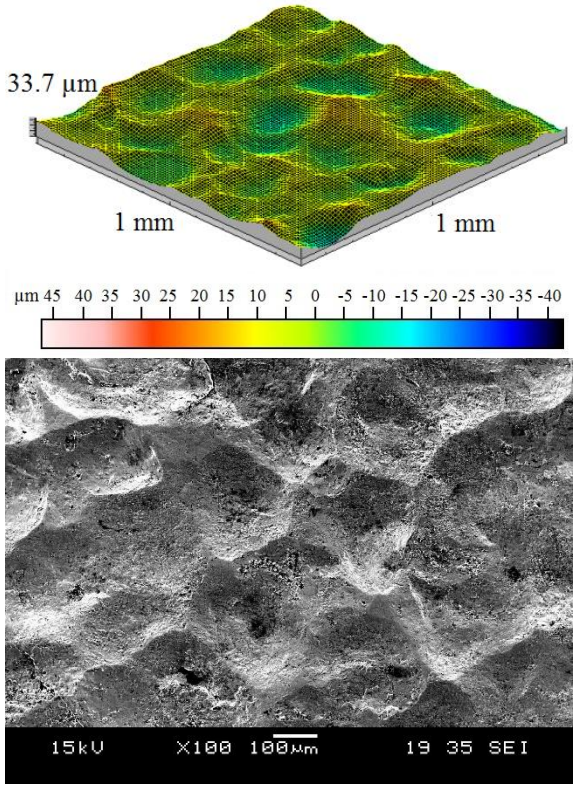

(c) S230-30

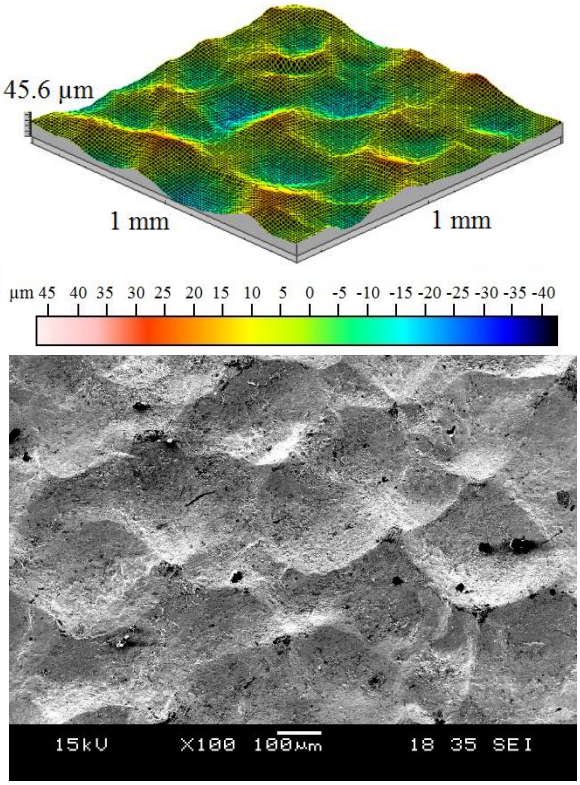

(d) S230-40

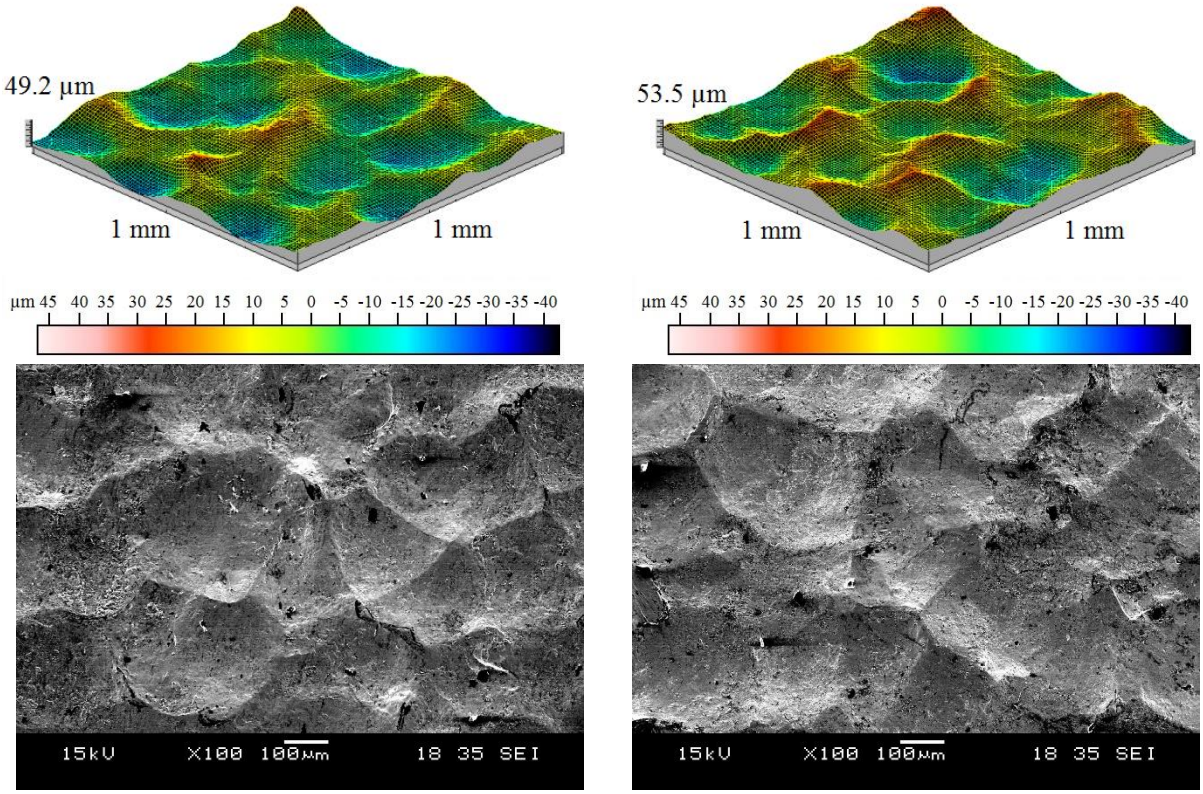

(e) S230-50 (f) S230-60

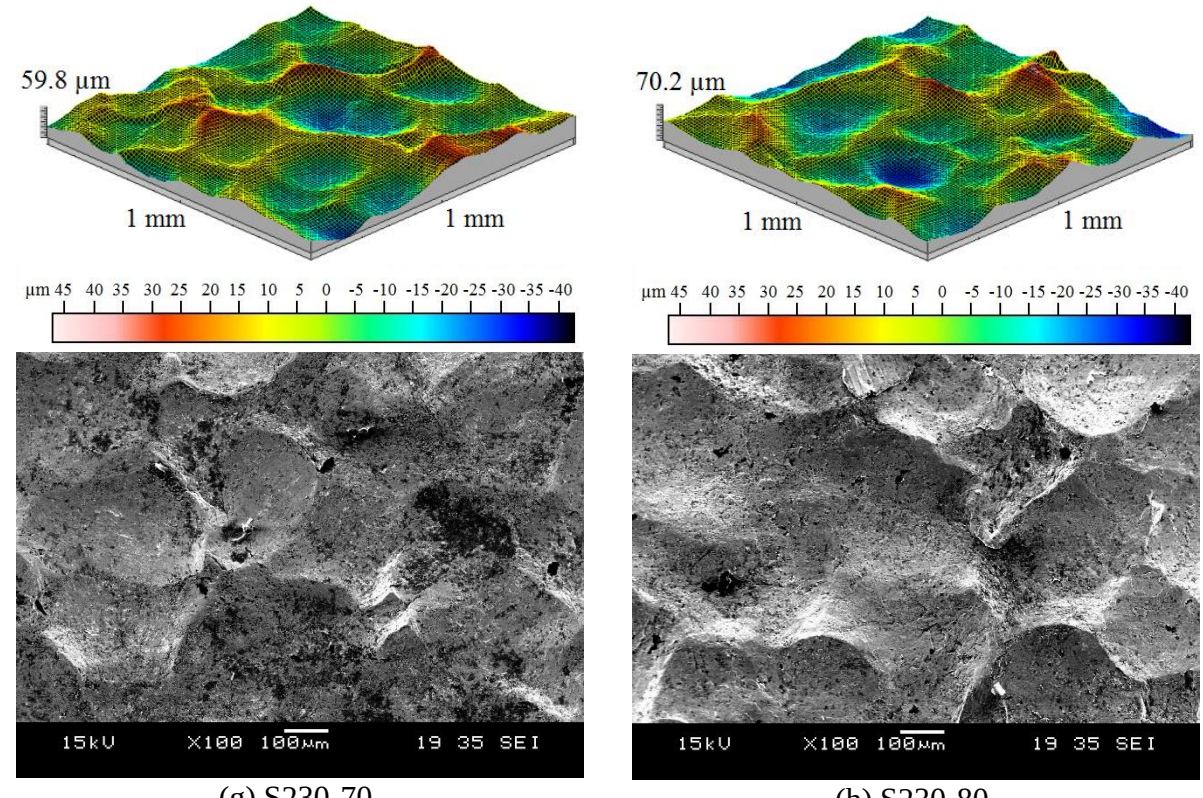

(g) S230-70 (h) S230-80

Figure 3-5. Surface topographies (above) and morphologies (below) of the shot peened AISI 4340 steel samples treated by the media S230: (a) S230-10, (b) S230-20, (c) S230-30, (d) S230-40, (e) S230-50, (f) S230-60, (g) S230-70 and (h) S230-80.

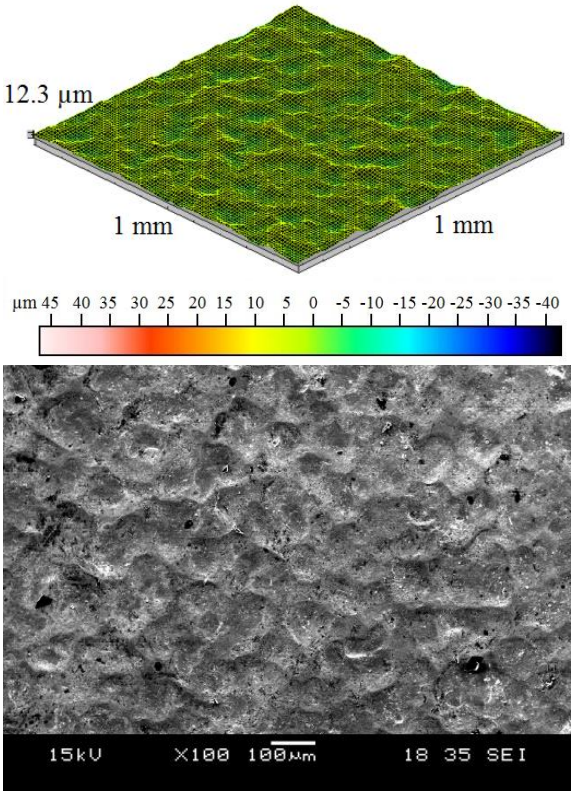

(a) S110-10

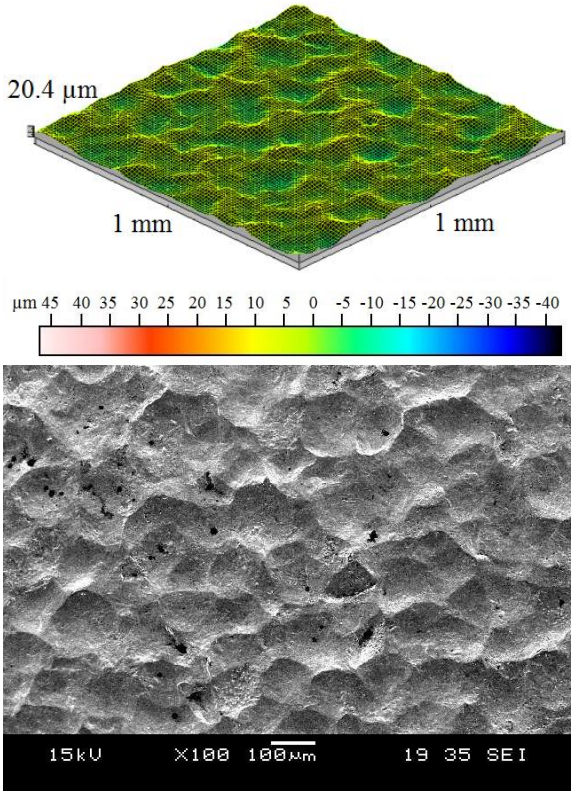

(b) S110-20

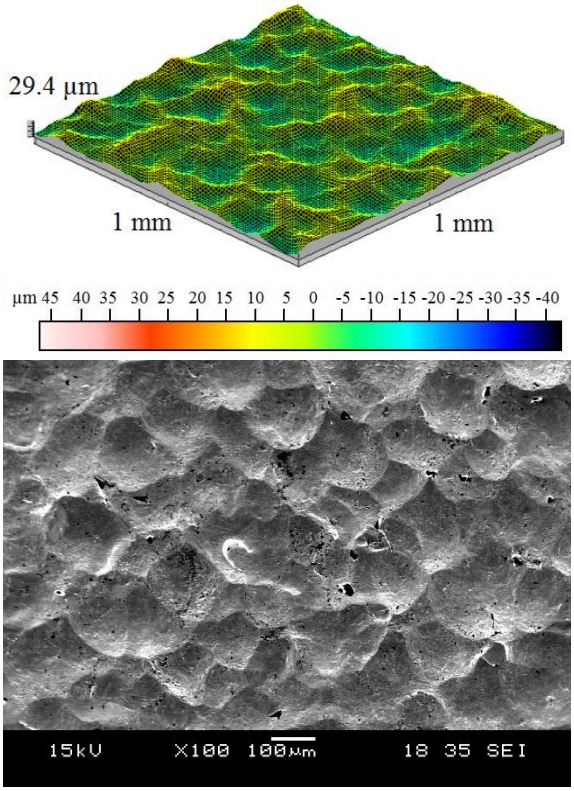

(c) S110-30

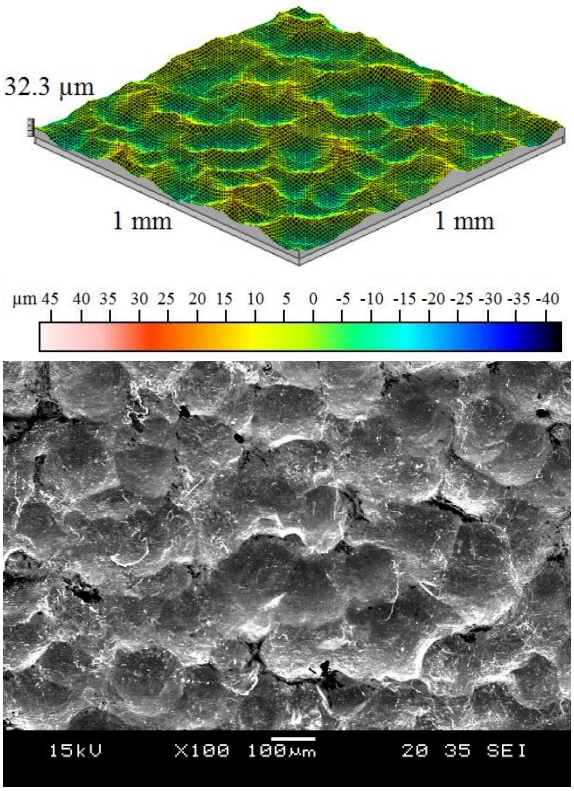

(d) S110-40

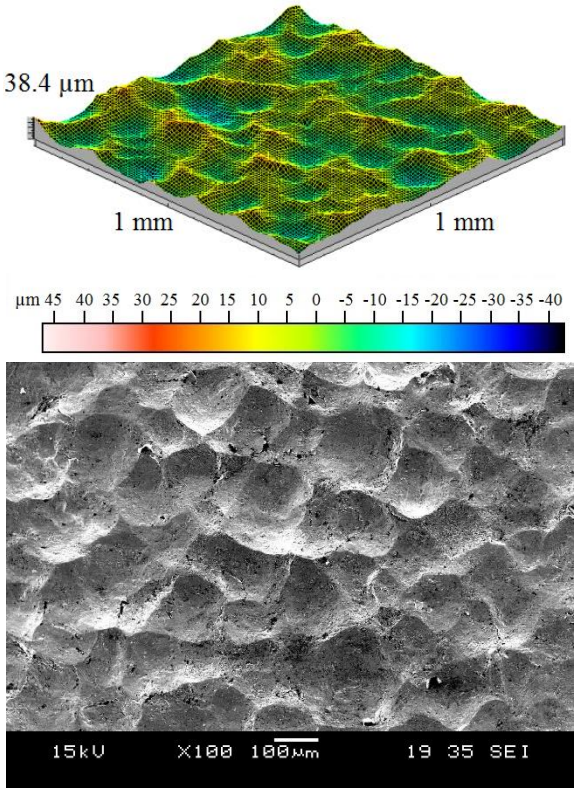

(e) S110-50

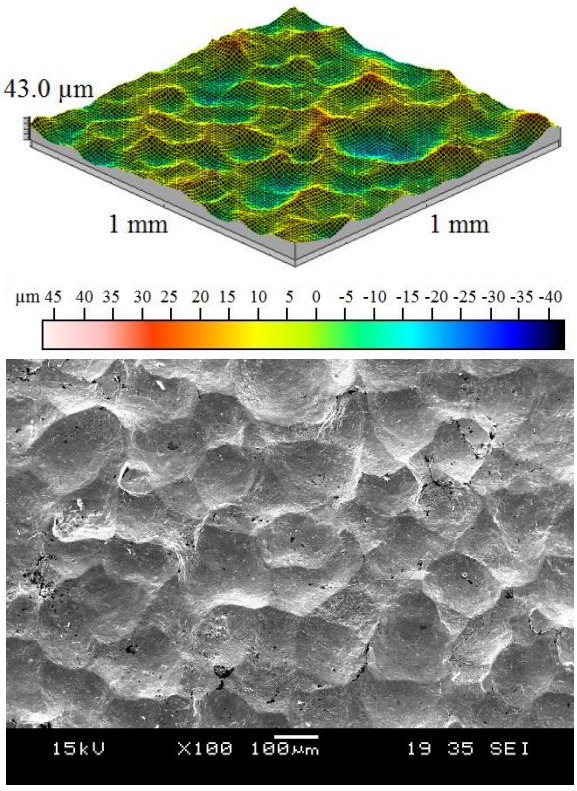

(f) S110-60

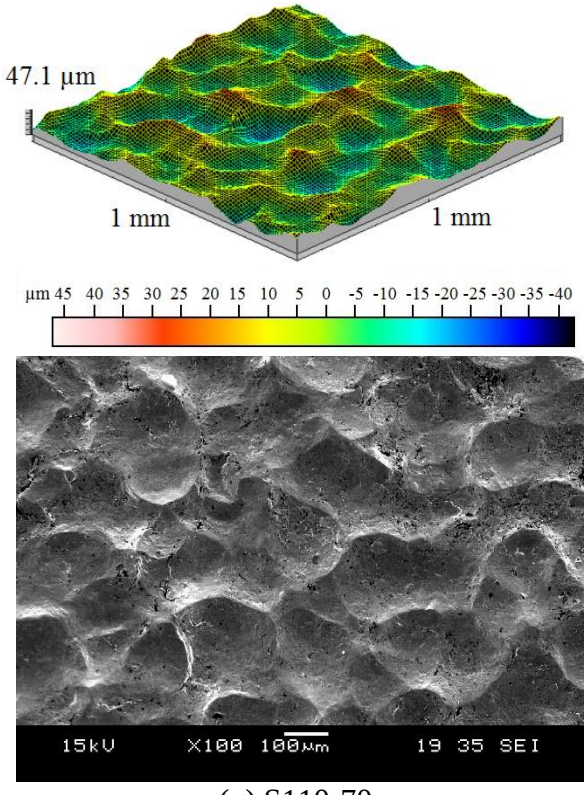

(g) S110-70

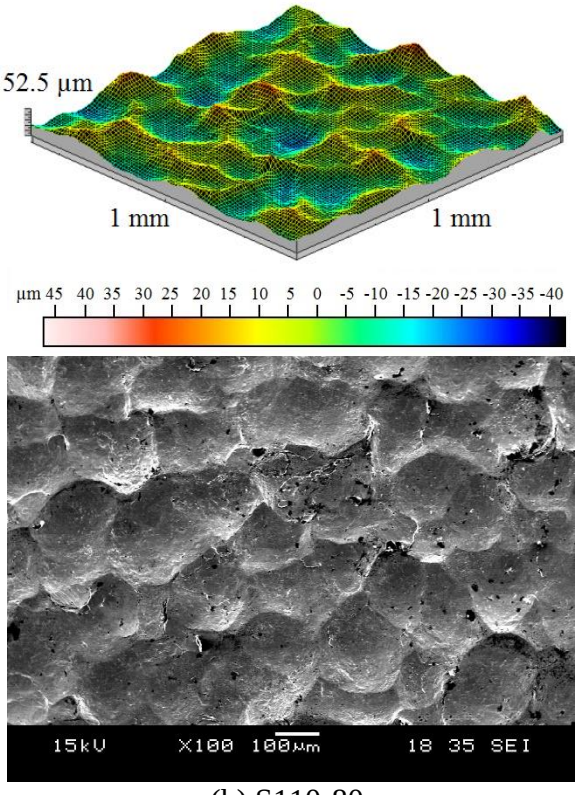

(h) S110-80

Figure 3-6. Surface topographies (above) and morphologies (below) of the shot peened AISI 4340 steel samples treated by the media S110: (a) S110-10, (b) S110-20, (c) S110-30, (d) S110-40, (e) S110-50, (f) S110-60, (g) S110-70 and (h) S110-80.

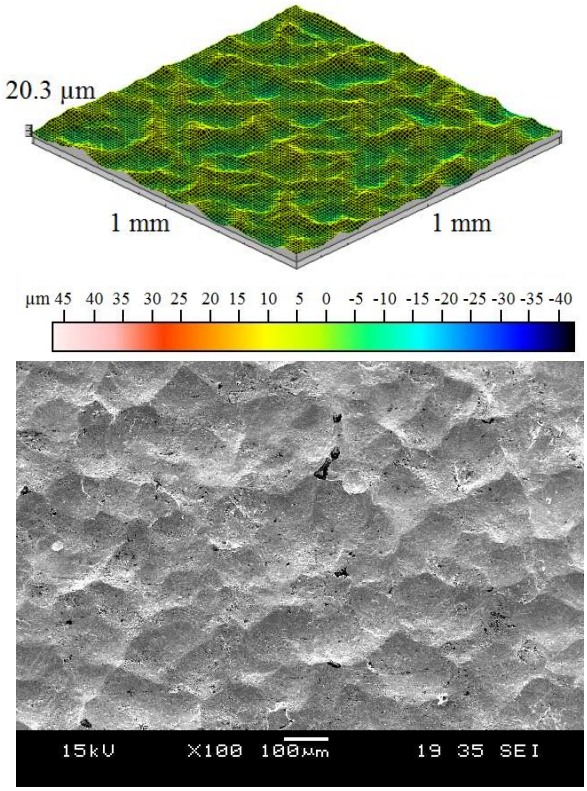

(a) DP-10-20

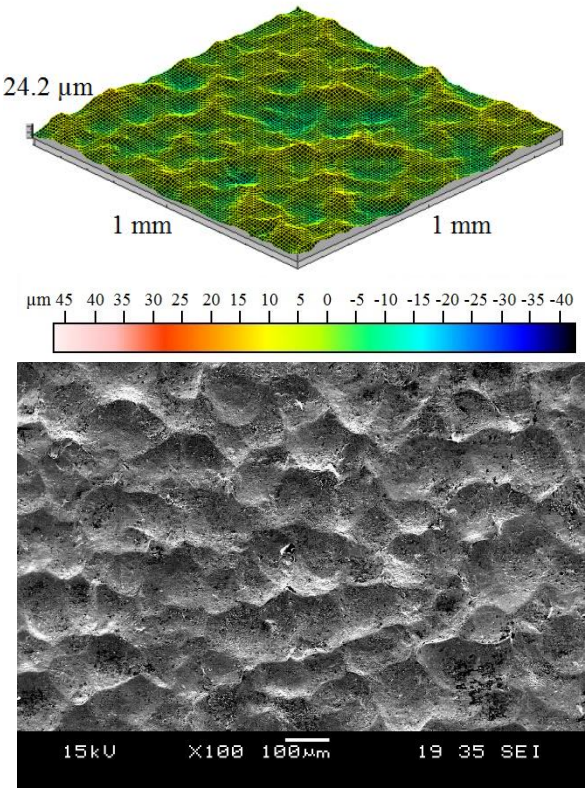

(b) DP-20-20

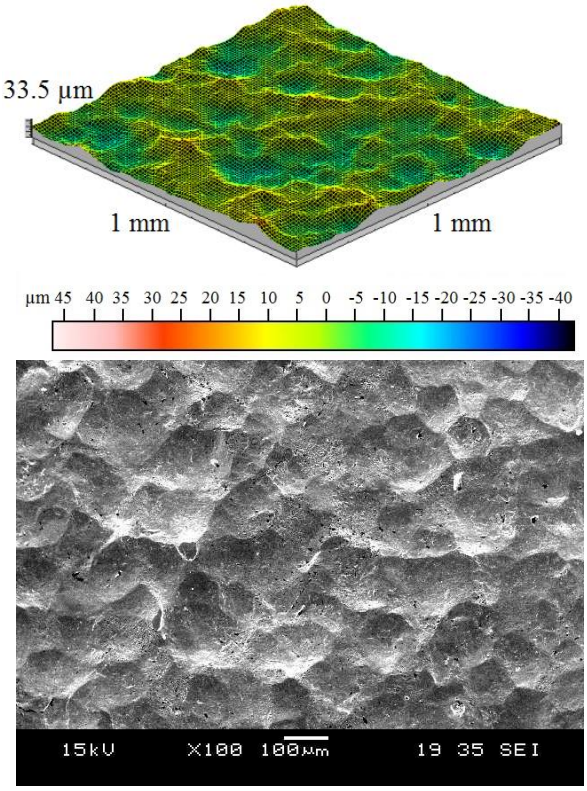

(c) DP-30-20

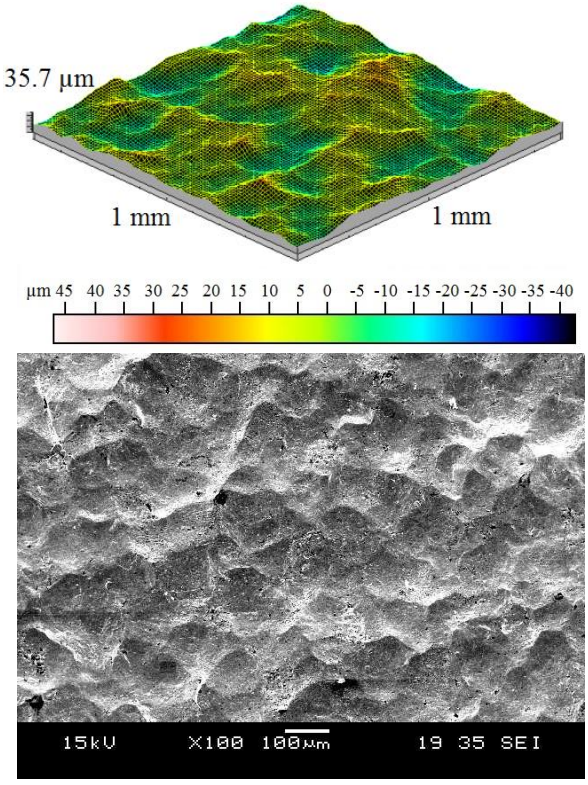

(d) DP-40-20

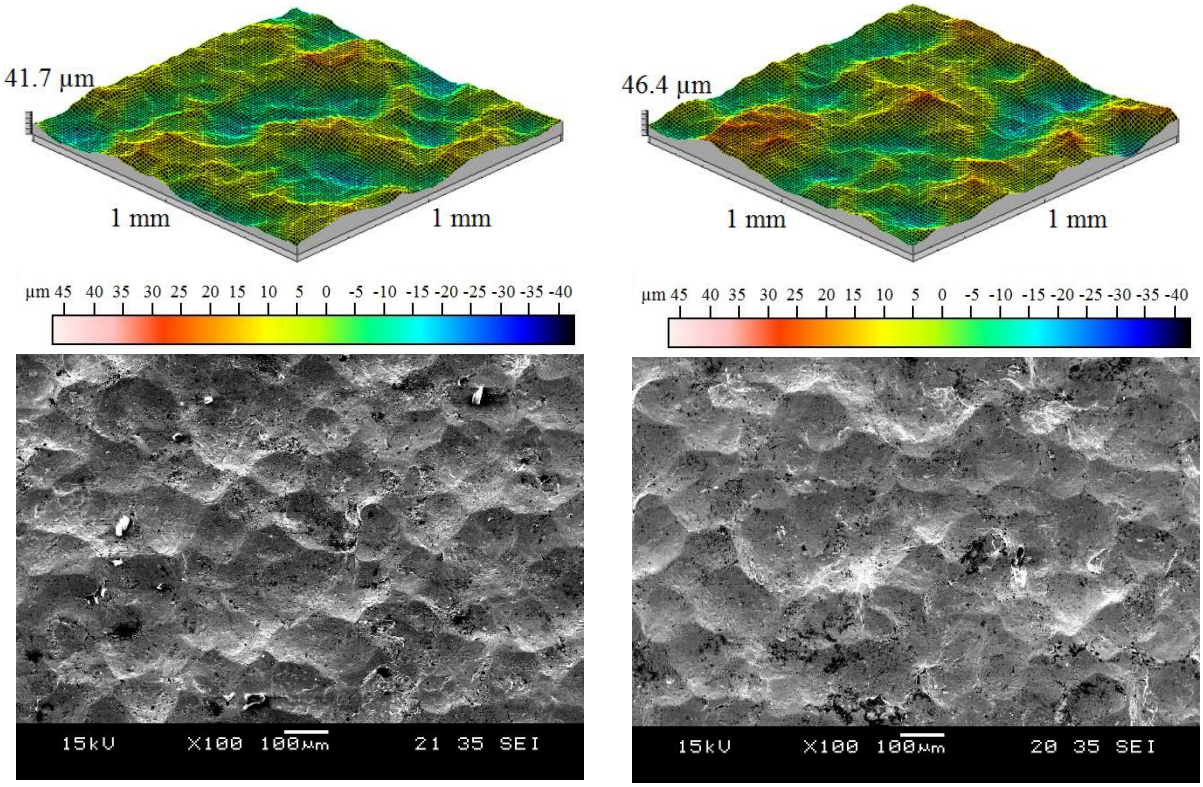

(e) DP-50-20 (f) DP-60-20

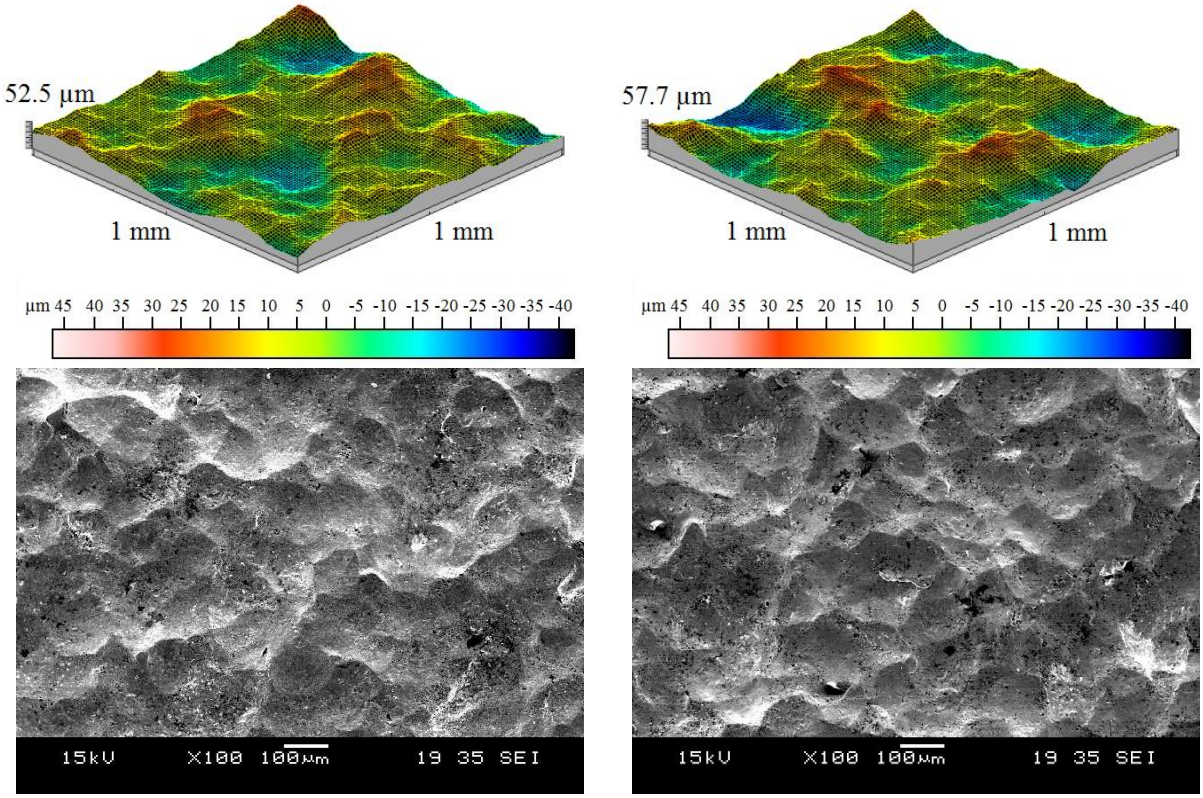

(g) DP-70-20 (h) DP-80-20

Figure 3-7. Surface topographies (above) and morphologies (below) of the shot peened AISI 4340 steel samples treated by the double shot peening process: (a) DP-10-20, (b) DP-20-20, (c) DP-30-20, (d) DP-40-20, (e)DP-50-20, (f) DP-60-20, (g) DP-70-20 and (h) DP-80-20.

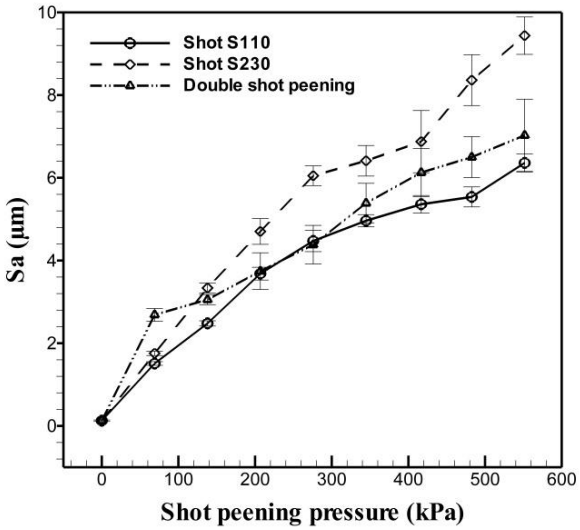

(a) S_a

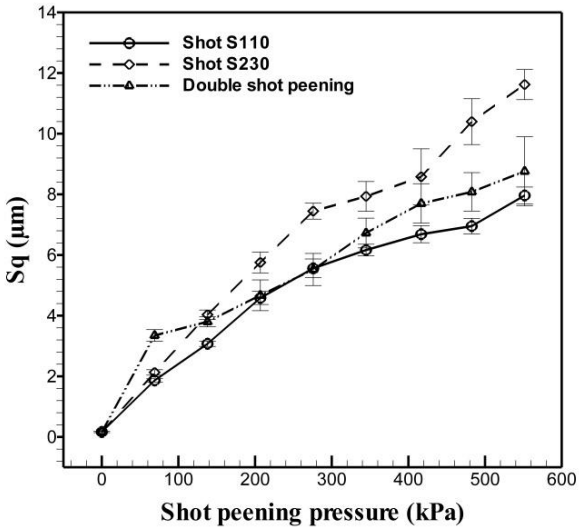

(b) S_q

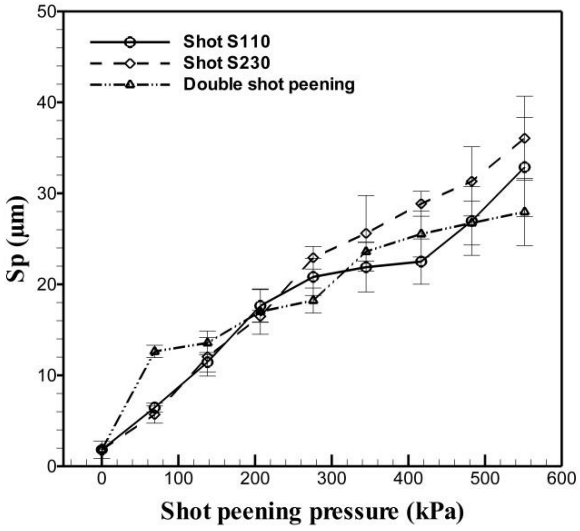

(c) S_p

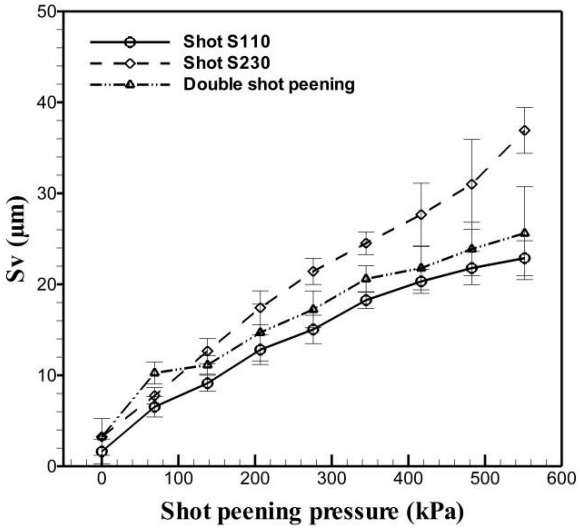

(d) S_v

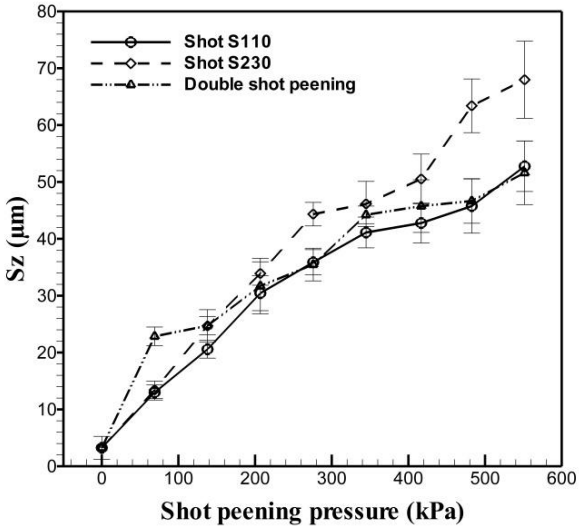

(e) S_z

Figure 3-8. (a) S_a, (b) S_q, (c) S_p, (d) S_v and (e) S_z parameters of the shot peened AISI 4340 steel samples as a function of shot peening pressure.

Figure 3-8 shows the areal roughness parameters for the shot peened AISI 4340 steel samples under different shot peening conditions. The average areal roughness as denoted by S_a and S_q show an increase in roughness with increasing shot peening pressure and the media size (figures 3-8*a* and *b*). A stronger trend is observed with a larger shot size which produces a maximum S_a value of approximately 10μm. The peak and valley components of the surface again follow a similar trend to that observed for S_a and S_q. The increase in S_p (figure 3-8*c*) and S_v (figure 3-8*d*) can be related to the impact of the shot on the surface which, with greater pressure, will cause the surface to deform to a greater depth (as represented by S_v) while at the same time, forcing the deformed material upwards (represented by S_p). As S_z is the sum of S_p and S_v, a similar trend is observed as is the case for S_v, which can be considered an average S_z value for the surface (figure 3-8*e*). What can be observed is that, by using double shot peening, the overall roughness is reduced when using a second peening stage with a smaller shot size.

The cross-sectional microstructures of the shot peened AISI 4340 steel samples under different conditions are shown in figure 3-9. After etching with 4% nital and 2% picral (in equal parts), the ferrite (α) grain in white, and the pearlite in black, are visible. In the microstructure of the as-received sample presented in figures 9*a* and *b*, the sizes of the ferrite grain are relatively even with a mean diameter of 3 μm. The results show that the sizes of ferrite grains become smaller with increased shot peening pressure or media size (figures 3-9*c*-*f*).

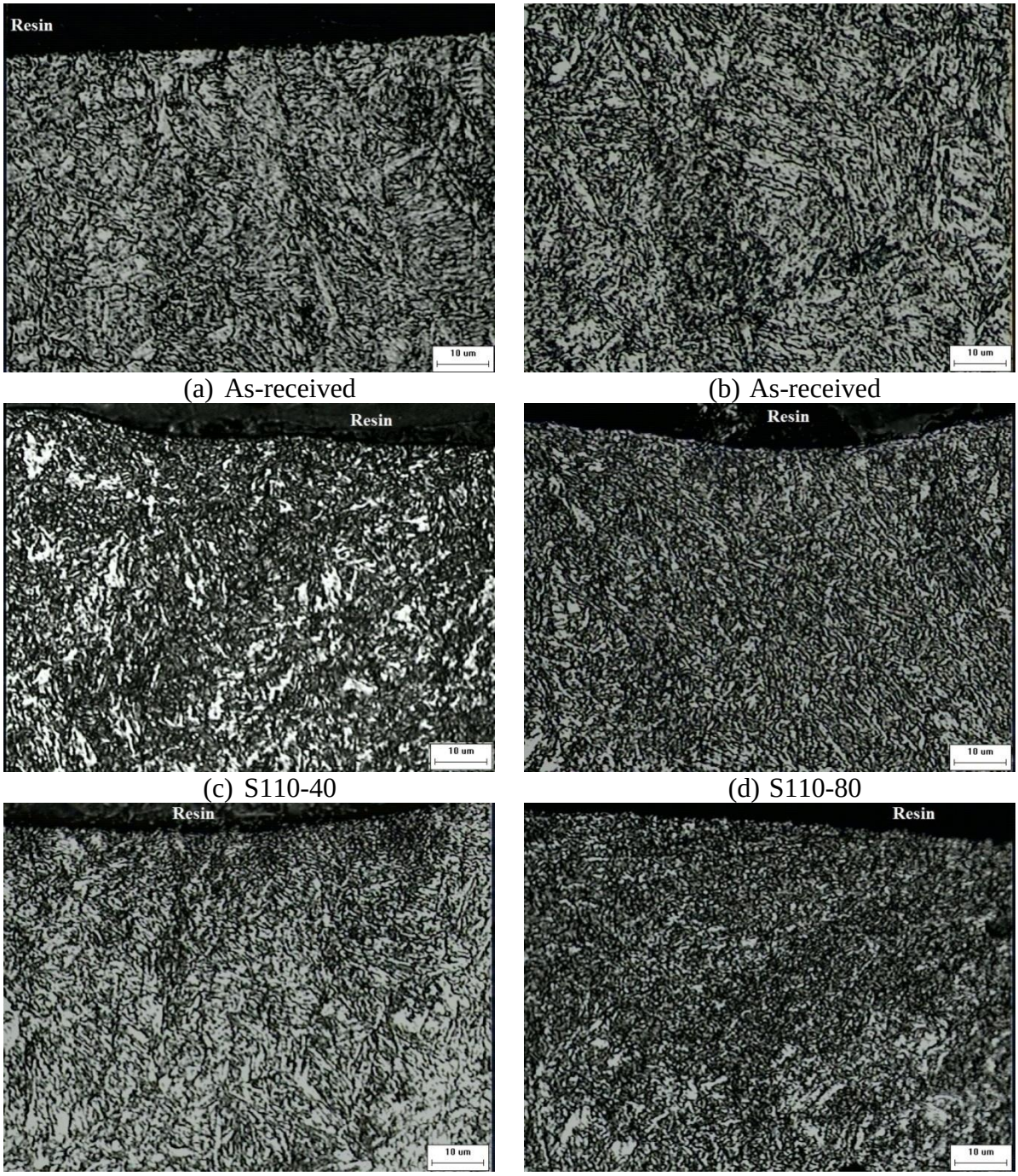

(a) As-received (b) As-received

(c) S110-40 (d) S110-80

(e) S230-40 (f) S230-80

Figure 3-9. Cross-sectional microstructures of the shot peened AISI 4340 steel samples under different shot peening conditions: (a) As-received, (b) Coarse-grained interior, (c) S110-40, (d) S110-80, (e) S230-40 and (f) S230-80.

Figure 3-10 presents the surface hardness of the AISI 4340 steel samples under different shot peening conditions. Due to the cold work hardening caused by the shot peening process, the surface hardness of the steel is higher after the treatment. The hardness of as-

received sample is about 3.12 ± 0.08 GPa, while the hardness of the steels after shot peening with S110, S230 steel shots and double shot peening under the pressure of 551.6 kPa are 3.92 ± 0.25, 4.11 ± 0.25 and 4.13 ± 0.22 GPa, respectively.

Shot peening treatment causes plastic deformation on the sample through the surface impact of the shot. The deformation depths induced by the media S110, S230, double shot peening at different pressures vary. Due to the cold work hardening occurring on the surface and the subsurface of the shot peened samples, the hardness reaches the largest value on the surface and gradually reduces with depth (figure 3-11). The hardness of samples S230-80, S230-40, S110-80, and S110-40 are 4.31 ± 0.11, 3.79 ± 0.15, 4.04 ± 0.16 and 3.54 ± 0.18 GPa on the surface and reduce to about 3.09 ± 0.20 GPa after 300 μm, respectively.

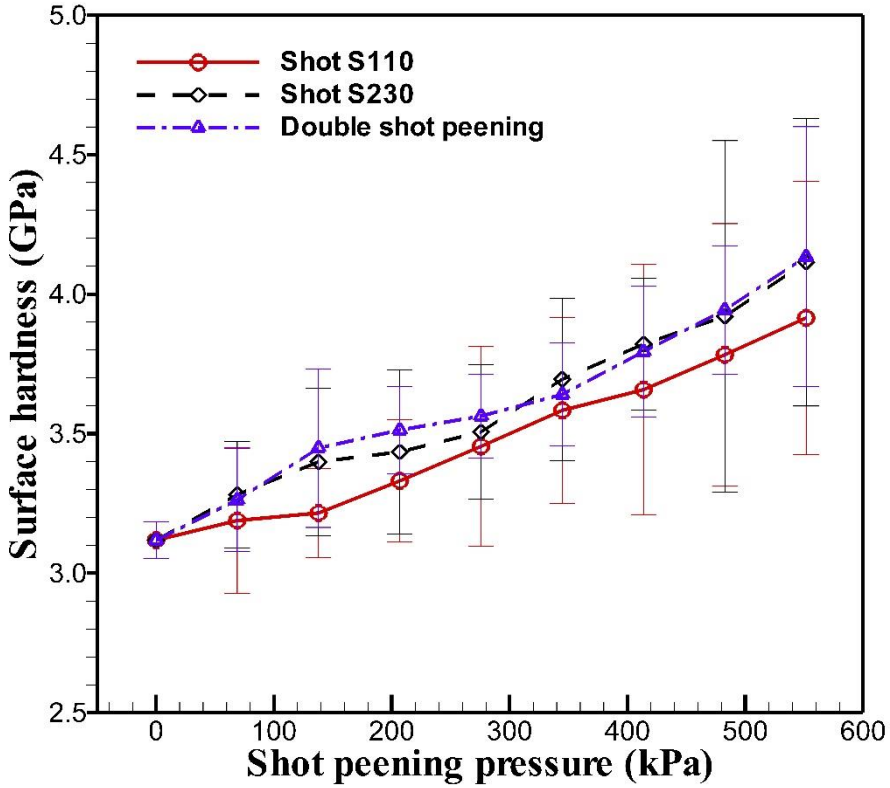

Figure 3-10. The surface hardness of the shot peened AISI 4340 steel samples under different shot peening conditions as a function of shot peening pressure.

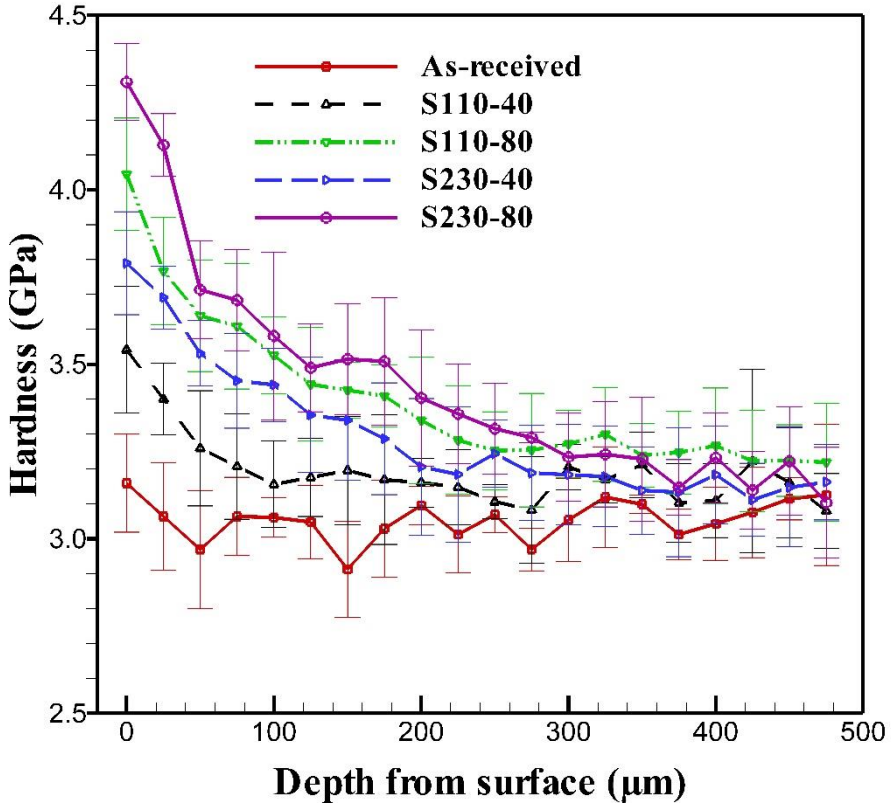

Figure 3-11. Cross-sectional hardness variations of the shot peened samples as a function of depth from the surface.

Figure 3-12 shows the friction coefficients of the as-received and the shot peened AISI 4340 steel samples under different conditions tested against a 100Cr6 steel ball in dry conditions. It is clear that the higher shot peening pressure results in a higher friction coefficient, from 0.47 of the as-received sample to 0.51, 0.55 and 0.52 of S110-80, S230-80, and DP-80-20 samples, respectively. Figure 3-12 also indicates that the shot peening with the larger shots (S230) results in, the higher friction coefficients for all the shot peening pressures. Besides, the second shot peening process (S110 with 137.9 kPa) can reduce the friction coefficients on the surface of the shot peened samples caused by the first shot peening process (by shot S230). The results also indicate that the rougher surface of the shot peened samples results in the higher friction through mechanical interlocking between two rubbing surfaces so that the friction of the shot peened steels under different conditions with

increased shot peening pressure can be correlated to the significant increase in their surface roughness (figure 3-8).

The friction coefficients of the shot peened steel AISI 4340 steel samples at different treatment conditions tested against 100Cr6 steel ball under 5 N in a dry condition as a function of the number of laps are displayed in figure 3-13. The as-received sample and the sample S230-80 display the lowest and highest friction coefficients respectively during the whole sliding test. The friction coefficient of all samples increases with increased laps for first 5000 laps (also called running-in period) due to the increased removal of asperities rubbing surfaces and then stabilize during the prolonged sliding [76, 84-87].

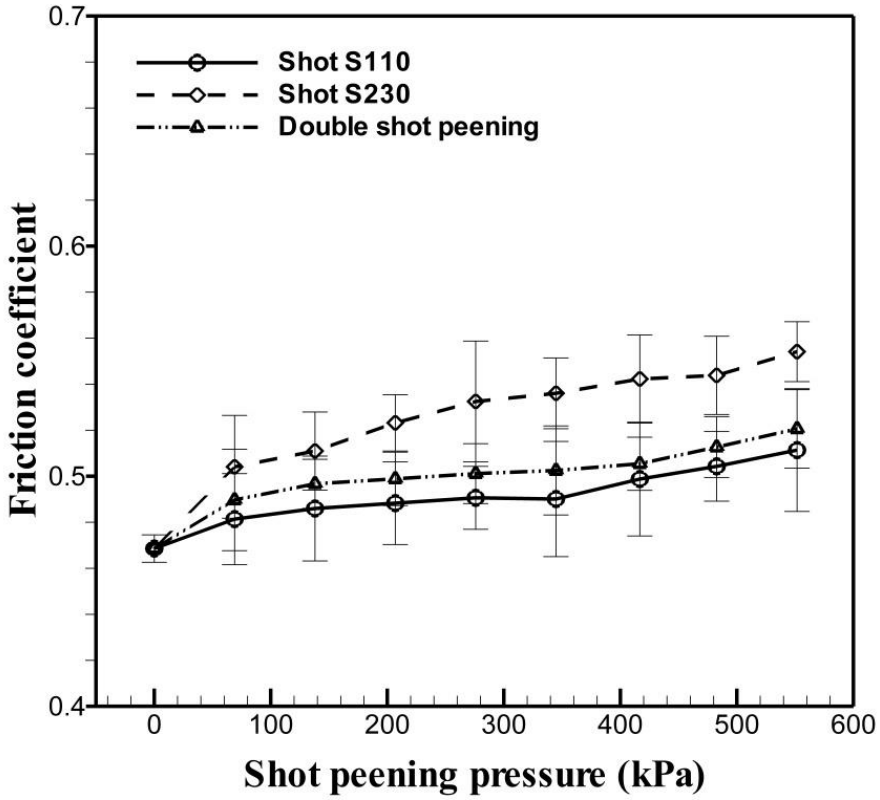

Figure 3-12. The friction coefficient of the shot peened AISI 4340 steel samples under different shot peening conditions as a function of shot peening pressure.

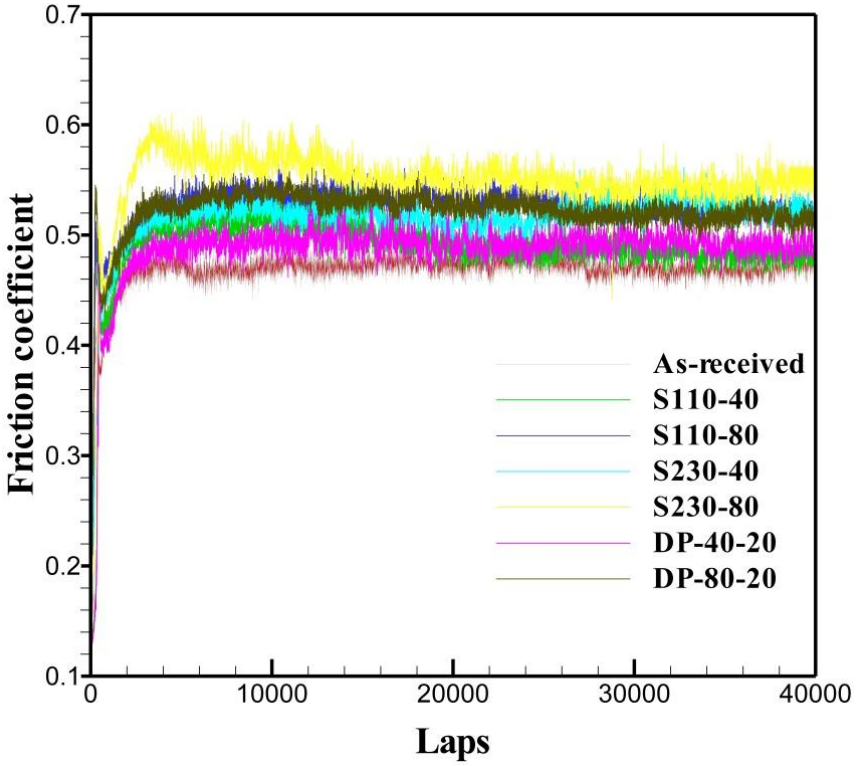

Figure 3-13. Friction coefficients of the shot peened AISI 4340 steel samples tested against a 100Cr6 steel ball under different shot peening conditions as a function of a number of laps.

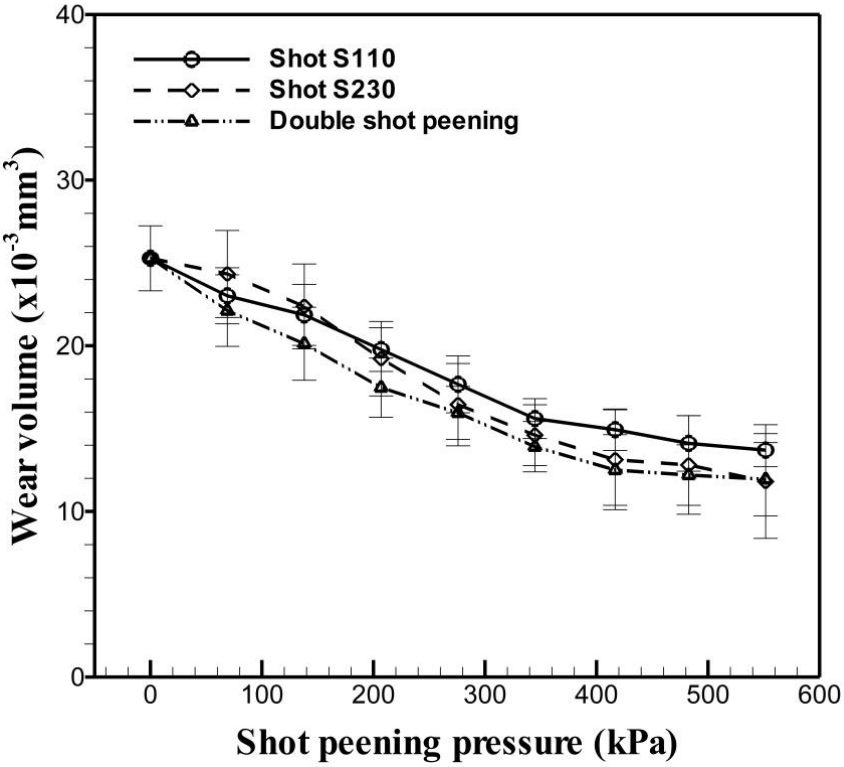

Figure 3-14. Wear volume of the shot peened AISI 4340 steel samples tested against a 100Cr6 steel ball under different shot peening conditions as a function of shot peening pressure.

Figure 3-14 presents the wear volume of the as-received, and the shot peened steel samples under different conditions as a function of the shot peening pressure. The wear volume of the as-received sample is about $25.3 \pm 1.9 \times 10^{-3}$ mm^3. Under the dry condition, due to the increased wear resistance associated with their higher hardness [76], the wear volume reduces gradually with the increasing of pressure in all tested conditions with media S110, S230, and double shot peening. Besides, at the low pressure (68.9 kPa and 137.9 kPa) the smaller shot size (S110) gives the better wear resistance, but the samples have a lower wear volume in the case of larger shot sizes when the pressure treatment is higher than 206.8 kPa. The reason is that the shot peened samples treated by media S230 do not achieve full coverage under the shot pressure at 68.9 kPa and 137.9 kPa (figures 5*a* and *b*). Figure 3-14 also indicates that second shot peening is a beneficial process to reduce the wear volume for the shot peened samples which were first treated by the shot S230 in all of the tests.

The wear topographies and morphologies of the as-received and shot peened AISI 4340 steel samples under different shot peening conditions are exhibited in figure 3-15. The as-received sample tested against the 100Cr6 steel ball has a larger wear track on the surface compared to those of the shot peened samples indicating that the latter have higher wear resistance. It is also clear that some dimples induced by the shot peening process are still visible on the wear track (figures 3-15*c*, *d*, *e* and *g*). It reveals that the dimples caused by the shot peening process at the high pressure are even deeper than the wear depth attributed to the sliding ball on the surface.

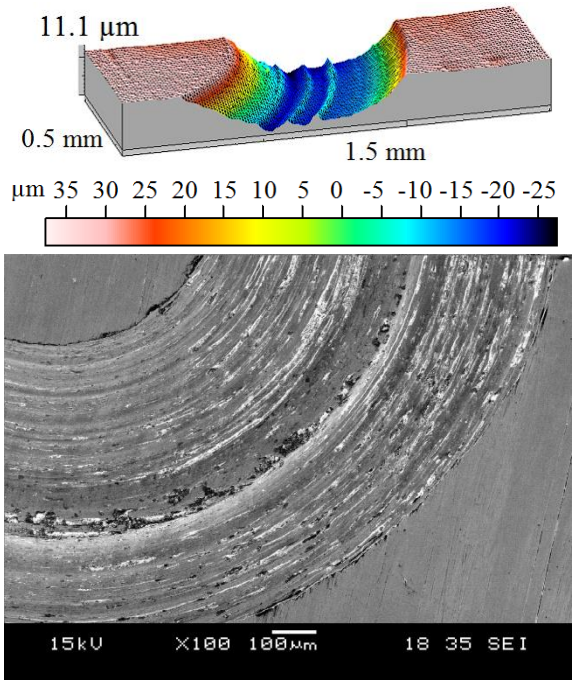

(a) As-received

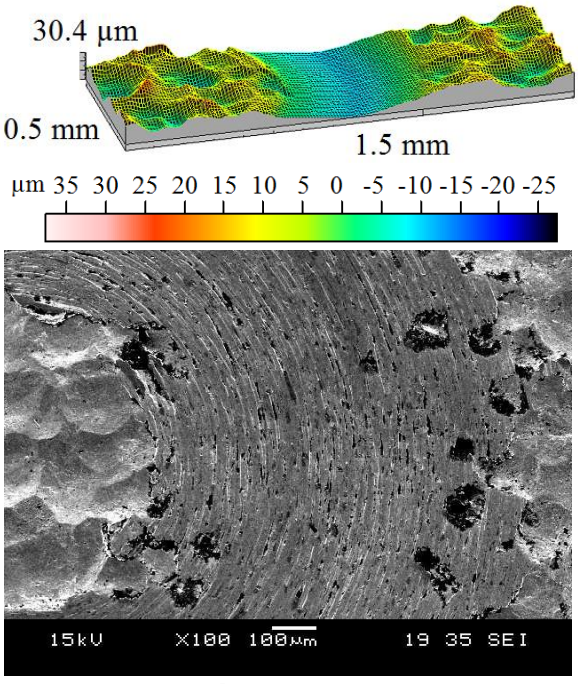

(b) S110-40

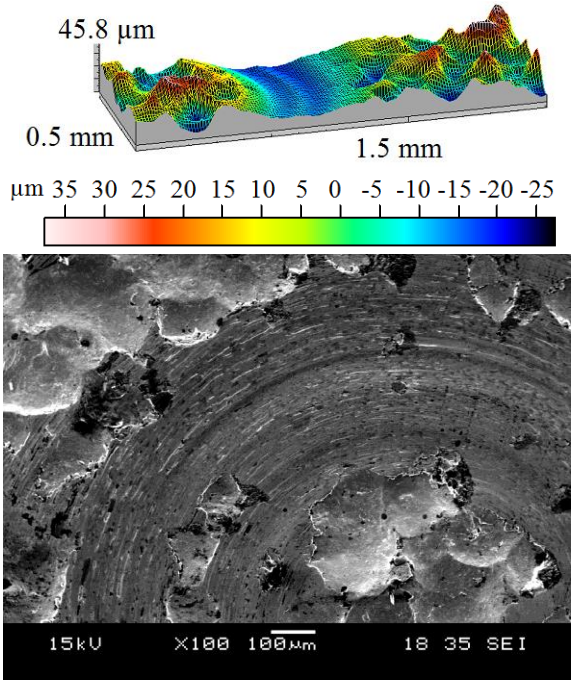

(c) S110-80

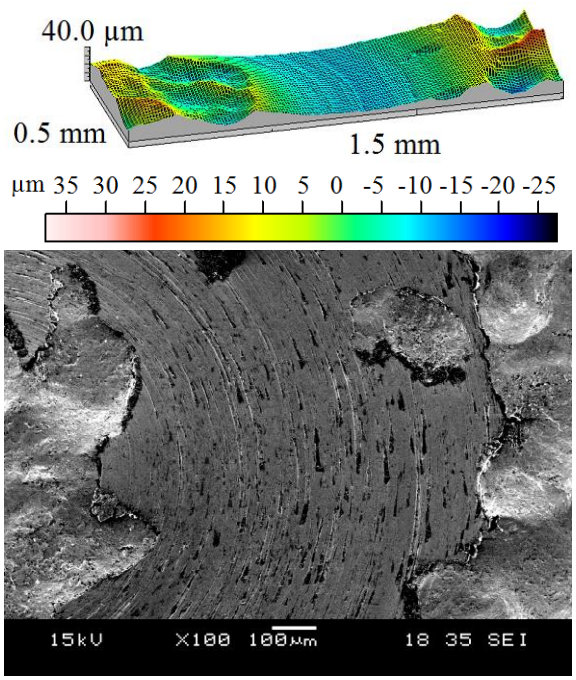

(d) S230-40

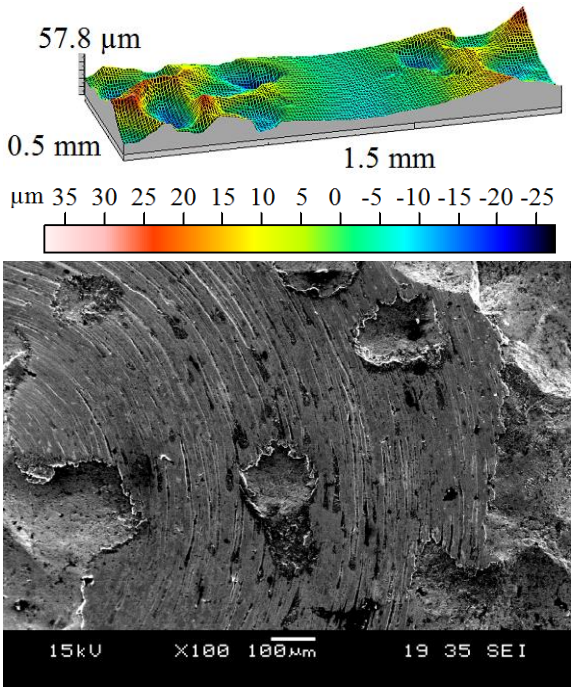

(e) S230-80

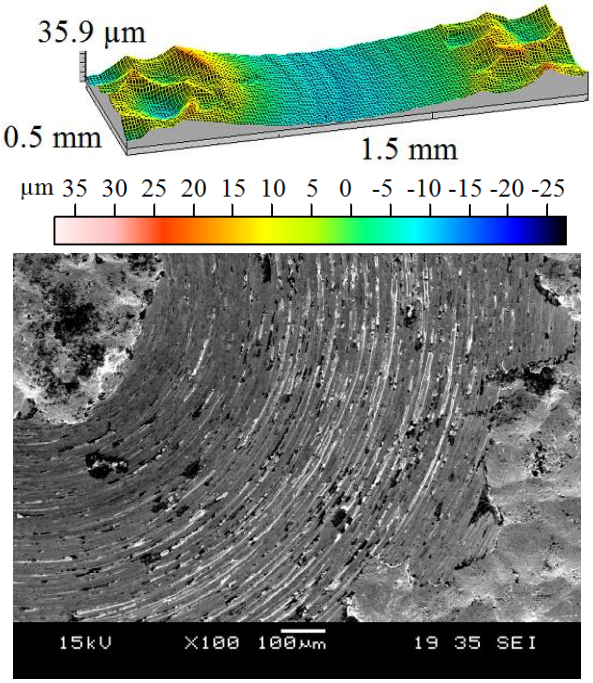

(f) DP-40-20

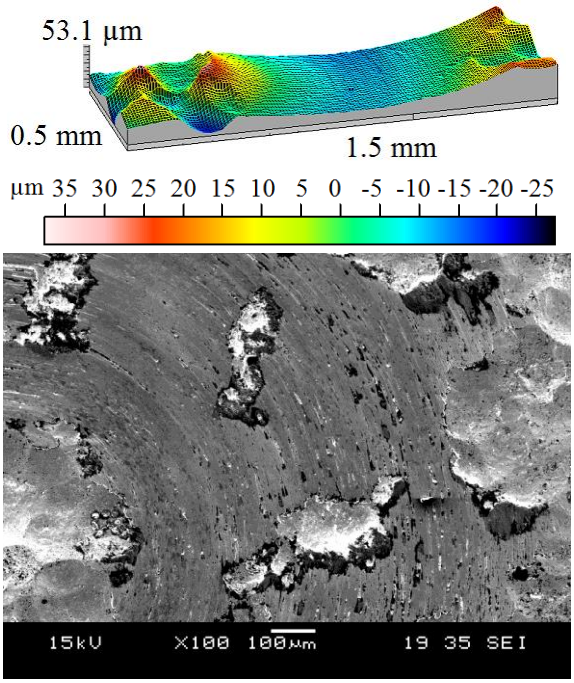

(g) DP-80-20

Figure 3-15. Wear topographies and morphologies of the shot peened samples: (a) As-received, (b) S110-40, (c) S110-80, (d) S230-40, (e) S230-80, (f) DP-40-20 and (g) DP-80-20.

Figures 3-16*a* and *b* show the wear morphologies of the 100Cr6 steel balls rubbed on the surfaces of the as-received sample and S230-80 sample, respectively. The larger wear

scar is found on the 100Cr6 steel ball slid on the treated sample. It indicates that the higher hardness and higher roughness of the shot peened sample are responsible for the much higher wear of its counter 100Cr6 steel ball.

In general, the above results show that the shot peening is a comprehensive process with a lot of operating parameters. These parameters include shot flow rate, shot velocity, impact angle, pressure of nozzle, distance from nozzle to workpiece (see figure 2-2), etc. Among these parameters, shot pressure and media size are importance because they can control the intensity and coverage are easily. The results in Chapter 3 reveals that shot pressure and media size have significant effects on the microstructure, mechanical and tribological properties of the low alloy steel. The details of the conclusion are presented in the next section.

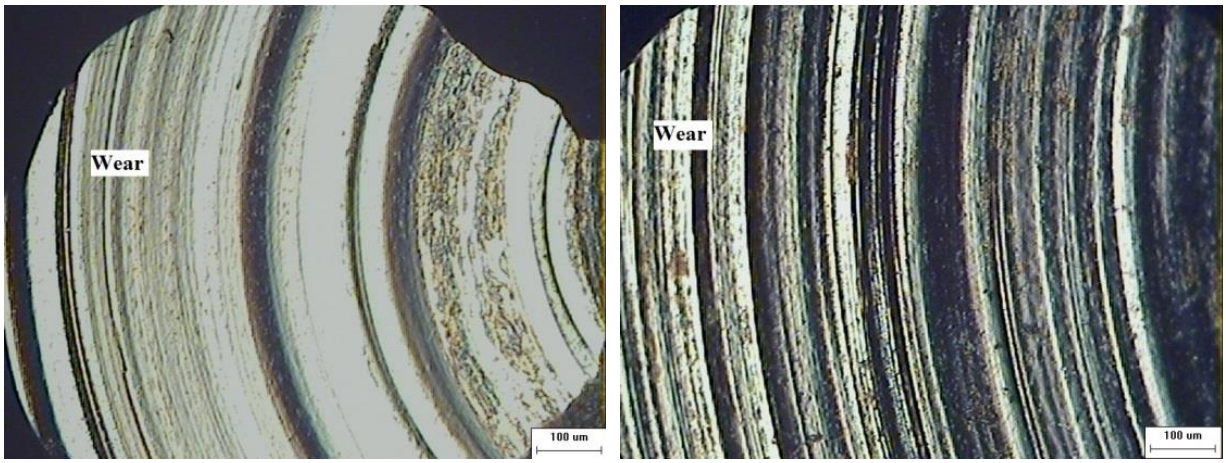

(a) (b)

Figure 3-16. Wear morphologies of 100Cr6 steel balls slid on AISI 4340 steel samples: (a) As-received and S230-80 sample.

3.4. Conclusion

The microstructure, mechanical and tribological properties of the shot peened AISI 4340 low alloy steel under different shot peening conditions were systematically investigated. The following conclusions can be drawn from the obtained results:

- Under the same nozzle pressure, the smaller S110 steel shots have higher velocities but smaller dynamic energies which result in lower measured intensities compared with S230 steel shots.
- In the case of low shot peening pressure of 68.9 kPa and 137.9 kPa, the shot peened samples cannot achieve full coverage with S230 steel shots but can with S110 steel shots. The coverage is full when the shot peening pressure is higher than 206.8 kPa for S230 steel shots.
- The hardness of the shot peened sample increases with the increasing shot pressure and media size due to higher cold working.
- The surface roughness of the shot peened sample increases with the increase in shot pressure and media size. It indicates that the steel shots with higher velocities (dynamic energies) and larger size form the deeper and wider dimples on the target material.
- The shot peening process influences the microstructure of shot peened steels by reducing the grain size on the sub-surface depth of influence.
- The increased shot peening pressure and media size result in increasing the friction coefficient but decreasing the wear volume of the shot peened samples due to the significant influences of their surface roughness and surface hardness.
- The larger wear scar found on the 100Cr6 steel ball rubbed on the rougher and harder shot peened sample.
- The double shot peening process not only reduces the surface roughness but also improves the tribological properties of the shot peened material.

Chapter 4: Investigation of the properties of conventional and severe shot peened low alloy steel

4.1 Introduction

Recently, ultrafine grain (nm in size) materials have attracted significant interest from both industry and academia for their high mechanical performance [7, 9, 10]. Surface properties have an important influence on the failure of engineering parts, for example in fatigue fracture, fretting fatigue, wear, and corrosion, etc [7]. Therefore, in many applications, it is recommended that it is not necessary to make entire components by ultrafine grain materials [7]. Thus, the material with ultrafine grain on the subsurface close to the surface is supposed to significantly improve the surface properties of the specimen without changing its chemical composition and shape [7, 9]. In order to create an ultrafine grain material, an aggressive form of shot peening is required with much higher intensity and coverage. This process is known as severe shot peening (SSP) and has been successfully used to generate the ultrafine grain layers on a variety of materials, including pure materials, alloys, and intermetallic compounds [7]. It also worth to note that at high intensity, severe shot peening process induces both high magnitude of compressive residual stresses as well as generate the ultrafine grain layer on the surface. However, the surface roughness of the severe shot peened target material is relatively high, which is considered as a negative side effect of this process. To improve the surface finish of the severe shot peened component, a secondary shot peening process with a smaller shot size media and a low intensity should be employed. This process is called as re-severe shot peening (or also named double severe shot peening).

Singh et al. [88] reported that the wear volume loss of quenched and tempered SAE 6150 steel could be reduced by employing the shot peening process. Mitrovic et al.[89] proved that both shot peened 36CrNiMo4 and 36NiCrMo16 alloy steel showed an improved wear resistance under dry and lubricated contact condition tests. Matsui et al. [90] investigated the tribological performance of steel under the dry rolling/sliding contact conditions and found that the samples with pre-shot peening treatment exhibited an improved wear resistance. The wear performance of AISI 1017 steel after severe shot peening was studied by Unal et al. [91]. This results suggest that the hardness and stiffness of the sample surface and wear durability were enhanced with the increasing shot peening [91].

In this chapter, heat-treated AISI 4340 low alloy steel samples were shot peened under conventional and severe conditions to investigate their mechanical and tribological properties. The hardness distribution against the depth from the surface of the shot peened components was evaluated by using a nanoindentor and their frictional and wear properties were studied using a ball-on-disc micro-tribological experiments.

4.2 Materials and methods

In this study, AISI 4340 steel was used as the material for all experiments. The nominal chemical composition of the AISI 4340 low alloy steel (weight %) is composed of C (~0.34), Si (~0.24), Mn (~0.51), Cr (~0.91) Ni (~1.54) and Mo (~0.25). The steel was heat treated at 815^{o}C, quenching in oil at ~20^{o}C, and followed by tempering at the temperature of ~230^{o}C for 2 hours.

Table 4-1. Shot peening parameter conditions used in chapter 4.

Specimen	**Almen intensity**	**Shot size**	**Coverage**	**Peening times**	**Pressure**
Conventional shot peening 1 (CSP1)	10A	S230 (ϕ600 μm)	120 %	150 s	200 kPa
Conventional shot peening 2 (CSP2)	12A	S230 (ϕ600 μm)	120 %	150 s	350 kPa
Severe shot peening (SSP)	24A	S230 (ϕ600 μm)	1200 %	1500 s	620 kPa
Re-Severe shot peening (Re-SSP)	24A	S230 (ϕ600 μm)	120 %	1500 s	620 kPa
	10 A	S110 (ϕ300 μm)	120 %	150 s	270 kPa
As-received	NA	NA	NA	NA	NA

The samples were then mounted on the fixture and shot peened under different conditions, as listed in table 4-1. To achieve a coverage of 120%, the specimen was shot peened in 150 seconds. Therefore, the peening time to obtain the coverage of 1200% is 1500s. The media employed in this research were S230, and S110, the round high-quality steel shot, which are the common media used in industry.

4.3 Results and discussion

Figures 4-1*a* and *b* show the cross-sectional optical microstructure of the as-received steel sample observed at different magnifications. The micrograph shows a 20 μm thick iron oxide layer due to heat-treated process. This iron oxide layer results in poor mechanical properties which are not useful in mechanical components. Therefore, the formation of this iron oxide layer in important mechanical parts is prevented by using vacuum furnace during heat treatment process or by conducting a polishing process after heat treatment. The normal mean grain size of the as-received sample measured by the optical microscope is about 10μm. Figures 4-1*c* and *d* present the cross-sectional microstructure of conventionally shot peened

sample 2 (CSP2) observed at different magnifications. The iron oxide layer is partly removed from the surface of the conventional shot peened sample (figure 4-1*c*) and remained over a depth of about 3-5 μm. Under the plastic deformation formed by the shot peening process, the mean grain size of the second layer over a depth of 100 – 150 μm is reduced to about 5μm (see figure 4-1*d*). The result demonstrates that shot peening is a good process to remove the iron oxide layer from the surface. Figures 4-1*e* and *f* show the cross-sectional microstructure of a severe shot peened (SSP) sample observed be specific magnifications. It can be clearly seen that the iron oxide layer is totally removed by the high energy impacted from the shots in the severe plastic deformation condition (figures 4-1*e* and *f*). There are three different grain size layers formed on the cross-sectional microstructure of the severe shot peened sample. The first layer with the ultrafine grain size, which cannot be discerned by the normal optical microstructure equipment, appears on the top surface of the shot peened steel sample. The depth of zone is about 20 μm, which is generated by receiving very high strain from the shot caused by severe plastic deformation. The next layer with a small grain size of approximately 2μm has the depth of 150 μm (measured by the optical microscope). This layer also underwent the high strain process. Therefore, the grain size of this layer was reduced to be smaller than the original grain size. The last layer is original grain size with the mean of grain size of about 10μm, where the effect of deformation caused by impacts is reduced significantly.

Hardness tests were performed using an Agilent G200 Nanoindenter. Figure 4-2*a* presents the microhardness distribution along the depth from the surface of the sample. During the heat treatment process in the normal furnace, elemental carbon is depleted from the surface over a depth of 300-500 μm, and the quantity of amount of escaped carbon reduces from the surface into inside material [92, 93]. This phenomenon caused a reduction

in the hardness of heat-treated sample at the surface and near surface layer (up to 500 μm) [92, 93].

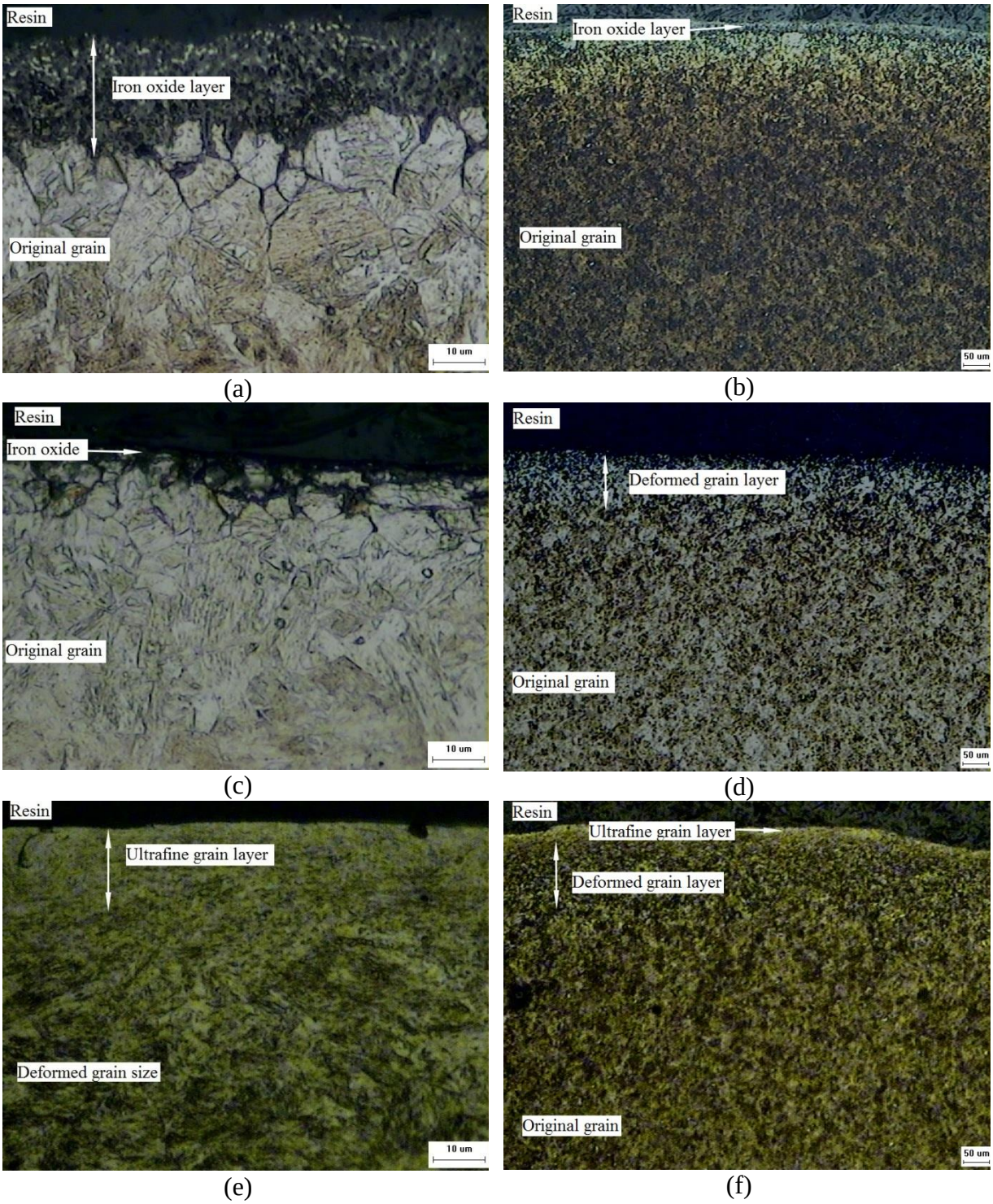

Figure 4-1. Cross-sectional microstructure of shot peened AISI 4340 steel at different magnifications: (a) and (b) as-received, (c) and (d) CSP2 sample, (e) and (f) SSP sample.

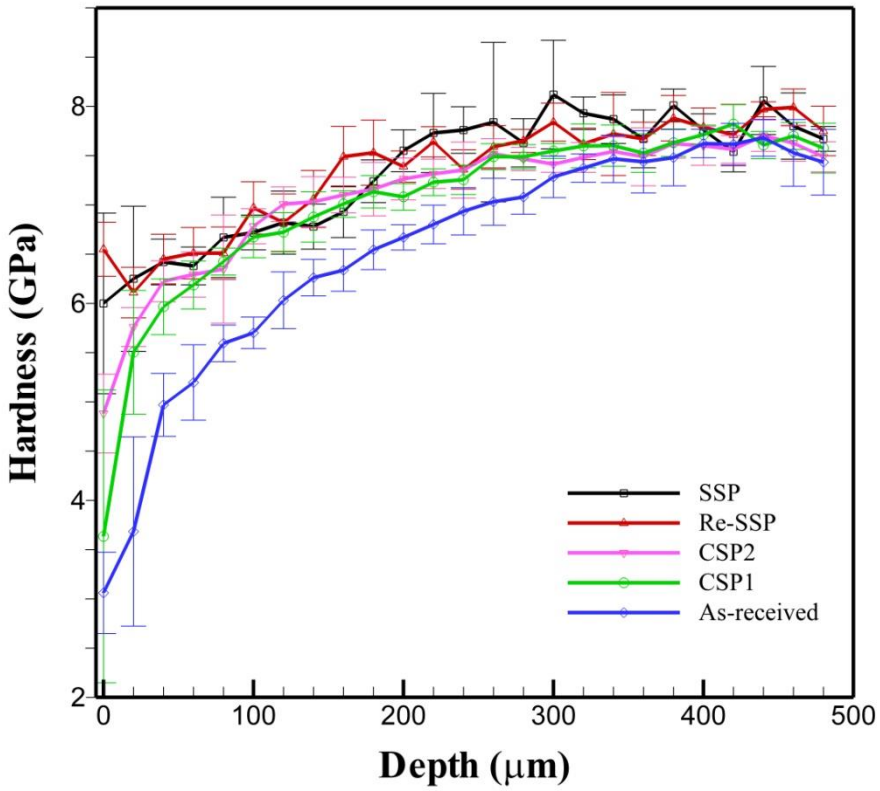

(a)

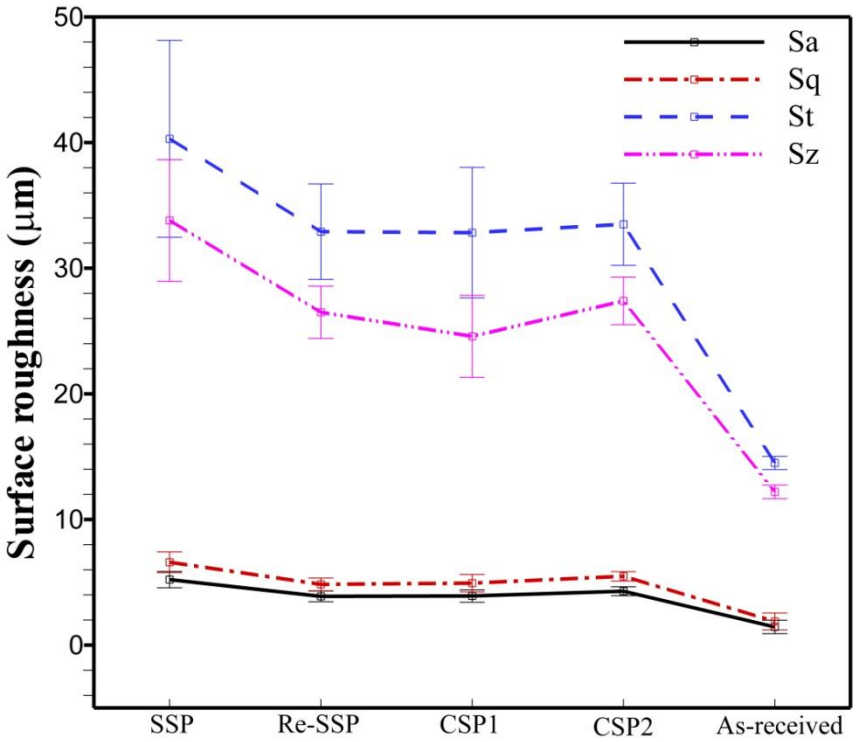

(b)

Figure 4-2. (a) Micro-hardness distribution along the depth from the surface of the sample and (b) Surface roughness of AISI 4340 steel after undergoing different shot peening conditions.

The shot peening process induced the plastic deformation on the surface of the target causing work hardening on these peened samples. It is also clearly seen that comparing with the as-received specimen, the near-surface hardness of SSP, Re-SSP, CSP1, CSP2 samples have increased. The hardness of the surface layer of Re-SSP, SSP, CSP1, CSP2, as-received samples is 6.5, 6.0, 4.8, 3.7 and 3.1 GPa, respectively. The difference in hardness profile between the severe and conventional shot peening condition occurs in about 50 μm from the surface, where the ultrafine grain is formed in the severe shot peened sample due to the high deformation process.

The surface roughness of the samples was measured using a surface profilometer (Taylor Hobson®, Talyscan 150). In figure 4-2*b*, the measured areal arithmetic average (S_a), root mean squared (S_q) surface roughness, the maximum height of surface (S_t) and the average distance between the five highest peak and five lowest valleys (S_z) values of the treated AISI 4340 samples are remarkably larger than those of the as-received sample. The difference between treated samples and as-received sample are more clearly in the case of S_t and S_z values because these values are sensitive to the height of peaks and depths valleys caused by shots. It also can be clearly seen that using a smaller shot after severe shot peening process can reduce the surface roughness in term of S_a, S_q, S_t and S_z values.

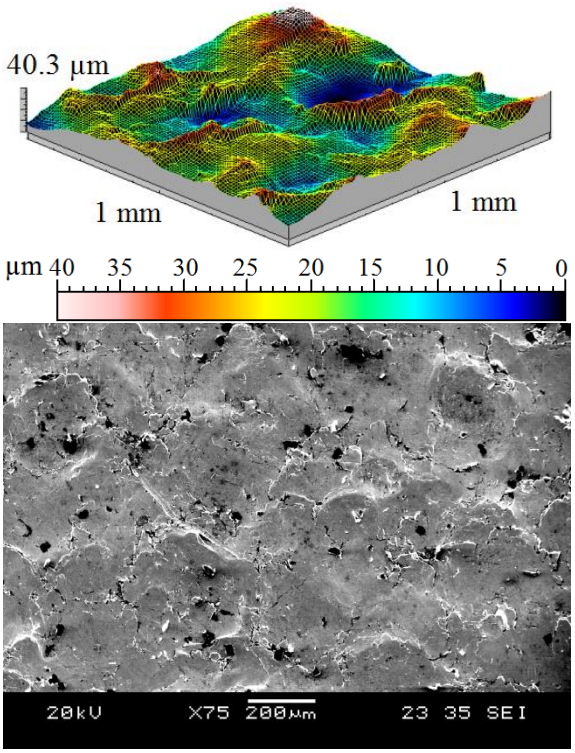
40.3 µm
1 mm
1 mm
µm 40 35 30 25 20 15 10 5 0
20kV X75 200µm 23 35 SEI

(a)

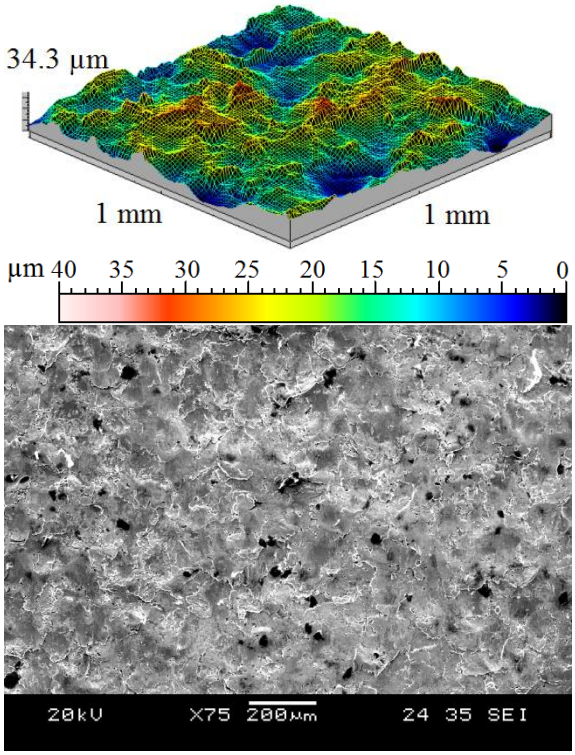
34.3 µm
1 mm
1 mm
µm 40 35 30 25 20 15 10 5 0
20kV X75 200µm 24 35 SEI

(b)

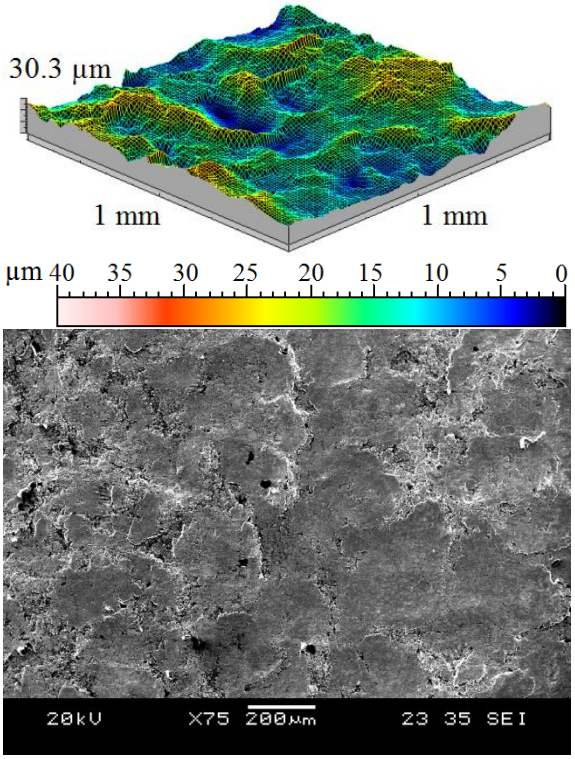
30.3 µm
1 mm
1 mm
µm 40 35 30 25 20 15 10 5 0
20kV X75 200µm 23 35 SEI

(c)

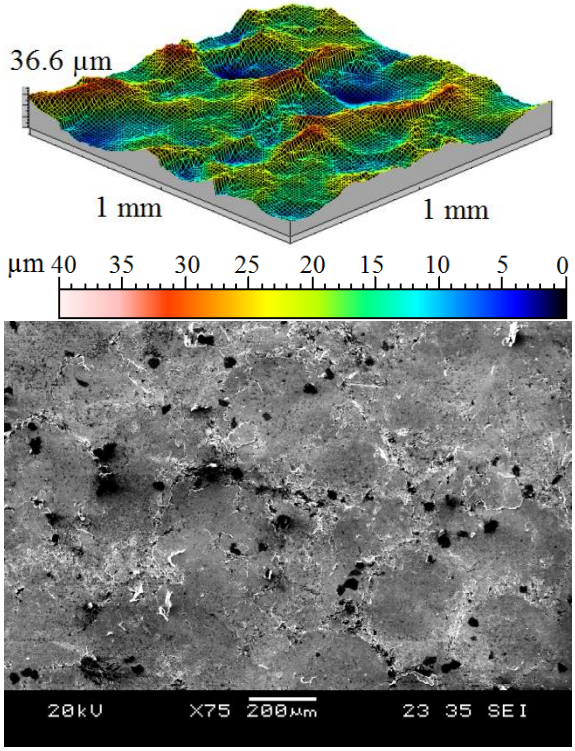
36.6 µm
1 mm
1 mm
µm 40 35 30 25 20 15 10 5 0
20kV X75 200µm 23 35 SEI

(d)

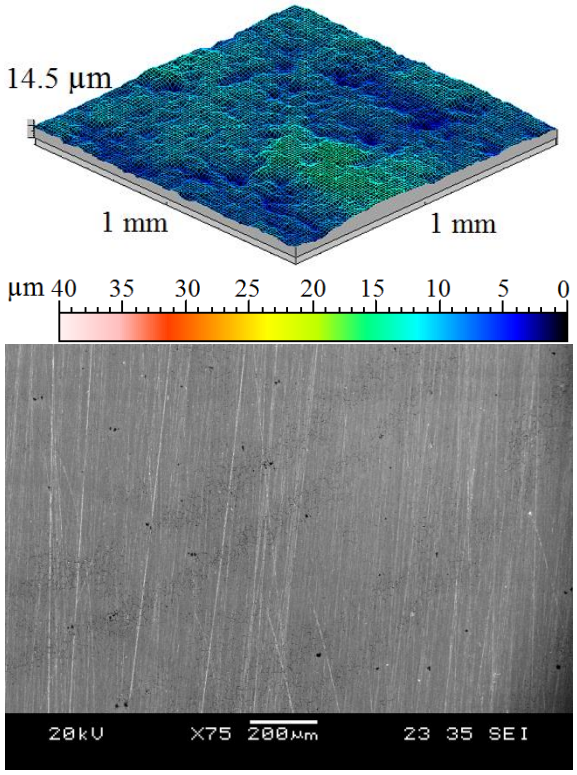

(e)

Figure 4-3. Surface morphologies and topographies: (a) SSP, (b) Re-SSP, (c) CSP1, (d) CSP2 and (e) as-received AISI 4340.

Figures 4-3*a-d* shows the surface morphology and topography of shot peened samples and figure 4-3*e* presents surface morphology and topography of the as-received sample. In figure 4-3*e*, the as-received sample has a relatively rough surface due to the formation of the iron oxide layer (caused by heat treatment process). Obvious dimples caused by the treatment appeared on the surface topographies of the peened sample as presented in figures 4-3*a-d*. The dimples become deeper, and the surfaces become rougher in the case of higher shot peening pressure [76]. It is also clearly seen that the re-severe shot peening process can make the surface topography smoother by reducing the height of the peaks after severe shot peening. This result is in agreement with the measured surfaces roughness of the treated topography in figure 4-2*b*.

The tribological properties of shot peened samples were investigated by the ball-on-disc micro-tribometer (CSM) machine. The sliding friction coefficient was measured by the

ratio of the friction force to the normal load on the pin. In this research, the pin stylus was kept stationary while the samples were mounted on the rotating disk. The tribological properties of the samples were studied by sliding against 100Cr6 steel balls (diameter of 6 mm) in a circular path (radius of 1.5 mm) for duration of 40000 laps with a sliding speed of 50 mm/s under a normal load of 5 N at room temperature (RT ~22 – 24^{o}C). During the sliding test, wear tracks were steadily made on the surface of the samples mounted on the rotating disc and on the surface of the top of the ball mounted on the stationary pin due to the material loss from friction/wear. The material removal can be associated with abrasive wear attributed to both two body and three body wear mechanisms. The average friction coefficient of each sample was obtained from three wear tests. Then, the width and the depth of wear tracks with surface profilometry were used to calculate the average wear volume (material loss) of each specimen. Figure 4-4*a* presents the friction coefficient between the shot peened samples against the 100Cr6 steel balls in the dry sliding wear tests. The results indicate that, compared with the as-received sample, the friction coefficient in the cases of conventional shot peened samples (CSP1, CSP2) slightly increases, while the values of SSP and Re-SSP samples are noticeably higher. The friction coefficients between the steel samples, i.e. SSP, Re-SSP, CSP1, CSP2, and as-received against the 100Cr6 steel balls are 0.53, 0.51, 0.47, 0.48 and 0.46, respectively. The possible reason is that the surface roughness plays an important role to raise a higher friction by mechanical interlocking between two rubbing surfaces [94, 95]. The results can show that the samples with higher surface roughness (figure 4-3 and figure 4-2*b*) exhibit a higher friction coefficient for all the tests. However, in the case of Re-SSP, the surface roughness value of Re-SSP sample is equal to that of CSP1 and smaller than that of CSP2, but the friction coefficient is still higher. As mentioned above, the ultrafine grain layers are formed on the surface and near-surface of the SSP sample and Re-SSP samples. This ultrafine grain layer has different properties compared with the original

grain size of the material [7]. Therefore, the highest friction coefficients in cases of Re-SSP come from the effect of this ultrafine grain layer. Figure 4-4*b* shows the friction coefficients of the shot peened steels against the steel ball under the load of 5N as a function of the number of laps. The friction coefficient increases gradually in the first 10,000 laps (also called running-in period) due to the increased wear of asperities rubbing surfaces [76, 84-87]. From 10,000 laps onwards, the tested samples exhibit a steady friction coefficient during the entire sliding test [76, 84-87].

Figure 4-5 illustrates the wear volume of the shot peened steel AISI 4340 samples under different peening conditions tested against the steel ball under a normal load of 5N. Wear volumes were calculated from the width and the depth of the wear track profiles. The wear track profile was measured after tested friction coefficient for 40000 laps by using a surface profilometer (Taylor Hobson®, Talyscan 150). It is clear that the decrease in the wear volume in the tested sample is probably due to the increased wear resistance associated with the corresponding increase surface hardness[76, 96]. It is further confirmed by considering the hardness distribution at the surfaces of these samples (see figure 4-2*a*). The highest hardness surface sample (Re-SSP) has the lowest wear volume of $8x10^{-3}mm^3$ and the lowest hardness surface sample (as-received) has the highest wear volume of $27x10^{-3}$ mm^3.

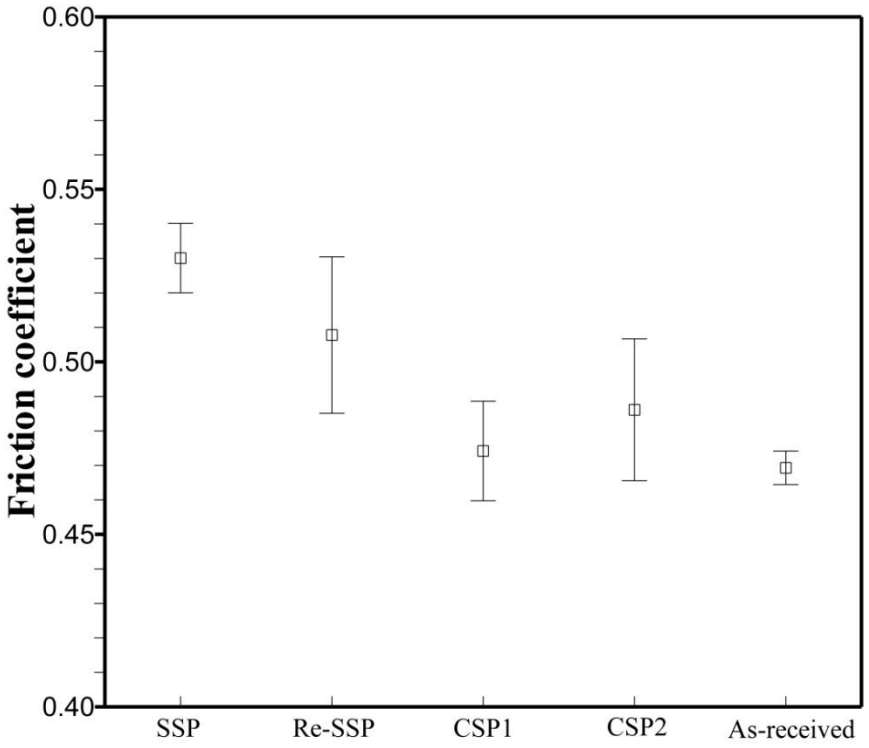

(a)

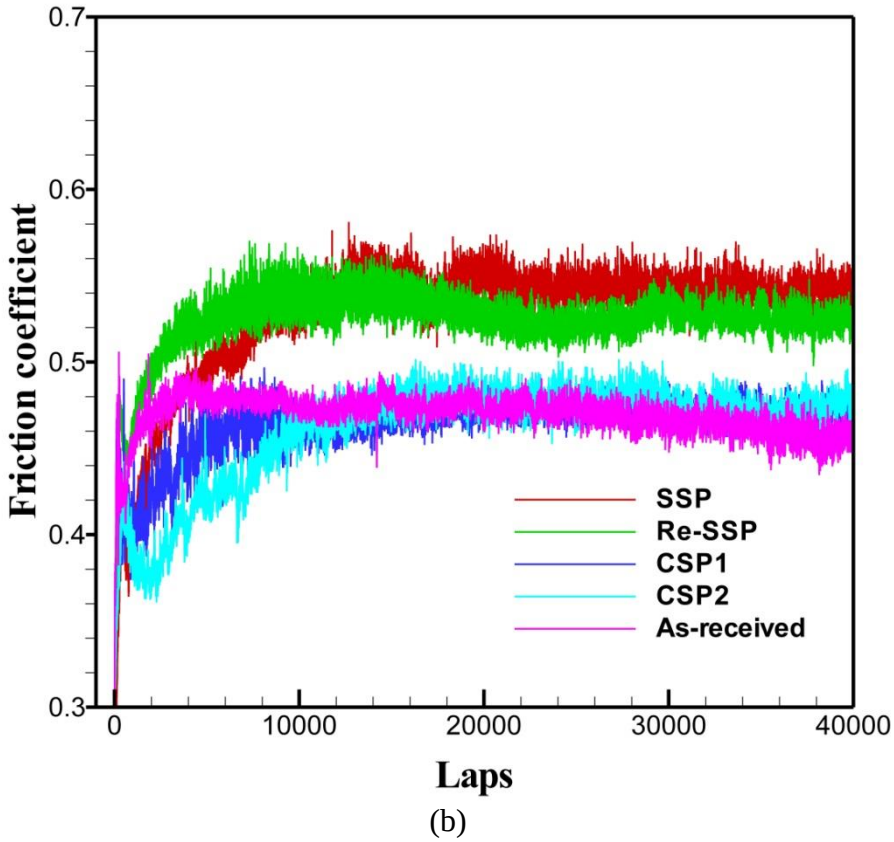

(b)

Figure 4-4. (a) The friction coefficient between the shot peened samples against the 100Cr6 steel balls in the dry sliding wear tests. (b) The friction coefficients of the shot peened steels against the steel ball under the load of 5N as a function of the number of laps.

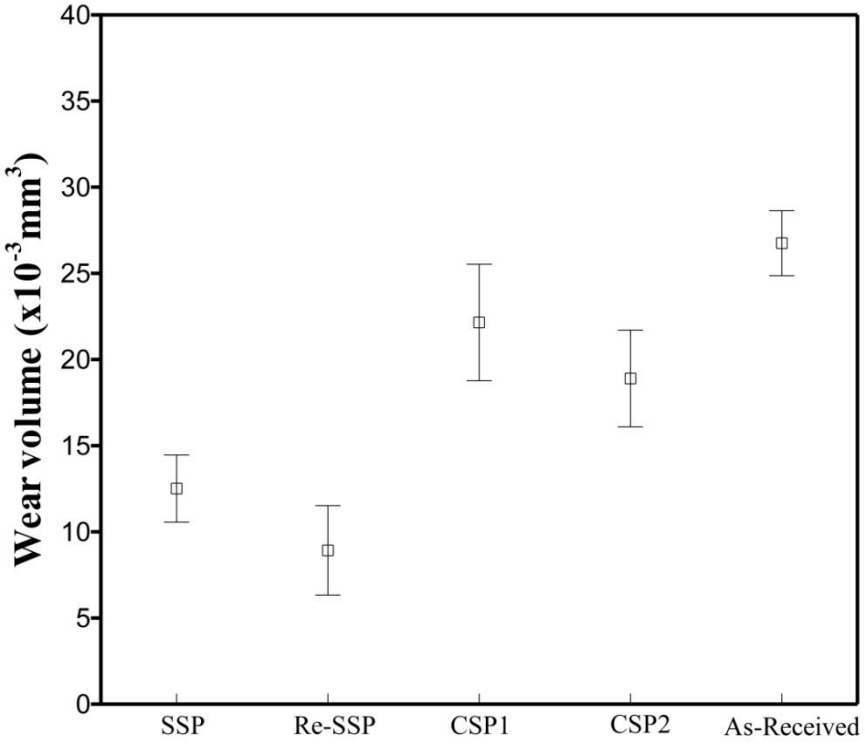

Figure 4-5. Wear volume of ASIS 4340 at different shot peening conditions.

Figure 4-6 shows the wear track morphology and topography of the shot peened AISI 4340 steel. Abrasive wear formed by the repeated sliding of the steel ball clearly creates grooves on the wear tracks under the load of 5N. The as-received sample has the largest wear track on the surface and consequently the highest material loss[76, 84-87]. The severe shot peened and re-severe shot peened samples have smaller wear tracks and wear volumes compared to the conventional shot peened samples. This is due to the higher wear resistance of the shot peened samples can reduce their wear tracks [76, 84-87]. Figures 4-6*a-b* also reveal that some dimples formed by the impact of the shot during shot peening have a higher depth than that of the material removed by the sliding ball and thus can still be seen.

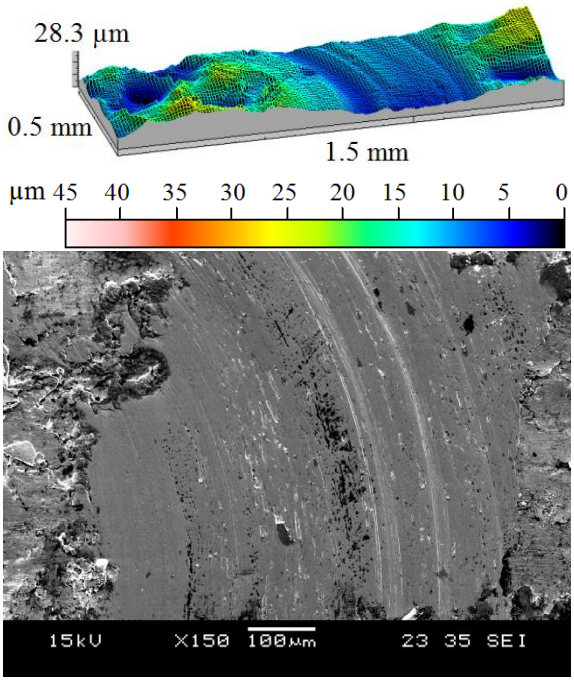
28.3 µm
0.5 mm
1.5 mm
µm 45 40 35 30 25 20 15 10 5 0
15kV X150 100µm 23 35 SEI

(a)

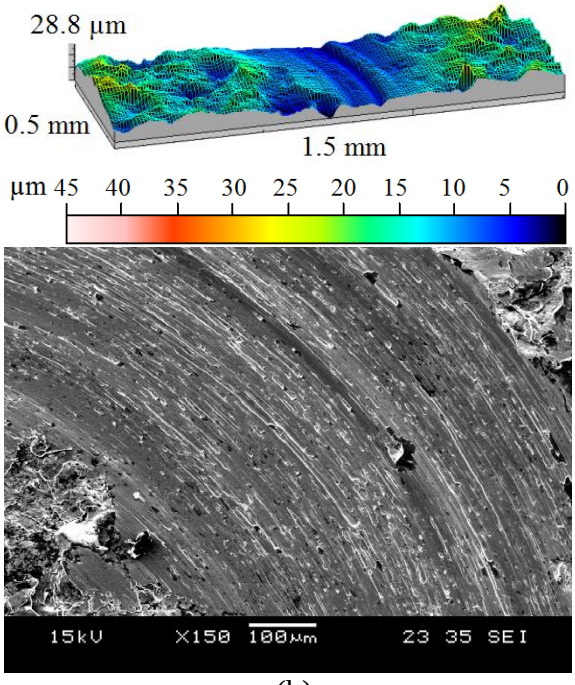
28.8 µm
0.5 mm
1.5 mm
µm 45 40 35 30 25 20 15 10 5 0
15kV X150 100µm 23 35 SEI

(b)

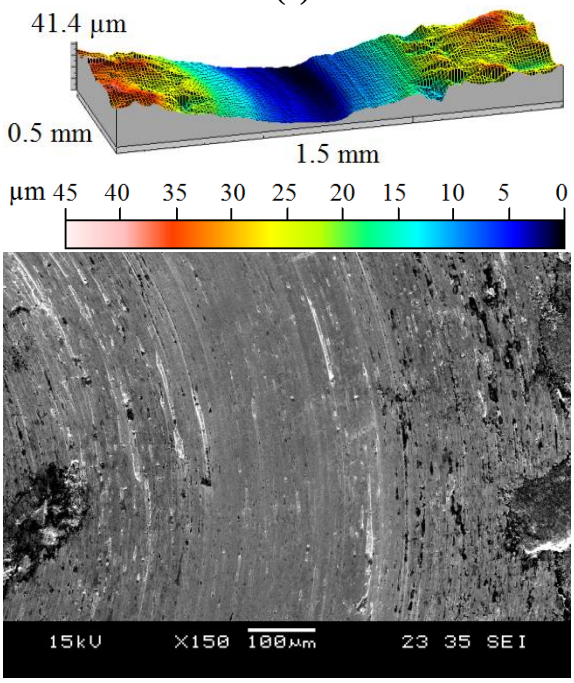
41.4 µm
0.5 mm
1.5 mm
µm 45 40 35 30 25 20 15 10 5 0
15kV X150 100µm 23 35 SEI

(c)

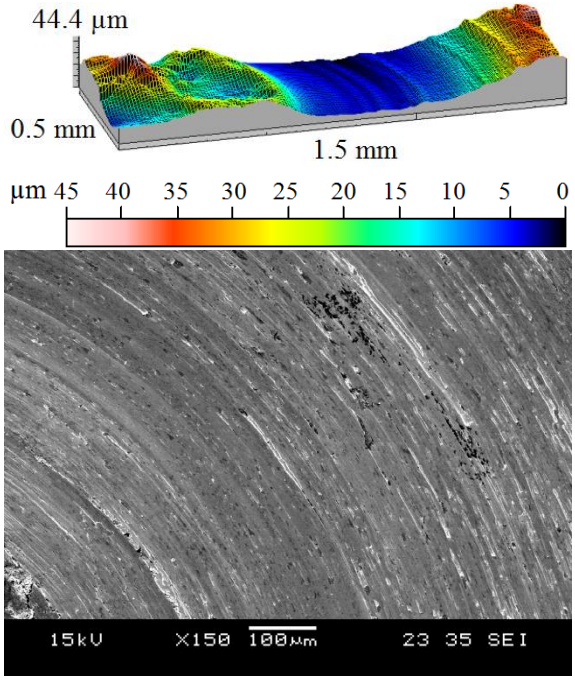
44.4 µm
0.5 mm
1.5 mm
µm 45 40 35 30 25 20 15 10 5 0
15kV X150 100µm 23 35 SEI

(d)

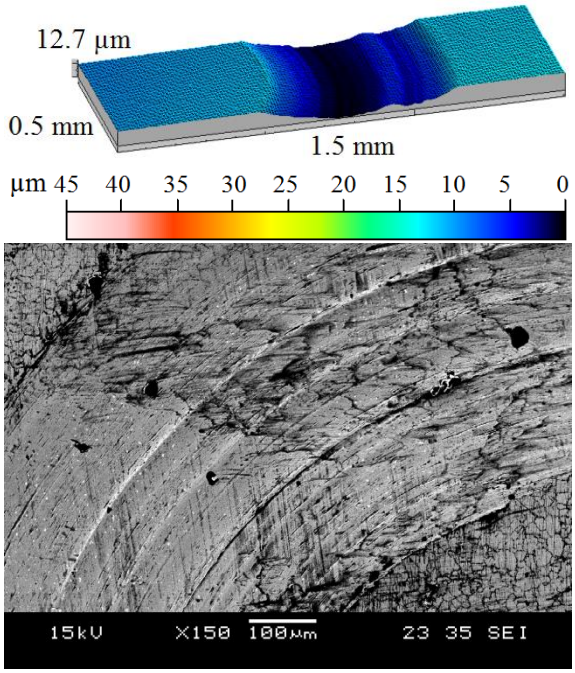

(e)

Figure 4-6. Surface morphologies and topographies of wear tracks: (a) SSP, (b) Re-SSP, (c) CSP1, (d) CSP2 and as-received AISI 4340 steel.

In general, a conventional shot peening parameter was used in industrial application for over fifty years, but a severe shot peening process was about a decade. The main purpose of the severe shot peening is to create an ultrafine grain on the surface of the material while the conventional shot peening aims to induce the compressive residual stress in the subsurface of the material. With the very high intensity (24A compared with 10A) and coverage (about 10 times compared with a conventional process), the severe shot peening caused a severe plastic deformation on the surface of the material. Therefore, severe shot peening process leads to a high surface roughness of the sample due to the formation of deep indentations on the surface.

4.4 Conclusion

In this chapter, the low alloy steel AISI 4340 after quenching and tempering was shot peened under conventional and severe conditions to investigate their mechanical and tribological properties. After heat treatment, there was an iron oxide layer with a depth of about 20 µm formed on the sample surface. The conventional shot peening process could

partly remove this layer and improve the properties of material while the severe shot peening process totally removed it from the surface.

The severe shot peening generated an ultrafine grain layer with a depth of 20 μm. The severe shot peening process increased the hardness of the surface and subsurface close to the surface of the material as a result of promoted cold work hardening effect. The increasing surface hardness by applying conventional shot peening and severe shot peening process could improve the wear resistance properties of material, as a result of decreasing the wear volume of peened samples.

Severe shot peening process leads to a high surface roughness of the sample due to the formation of deep indentations on the surface. Therefore, the increase of surface roughness of severe shot peened sample was responsible for their increased friction coefficient against the steel ball. The high surface roughness was considered as a side effect of severe shot peening process. To reduce its side effect, additional shot peening process with smaller media was employed. This method not only reduced the surface roughness on severe shot peened surface samples but also improved the wear resistance of the low alloy steel (Re-SSP).

It could be concluded that the severe shot peening process could remove the iron oxide layer and generate an ultrafine grain layer on the surface of a low alloy steel; the experimental results showed that this layer had an influence on the mechanical and tribological properties of the treated AISI 4340 low alloy steel specimens.

Chapter 5: Three-dimensional modeling of shot peening process

5.1 Introduction

Computational modeling is widely used for a number of manufacturing processes including shot peening in order to avoid the expensive and time consuming experiments to process optimisation [97, 98]. Its results can be used to predict for the experimental studies, etc. It can also reduce the number of experiments required to establish the ideal processing parameters. Different approaches are proposed to study the numerical simulation of the shot peening process [48, 65-69]. It is observed that three-dimensional multiple-shot impact models did not concentrate on the coverage parameter, but on the development of stress state during the impact process. These the multiple-shot impact simulations studied uniformly distributed positions and prearranged sequences. The details of these impact patterns have been discussed in a review paper by Bagherifard et al. [70]. Though the use of symmetry patterns reduces the computational costs, cannot totally define the random nature of practical shot peening process. Therefore, these patterns often fail to simulate a full coverage condition for the actual shot peening process.

A random impact model was developed by Miao et al.[49], where the center of shot coordinates was generated by equation (5-1).

$$\begin{aligned} x &= 0.75 + 1.5 \times rand(1,1) \\ y &= 0.75 + 1.5 \times rand(1,1) \\ z &= -0.5 - (N-1) \times 1.5 \times rand(1,1) \end{aligned} \qquad (5\text{-}1)$$

where *rand*(1,1) is a uniform pseudo-random number generator in the interval [0,1] and N is the number of impacts.

Bagherifard et al. [50] developed a multiple-shot random impact simulation model to predict the generation of the nanostructured surface layer. In this research, to obtain the coverage parameter, the Kirk and Abyaneh model [99] given by the Avrami equation (equation 5-2) was applied.

$$C\% = 100[1 - e^{-Ar}]$$
$$Ar = \frac{N \times \pi\left(\frac{d}{2}\right)^2}{\pi\left(\frac{D}{2}\right)^2} = N\left(\frac{d}{D}\right)^2 \qquad (5\text{-}2)$$

where N is the number of shots, d is the diameter of a dimple caused by a single shot; D is the diameter of impact region of the target material. In shot peening experiments, a coverage of 98% can still be assessed visually [1], and is considered as full coverage. To obtain 98% coverage, the Ar value is equal to 4.

It is also worth noting that the high shot intensity obtained with large shots at a high velocity is effective to induce a high magnitude of compressive stress in the target material. However, the surface roughness of the shot peened target material is relatively high. To improve the surface finish of shot peened components at high intensity, lower shot intensity obtained with smaller shots at a lower velocity is used to reduce the surface roughness. This process is called double shot peening. The experimental results of the double shot peening process are reported by Vielma [71] and Scuracchio [72], but there is the lack of modeling and simulation knowledge.

In this chapter, a new method is introduced to estimate the number of shots and the arrangements required to achieve full coverage of the target material. A multiple-shot impact model, implemented in a commercial explicit FE analysis program LSDYNA, was used to investigate the effect of different shot peening parameters on the compressive residual stress

distribution of the material. The effect of double shot peening on the residual stress distribution of the material was also studied in the simulation.

5.2 Materials and methods

In this research, a new approach method is introduced to estimate the coverage of target material using a simulation model. This model is based on the assumptions of the Kirk and Abyaneh model [99]. The assumptions are that during shot peening process, a simplified model is considered, in which a fixed diameter of circular impression is created by uniformly sized spheres impacting a flat surface. A new approach can provide the number and arrangement of required shots for the coverage of 98%. To estimate the level of coverage parameter, a Matlab^{TM} code is developed as per the flow chart in figure 5-1.

The first step of this flowchart is the calculation of the diameter of a dimple on target material surface caused by a single impact. Figure 5-2*a* presents the original region of a target area which is divided into several small cells. The value of each node of the cell is set equal to 1 at the beginning of the process. Value "1" means that the node is not peened. The first ball, which has the radius "*R",* randomly impacts on a target (the center of the ball is located in the target area) to generate an indentation with radius "*r"* on the target surface. Therefore, the values of all nodes, which are located inside the circle, change from "1" to "0", and value "0" remains unchanged (figure 5-2*b*). Value "0" means that the node is peened. After each shot, the degree of coverage is calculated by equation (5-3). If this ratio is less than 98%, an additional ball will impact the region area (figure 5-2*c*) until this ratio is larger than 98%, so that the program will stop and provide coordinates of all impacted balls and the final coverage of the process.

$$C\% = \frac{number\ of\ \ nodes\ with\ value\ "0"}{total\ \ number\ of\ \ nodes} \qquad (5\text{-}3)$$

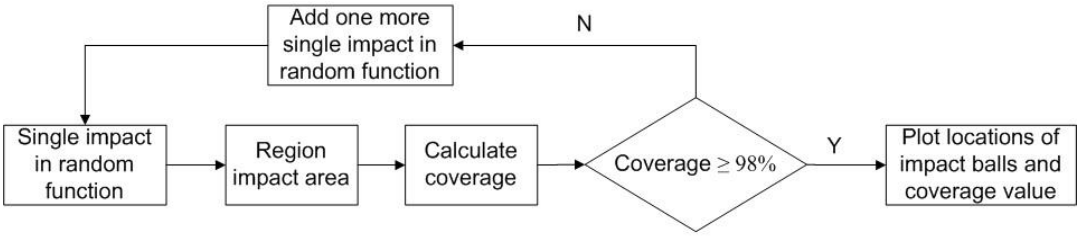

Figure 5-1. A sequence of multiple-shot impact shot peening process with the aid of Matlab™.

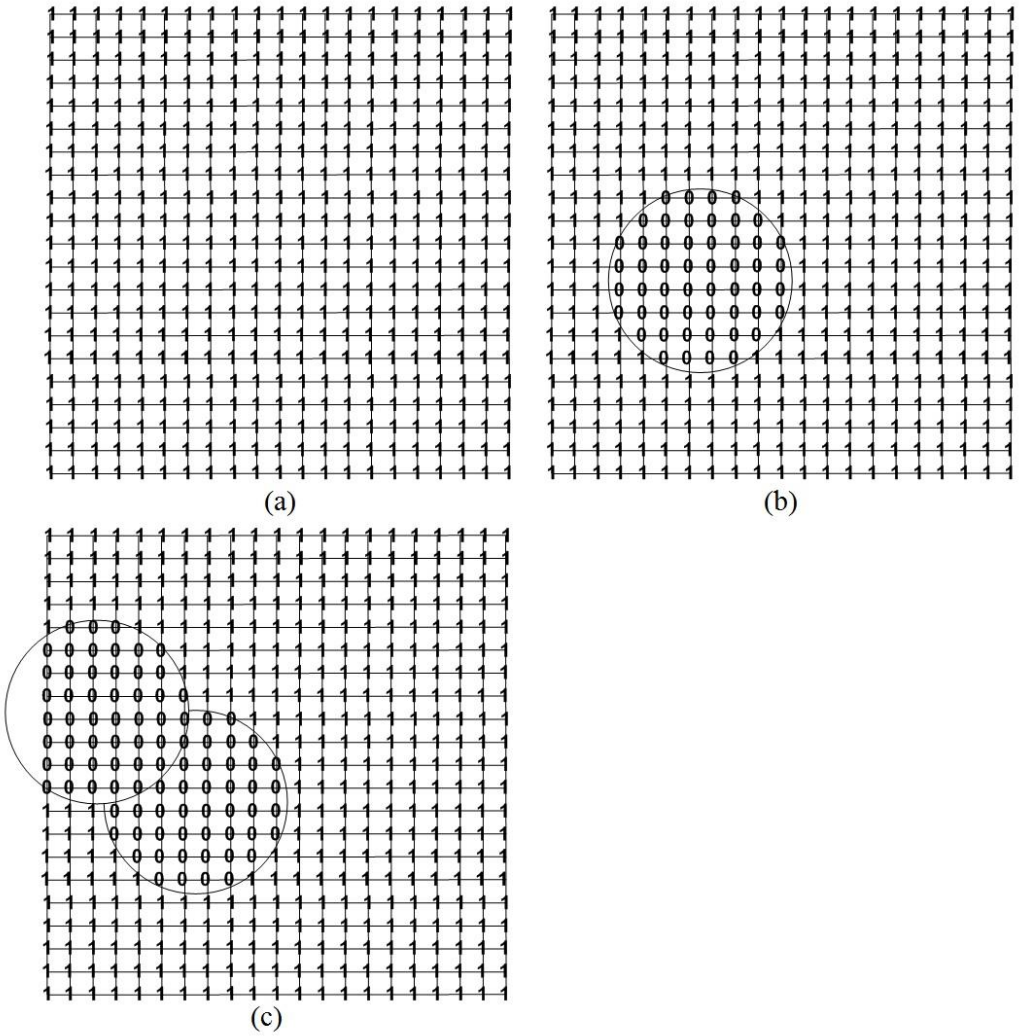

Figure 5-2. A sequence of a new method: (a) an original target surface, and shot peened

surfaces after (b) first impact, and (c) first two impacts.

To validate the result of this newly introduced method to estimate the coverage of the shot peening process, a multiple-shot impact FEM model was developed. The steel target material parameter was set based on Majzoobi study [48], in which mass of density ρ = 7800 kg/m^3, a Young's modulus E = 210 GPa and the initial yield stress σ_o = 1500 MPa. The shots used were assumed to be rigid with two radii of 0.15 and 0.3 mm. The dimensions of the target material were 2 mm x 2 mm x 1.5 mm, and the shot peened target area was 1 mm x 1mm. The target material and the shots were meshed using an eight-node brick element with an element size of 0.04 mm. The dynamic friction coefficient between the shots and target is set at f 0.1 [48]. The plastic strain-rate dependent behaviour follows that of the Cowper-Symonds law was given by (5-4).

$$\sigma = \sigma_0 \left[1 + \left(\frac{\dot{\varepsilon}}{C} \right)^{1/p} \right] \qquad (5\text{-}4)$$

in which σ_o is static yield stress, C and p are material constants. The values C and p of steel are 2.1e+11 and 3.3, respectively [48].

The rigidity of shots was based on the fact that the yield strength and hardness of typical steel shots are required to be significantly higher than those of the target material [12]. The interaction between shots was ignored. The shots in the simulation have a perfectly spherical shape and impacts with the same velocity. The velocity was studied from 30 m/s to 50 m/s. The bottom surface of the target is fully constrained.

5.3 Results and discussion

5.3.1. Coverage parameters

Figure 5-3 presents an example result of the introduced method, i.e. an indentation with r = 0.064 mm caused by the impact between a 0.3 mm diameter shot at 40 m/s on 1 mm x 1 mm target. Figure 5-3*a* provides the result of locations of all shots and the coverage of 98.11% after peened with 311 shots. Figure 5-3*b* presents the coverage of target surface as a function of the number of shots. The curve is close to the Arvami curve when the single dimple area $(\pi d^2/4)$ is very small compared with the shot peened target area $(\pi D^2/4)$. The ratio of the area, (d^2/D^2), is small, meaning that N is large.

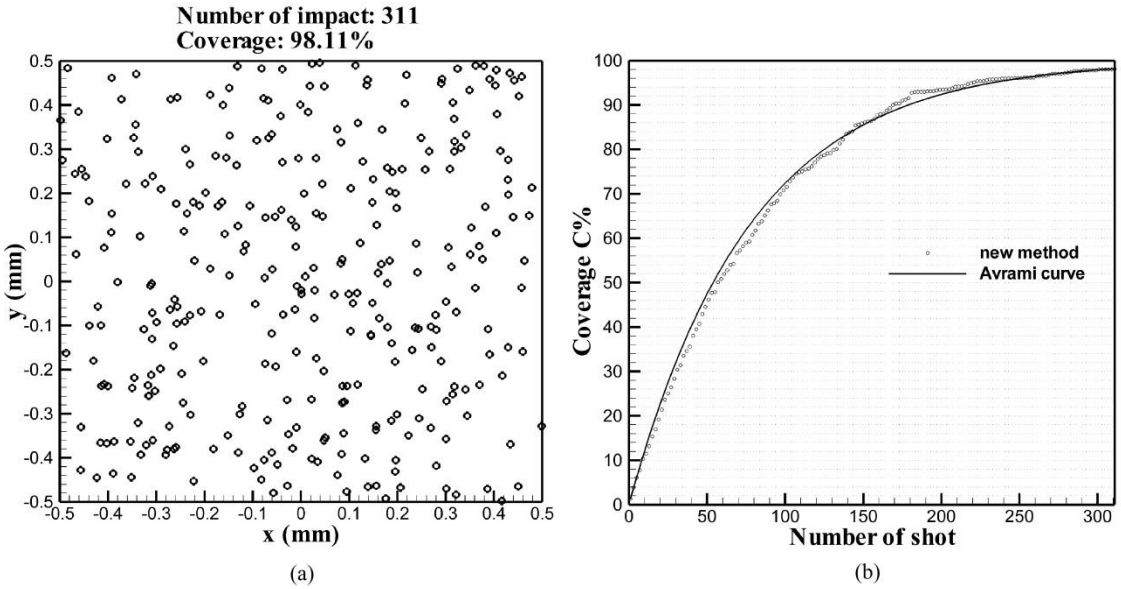

Figure 5-3. (a) Coordinates of impact shots employed to obtain coverage of 98%, and (b) dependence of the degree of coverage on a number of shots.

In this method, the random function was used to generate the position of shots including the number of shots and their locations and the degree of coverage varied with different repeated runs. For example,when R = 0.15 and v = 40 m/s, the number of shots required to obtain the coverage of 98.11%, 98.05%, 98.03%, 98.12%, and 98.01% in five consecutive repeated runs are 311, 309, 315, 314, and 310 respectively. It is worth noting that

the difference in the number of shots required to obtain a coverage of 98% in different consecutive repeated runs become more significant with the large ratio of $(d/D)^2$.

A practical shot peening process is a random process thus the number of shots used to achieve the full coverage in one unit of the surface target area is a random number followed the standard normal distribution. Hence, it is missing in the Kirk and Abyaneh's model e.g. the equation (5-2) only provides one result. Therefore, the result of equation (5-2) only becomes accurate when the N is sufficiently large. In that case, the value of N is approximately equal to the mean value μ of the standard normal distribution. It can be seen that if the number of shots N is sufficiently large, the Kirk and Abyaneh's model based on the Avrami's equation is approximately equal to the mean value μ of the standard normal distribution, so there is an agreement of the Kirk and Abyaneh's model with this proposed method result. Figure 5-3 shows this comparison.

However, when the number of shots N is small, the Kirk and Abyaneh's model is not accurate. For example, a shot with a diameter of 1.2 mm was employed to impact the material at the velocity of 115 m/s. The single indentation was formed on the surface of the material with a diameter of 0.58 mm. The equation (5-2) provides the result of N = 15 impacts to achieve the full coverage of 98% in the unit of 1 mm^2. It can be concluded that this result is not accurate. Figures 5-4*a-f* displays the number of shots and their coordinates to obtain the full coverage of 98% in six consecutive repeated runs using this proposed method. It shows that 23, 24, 20, 14, 17 and 26 impacts were employed to achieve coverages of 100%, 98.30%, 99.98%, 99.24%, 98.82% and 99.89% respectively. The comparison shows that there is a large difference in six consecutive repeated runs due to the random function of the shot peening process. Figure 5-4*g* illustrates a dependence of coverage on the number of shots of the Kirk and Abyaneh's model and six consecutive repeated runs of the proposed method.

The figure presents the coverage of target surface as a function of the number of shots. Increasing the number of shots results in the increment of shot-peened coverage. However, the proposed curves follow the same trend but are close to the Arvami curve.

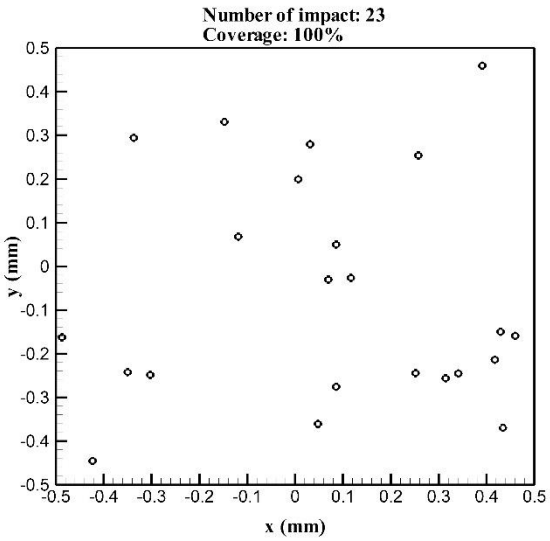

(a) Run 1

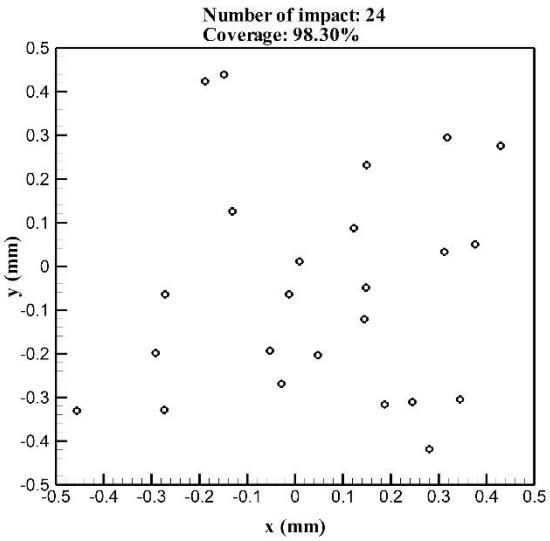

(b) Run 2

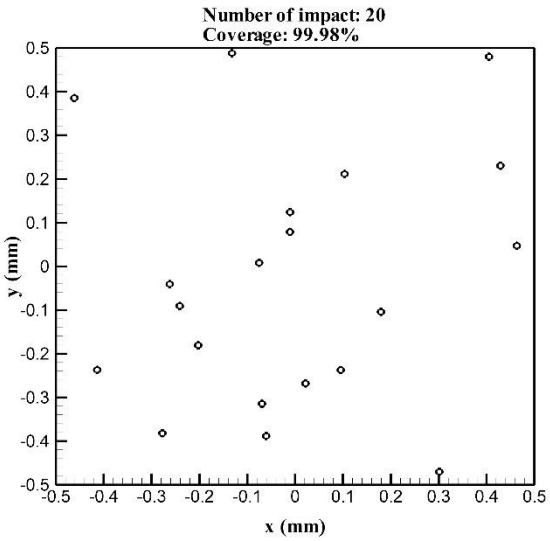

(c) Run 3

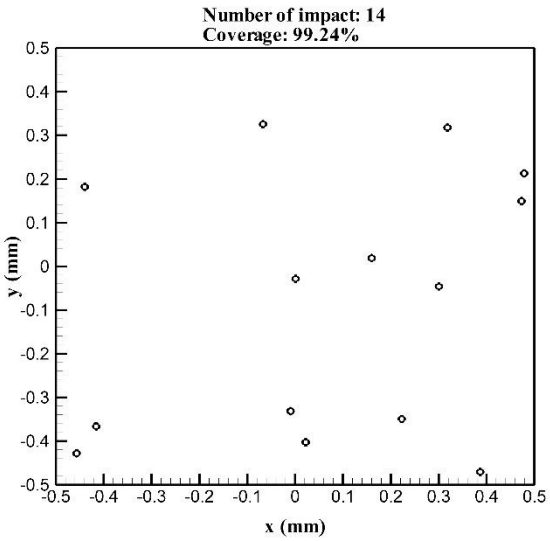

(d) Run 4

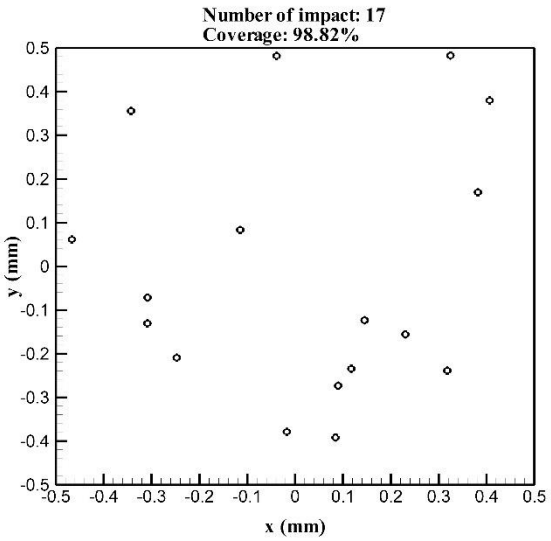

(e) Run 5

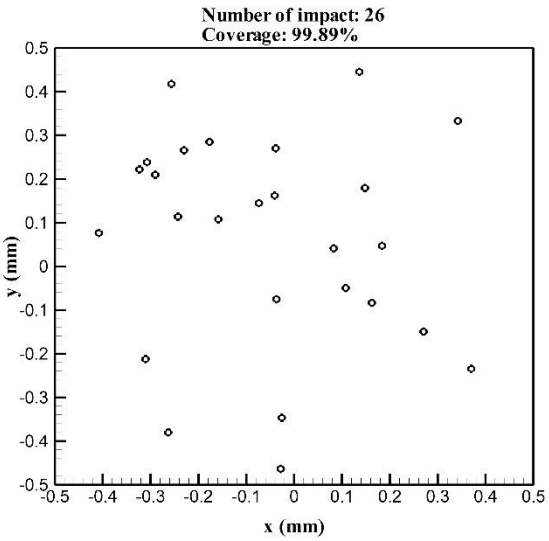

(f) Run 6

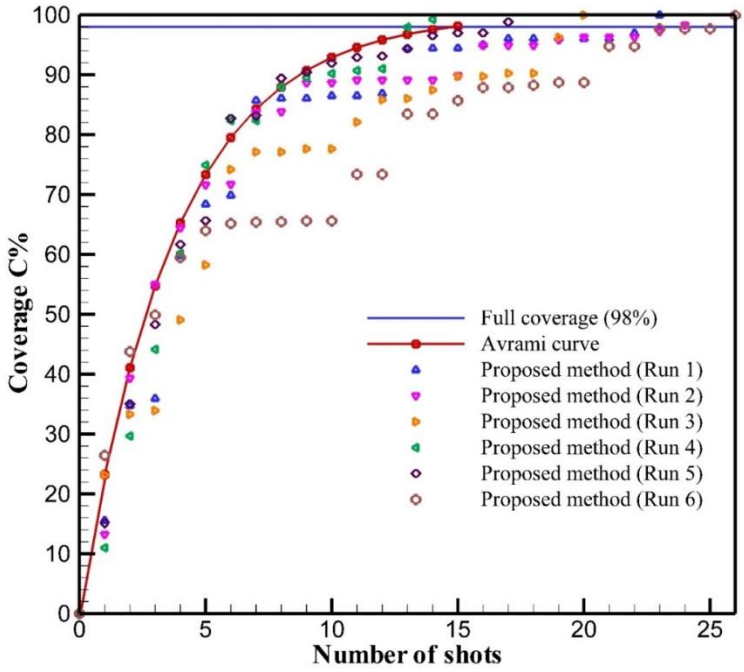

(g)

Figure 5-4. (a-f) Coordinates of impact shots employed to obtain coverage of 98% in six consecutive repeated runs, and (g) dependence of the degree of coverage on a number of shots.

5.3.2. FEM multiple-shot impact model

To investigate the effect of full coverage of shot peening process, the result of the new proposed method was applied in the multiple-shot impact model. In the random multiple-shot impact model presented in figure 5-5, multiple shots were impacted onto the surface of a

kinematic plastic model. The effect of coverage, velocity of shot, and shot size on the distribution of residual stress and surface roughness of target material under different process conditions were investigated.

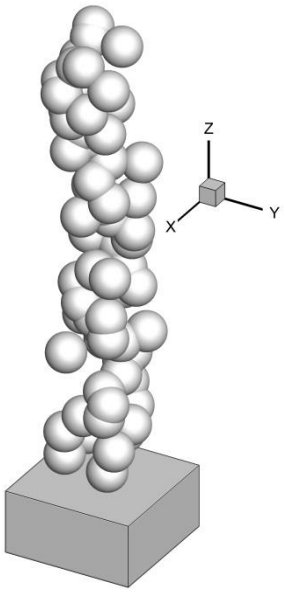

Figure 5-5. Finite element model of multiple-shot impacts.

5.3.2.1 Mesh sensitivity analysis

In finite element modeling, there is a trade-off between greater accuracy which is achieved by smaller mesh size mesh and computational power or time needed. Therefore, it is important to evaluate the effect of mesh size on the simulated results. By doing this, the appropriate number of elements which allows adequate simulation time without compromising the accuracy can be determined. In current study, the simulated distribution of residual stresses in the centre plane (y = 0) and along the z direction (in the centre plane) at the contact point are obtained by using five different mesh sizes (0.06 mm, 0.05 mm, 0.04 mm, and 0.03 mm) as shown in figure 5-6. The results converge when the mesh size becomes less than 0.05 mm. In this research, the mesh size 0.03 mm is chosen for the simulation.

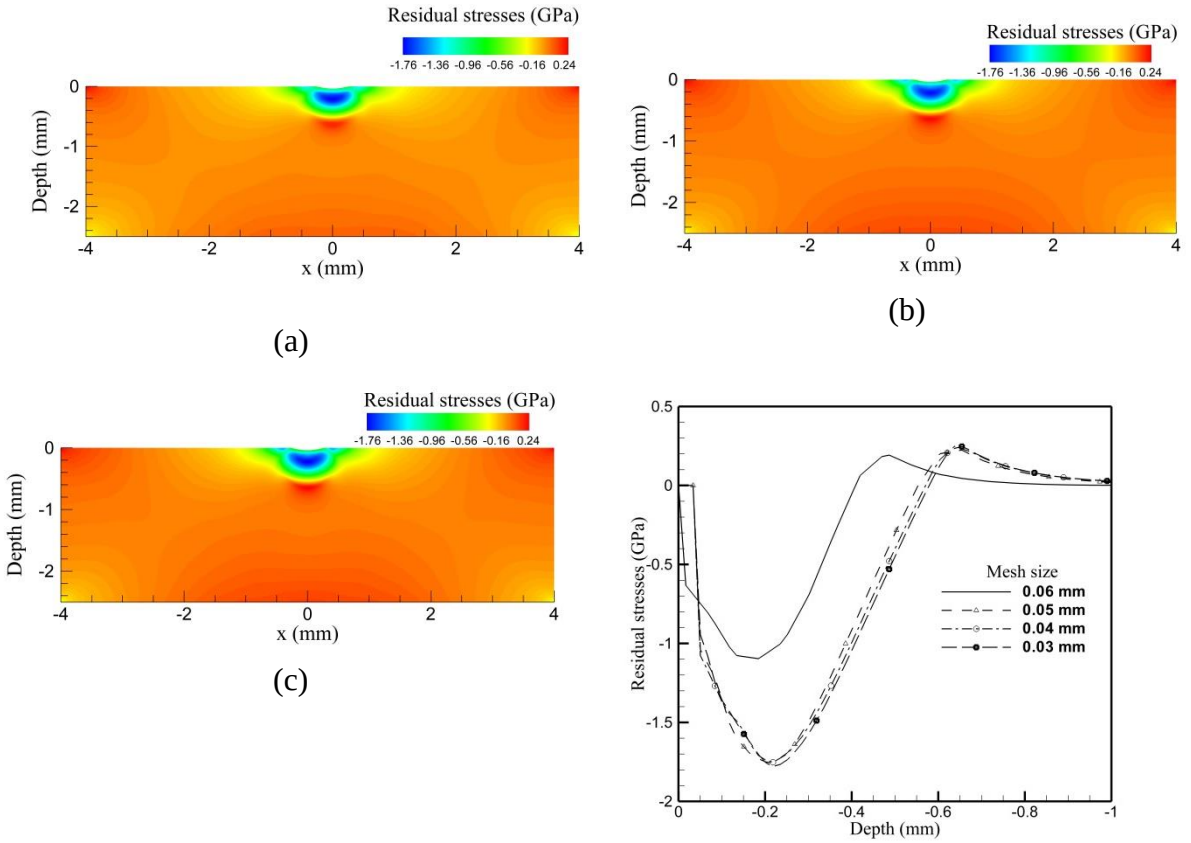

Figure 5-6. Residual stress distribution: (a) on plane y = 0 with mesh size of 0.05 mm, (b) on plane y = 0 with mesh size of 0.04 mm, (c) on plane y = 0 with mesh size of 0.03 mm, and (d) along the z direction below the contact point at different mesh sizes.

5.3.2.2 Validation the studied FEM model with the reference model

To validate the result of the studied FEM model, a comparison between the studied results with the reference model was made at the velocity of 50 m/s. Figure 5-7*a* and *b* show the multiple shot impact model and target plate with indentations created by shot impacts employed in Majzoobi research [48]. The comparison between the numerical study of Majzoobi research [48] and the experimental work of Torres [100] with this studied FEM model depicts that the results of Majzoobi research [48], Torres [100] and this study are very close, i.e. the similar compressive residual stress profile is found, the maximum

compressive stress is about 1.2 GPa, and the depth of the compressive residual stresses zone is about 200 μm. However, a significant difference between this studied result with these reference results is the residual stresses in the subsurface below the depth of 200 μm. The literature review in Chapter 2 indicates that under the deformation process, the compressive residual stress in the subsurface results in the formation of the tensile stresses in the rest of the material for equilibrium.

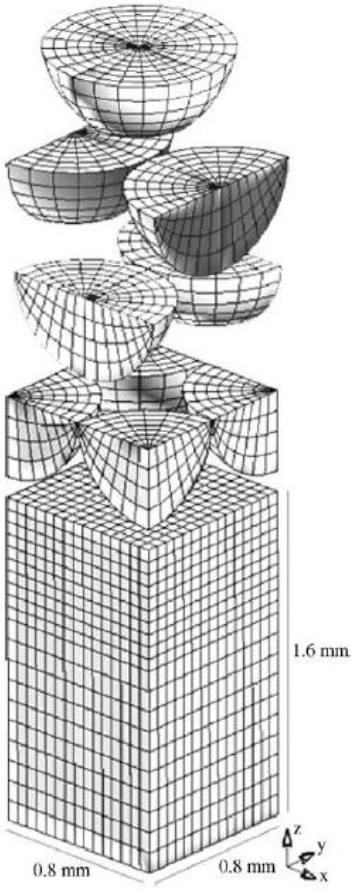

(a) The multiple shot impacts model of Majzoobi [48]

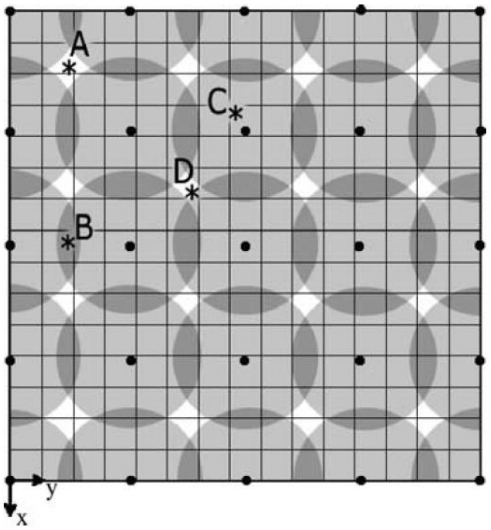

(b) The target plate with indentations created by shot impacts of Majzoobi' model [48]

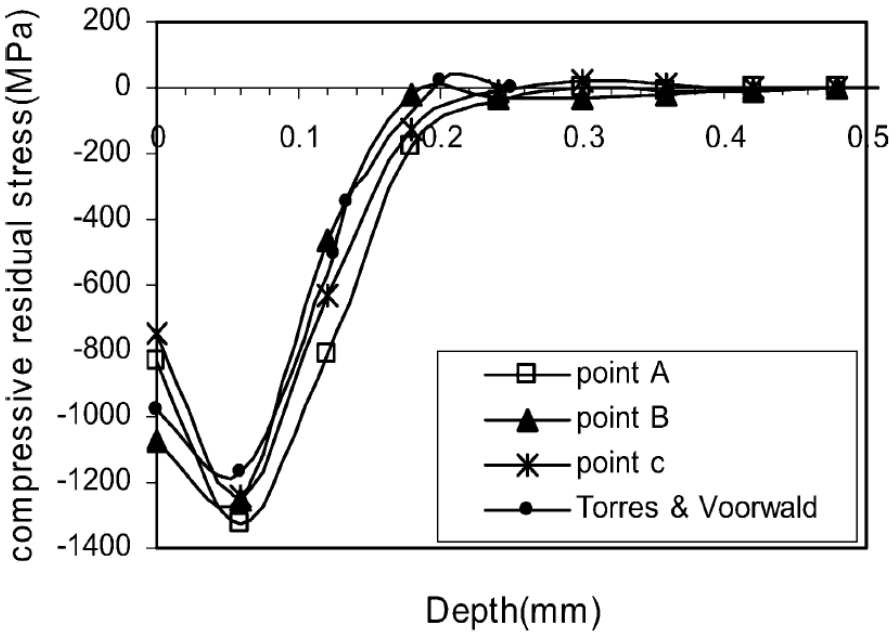

(c) The residual stresses profile distribution at different points of Majzoobi's report [48] and Torres's work [100] at the velocity of 50 m/s

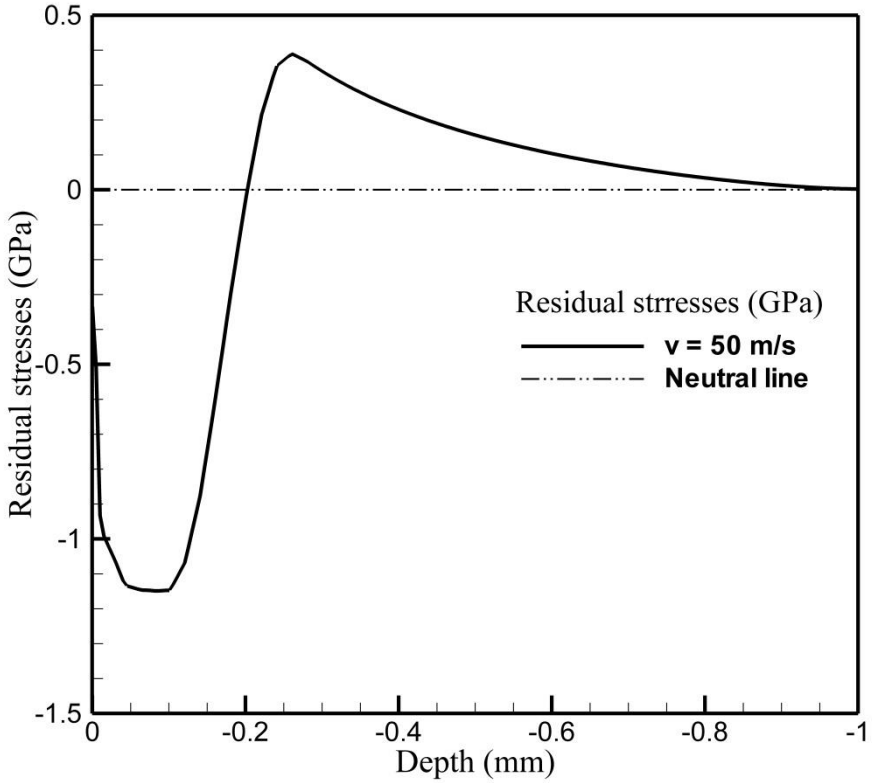

(d) The residual stresses profile distribution in this study

Figure 5-7. The residual stresses profile distribution in this studied FEM model at the velocity of 50 m/s

5.3.2.3 Effect of shot peening process parameters on the residual stress distribution

The effect of the coverage on residual stress of target material were examined and depicted in figure 5-8. Multiple impacts with 0.3 mm radius shot onto the target material at a velocity of 50 m/s.

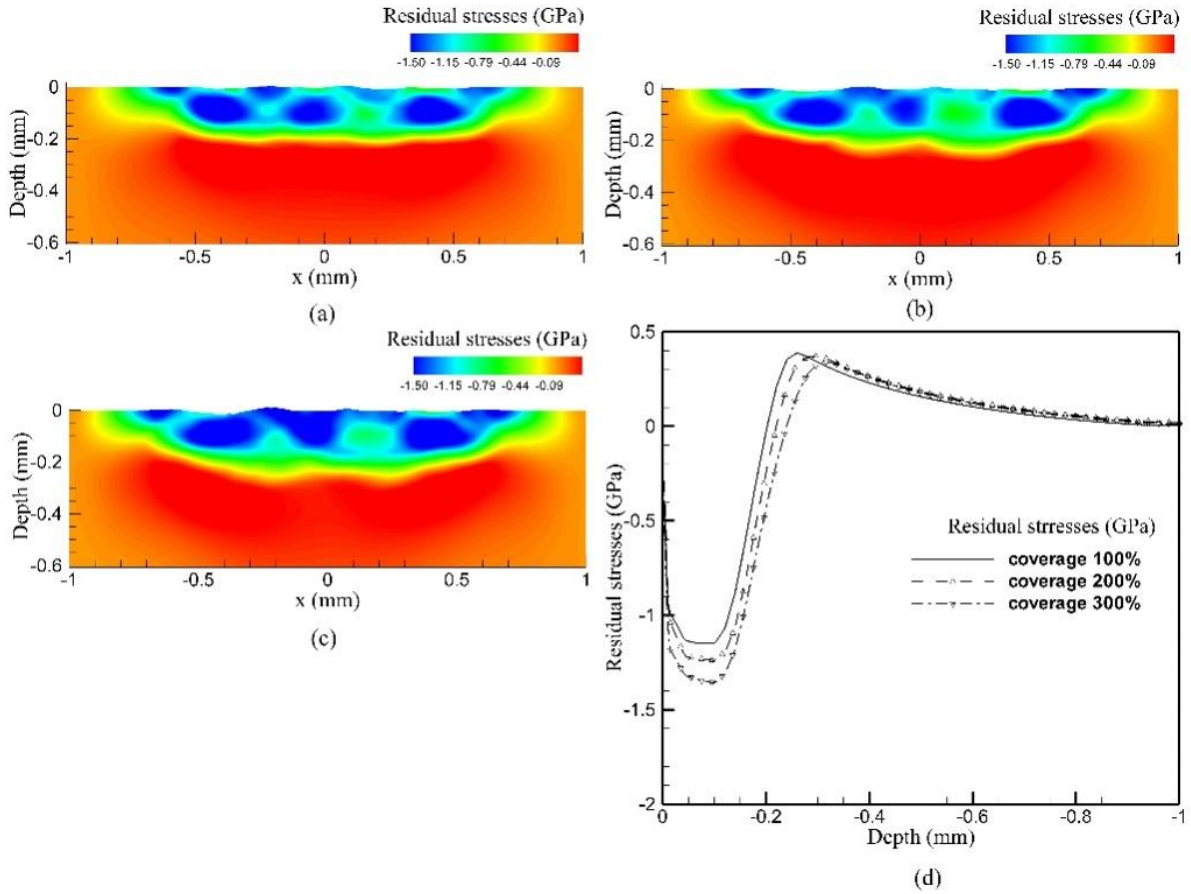

Figure 5-8. Residual stress distribution: (a) on centre plane (y = 0) at coverage of 100%, (b) on plane y = 0 at coverage of 200%, (c) on centre plane (y = 0) at coverage of 300%, and (d) average residual stress long z direction (x = 0, y = 0) on the target area at different coverage degrees.

Figures 5-8*a-c* display that, on the centre plane (y = 0), the compressive zone becomes slightly deeper, when the coverage increases from 100% to 300%. The number of

shots employed to obtain coverages of 100%, 200%, and 300% were 69, 137, and 208, respectively. Figure 5-8*d* presents the distribution of the average residual stress along the z direction on the target peened area. The maximum value of compressive residual stress in the case of 100% coverage is -1.15 GPa which is smaller than -1.40 GPa achieved with 300% coverage (figure 5-6*d*). Moreover, the depth of influence (of compressive stresses) also increases. The simulation results in this research present that increasing the coverage is an effective approach to obtain a higher compressive residual stress in the target material [101].

The effect of the shot velocity with R of 0.3 mm was examined in the multiple-shot impact model using various velocities of 30, 40, and 50 m/s. The indentation size caused by each single shot increases with increasing shot velocity, therefore the number of shots needed to achieve the required 98% coverage with these velocities were 82, 73, and 69, respectively.

Figures 5-9*a-c* illustrate that increasing the velocity increases the compressive residual stress region. Figure 5-9*d* shows that the largest value of compressive residual stress caused by the shots with a velocity of 50 m/s would be higher than that of the one caused by the shot with a velocity of 30 m/s. In addition, the compressive stress zone increases from 0.125 mm to 0.200 mm when the velocity of shot increases from 30 m/s to 50 m/s. Therefore, the result illustrates that increasing the velocity of shots is an effective approach to obtain deeper compressive stress zone in the target material. Similar observation was made by Meguid et al. [12, 102] and Majzoobi et al. [48], the effect of velocity on the distribution of residual stress on the shot peened material is achieved.

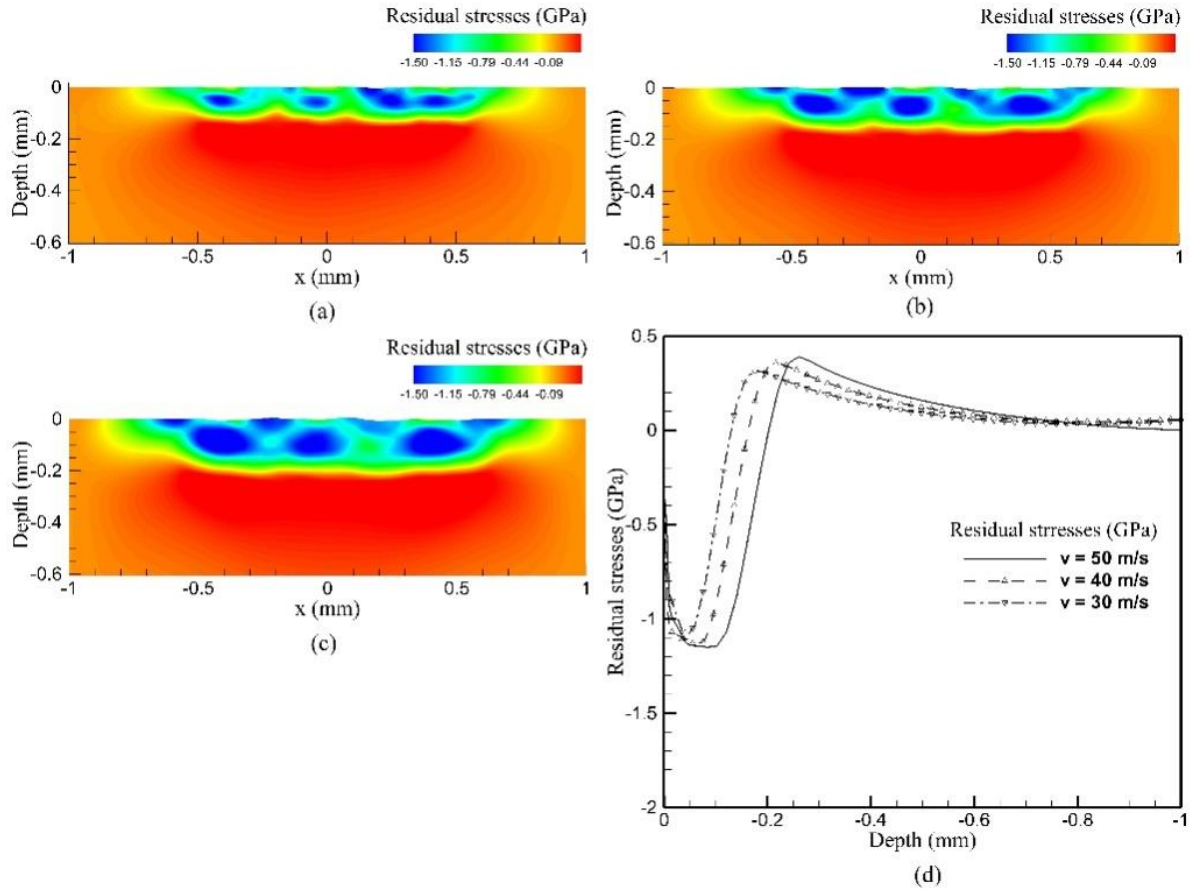

Figure 5-9. Residual stress distribution: (a) on plane y = 0 at velocity of 30 m/s, (b) on plane y = 0 at velocity of 40 m/s, and (c) on plane y = 0 at velocity of 50 m/s, and (d) average residual stress long z direction on the target area at different velocities.

The effect shot size was studied by applying two different shot radii 0.15 mm and 0.3 mm. In this section, the velocity of the shot was 50 m/s. The size of the dimple formed by each single impact increases when the size of shots was increased; therefore, the number of shots employed to obtain a full coverage were 311 and 69 for the shot radii of 0.15 and 0.3 mm, respectively. The compressive residual stress region after shot peening is wider and deeper for the larger shot radius due to the higher impact energy of the shots (figure 5-10). The result suggests that increasing the shot size is an effective approach for obtaining a higher compressive residual stress and deeper compressive residual stress zone in the target material [102].

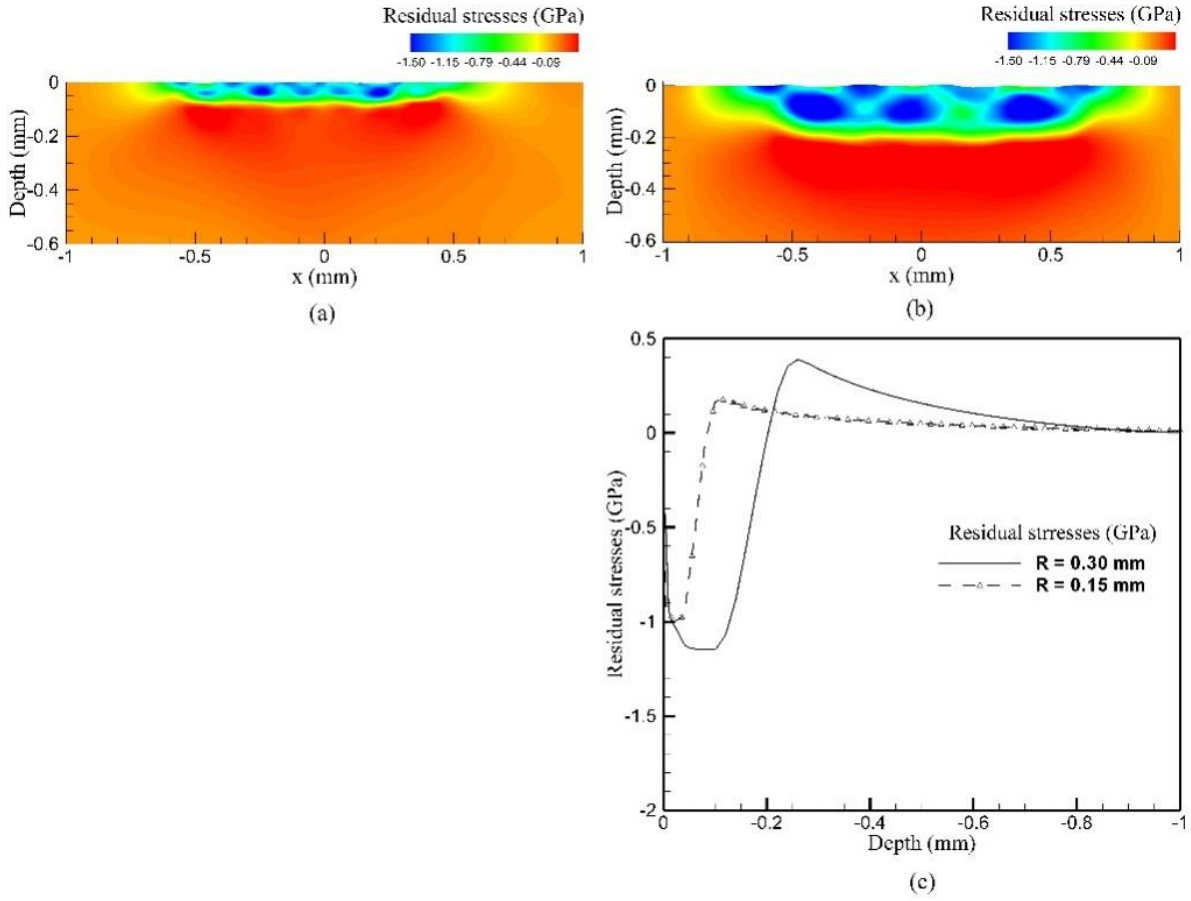

Figure 5-10. Residual stress distribution: (a) on plane y = 0 at shot radius of 0.15 mm, (b) on plane y = 0 at shot radius of 0.3 mm, and (c) average residual stress along z direction on the target area at a velocity of 50 m/s.

The results reported in the previous paragraph also suggest that a larger shot size can induce higher compressive stress in the subsurface of the target material. However, it was mentioned that a smaller shot size can result in a more uniform compressive residual stress distribution and a smoother target surface finish. Therefore, it is possible to use two different sizes of shots for double shot peening to obtain their combined effects. The target material after shot peening with large shots of 0.3 mm in radius at a velocity of 50 m/s for 100% coverage was shot peened by using smaller shots of 0.15 mm in radius at the velocity of 30 m/s (DP1) and 50 m/s (DP2) for the 100% coverage. Figure 5-11 shows that consecutive second shot peening with the smaller shots of 0.15 mm in radius slightly lowers the

maximum value of the compressive residual stress, but does not affect the depth of compressive zone obtained after first shot peening of the target material with the larger shots of 0.3 mm in radius. However, the compressive residual stress becomes more uniform, and the surface profile looks smoother after the double shot peening process [71, 72].

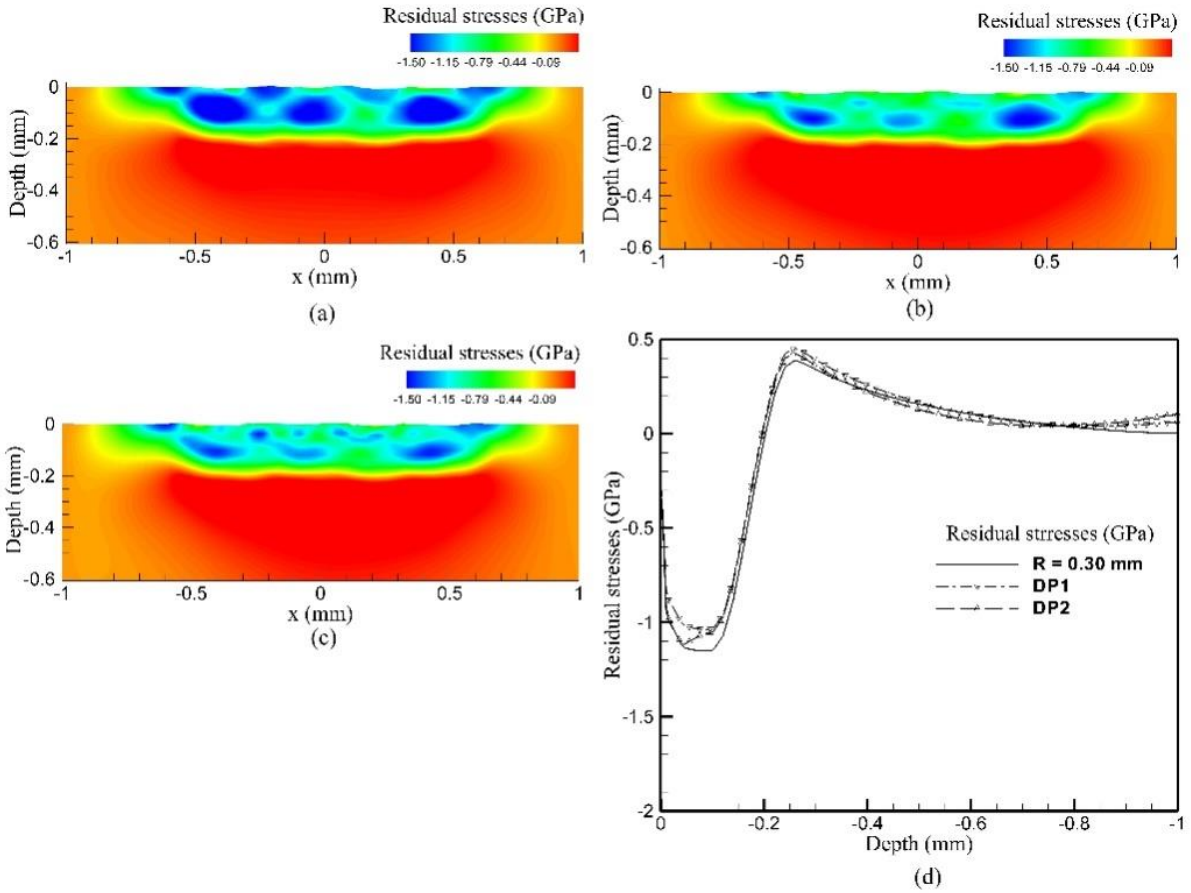

Figure 5-11. Residual stress distribution: (a) on plane y = 0 at first shot peening with shots of 0.3 mm in radius, (b) on plane y = 0 at double shot peening with velocity of second shot of 30 m/s, (c) on plane y = 0 at double shot peening with velocity of second shot of 50 m/s, and (d) average residual stress along z direction on the target area.

5.4 Conclusion

A new approach was introduced to estimate the number of shots and their arrangements to obtain the desired coverage. This method could provide the number of shots,

and their coordinate positions required to obtain full coverage. Based on the new approach, multiple-shot impact models of the shot peening process were studied using a finite element simulation. The simulation results suggested that increasing the coverage, shot velocity and shot size were effective approaches to obtain a higher level of compressive residual stress and deeper the compressive stress zone in the target material. Also, the simulation results suggested that it was possible to apply the smaller shots after peening the target material with the large shots. The double shot peening simulation results showed that the smaller shots reduced slightly the compressive residual stress previously induced by the larger shots but did not affect the depth of the compressive stress zone. The second shot peening process could be used in low intensity, in that case, double shot peening was considered as a simple, low-cost method for improving the surface finish of shot peened components.

Chapter 6: Experimental and numerical investigation of the effect of shot peening process parameters on the surface topography, residual stress distribution of shot peened low alloy steel

6.1 Introduction

Recently, Bagherifard et al. [58] indicated that the shot peening process can improve the fatigue life for the treated sample but also create the high surface roughness of the material surface. The rough surface has a detremental effect which reduced the fatigue life of the material. It is reported that the initiation crack of the fatigue fracture usually occurs at the weakness link, which has the low restraint on the slip, in the material [103]. Therefore, the free surface roughness or the appearance of inclusions i.e. impurities or small defects are the preferable conditions for the initiation of the micro cracks [104]. As a consequence, the increase in the surface roughness in the case of shot peening process with high intensity or large media size make the treated surface material become a favorable condition for a formation of nucleation cracks prevent [105]. In addition, the shot peening process is often the final surface treatment method for the mechanical components, which often have the high price or are employed at important positions in the equipment or system [1]. That reason explains why these products require high surface finishing after surface treatment. Therefore, to maximize the benefits of the shot peening process, the operating process parameters need be optimized.

The numerical simulations of the shot peening process are studied and reported in

many published papers [12, 13, 49, 50, 73]. In these studies, the surface target material is set as a flat surface. It is based on the fact that, in practice, prior to the shot peening process, the samples are polished to reduce the initial surface roughness. In addition, this assumption reduces the complexity of the simulation process. However, the flat surface somehow reduces the accuracy of the numerical simulation results and cannot be applied to consider the effect of the as-received surface roughness condition on the surface topographies of the shot peened samples.

In this chapter, a multiple-shot impact FEM model introduced in Chapter 5 was employed to validate with the experimental data conducted in Chapter 3. In addition, the original surface of the FEM model was created by using the data point coordinates of the as-received sample, which was collected by 3D scanning the surface of the as-received component. In this Chapter, the AISI 4340 high strength steel continued to be selected as a material for the numerical and experimental investigation of the effects of the shot peening process on the sample topography.

6.2. Experimental details

Commercial AISI 4340 high strength steel was selected as a material for both numerical and experimental study. The nominal chemical composition of the steel in weight % is C (~0.34), Si (~0.24), Mn (~0.51), Cr (~0.91) Ni (~1.54) and Mo (~0.25).

Figure 6-1 presents the flowchart of the numerical and experimental study to investigate the effect of shot peening process on the surface topography of the components. The test samples were cut from an ingot of 16mm diameter and were 10mm thick. To reduce the effect of the cutting process as well as the initial surface roughness of the as-received

components, prior to the shot peening experiment, the steel samples were polished using sandpapers with the grit size of 240, 600, 1000 and 1500.

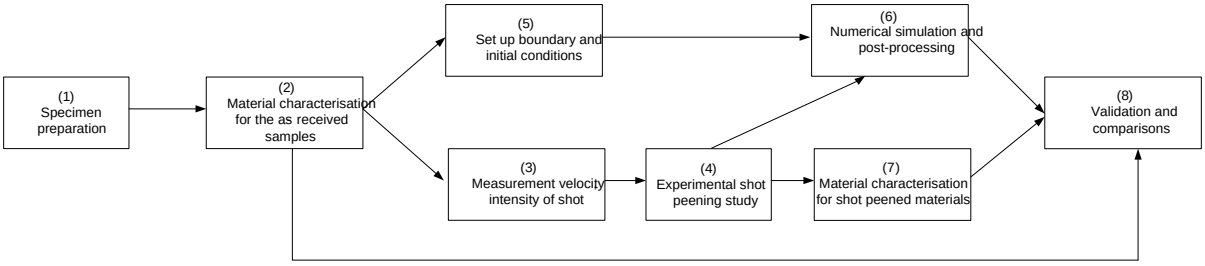

Figure 6-1. The flowchart of the numerical and experimental shot peening study.

A dog-bone sample was machined, and tested under uniaxial tensile test under displacement control of 0.1 mm/mm. The measured properties are Young's modulus of elasticity (E) 210 GPa, initial yield stress (σ_o) 1000 Mpa, and ultimate tensile strength (UTS) 1105 MPa. Density (ρ) of the steel is 7800 kg/m^3. These parameters are used as input parameters for FEM model. The specimens were mounted on the fixture and shot peened under various conditions with both single media S230 and S110 and a combination of these two media. The shot peening process parameters are shown in table 6-1.

The surface roughness and topography of the as-received and shot peened samples were studied using a surface profilometer (Taylor Hobson®, Talyscan 150). Five areal measurements per samples were performed to calculate the average surface roughness value e.g. arithmetical mean height of scale-limited S_a [42].

The residual stresses of the as-received and shot peened samples were measured using a Prism instrument (Stresstech®) with the help of the drill bits of 0.7874 millimeters (0.031 inch) in the diameter. It is an advanced hole-drilling equipment to measure residual stresses quickly and accurately with minimum surface preparation [41]. This method has a similar measuring mechanism with the conventional strain gage hole-drilling systems, it measures

changes in the part surface caused by the hole drilling and determines the previously existing residual stresses [39]. Nevertheless, this method can avoid time-consuming application of strain gages and large required areas for the measurement.

Table 6-1. Shot peening process parameters used in chapter 6.

Samples	Media type	Pressure (kPa)	Pressure (Psi)
S110-10	S110	68.9	10
S110-20	S110	137.9	20
S110-30	S110	206.8	30
S110-40	S110	275.8	40
S110-50	S110	344.7	50
S110-60	S110	413.7	60
S230-10	S230	68.9	10
S230-20	S230	137.9	20
S230-30	S230	206.8	30
S230-40	S230	275.8	40
S230-50	S230	344.7	50
S230-60	S230	413.7	60
DP-10-20	S230	68.9	10
	S110	137.9	20
DP-20-20	S230	137.9	20
	S110	137.9	20
DP-30-20	S230	206.8	30
	S110	137.9	20
DP-40-20	S230	275.8	40
	S110	137.9	20
DP-50-20	S230	344.7	50
	S110	137.9	20
DP-60-20	S230	413.7	60
	S110	137.9	20
As-received	NA	NA	NA

The random multiple-shot impact model was developed by using the commercial finite code LS-DYNA [51]. The input parameters were set up based on the measured results, such as E, ρ, σ_o, UTS. The dimension of the target was 2 x 2 x 1 mm and the shot peened area was 1 x 1 mm. In this model, the multiple shots impacted onto the kinematic hardening model. The details of this model were presented in Chapter 5.

6.3. Results and discussions

Prior to the shot peening process, to determine the shot velocity at different pressures in the range of 68.9 to 413.7 kPa, a shot Meter G3 – partial velocity sensor equipment was employed at a distance of 150 mm from the outlet of the pressure nozzle. This result provides a relation between the experimental operation parameter (e.g. pressure) and the input numerical parameter (e.g. velocity) of the shot. In addition, the standard Almen test A strip, Almen gauge and holding fixture were also used to determine the shot intensity.

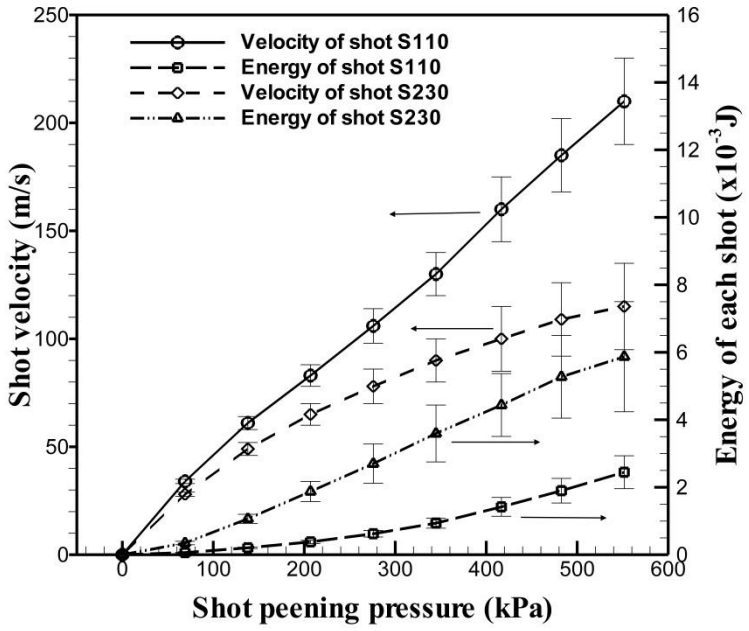

(a)

Figure 6-2. The velocity of shot and dynamic energy of each S230 and S110 steel shot measured under different shot peening pressures

Figure 6-2 shows the velocity and intensity of shots S230 and S110 as a function of peening pressure. Increasing the nozzle pressure increases the shot velocity and thereby peening intensity. This figure also shows that the smaller media S110 has a higher velocity but is lower in intensity compared with media S230. The reason is that the larger size media has a higher dynamic energy due to its mass in the energy equation $E = ½\ mv^2$, where m and v are mean mass and mean velocity of each shot.

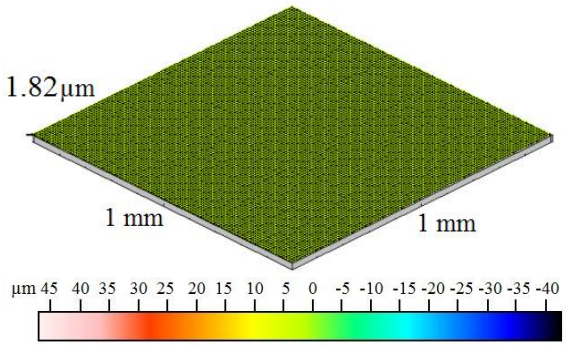

(a)

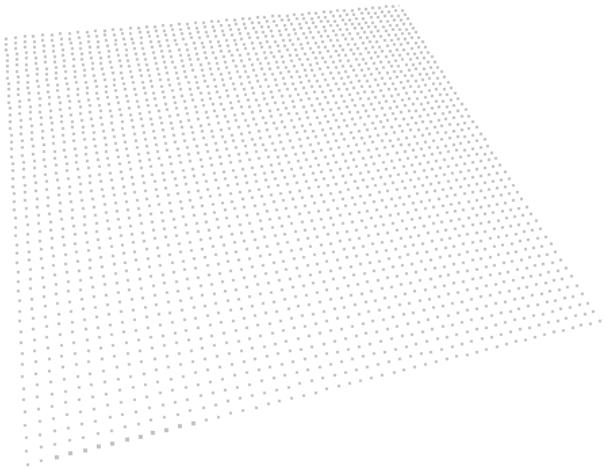

(b)

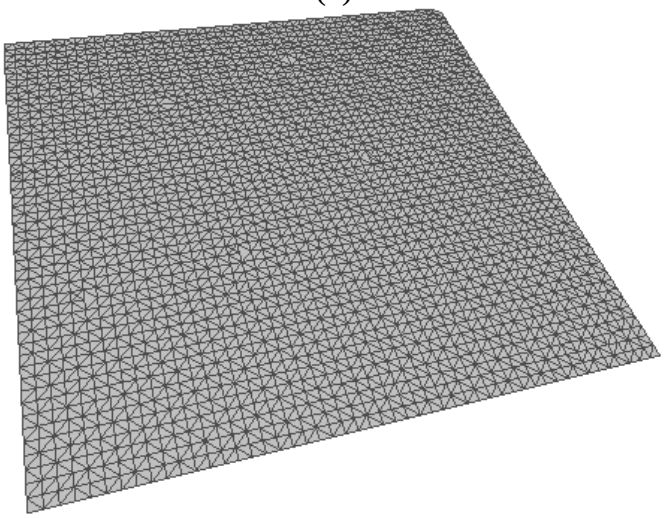

(c)

Figure 6-3. (a) Surface topography, (b) Surface layer point cloud of as-received AISI 4340 steel sample and (c) Surface reconstruction from the point clouds for the FEM model.

Figure 6-3*a* illustrates the surface topography of the as-received sample. It is shown that the surface is smooth after polishing with the arithmetical mean height of scale-limited

surface S_a = 0.5 ± 0.05 µm. The measurement result from the stylus scan also provides the three-dimensional coordinates of points on the as-received surface. These point clouds are presented on figure 6-3*b*, with the help of Meshlab software and were meshed into a free surface (figure 6-3c). Finally, this free surface was developed to be a three-dimensional block and applied as a target material for the shot peening process (figure 6-6).

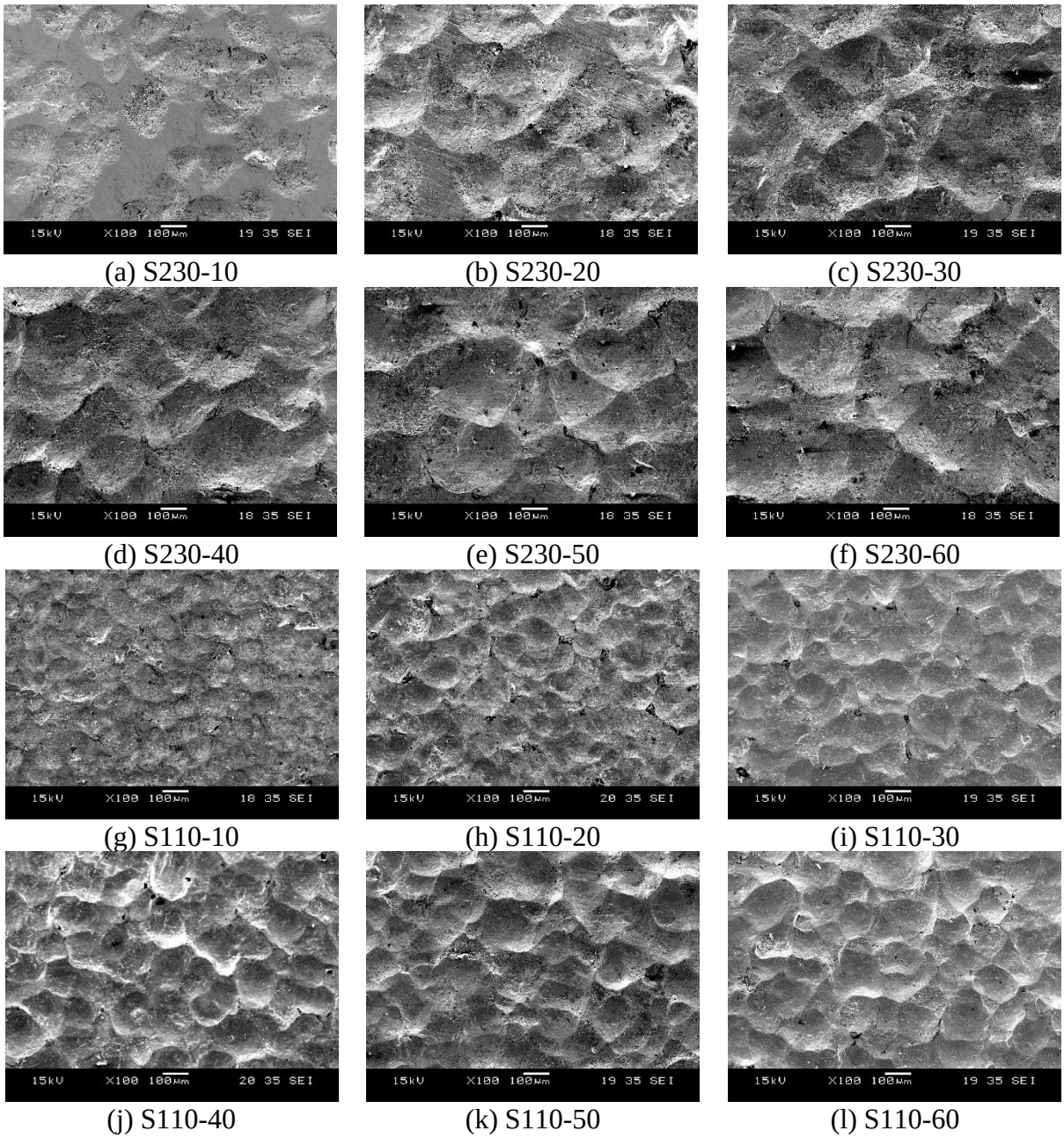

(a) S230-10 (b) S230-20 (c) S230-30

(d) S230-40 (e) S230-50 (f) S230-60

(g) S110-10 (h) S110-20 (i) S110-30

(j) S110-40 (k) S110-50 (l) S110-60

Figure 6-4. Surface morphologies of shot peened AISI 4340 steel samples.

Figure 6-4 depicts the surface morphologies of shot peened samples under various pressures with media S230 and S110. The figure indicates that the higher pressure and larger media size can cause larger and deeper indentations on the target material. It is observed that at 68.9 kPa and 137.9 kPa, the surface of shot peened specimens did not achieve full coverage (≥98%). The full coverage is obtained at 206.8 kPa for S230. In the case of the treatment with media S110, the surface can achieve about 95-98% at 68.9 kPa. This result provides an important information to calculate the required number of shots which should be used. The velocity of the shots S230 and S110 in the simulation work were initial set up based on the measured velocity of shots at 206.8 kPa and 68.9 kPa respectively. In the experimental work, the shot peening time and mass flow rate are kept constant at 20 seconds and 3 kg/s, respectively under different pressures. Hence, in the FEM model, the number of shots for media were also maintained under various velocities. This explains why the initial condition is important.

To simulate the shot peening process with multiple-shot random impact model, the number of shots and their coordinates are determined. The proposed method to estimate the number of shots and their locations were presented in detail in chapter 5 [106, 107]. In the case of the shot peening process with media S230, the velocity of shot S230 with a mean diameter of 600 μm at a pressure of 206.8 kPa is 65 ± 5 m/s. Therefore, 65 m/s shot velocity was used in the simulations. The results show that the number of shots required to achieve the full coverage (≥98%) of 98.05%, 98.11%, 98.14%, 98.08% and 98.02% in five consecutive repeated runs were 69, 60, 75, 64 and 75 respectively. Figure 6-5*a* presents an example of the coordinates of the 69 impact shots employed to obtain full coverage of 98.05%. A similar process was used with the media S110. The number of shots required to achieve the full coverage of 98.08%, 98.01%, 98.03%, 98.05% and 98.07% in five consecutive repeated runs

were 259, 268, 250, 265 and 255 respectively. Figure 6-5*b* illustrates an example of the coordinates of the 259 impacts employed to obtain the full coverage of 98.08%.

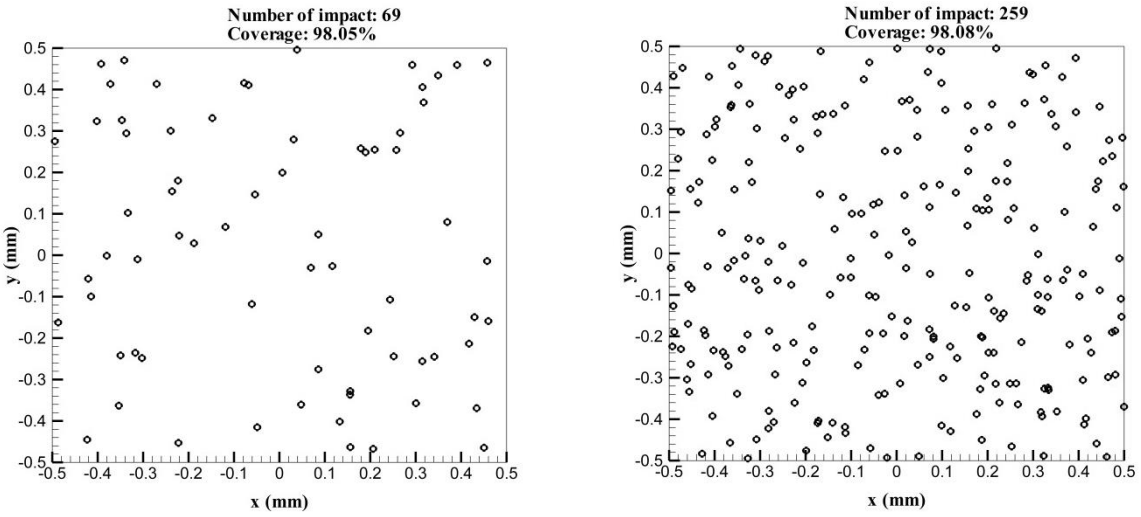

(a) (b)

Figure 6-5. Coordinates of impact shots employed to obtain full coverage (>98%): (a) S230 media and (b) S110 media.

The shot peening time and mass flow rate in the experiment were kept constant under different pressures, therefore in the numerical study, the number of shot and their coordinates were also the same under various shot velocities. To obtain an average surface roughness value, at each pressure, five measurements were conducted in the experiment. Hence, in the numerical study, under each velocity, the calculation was performed five times with five different impact models having a different number of shots and their coordinates. Five multiple-shot impact models for each media were used to perform the process e.g. media S230 used 69, 60, 75, 64 and 75 impacts and media S110 employed 259, 268, 250, 265 and 255 impacts. Figures 6-6*a* and *b* present an example of one multiple-shot impact model for each media S230 and S110, respectively with an assumption that the interactions between shots were ignored to reduce the complexity of the calculation.

To simulate the double shot peening, the two media were used in a multiple-shot impact model (figure 6-6c), in which the smaller shot was set above the larger shot to make sure that the S110 shot impacts only when all of the media S230 impact the target.

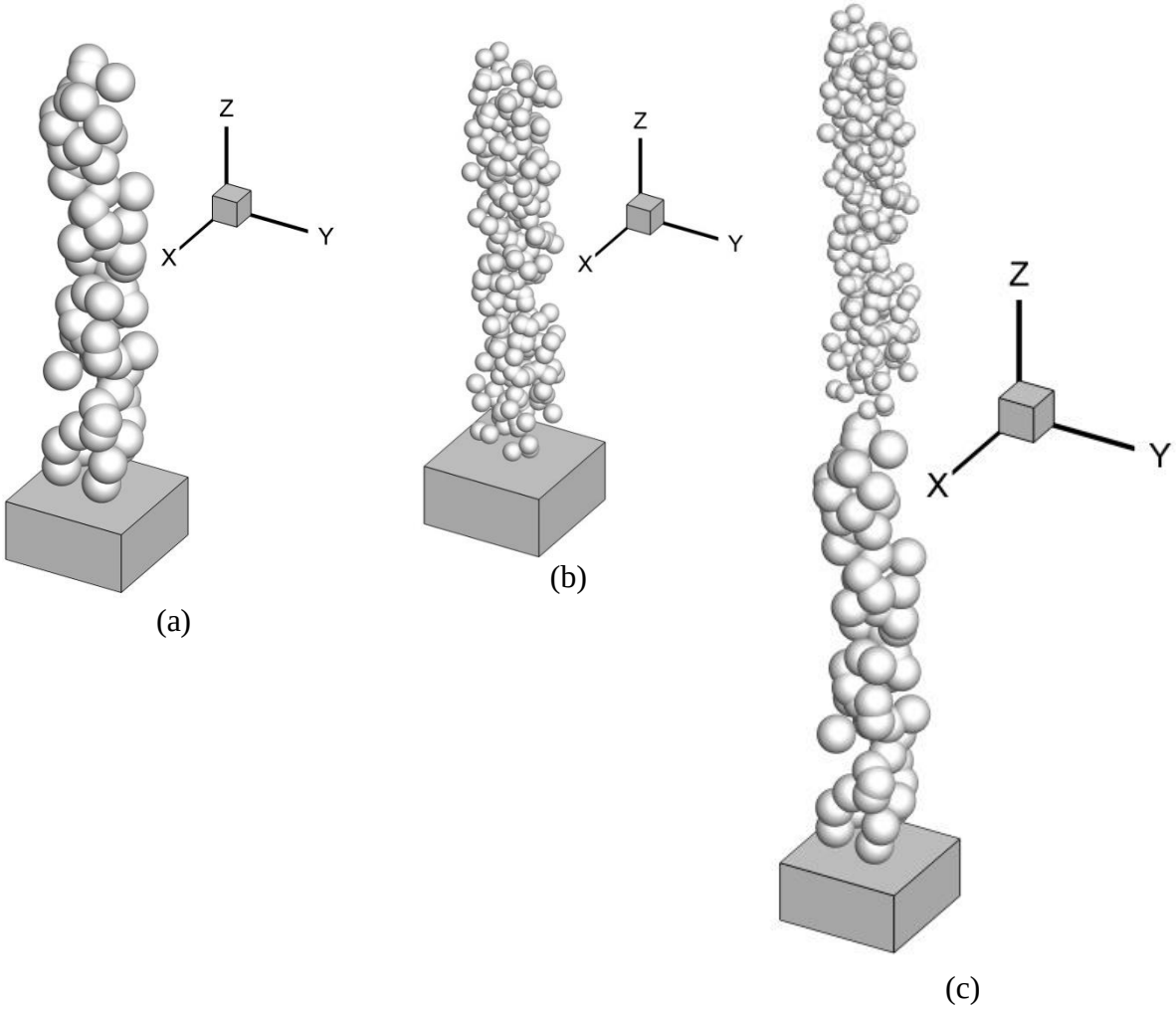

Figure 6-6. Finite element model of multiple-shot impacts: (a) S230 media, (b) S110 media and (c) Double peening process.

Figures 6-7, 6-8 and 6-9 depict the surface topography of the shot peened AISI 4340 steel samples investigated via simulations (left) and experiments (right) with the media S230, S110 and double shot peening respectively. It can be seen that, at the pressure of 68.9 kPa, the surface of material treated with S230 has partial coverage, with about 60±5% in both numerical and experimental works (figures 6-7*a* and *b*). At 137.9 kPa (figures 6-7*c* and d), the indentations caused by the shots are deeper and wider so the surface becomes rougher

compared with the process treated at 68.9 kPa. Figures 6-7*c* and *d* also present that the coverage increases to about 80±5%. It can be concluded that the high velocity induced by the high pressure can increase the coverage of the shot peened components (under the same shot peening time). When the pressure was increased to 206.8 kPa (figures 6-7*e* and *f*), the larger and deeper indentations make the surface further rougher and also increase the coverage for the samples (about 98%). At higher pressure, ranging from 275.8 to 413.7 kPa (figures 6-7*g-l*), the treated samples archived full coverage (even higher than 100%).

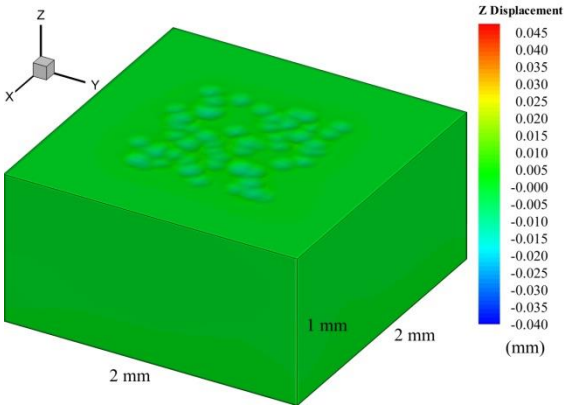

(a) S230-10

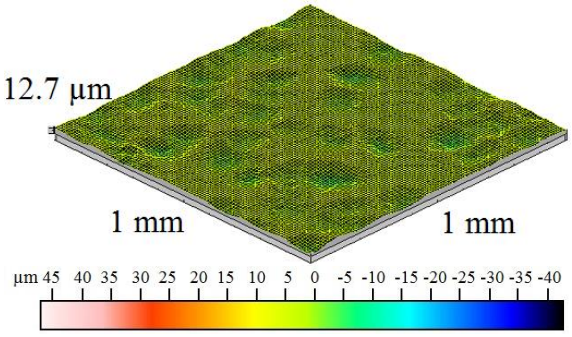

(b) S230-10

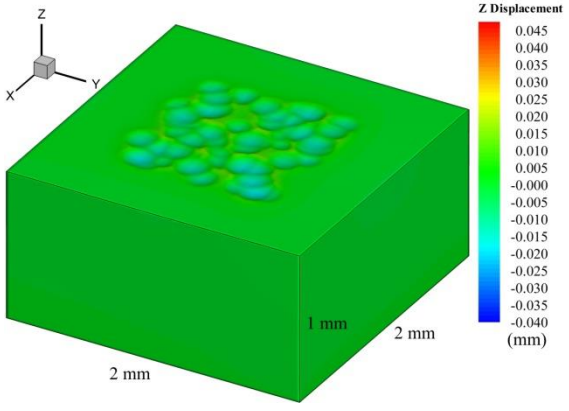

(c) S230-20

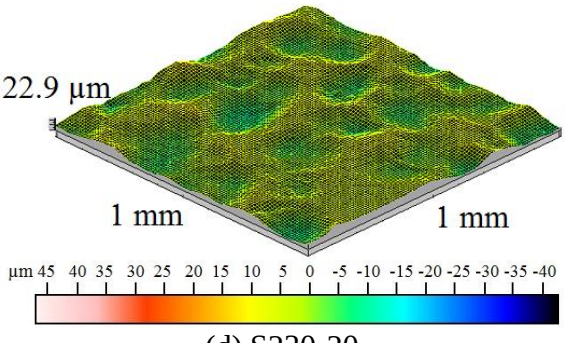

(d) S230-20

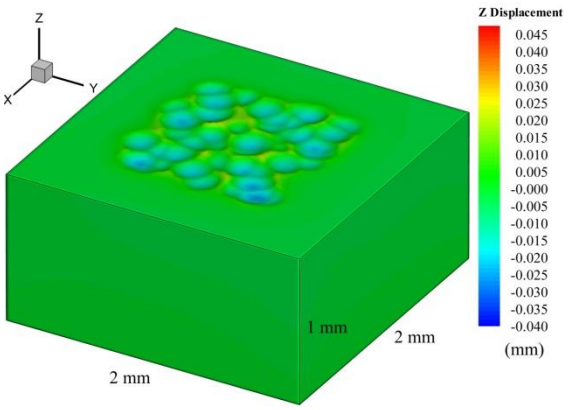

(e) S230-30

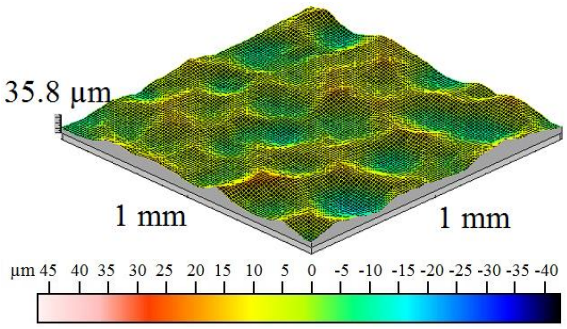

(f) S230-30

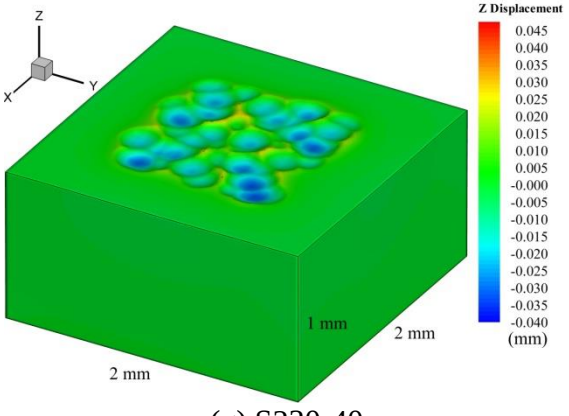

(g) S230-40

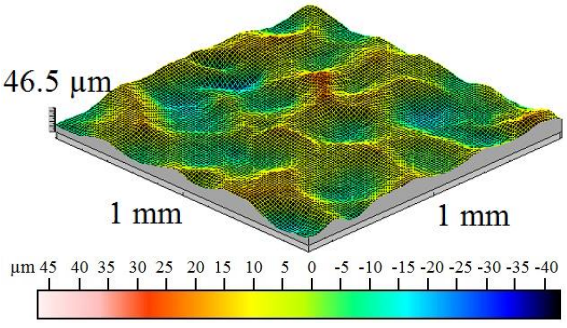

(h) S230-40

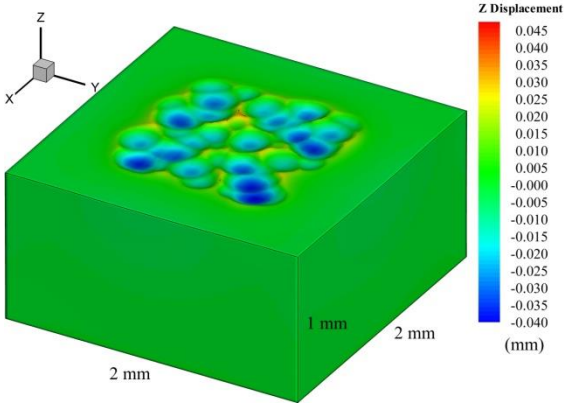

(i) S230-50

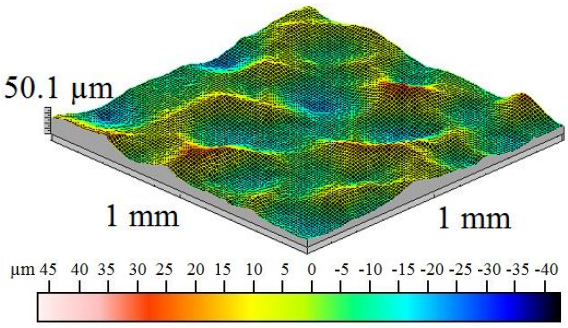

(j) S230-50

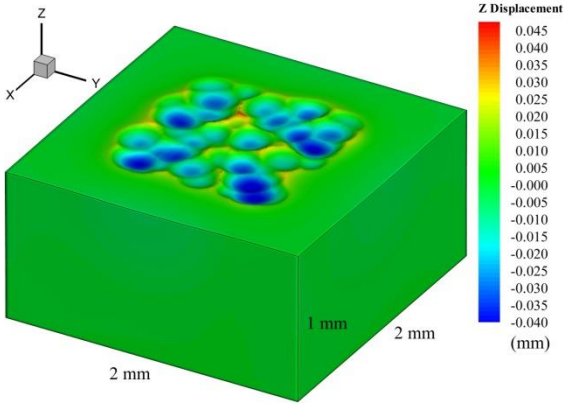

(k) S230-60

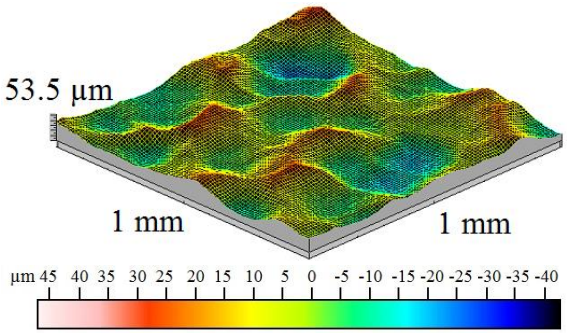

(l) S230-60

Figure 6-7. Surface topographies of shot peened AISI 4340 steel sample shot peened by S230 media (left: numerical study and right: experimental result).

The topography of the shot peened samples treated with media S110 (figure 6-8) have similar trend as with S230 e.g. the higher velocity or pressure causes the larger and deeper indentations on the target surface leading to rougher surface. Besides, 95% to 98% coverage achieved even at the low pressure of 68.9 kPa and full coverage obtained at 137.9 kPa.

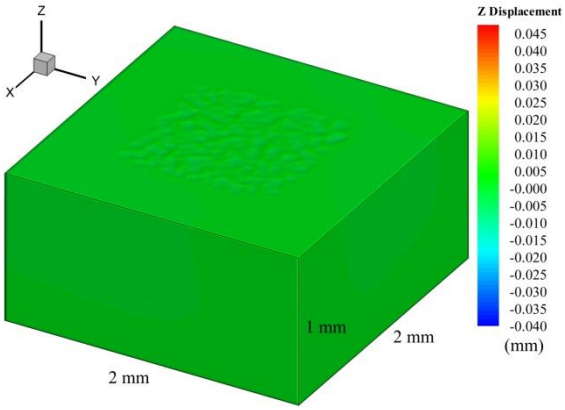

(a) S110-10

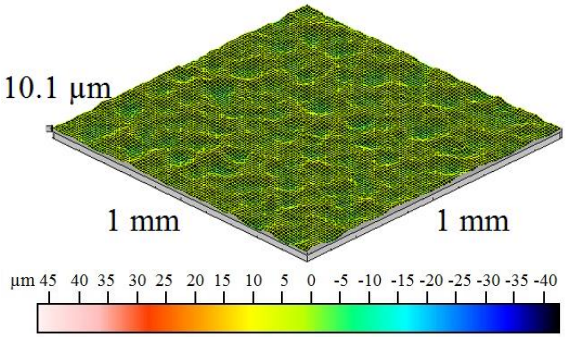

(b) S110-10

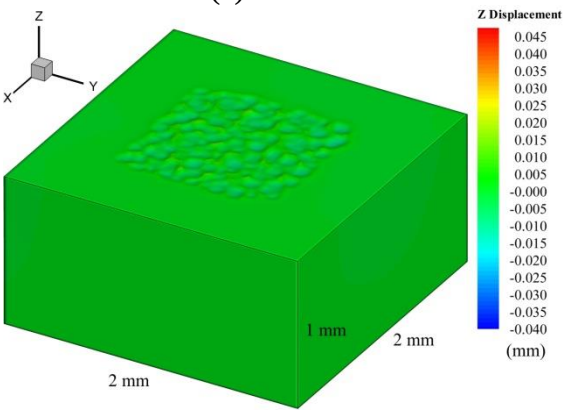

(c) S110-20

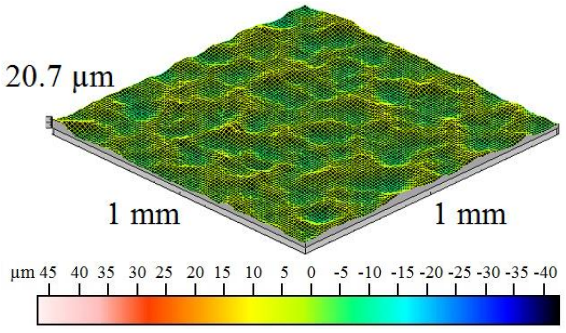

(d) S110-20

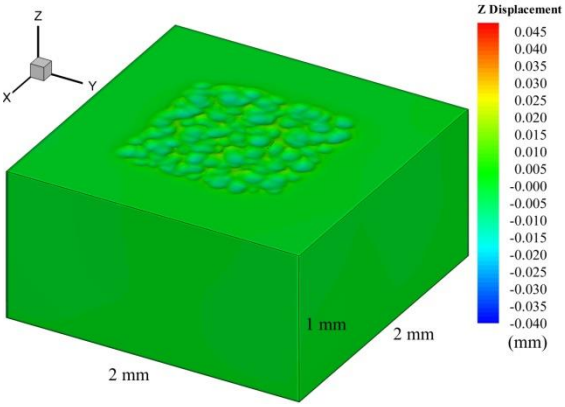

(e) S110-30

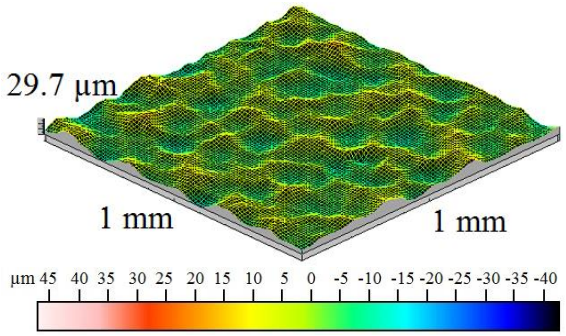

(f) S110-30

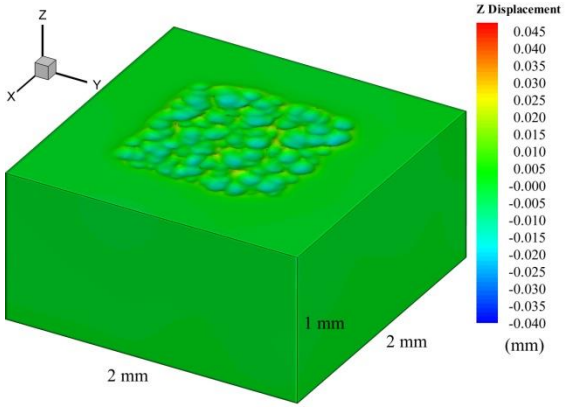

(g) S110-40

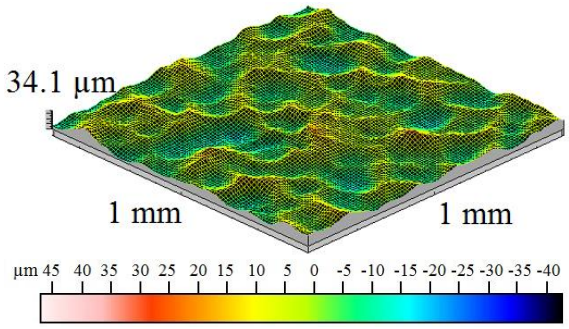

(h) S110-40

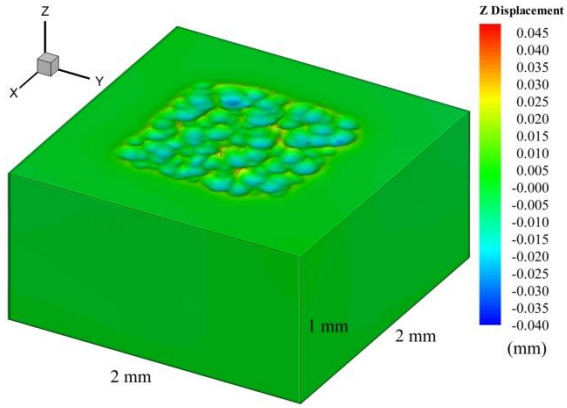

(i) S110-50

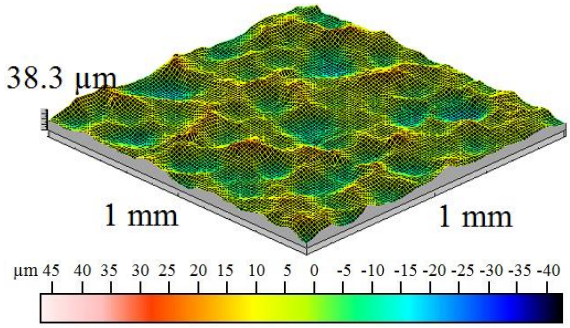

(j) S110-50

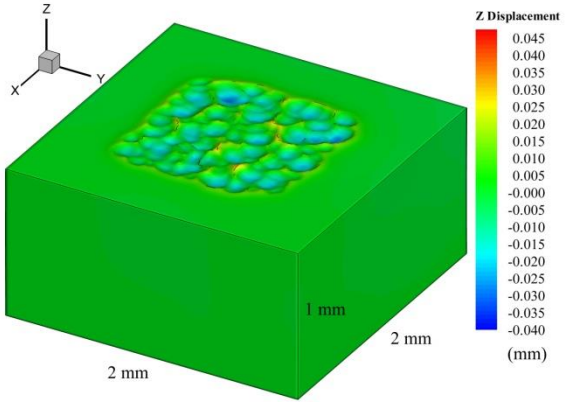

(k) S110-60

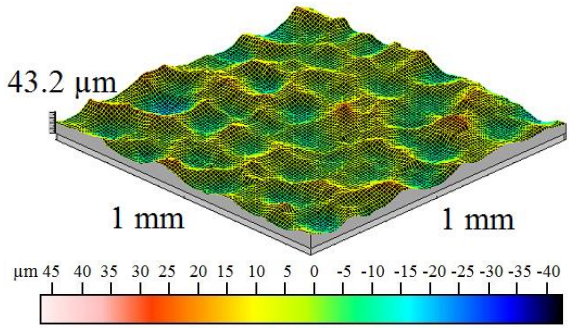

(l) S110-60

Figure 6-8. Surface topographies of shot peened AISI 4340 steel sample shot peened by S110 media (left: numerical study and right: experimental result).

In the double shot peening process (figure 6-9), the secondary shot peening process with media S110 was used to after treating them with media S230, to reduce the high surface roughness caused by the previous treatment. The secondary shot was applied at a pressure of 137.9 kPa corresponding to the shot velocity of 61 m/s. Figures 9 *a-b* and 9 *c-d* show that full coverage of the double peened samples are achieved, as the media S110 itself can make the

target surface achieve full coverage at 137.9 kPa. Up to 206.8 kPa, the peening effect of S230 is low so the surface of the sample becomes rougher after applying the secondary shot peening. Consequently, it can be concluded that the secondary shot peening process is not necessary. However, when the pressure is higher than 275.8 kPa, the high peaks caused by the high velocity shot impacts in the previous treatment are lower and the surface becomes smoother after the second process. Hence, the secondary shot peening process becomes polishing to reduce the surface roughness.

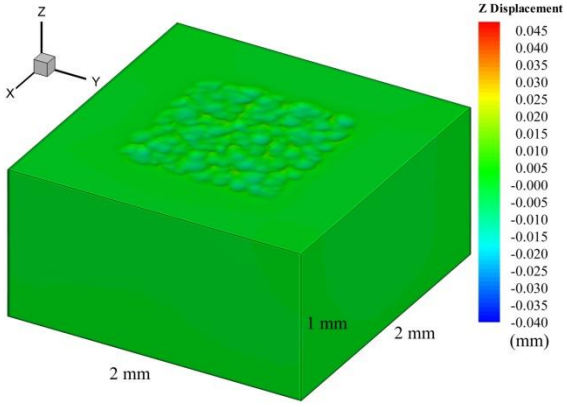

(a) DP-10-20

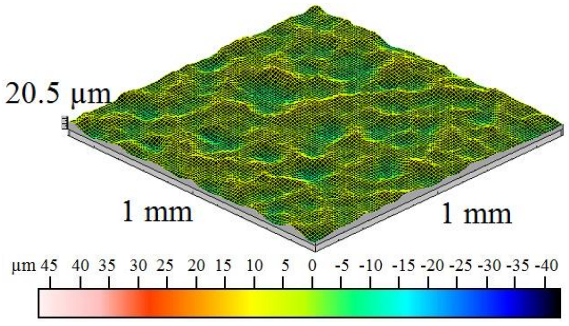

(b) DP-10-20

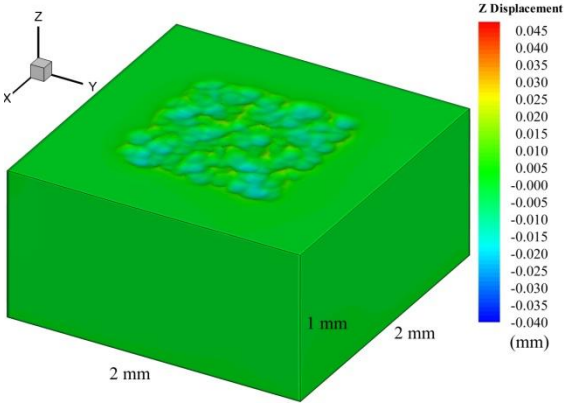

(c)DP-20-20

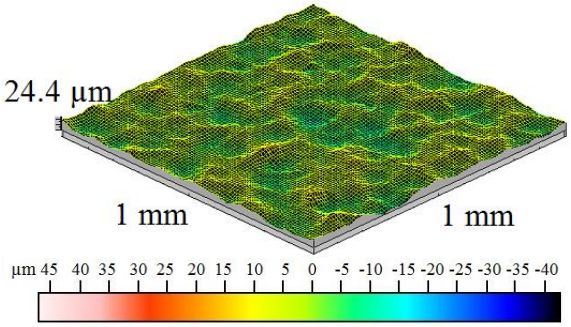

(d) DP-20-20

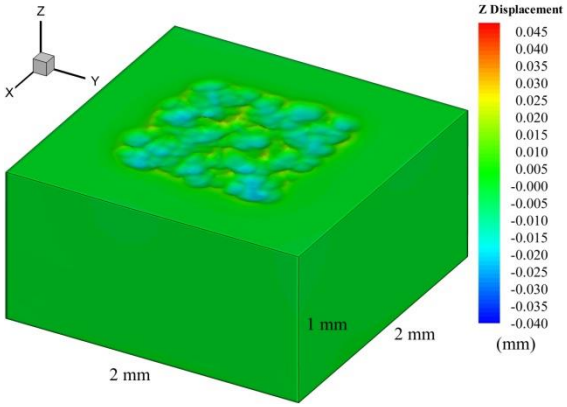

(e) DP-30-20

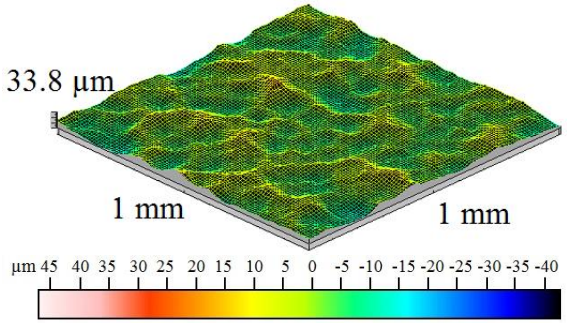

(f) DP-30-20

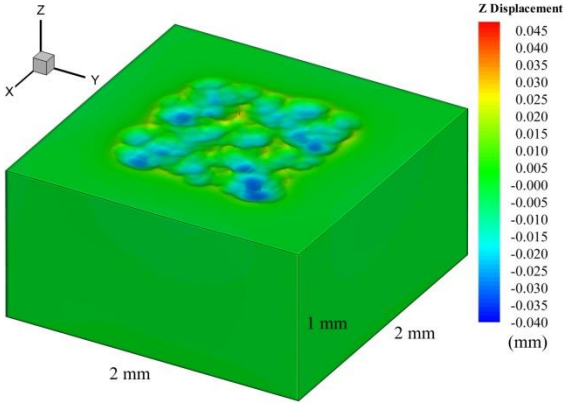

(g) DP-40-20

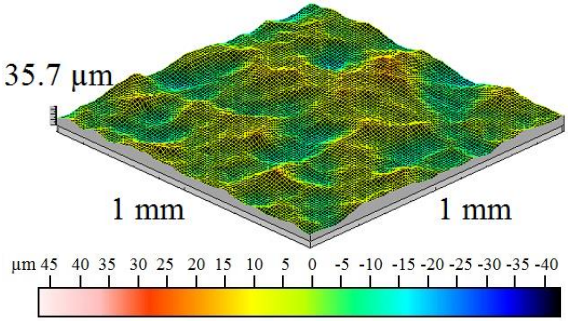

(h) DP-40-20

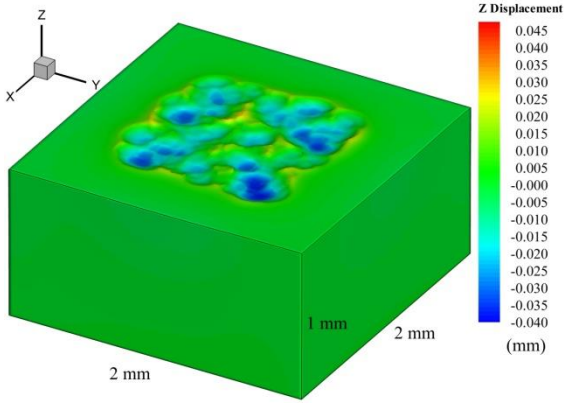

(i) DP-50-20

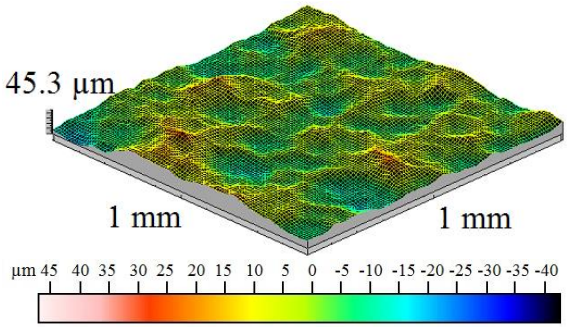

(j) DP-50-20

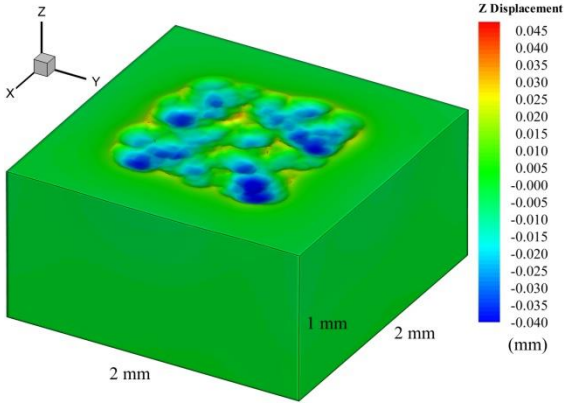

(k) DP-60-20

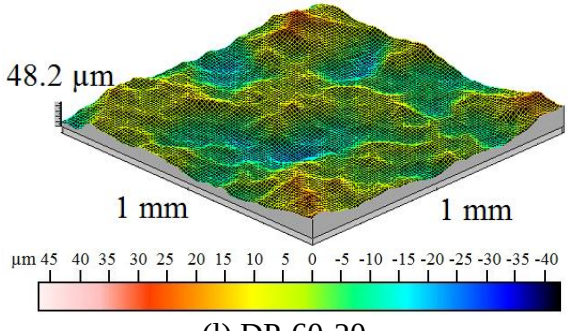

(l) DP-60-20

Figure 6-9. Surface topographies of shot peened AISI 4340 steel sample shot peened by double shot peening process (left: numerical study and right: experimental result).

Figure 6-10 shows the arithmetical mean height of scale-limited surface (S_a) of the shot peened samples. There is a good agreement with the morphologies (figure 6-4) and topographies (figures 6-7, 6-8, and 6-9) that the increment of shot pressure or shot velocity results in increased surface roughness. It also can be concluded that at low pressures, the double shot peening process is not recommended as it cause an unexpected side effect on the surface roughness of the previously treated samples. However, at higher pressures, it polishes the earlier peened surface. Therefore, the secondary shot peening process should be selected wisely to obtain the benefits of the double shot peening process.

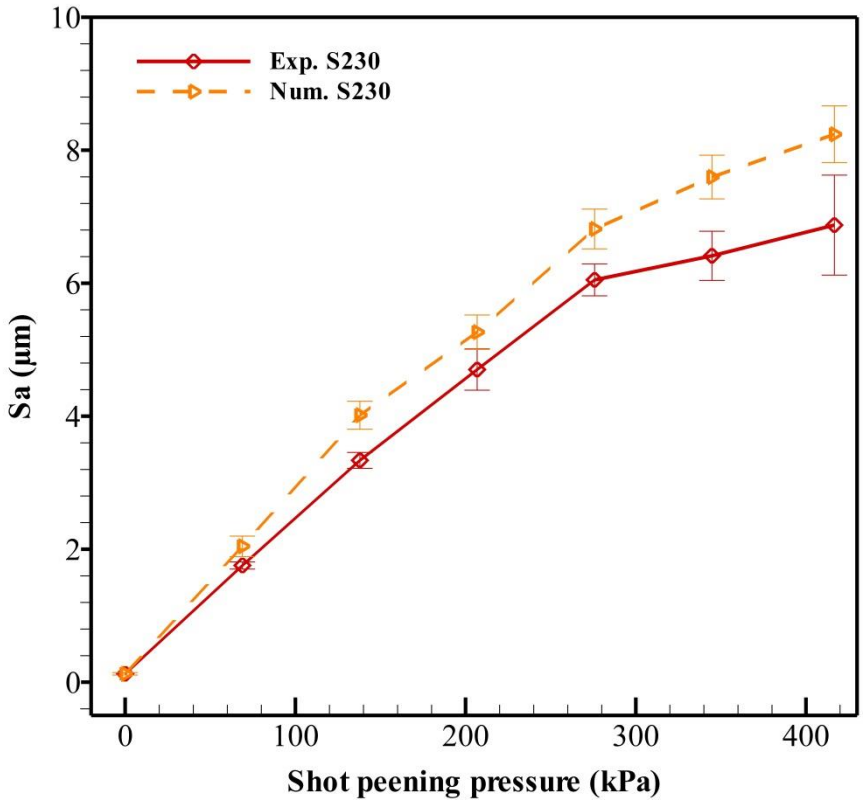

(a) S230

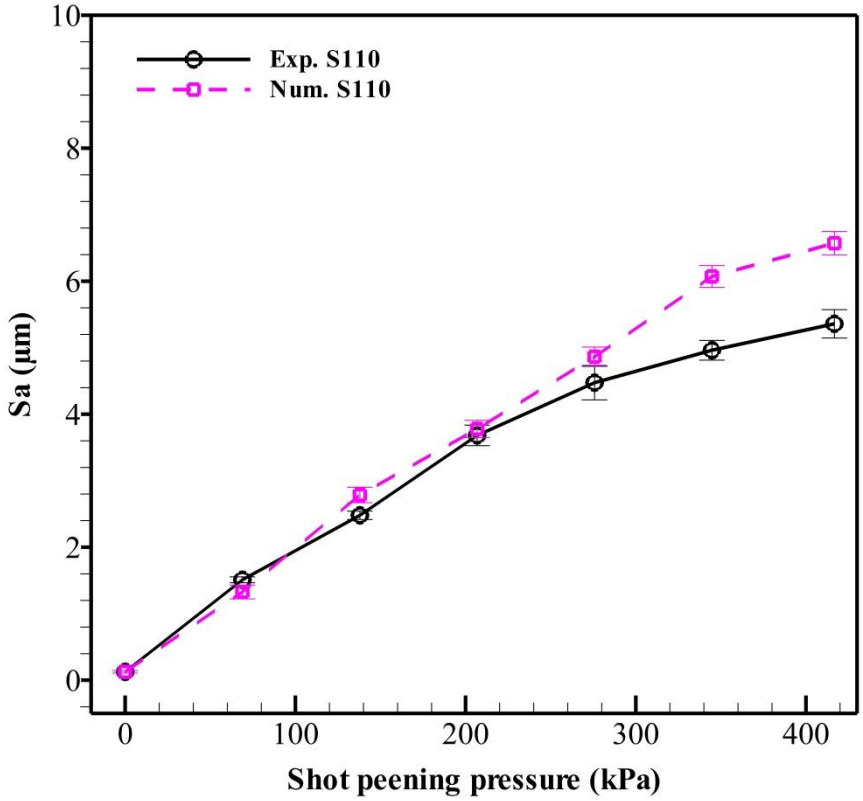

(b) S110

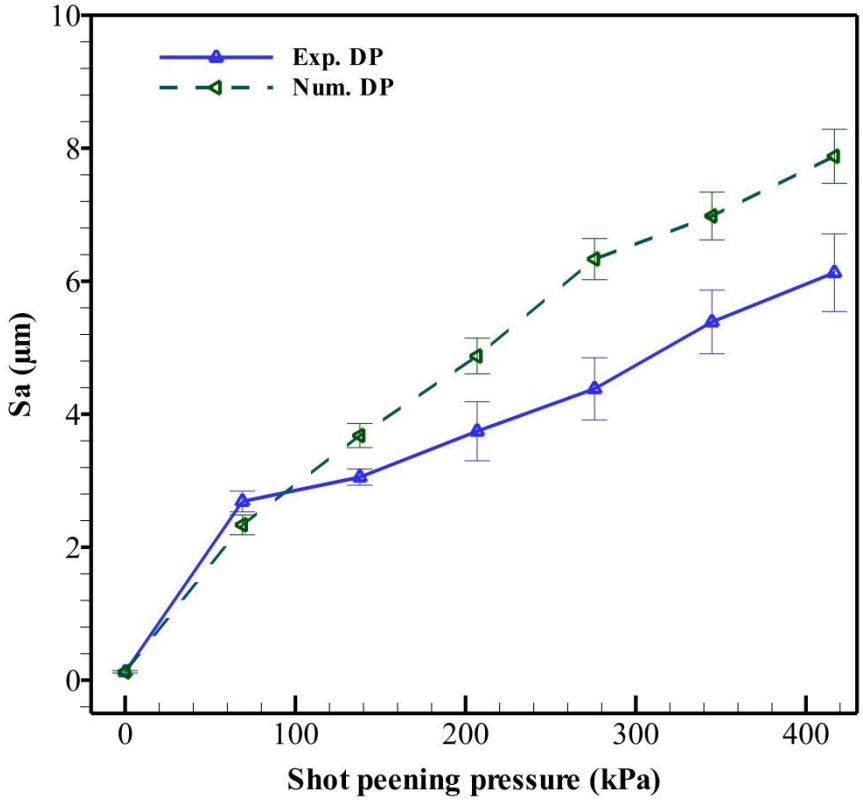

(c) Double shot peening

Figure 6-10. The arithmetical mean height of scale-limited surface S_a of the shot peened AISI 4340 steel samples as a function of shot peening pressure.

Figures 6-10*a-c* also compares the arithmetical mean height of scale-limited surface (S_a) in the numerical study and experimental work as a function of pressures. The results show that S_a value increases gradually with pressure in both cases. However, under the same pressure conditions, the measured S_a value (in the experimental study) is always smaller than that of calculated S_a value (in the simulation). The discrepancy could due to neglecting the temperature effect and considering the shots as rigid in the numerical simulations.

Figures 6-11 to 6-14 show the distribution of the residual stresses within the material under various shot peening conditions. The residual stresses are compressive on the surface and are maximum in the sub-surface and then reduce to balancing tensile stresses into the depth, finally turning to the neutral value. The depth at which maximum compressive stress occurs depends on the shot peening process parameters. Studies on of the fatigue life of the shot peened material [103, 108] reveals that the initial crack usually starts from the point located at the sub-surface close to the free surface of the as-received samples. The primary failure initiates at the weakest region of the material under fatigue testing [103, 104, 108]. Therefore, the presence of the compressive residual stresses from the surface to a depth of 80 to 350 μm (depending on the shot peening conditions) shifts the nucleation crack location to the surface. As a consequence, when the weakest link occurs on the free surface of the shot peened material, the effect of the surface texture of the material on the fatigue life becomes more significant. In this case, the indentations caused by the shot impacts on the material become a preferable condition for the initial fatigue failure. The residual stresses of the as-received sample is almost zero, so under the deformation process, the compressive residual stress formed in the subsurface results in the formation of the tensile stresses in the rest of the material for equilibrium.

Figures 6-11 and 6-14*a* illustrate the distribution of the residual stresses in the subsurface of the S230 shot peened samples. The depth of the compressive residual stress layer increases with the pressure, starting from about 140 µm at a pressure of 68.9 kPa to 350 µm at a pressure of 413.7 kPa. It can be seen that, although the coverage of the shot peened samples are not full i.e. about 60% and 80% at the low pressure of 68.9 kPa and 137.9 kPa, the layers at the depth of 150µm and 200 µm are fully compressive. Due to the random nature of the peening process, the residual stresses are not uniform across the section, i.e. the variation is with ± 50 MPa. Good agreement between the figures 6-11 and 6-14*a*, which is the depth of the compressive stress zone, increases the shot peening pressure. It is also noted that the maximum value of the compressive residual stress is a function of the shot velocity is 65% to 85% of initial yield stress.

Figures 6-12 and 6-14*b* show the distribution of the residual stresses within the shot peened material under various pressures with media S110. A similar trend can be seen in the treated samples, i.e. the depth of the compressive stress layer increases with the increment in pressure, from 80 µm to 200 µm at the pressure of 68.9 kPa and 413.7 kPa respectively. The results also reveal that the depth of the compressive stress zone of the S230 treated sample is about two times deeper than that of the S110 peened material at the same peening pressure (note that the diameter of the media S230 is twice that of S110). In the case of the maximum compressive stress value, it can be concluded that the shot size has an effect on this value under the same shot peening pressure.

Comparing figures 6-14*a* and 6-14*b* displays that, although the depth of the compressive stress layer in the subsurface of S230 shot peened samples are two times larger, the compressive stress at the surface and subsurface near the free surface are smaller than

S110. It also was reported that the compressive stress has more significant influence on the fatigue life of sample when it exists near the surface [103, 108].

Therefore, it can be concluded that distribution of the residual stresses has three important parameters i.e. the depth of compressive stress layer, the maximum compressive stress value and the compressive stress value in the subsurface which is near the free surface. The treatment with the larger media results in the deeper compressive residual stress zone but in the case of the last factor the smaller media gives the better result. It can be seen that the shot peening pressure and media size have a significant effect on the maximum compressive stress value.

The results reported in this paper suggest that the media S230 can introduce up to a two times deeper the compressive stress zone in the subsurface of the material but the smaller media S110 can induce higher compressive stresses at the surface and subsurface near the free surface of the material. In addition, the surface finishing of S110 shot peened material has an average areal roughness parameter S_a lower than that of S230. Therefore, it is possible to use two media S230 and S110 in the double shot peening process to achieve the combined effects. Comparing figures 6-11 and 6-13 shows that on the plane y = 0, the distribution of the residual stresses of the double shot peened material is more uniform. In addition, comparing figures 6-14*a* and 6-14*c* shows that the secondary process makes the compressive stress layer to be slightly deeper but this parameter is not the main purpose of this method. Instead, the secondary shot peening can induce the compressive stress value at the surface and subsurface near the free surface more largely, especially in the cases of pressures ranging from 137.9 kPa to 275.8 kPa. As a consequence, the prediction can be made that the fatigue life of the double shot peened samples will be higher than that of S230 under these shot peening pressure conditions.

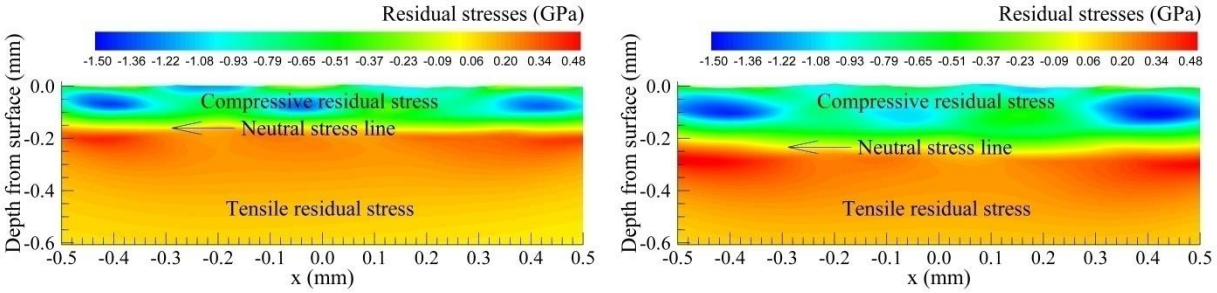

a. S230-10

b. S230-20

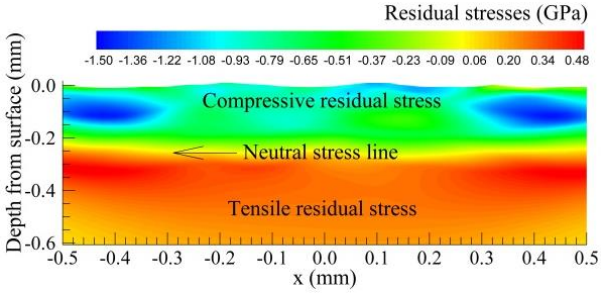

c. S230-30

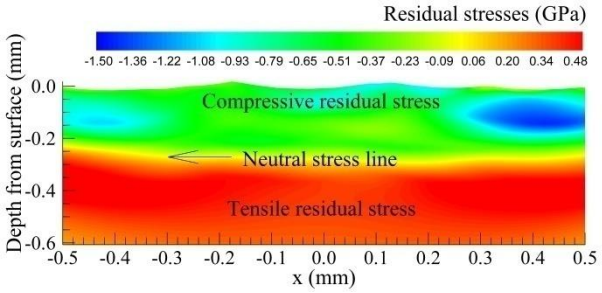

d. S230-40

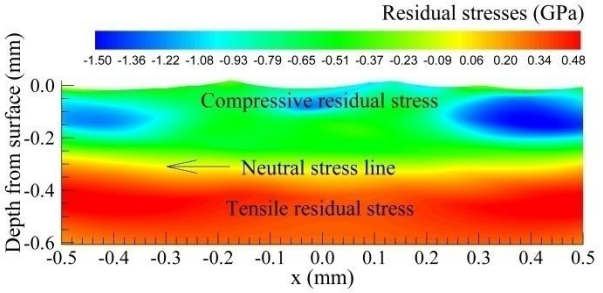

e. S230-50

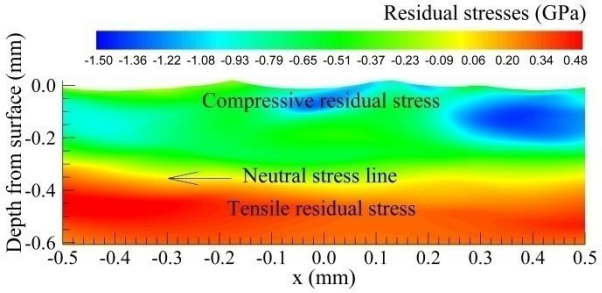

f. S230-60

Figure 6-11. Residual stress distribution of the S230 shot peened samples on plane y = 0 under various shot peening pressures.

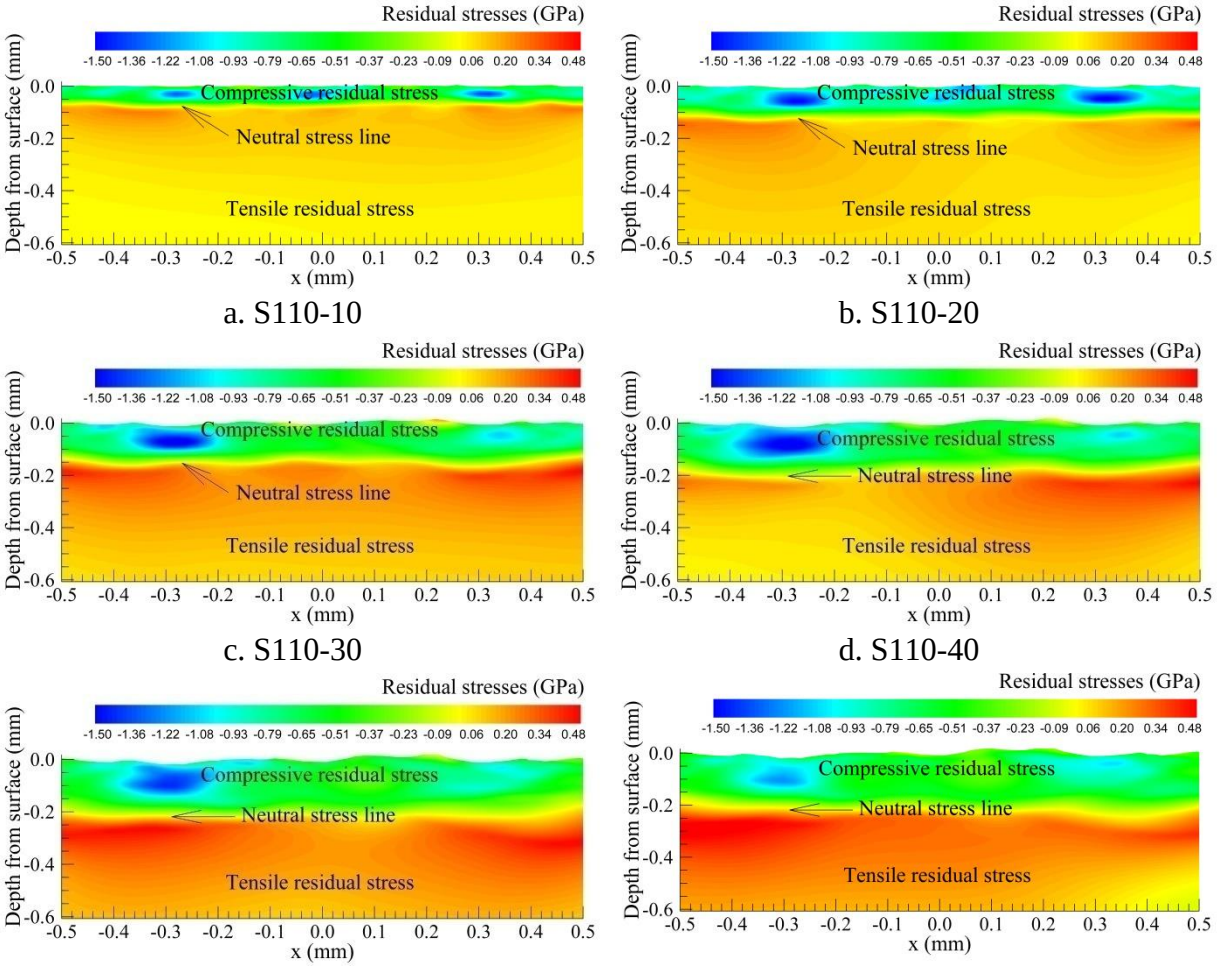

a. S110-10 b. S110-20

c. S110-30 d. S110-40

e. S110-50 f. S110-60

Figure 6-12. Residual stress distribution of the S110 shot peened samples on plane y = 0 under various shot peening pressures.

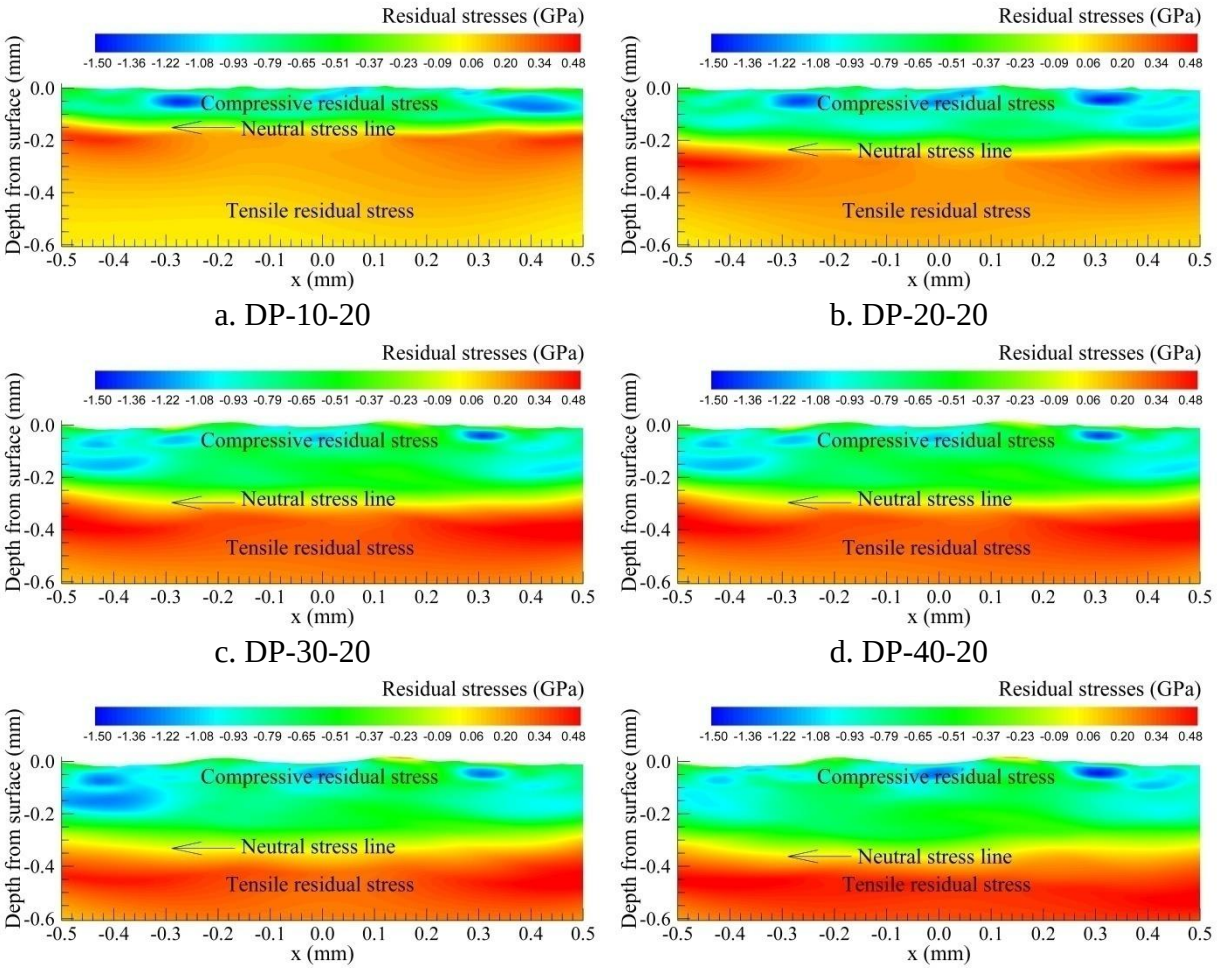

a. DP-10-20 b. DP-20-20

c. DP-30-20 d. DP-40-20

e. DP-50-20 f. DP-60-20

Figure 6-13. Residual stress distribution of the double shot peened samples on plane y = 0 under various shot peening pressures.

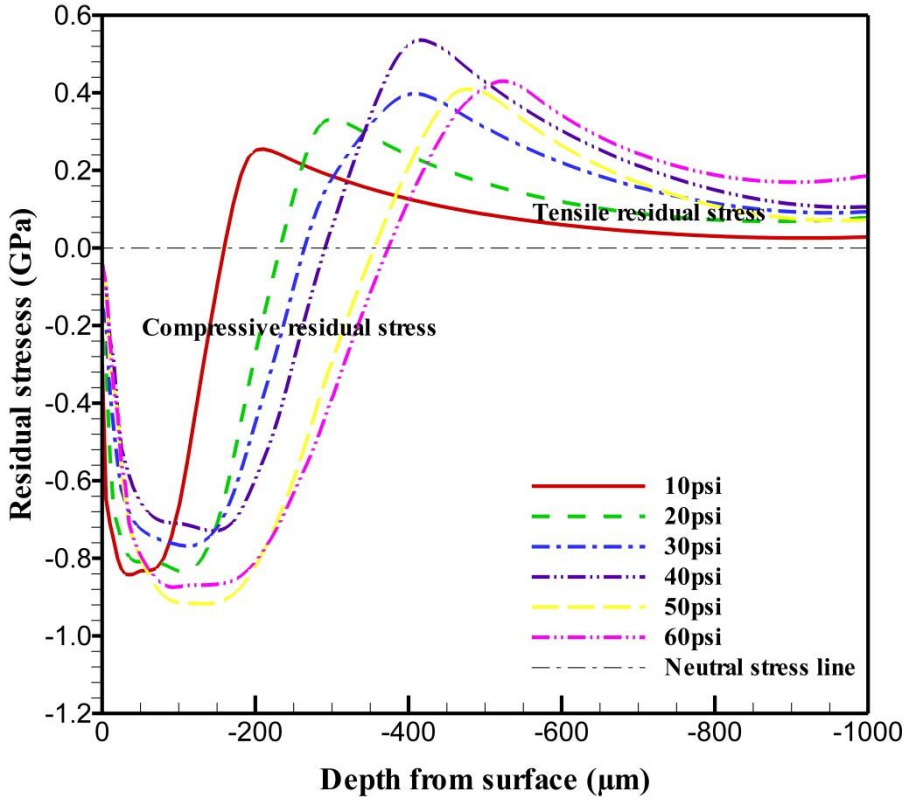
Residual stresess (GPa)
0.6
0.4
0.2
0.0
-0.2
-0.4
-0.6
-0.8
-1.0
-1.2
0
-200
-400
-600
-800
-1000
Depth from surface (μm)
Tensile residual stress
Compressive residual stress
10psi
20psi
30psi
40psi
50psi
60psi
Neutral stress line

(a) S230

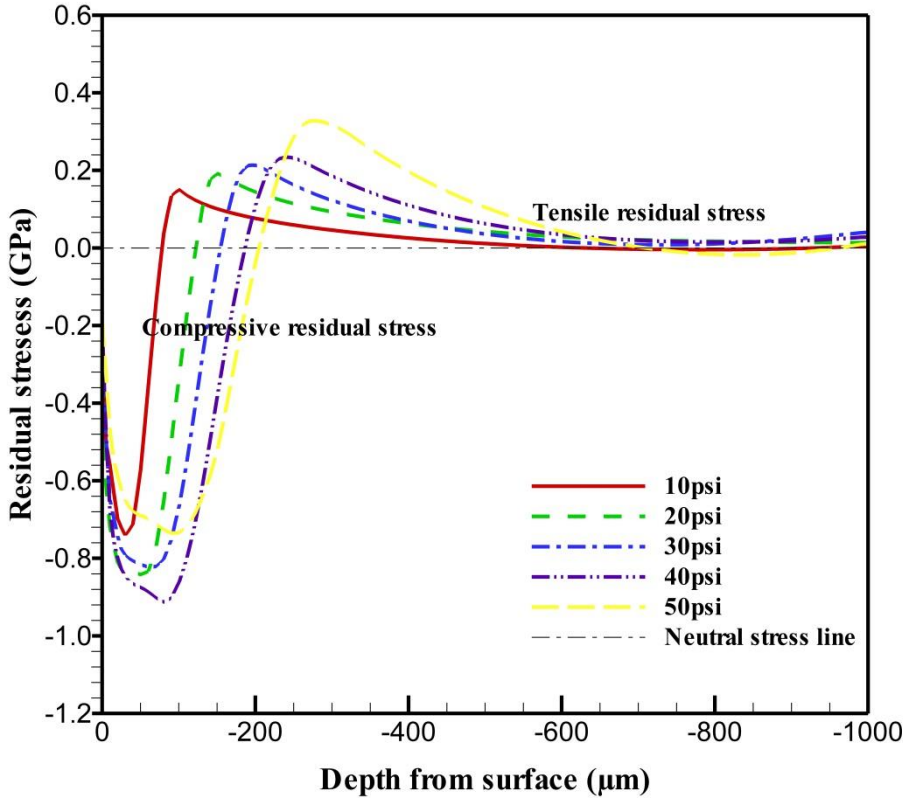
Residual stresess (GPa)
0.6
0.4
0.2
0.0
-0.2
-0.4
-0.6
-0.8
-1.0
-1.2
0
-200
-400
-600
-800
-1000
Depth from surface (μm)
Tensile residual stress
Compressive residual stress
10psi
20psi
30psi
40psi
50psi
Neutral stress line

(b) S110

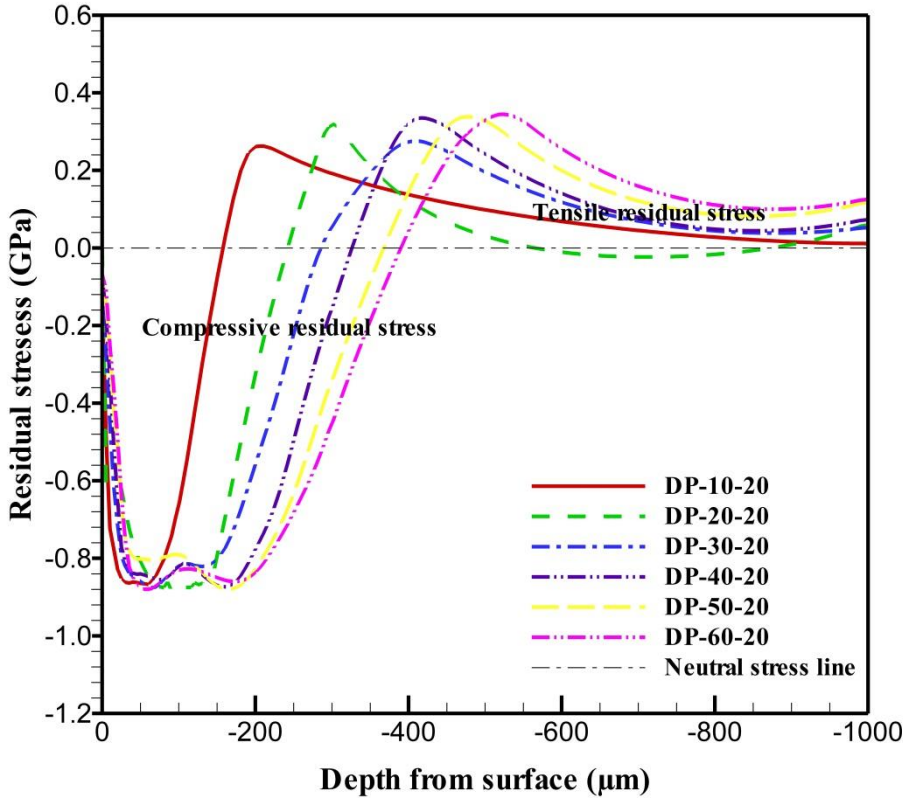

(c) Double peening

Figure 6-14. Average longitudinal residual stress distribution under various shot peening pressures in the numerical study: (a) S230 shot peened samples, (b) S110 shot peened samples and (c) Double shot peened samples.

Figure 6-15 illustrate the average longitudinal residual stress measured under various shot peening pressures in the experimental study. It can be seen that, the tensile residual stresses are presented in the subsurface of the as-received components. Due to the surface polishing operation carried out, these tensile stresses of 70±40 MPa appeared over a depth of 400 µm.

Figures 6-15*a* and *b* show the measured residual stresses of the shot peened samples. It is shown that the compressive residual stress areas are formed close to the peened surface followed by the tensile stress areas. A similar trend with the numerical results can be seen in both measured treated samples (see figure 6-14), i.e. the depth of the compressive stress layer increases with pressure and media size, from 150 µm to 230 µm (S110) and from 230 µm to 370 µm (S230) and at the pressure of 137.9 kPa and 413.7 kPa respectively. The shot peening

pressure and the media size have significant effects on the maximum compressive stress value but the changing trend is not clear. For example, the maximum compressive stress of the treated samples is 755 MPa at 137.9 kPa and reduces to 632 MPa at 275.8 kPa and again increases to 682 MPa at 413.7 kPa. In addition, figure 6-15*c* shows that secondary peening process (by smaller shot) makes the compressive stress layer to be slightly deeper than the S230 treated samples. The secondary process can improve the depth of compressive zone, the maximum compressive stress value.

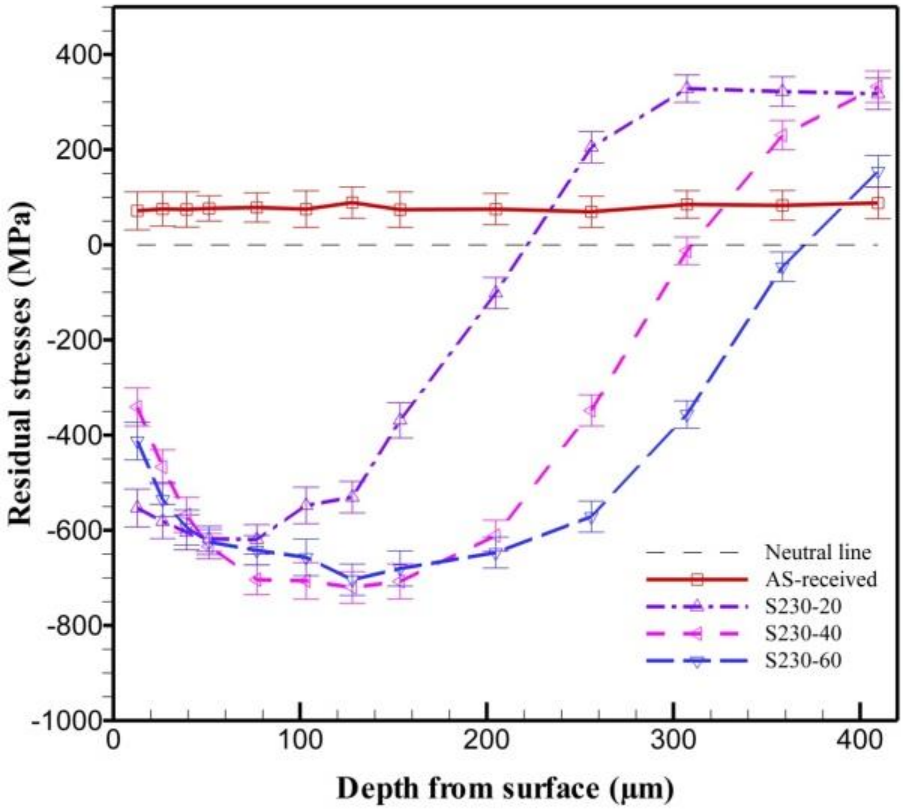

(a) S230 shot peened samples

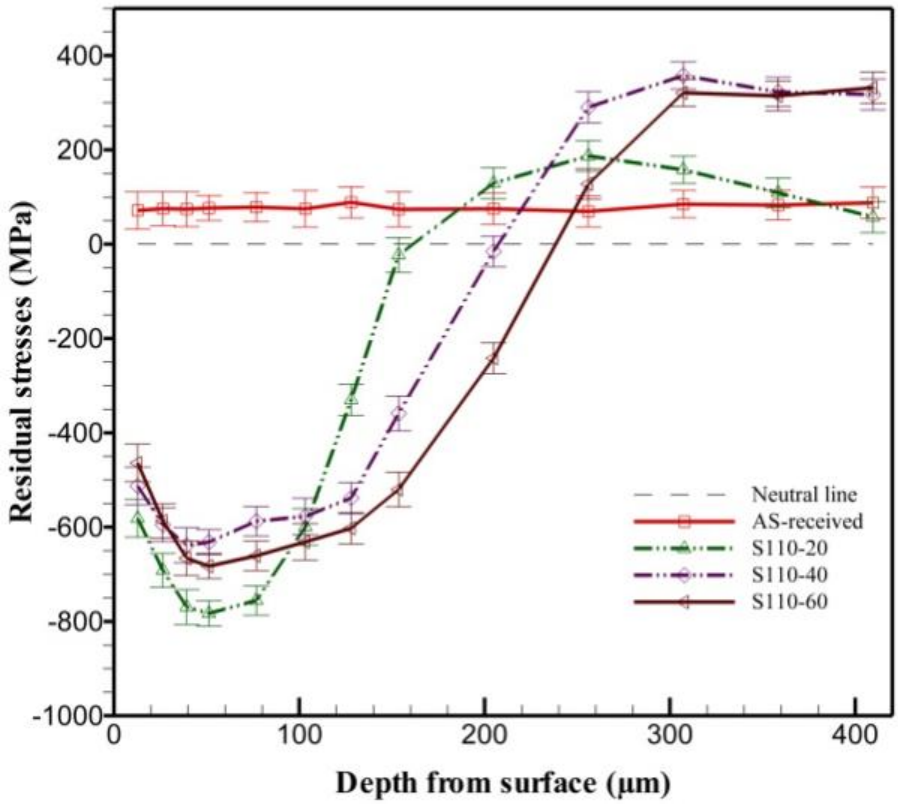

(b) S110 shot peened samples

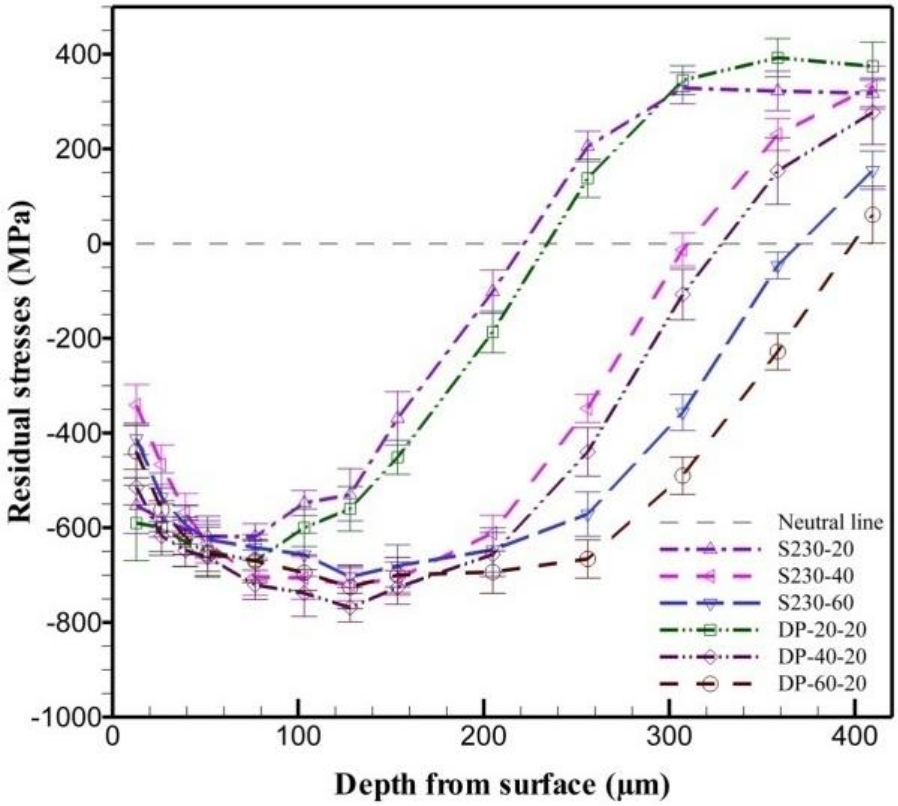

(c) Comparison between S230 shot peened samples and double shot peened samples

Figure 6-15. Average longitudinal residual stress distribution under various shot peening pressures in the experimental study: (a) S230 shot peened samples, (b) S110 shot peened samples and (c) Comparison between S230 shot peened samples and double shot peened samples.

A comparison between the numerical and experimental residual stress distributions (figure 6-14 and figure 6-15, respectively) demonstrates that the shot peening pressure and media size are two main factors affecting on the presence of compressive residual stresses in the subsurface of the material in both studies. The compressive residual stress increases with depth and achieve the largest compressive value at the depth from 150 µm to 370 µm (depending on media size and shot pressure). The compressive stress layers are located close to the free surface and followed by the tensile stress areas. It also reveals that in both studies, at the same shot peening pressure, the larger media causes the deeper compressive stress layer in the subsurface of the material. Moreover, the results in both studies displayed that the treatment with higher pressure results in the deeper compressive zone in the subsurface material of the components treated with the similar shot media. However, it only can conclude that the pressure and media size have significant effects on the value of the largest compressive value and its location in the subsurface but it is hard to predict the changing trend. In addition, the secondary process was proved by both studies that it is a promising process can be used to enhance the compressive stresses in the material but the parameters should be carefully selected to prevent detrimental results. In general, the numerical and experimental studies give a good agreement in the results of the distribution of the residual stresses in the subsurface of the shot peened material, but it can be seen that there is a difference between the numerical and experimental results, i.e. the numerical value is higher than the later study result. The reason of this difference can be explained that in the numerical study, some physical conditions of the process were ignored to reduce the complexity of the calculation, i.e. the impacting of the media (the interaction of the reflective shots (after hitting the surface) and the incident shots), the heating transfer due to the deformation process and the initial residual stresses of the as-received samples (the initial measured value is 70 ± 40 MPa).

6.4. Conclusion

The numerical and experimental study of the effect of the shot peening process parameters on AISI 4340 high strength steel under different conditions were systematically investigated. The following conclusions are drawn:

- Both studied results confirmed that full coverage only achieved at a pressure of 206.8 kPa in the case of S230 and at a pressure of 68.9 kPa in the peening process by shot S110.
- The higher velocity caused by the high pressure increases the surface roughness.
- The bigger media had the larger intensity although having smaller velocity hence it could impact the surface target with higher dynamic energy creating deeper and wider indentations.
- The secondary shot peening treatment is a promising method to reduce the surface roughness caused by the previous shot peening process with high intensity and larger media. While this can be seen as a beneficial process, the operating parameters should be carefully selected to prevent detrimental results.
- A comparison of S_a value between two numerical and experimental process reveals that this value increases gradually with the increment of pressures. However, the value in the later process is always smaller than that of the previous one under the same pressure condition due to some physical conditions were ignored in the numerical process to reduce the complexity of the calculation.
- The depth of the compressive residual stress layer in the S230 shot peened material is about two times higher than that of S110. However, the compressive residual stress at the surface and subsurface near the free surface is higher.

- The increase in the shot peening pressure and media size results in the increment of the depth of the compressive residual stress zone. However, the effect of these parameters on the changing trend of the maximum compressive residual stress value is not clear.
- The comparison between the numerical and experimental studies gives a good agreement of the distribution of the residual stresses in the subsurface of the shot peened material. The shot peening pressure and media size are two main factors affecting on the presence of compressive residual stresses in the subsurface of the material.

Chapter 7: Fatigue life of shot peened low allow steel

7.1 Introduction

Shot peening process can significantly improve the fatigue strength of engineering components [7]. Hassani-Gangaraj et al. [59], Voorwald et al. [74], and Závodská et al. [109] have described shot peening as a viable method to introduce the compressive residual stresses to retard the crack propagation in the material but, Bagherifard et al. [58] indicated that the high surface roughness, which occurs during the peening process, has a deterimental effect in reducing the fatigue life of the shot peened steel. Hence a secondary polishing step is recommended to decrease the surface roughness of the treated samples: these could be prolonging the treatment time, removing a thin layer of material (abrasive grinding and electropolishing), or re-shot peening.

Miková et al. [64] specified that the fatigue strength of the shot peening specimens increased in both cases for the smooth and notched samples. Nevertheless, the increment in the notched sharp sample compared with the relative as-received sample is much more significant. Although shot peening is a commonly used industry process, little published data is available about the influence of the shot peening process on fatigue life of components which are either single or double shot peened.

In the previous chapters, AISI 4340 steel was chosen as a material to examine the microstructural, mechanical and tribological properties of the specimens under different shot peening conditions. In this chapter, the focus will be on the fatigue life analysis of AISI 4340 steel under various shot peening conditions.

7.2 Experimental details

7.2.1 Material

As in the previous work-chapters, commercial AISI 4340 low alloy steel was chosen as the material for all of the experimental tests. The nominal chemical composition of the AISI 4340 low alloy steel (weight %) is composed of C (~0.34), Si (~0.24), Mn (~0.51), Cr (~0.91) Ni (~1.54) and Mo (~0.25).

7.2.2 Shot peening

The mechanical drawing of the specimen shown in figure 7-1 was designed according to the ASTM standard E466-07 [110] (all the dimensions had a unit in mm). A fixture was designed and fabricated to mount the sample firmly on it by Abrasive Engineering Pte Ltd ®. All specimens were shot peened under various conditions at for the same duration of 150 seconds with two types of media S230 and S110 (the same hardness of about 500 ± 30 Hv), which have a mean diameter of about 600 µm and 300 µm respectively. In the double shot peening process, the samples were first shot peened by the larger shot S230 and then treated by the smaller media S110. The shot peened samples were analyzed for the level of coverage with the help of an optical microscope at 50 times magnification. The details of the shot peening operation parameters are provided in table 7-1.

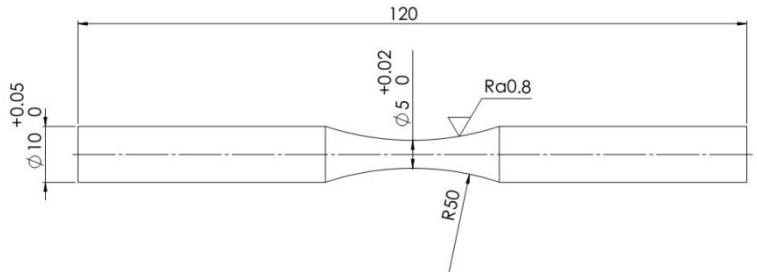

Figure 7-1. The geometry of the specimens used for all the experimental tests.

Table 7- 1. Shot peening process parameters used in chapter 7.

Samples	Media type	Pressure (kPa)
S110-10	S110	68.9
S110-20	S110	137.9
S110-30	S110	206.8
S110-40	S110	275.8
S110-50	S110	344.7
S110-60	S110	413.7
S110-70	S110	482.6
S110-80	S110	551.6
S230-10	S230	68.9
S230-20	S230	137.9
S230-30	S230	206.8
S230-40	S230	275.8
S230-50	S230	344.7
S230-60	S230	413.7
S230-70	S230	482.6
S230-80	S230	551.6
DP-10-20	S230	68.9
	S110	137.9
DP-20-20	S230	137.9
	S110	137.9
DP-30-20	S230	206.8
	S110	137.9
DP-40-20	S230	275.8
	S110	137.9
DP-50-20	S230	344.7
	S110	137.9
DP-60-20	S230	413.7
	S110	137.9
DP-70-20	S230	482.6
	S110	137.9
DP-80-20	S230	551.6
	S110	137.9
As-received	NA	NA

7.2.3 Fatigue test

Fatigue testing was carried out using a MTS 810 (MTS®), a servo-hydraulic testing machine. The fatigue tests were performed under the tension-compression axial loading condition with the maximum applied load started from 0.70% (700 MPa) to 0.45% (450 MPa) of the static yield strength with the cycling frequency of 5 Hz. It was reported that the

fully reversed condition, R = -1, gives the least fatigue life [103]. The fatigue life of the shot peened sample was investigated in the most severe fatigue condition tests. After failure, all specimens were sectioned transversely to the loading direction for fractographic studies.

7.3 Results and discussion

The fatigue response of the as-received samples in terms of maximum stress versus the number of cycles (N) to fracture is shown in figure 7-2. It was reported that the fully reversed condition, R = -1, gives the least fatigue life [103]. The fatigue tests were performed under the tension-compression axial loading condition with the maximum applied load started from 0.70% (700 MPa) to 0.45% (450 MPa) of the static yield strength. The fatigue life of the shot peened sample was investigated in the most severe fatigue condition tests. The Figure 7-2 also shows that the fatigue limit of the AISI 4340 is 475±10MPa. At that maximum stress, the fatigue tests run out, so the tests were stopped after 4×10^7 cycles without fracture.

The fatigue life of the shot peened samples is shown in figure 7-3. All of the tests were performed under the maximum stress of 550 MPa to fracture. The as-received samples fractured at $40\pm3\times10^3$ cycles while all of the shot peened specimens witnessed a significant improvement in the fatigue life. In the shot peening process with media S110, the fatigue life reaches the highest value of $93\pm3\times10^3$ cycles at the pressure of 344.7 kPa then gradually reduced to $84\pm5\times10^3$ cycles. In the case of the media S230, the fatigue life of samples achieves the highest value of $84\pm4\times10^3$ cycles at the pressure of 413.7 kPa and reduced significantly to $61\pm3\times10^3$ cycles. The figure also shows that at the same shot peening pressure condition, the media S110 can improve the fatigue life of shot peened samples higher than media S230. In the previous chapter[105], the intensity of shot S110 and S230 and the topography of the shot peened samples were investigated. The higher intensity,

caused by the higher shot peening pressure, could introduce a higher compressive residual stress in the subsurface of the treated components [1, 105]. This explains the increased fatigue life when pressure rises from 0 kPa to 344.7 kPa (with media S110) and from 0 kPa to 413.7 kPa (with media S230). The topography of shot peened steels reveals that the higher shot peening pressure resulted in increased surface roughness [105, 111] when the shot peening pressure is higher than 344.7 kPa. The increased surface roughness was known to be a detrimental effect the shot peening process. This is why the shot peening media S110 improve the fatigue life of the material compared to the sample treated by media S230 at the same operating pressure although having a lower intensity. The increased pressure leads to greater shot peening intensity and also coarser surface finish. These factors have an opposite effect on the fatigue strength of the material. In case of pressure lower than 482.6 kPa, the effect of compressive residual stress dominate in improving the life, whereas pressure from 551.6 kPa causes the increased surface roughness so reduced the fatigue life.

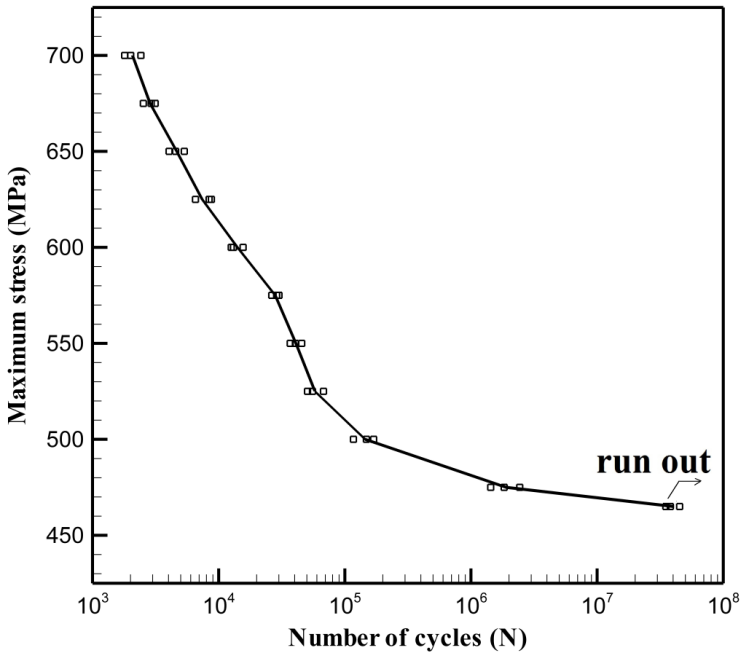

Figure 7-2. The S-N curve of the as received AISI 4340 samples in the tension-compression axial loading.

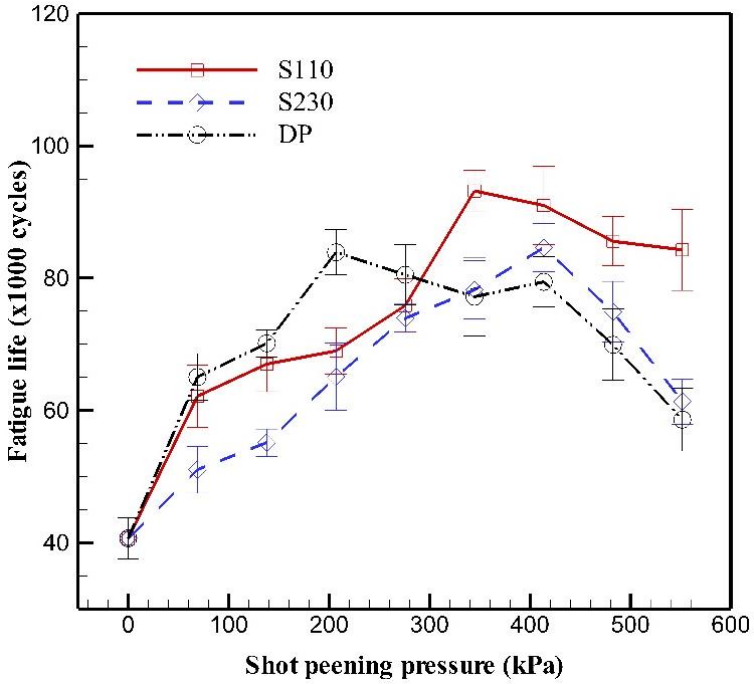

Figure 7-3. The fatigue life of shot peened samples under the maximum stress of 550 MPa.

The double peening process is considered as a promising method to improve the surface roughness of the shot peened samples [58, 71, 105]. In the double peening process, the materials first undergo the primary shot peening process with large media with high intensity and are then subjected to a secondary peening with smaller media and lower intensity [58]. In figure 7-3, the fatigue life of the double shot peened samples increases significantly and reaches the highest value of $83\pm5\times10^3$ cycles at 206.8 kPa and then reduces with the peening of pressure. At the first three levels of pressure (from 68.9 to 206.8 kPa), the primary shot peening process with media S230 cannot achieve the full coverage [105], and the compressive residual stress is low due to the reduced shot intensity. Therefore, with the second treatment by media S110 at 137.9 kPa, the components achieve full coverage and the fatigue life increases by $12\pm3\times10^3$ cycles or 27±2% compared with the fatigue life of media S230. However, when the pressure increases beyond 344.7 kPa, the fatigue life drops significantly and has a value even smaller than the samples peened with S230. Therefore, the operating parameters of the shot peening should be analyzed and selected suitably to prevent detrimental results.

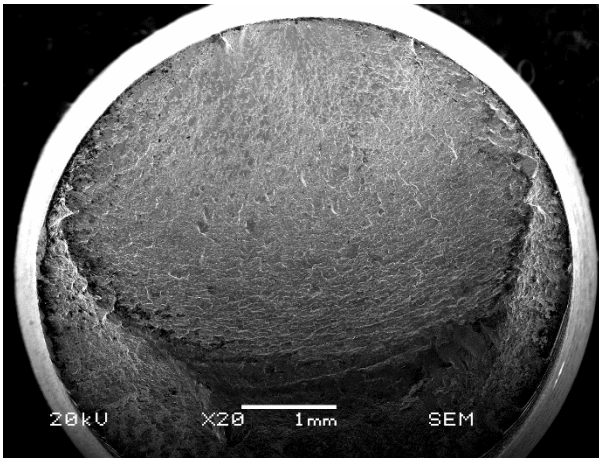

(a) (x20)

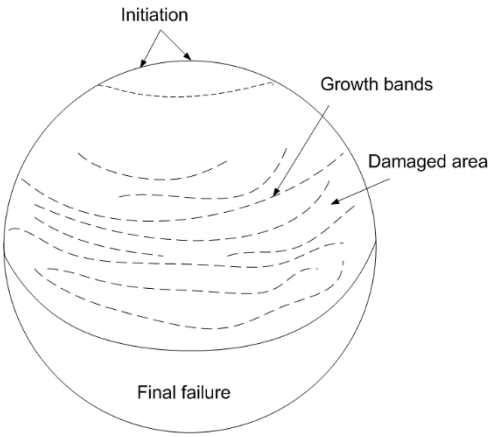

(b)

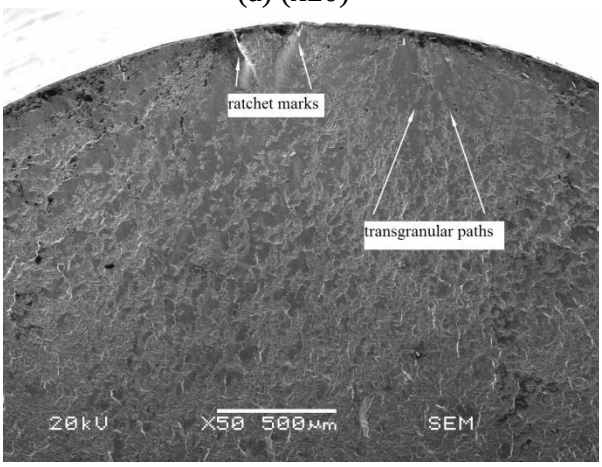

(c) x50

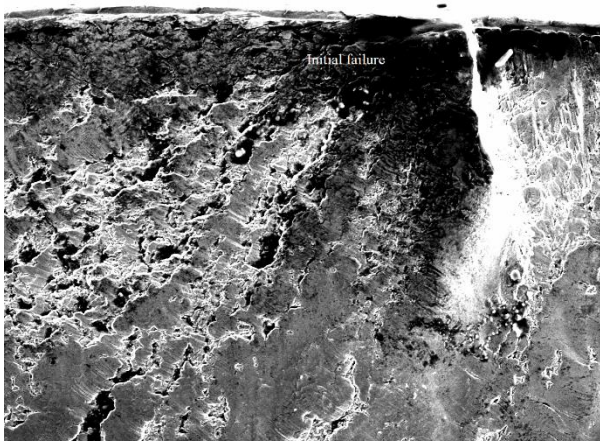

(d) x300

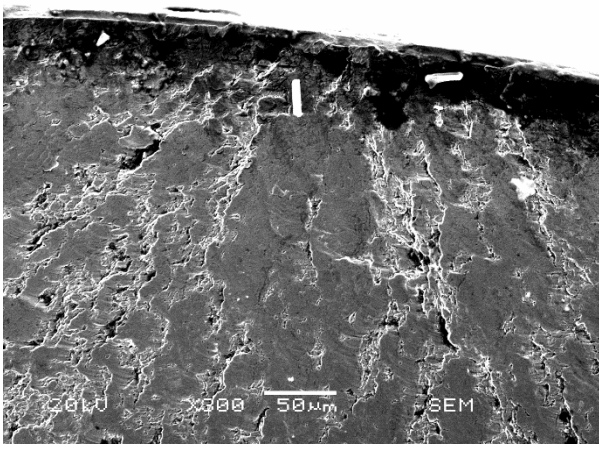

(e) (x300)

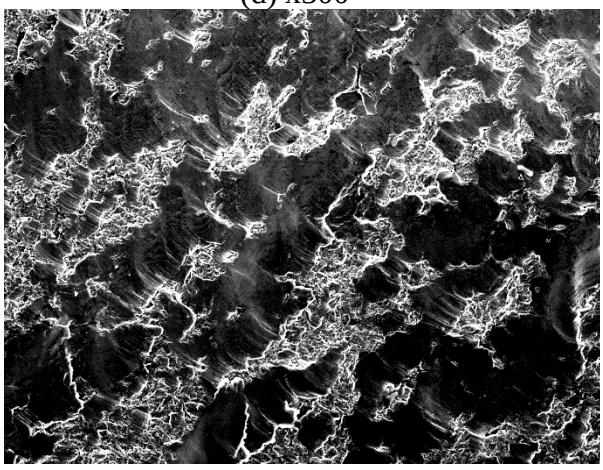

(f) (x300)

Figure 7-4. SEM micrographs showing the fatigue fracture surface of the as-received AISI 4340 samples at different magnifications: (a) over view of the fracture surface, (b) the fatigue failure diagram, (c) close view of the initial failure at the magnification of 50 times, (d) close view of the main first initial fracture, (e) close view of the second main initial fracture, and (f) close view of the crack growth zone.

After failure, all fractured specimens were cut across the transverse section from the loading direction to investigate the fracture process. Figure 7-4 depicts a fracture surface of the as-received sample failed at 42159 cycles at the stress value of 550 MPa. The striation marks indicate three zones on this surface, e.g. failure initiation, crack growth and final failure as shown in figure 7-4*a* and schematically depicted in the figure 7-4*b*. Figure 7-4*a* and *c* also demonstrate that there are two initiation cracks on this surface, in which the right one is larger. The SEM micrographs of these two initiation cracks are illustrated in figures 7-4*d* and *e*. It can be seen that the initial failure is located in the subsurface at a depth of 10 to 20 µm from the free surface of the sample. Failure initiates at the weakest link of material under fatigue loading [103, 108]. Therefore, the free surface and the appearance of inclusions, such as impurities or very small defects inside the material, are the preferable conditions for nucleation of the micro crack (due to the low restraint on slip) [103, 104]. As a consequence, the observation of the nucleation of a micro crack shows that the initial failure usually occurs in the subsurface (at the inclusion) but very close to the free surface or even on the free surface of the material [103, 108].

The transgranular paths shown in figure 7-4*c* paths start from the initiation crack and grow to the center of the specimen. The fatigue cracks grow along the transgranular path, i.e. across the grains [103, 108]. The figures 7-4*c* and *d* illustrate that there are some ratchet marks appearing on the failure surface shown as the bright paths. The marks are created when more than one growth crack or initiation crack at different locations join together. Therefore, in general, counting the number of ratchet marks can roughly provide the information of the number of crack initiation or crack growth paths [108]. Figure 7-4*f* exhibits the striations on the failure surface of the as-received sample. The SEM micrograph reveals that striations

occur in pairs, which implies that each pair of striation corresponds to one cycle of load fatigue test (tension and compression test).

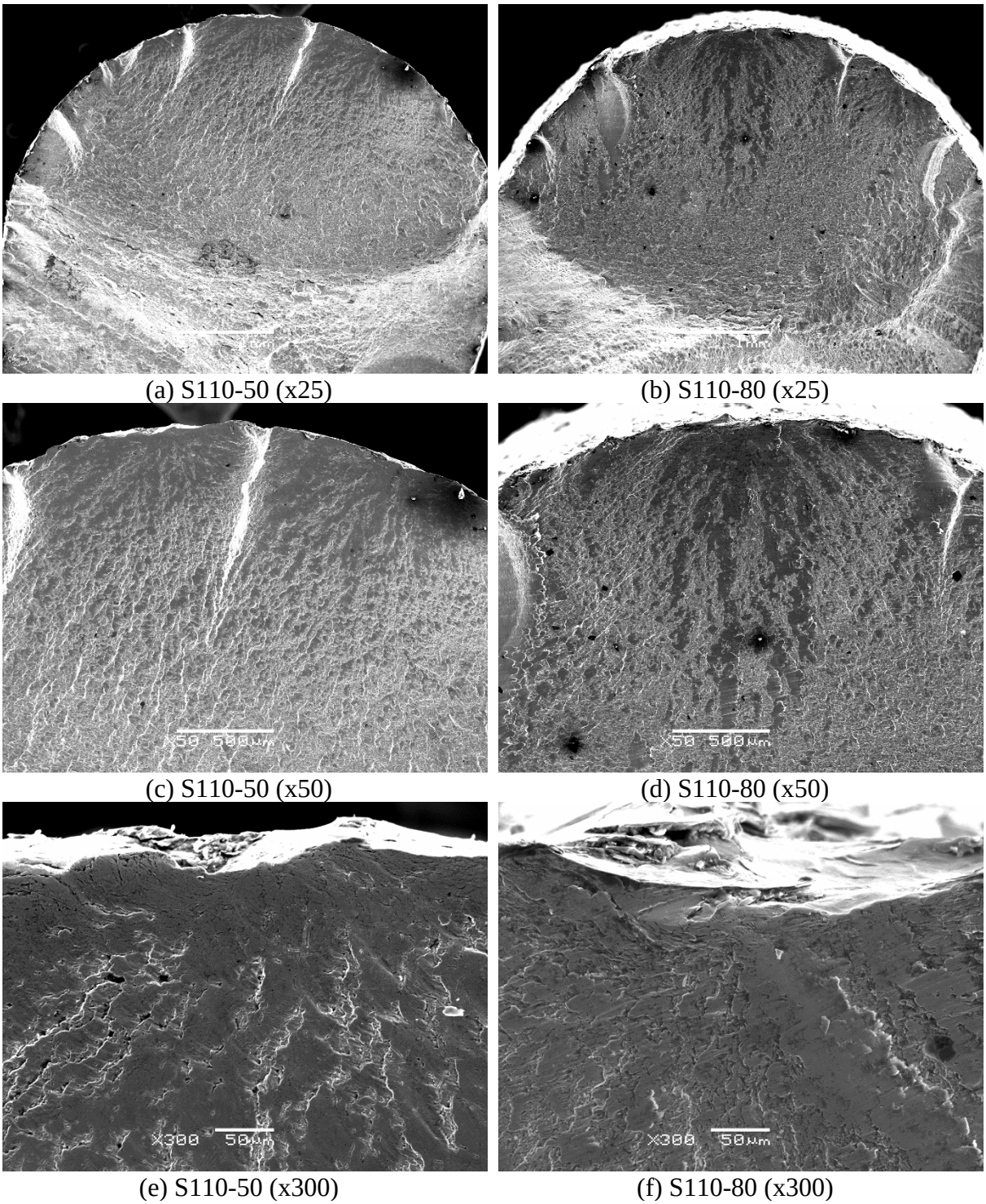

(a) S110-50 (x25) (b) S110-80 (x25)

(c) S110-50 (x50) (d) S110-80 (x50)

(e) S110-50 (x300) (f) S110-80 (x300)

Figure 7-5. SEM micrographs showing the fatigue fracture surface of the shot peened AISI 4340 samples at different magnifications: (a) and (b) over view of the fracture surface, (c) and (d) close view of the initial failure at the magnification of 100 times and (e) and (f) close view of the one main initial fracture of the S110-50 and S110-80 sample, respectively.

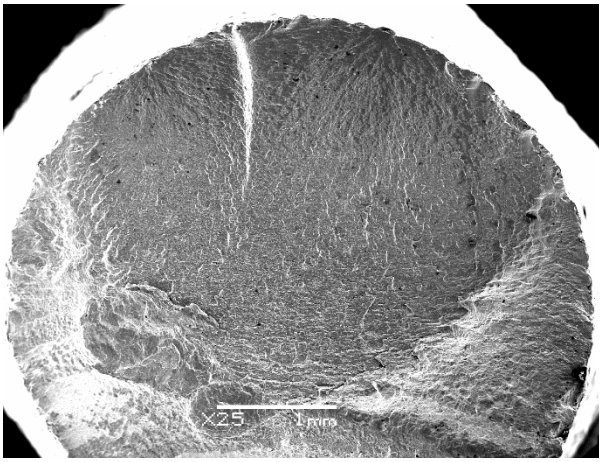

(a) S230-50 (x25)

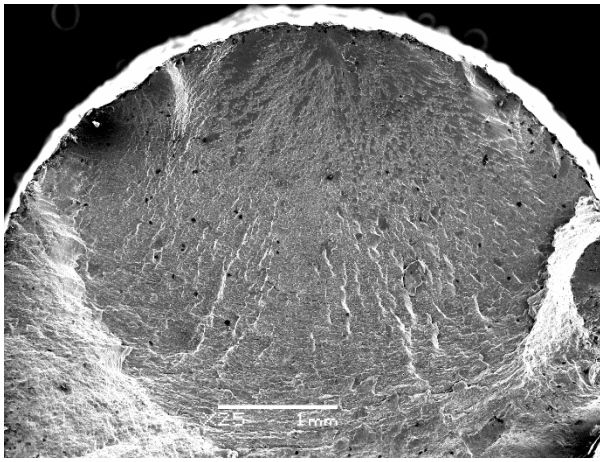

(b) S230-80 (x25)

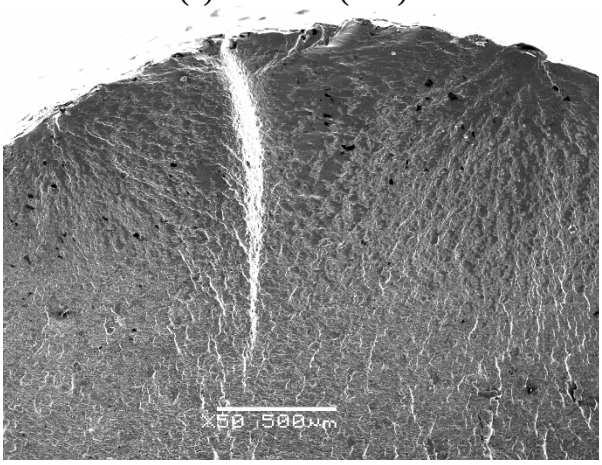

(c) S230-50 (x50)

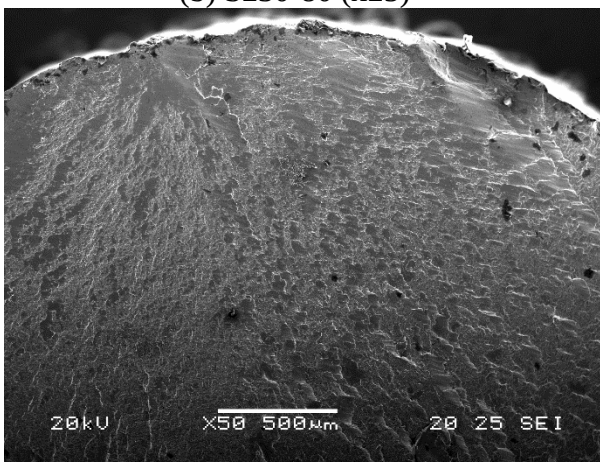

(d) S230-80 (x50)

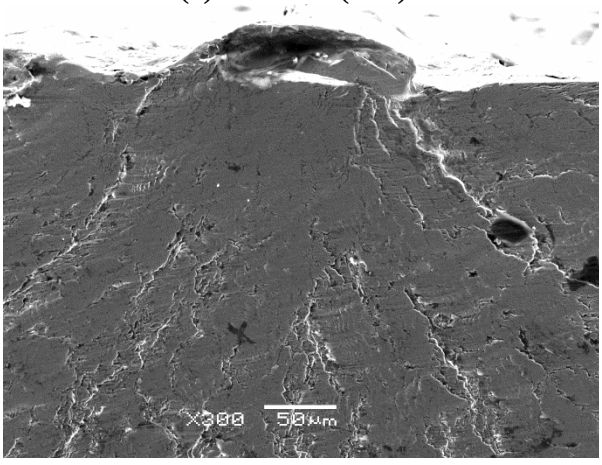

(e) S230-50 (x300)

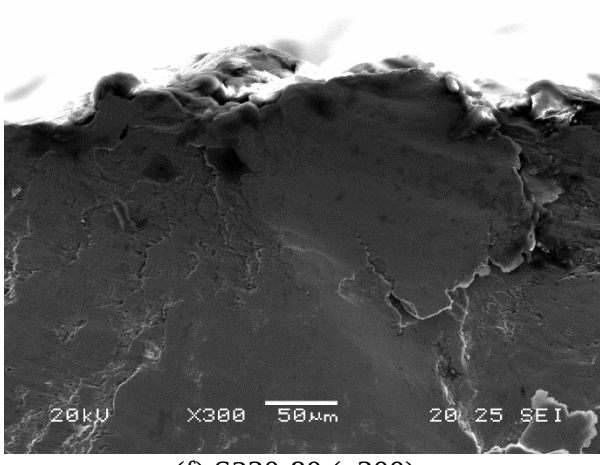

(f) S230-80 (x300)

Figure 7-6. SEM micrographs showing the fatigue fracture surface of the shot peened AISI 4340 samples at different magnifications: (a) and (b) overall view of the fracture surface, (c) and (d) close view of the initial defect at the magnification of 100 times, (e) and (f) close view of the one main initial fracture of the S230-50 and S230-80 sample, respectively.

Figures 7-5 and 7-6 present the SEM micrographs of the fatigue fracture surface of the S110-50, S110-80, S230-50 and S230-80 samples at different magnifications. Figures 7-

5*a* and *b* show the overview of the fracture surface; it shows that the fracture failures of the shot peened samples are also similar to that of the as-received specimens, e.g. having three failure regions (initiation crack, crack growth and final failure). The number of initiation cracks are more than two, as indicated by the multiple ratchet marks. The transgranular paths and striations also appear on all of the shot peened fracture fatigue surfaces. However, there is an important difference which demonstrates the improvement of the fatigue life of the shot peened samples; that is the location of the nucleation crack. All of the nucleation cracks appear on the free surface of the shot peened samples, not in the subsurface anymore. In the as-received steel, the fracture initiated at the subsurface of the sample with the depth from 10 to 20 μm from the free surface. Nevertheless, due to the shot peening process, the compressive residual stress is induced to the subsurface of the specimen [1]. As a result, the weakest link is no longer at the subsurface, and it moves up to the free surface. When it happens to be on the free surface, the effect of surface roughness on the fatigue life becomes significant. In this case, the indentations caused by the shot peening process become a preferable location for the micro concentration and consequently the initiation crack has a favorable condition to appear stress at the rough surface.

Figure 6-15 (chapter 6) illustrates the average longitudinal residual stress measured under various shot peening pressures in this study. It can be seen that, in the subsurface of the as-received material, due to the preparation process (cutting and polishing process) the tensile residual stresses are located at the areas close to the surface. As a consequence, in the fatigue test, the initiation cracks are easily formed on the surface or in the subsurface (which is close to the surface). In addition, the results indicated that the fatigue life of the as-received sample is low because the tensile residual stresses are the favorable condition to for the development of the crack propagation. The shot peening process was removed the tensile stresses and

induced the compressive stresses to the subsurface of the treated material, as a result the fatigue life of all shot peened samples are significantly higher than that one of the as-received sample. The depth of compressive residual stresses increased with the increase of pressure and media size. The increment of compressive stresses results in the enhancement of the fatigue life. However, to induce the high compressive stresses to the subsurface of the material, a higher pressure and media size should be employed. The increase of the later parameters caused the side effects on the surface topology of the shot peened material so it reduces the fatigue life of samples. In addition, figure 6-15*c* shows that secondary process makes the compressive stress layer to be slightly deeper than the S230 treated samples. The secondary process can improve the depth of compressive zone, the maximum compressive stress value and therefore enhance the fatigue life of the double shot peened samples when the shot peening parameters were selected widely. Therefore, the operating parameters should be carefully selected to prevent detrimental results.

7.4 Conclusion

The fatigue life of the shot peened AISI 4340 low alloy steel under different shot peening conditions was systematically investigated. The resulting conclusion can be drawn from the obtained results:

- The fatigue endurance of the as-received AISI 4340 steel specimen was 475±10 MPa.
- The highest fatigue cycle of the shot peened samples with the media S110 (at a pressure of 344.7 kPa), media S230 (at a pressure of 413.7 kPa) and double peening (at a pressure of 206.8 kPa) are about two times higher than the fatigue life of the as-received sample.

- For a same shot peening pressure, the media S110 can improve the fatigue life of the treated samples better than the media S230.
- The double shot peening is a promising method to improve the fatigue life, but shot peening pressure has to be carefully selected based on the analytical study to prevent detrimental results.
- In the case of the as-received samples, the initiation cracks occurred in the subsurface of the specimens at a depth from 10 to 20 µm. However, all the initiation cracks of the shot peened steel start from the free surface.

Chapter 8: Conclusion and future work

8.1 Conclusion

This report presented experimental and numerical investigation of the effect of shot peening process parameters on the surface topography and mechanical performance of low alloy steel 4340. A comprehensive literature review has been undertaken in the first two chapters to understand the shot peening process, the equipment, the limitations and the measurement techniques.

To further understand the shot peening process and provide a foundation for this research, a number of the experiments were undertaken as reported in Chapters 3 and 4. The experimental results in Chapter 3 concludes that, for a given nozzle pressure, the smaller S110 steel shots have higher velocities but smaller kinematic energy which result in lower measured intensities compared with S230 steel shots. Moreover, at low shot peening pressure of 68.9 kPa and 137.9 kPa, the shot peened samples didnot achieve full coverage with S230 steel shots whereas the S110 steel shots able to. The coverage is full when the shot peening pressure is higher than 206.8 kPa for S230 steel shots. It also can be seen that the hardness of the shot peened sample increases with the increasing shot pressure and media size due to the promoted cold work hardening. The surface roughness of the shot peened sample increases with the increase in shot pressure and media size. It indicates that the steel shots with higher velocities (kinematic energy) and larger size formed the deeper and wider dimples on the target material. The increased shot peening pressure and media size result in increasing the friction coefficient but decreasing the wear volume of the shot peened samples due to the significant influences of their surface roughness and surface hardness.

The investigation of the properties of conventional and severe shot peened low alloy steel in Chapter 4 reveals that there was an iron oxide layer with a depth of about 20 μm formed on the sample surface due to the prior heat treatment. This layer had poor mechanical properties and reduced the surface quality of mechanical parts. The conventional shot peening process partly removed this layer and improved the properties of material while the severe shot peening process totally removed it from the surface. The severe shot peening generated an ultrafine grain layer with a depth of 20 μm. The severe shot peening process increased the hardness of the surface and subsurface close to the surface of the material as a result of promoted cold work hardening effect. The increase in surface hardness by applying conventional shot peening and severe shot peening process could improve the wear resistance properties of the material, as a result of decreasing the wear volume of peened samples. However, the severe shot peening process caused the high surface roughness of the surface. To reduce it, additional shot peening process with smaller media was employed. This method not only reduced the surface roughness on severe shot peened surface samples but also improved the wear resistance of the low alloy steel (Re-SSP).

A number of numerical finite element models were developed based on both single and multiple impacts. The single impact model was developed first to provide a deeper understanding of the relationship between the shots, the workpiece surface, and the peening parameters. The surface deformation during from the shot impact could be better understood. In order to better represent the actual shot peening process, a multiple impact model was developed, which allowed for further such as coverage and intensity to be considered. However, according to the literature review (Chapter 2 and 5), most of the studies used the multiple-shot impact model using uniformly distributed positions and prearranged media in a sequence of impact. The use of symmetry patterns can help to reduce computational costs. Nevertheless, this assumption cannot totally define the random nature of practical shot

peening process. Hence, these patterns often fail to simulate a full coverage condition of the actual shot peening process. Therefore, a new approach is introduced in Chapter 5 to estimate the number of shots and the arrangements required to achieve full coverage of the target material. A multiple-shot impact model, developed using a commercial FE analysis program LSDYNA, was used to investigate the effects of shot peening process parameters on the compressive residual stress distribution of the material. The simulation results suggested that increasing the coverage, shot velocity and shot size were effective approaches to obtain a higher level of compressive residual stress and deeper the compressive stress zone in the target material. Also, the simulation results suggested that it was possible to apply the smaller shots after peening the target material with the large shots. The double shot peening simulation results showed that the smaller shots reduced slightly the compressive residual stress previously induced by the larger shots but did not affect the depth of the compressive stress zone. The second shot peening process could be used at low intensity, in that case, double shot peening was considered as a simple, low-cost method for improving the surface finish of shot peened components.

In Chapter 6, comparison of numerical results with experiment measurements confirmed that full coverage was achieved at a pressure of 206.8 kPa in the case of S230 and at a pressure of 68.9 kPa in the peening process by shot S110. A comparison of S_a value between two numerical and experimental process reveals that this value increases gradually with the pressure. However, the value in the later process is always smaller than that of the previous one under the same pressure condition due to some physical conditions were ignored in the numerical process to reduce the complexity of the calculation. The increase in the shot peening pressure and media size results in the increment of the depth of the compressive residual stress zone. However, the effect of these parameters on the changing trend of the maximum compressive residual stress value is not clear. It can be concluded that

the numerical and experimental studies show a good agreement in the results of the residual stress distribution in the subsurface of the shot peened material. The shot peening pressure and media size are two main factors affecting the presence of compressive residual stresses in the subsurface of the material.

The main objective of the shot peening process is to enhance the fatigue life of the shot peened material, so the study of the effect of this treatment process on the material was discussed in Chapter 7. It has been seen that the highest fatigue cycle of the shot peened samples with the media S110 (at a pressure of 344.7 kPa), media S230 (at a pressure of 413.7 kPa) and double peening (at a pressure of 206.8 kPa) are about two times higher than the fatigue life of the as-received sample. Besides, at the same shot peening pressure, the media S110 can improve the fatigue life of the treated samples better than the media S230. In addition, in the case of the as-received samples, the initiation cracks occur in the subsurface of the specimens at a depth of about 10 to 20 μm. However, failure initiates on the free surface of the shot peened material.

The results from works in from Chapter 4 to 7 present that the secondary shot peening treatment (or the double shot peening process) is a promising method to reduce the surface roughness and to improve the fatigue life of the shot peened samples treated by the previous shot peening process with high intensity and larger media. While this can be seen as a beneficial process, the operating parameters should be carefully selected to prevent detrimental effects.

8.2 Scope for further work

The following future research directions and recommendations are proposed base on this scope:

- Double shot peening process is a promising method to reduce the surface roughness and to improve the fatigue life for the shot peened samples. However, the operating parameters should be carefully selected to prevent detrimental results. Therefore, to further understand the double shot peening process and provide optimized operating parameters for this treatment process in the different target material, a number of the experiments should be undertaken and analyzed.

- Severe shot peening process is one of the modern trends of the application of shot peening process since it generates the ultrafine grain size for the surface layer of the material. However, it is necessary to find the potential application for the severe shot peening for industrial usage.

- The numerical model should be further enhanced by taking into account the grain refinements, crystal plasticity, thermal effect, etc.

- A comprehensive study on the fatigue response of shot peened samples under varying loading parameters should be proposed. A fatigue life model needs to be developed for practical designs.

Appendix A - Contributions

The main contributions of this Ph.D. work are as follows:

- Providing the data on mechanical and tribological properties of shot peened low alloy steel under different shot peening conditions, and double shot peening process (Chapter 3 and 4).

- A new approach was introduced to estimate the coverage of target material using a simulation model. This approach can provide the number of required shots for the coverage of 98%, the arrangement of shots and the dependence of the degree of coverage on the number of shots.

- According to the literature review, this is the first time the double shot peening process was analyzed and reported in numerical work. It is worth noticing that the numerical study of the surface topographies of the shot peened material were firstly reported and validated with the experimental results. In addition, it was also a first time the initial surface of the FEM shot peening model was not assumed as a flat surface. Instead, it was developed based on the scanned surface.

- SEM micrographs of the fatigue fracture surface showed the location of the initial fracture, it was one of evidence used to explain why the shot peened material has a better figure life compared to the as-received one. According to my best knowledge, this evidence was firstly reported to explain how the shot peening process can improve the fatigue life.

Appendix B - List of Publications

* Published

Journal papers

[1] Khun N W, **Trung P Q** and Butler D L, Mechanical and tribological properties of shot peened SAE 1070 steel, Tribology Transactions, 59 (2016) 932-943. DOI: 10.1080/10402004.2015.1121313.

[2] **Pham Quang Trung**, Nay Win Khun and David Lee Butler, Effects of shot peening pressure, media type and double shot peening on the microstructure, mechanical and tribological properties of low alloy steel, Surface Topography: Metrology and Properties, 4 (2016). DOI: 10.1088/2051-672X/4/4/045001

[3] **Pham Quang Trung**, Nay Win Khun and David Lee Butler, New Approach to Estimate Coverage Parameter in 3D FEM Shot Peening Simulation, Surface Engineering, 33 (2016) 687-695. DOI: 10.1080/02670844.2016.1274536

[4] **Pham Quang Trung**, Nay Win Khun and David Lee Butler, An investigation of the properties of conventional and severe shot peened low alloy steel, Materials Research Express, 4 (2017). DOI: 10.1088/2053-1591/aa6b22

[5] **Pham Quang Trung**, Nay Win Khun and David Lee Butler, Effect of shot peening process on the fatigue life of shot peened low alloy steel, Journal of Engineering Materials and Technology, 2017. DOI: 10.1115/1.4037525

Conference papers

[1] **Pham Quang Trung** and David Lee Butler, "Three dimensional dynamic modelling of shot peening process: The effects of shot peening parameters on residual stresses", The AUN/SEED-NET Regional Conference 2015 on Materials Engineering (RCME 2015), Bangkok, Thailand, 2015.

[2] **Pham Quang Trung**, Nay Win Khun and David Lee Butler, "Three-dimensional dynamic finite element modelling of shot peening process: New approach to estimate level of the coverage parameter", XXX International conference on surface modification technologies (SMT30*)*, Milan, Italy, 2016.

[3] **Pham Quang Trung**, Nay Win Khun and David Lee Butler, "Comparison of the

effects of conventional shot peening and severe shot peening processes on the mechanical and tribological properties of shot peened AISI 4340", XXX International conference on surface modification technologies (SMT30), Milan, Italy,2016.

[4] **Pham Quang Trung** and David Lee Butler, "Three dimensional dynamic modelling of shot peening process: The effects of shot peening parameters on residual stresses", The AUN/SEED-NET Regional Conference 2016 on Materials Engineering (RCME 2016), Yangon, Myanmar, 2016.

[5] **Pham Quang Trung** and David Lee Butler "A Study on the Effects of the Shot Peening Process Parameters on the Shot Peened Low Alloy Steel", 9th AUN/SEED-Net Regional Conference on Mechanical and Manufacturing Engineering, Vientiane, Lao PDR, 2017.

* Submitted

Journal papers

[1] **Pham Quang Trung**, David Lee Butler and Sridhar Idapalapatiat, A study of residual stress distribution on the shot peened steel, Journal of Engineering Materials and Technology, 2017.

References

[1] S. Baiker, Shot peening: a dynamic application and its future, fourth ed., ISBN 9783033020269, Metal finishing news, 2014.

[2] Y. Harada, K. Fukaura, Influence of shot peening on surface characteristics of high speed steel, Steel Research International, 79 (2008) 57-64.

[3] S.E. Homer, R.D. Van Luchene, Aircraft wing skin contouring by shot peening, Journal of Materials Shaping Technology, 9 (1991) 89-101.

[4] M. Kobayashi, T. Makino, Y. Kurihara, Y. Murakami, T. Toriyama, R. Ebara, Fatigue strength prediction of automobile suspension spring steels. Explicit analysis of nonmetallic inclusions, shot peening, decarburized layer, surface roughness and corrosion pits, in: American Society of Mechanical Engineers, Materials Division, 1991, pp. 171-183.

[5] G. Donzella, A. Pola, L. Solazzi, G.P. Marconi, Effect of shot peening on carburized surfaces, International Journal of Materials and Product Technology, 15 (2000) 117-130.

[6] G.H. Majzoobi, K. Azadikhah, J. Nemati, The effects of deep rolling and shot peening on fretting fatigue resistance of Aluminum-7075-T6, Materials Science and Engineering A, 516 (2009) 235-247.

[7] S. Bagheri, M. Guagliano, Review of shot peening processes to obtain nanocrystalline surfaces in metal alloys, Surface Engineering, 25 (2009) 3-14.

[8] Y.Q. Wu, T. Bitoh, K. Hono, A. Makino, A. Inoue, Microstructure and properties of nanocrystalline Fe–Zr–Nb–B soft magnetic alloys with low magnetostriction, Acta Materialia, 49 (2001) 4069-4077.

[9] K. Lu, J. Lu, Nanostructured surface layer on metallic materials induced by surface mechanical attrition treatment, Materials Science and Engineering: A, 375–377 (2004) 38-45.

[10] R. Valiev, Nanostructuring of metals by severe plastic deformation for advanced properties, Nat Mater, 3 (2004) 511-516.

[11] S.A. Meguid, G. Shagal, J.C. Stranart, Finite element modelling of shot-peening residual stresses, Journal of Materials Processing Technology, 92-93 (1999) 401-404.

[12] S.A. Meguid, G. Shagal, J.C. Stranart, 3D FE analysis of peening of strain-rate sensitive materials using multiple impingement model, International Journal of Impact Engineering, 27 (2002) 119-134.

[13] T. Kim, H. Lee, S. Jung, J.H. Lee, A 3D FE model with plastic shot for evaluation of equi-biaxial peening residual stress due to multi-impacts, Surface and Coatings Technology, 206 (2012) 3125-3136.

[14] W.H. Friske, J.P. Page, Shot peening to prevent the corrosion cracking of austenitic stainless steels, Journal of Materials for Energy Systems, 1 (1979) 20-32.

[15] K. Inoue, M. Kato, Crack growth resistance due to shot peening in carburized gears, Journal of Propulsion and Power, 11 (1995) 973-979.

[16] T. Honda, M. Ramulu, A.S. Kobayashi, Shot peening and fatigue crack growth in 7075-T7351 aluminum, in: Key Engineering Materials, 2005, pp. 72-77.

[17] T. Honda, M. Ramulu, A.S. Kobayashi, Effect of shot peening on fatigue crack growth in 7075-T7351, in: ASTM Special Technical Publication, 2008, pp. 33-46.

[18] T. Honda, M. Ramulu, A.S. Kobayashi, Effect of shot peening on fatigue crack growth in 7075-T7351, Journal of ASTM International, 2 (2005) 39-52.

[19] M.A. Hossian, M. Lim, S. Huh, W. Park, A study on fatigue crack propagation properties using the x-ray diffraction method, in: Materials Science Forum, 2008, pp. 1162-1169.

[20] O. Takakuwa, M. Nishikawa, H. Soyama, Suppression of fatigue crack growth in austenite stainless steel by cavitation peening, in: Key Engineering Materials, 2011, pp. 641-644.

[21] H. Bae, Experimental Study of Shot Peening Process and its Effects on High Cycle Fatigue in Aero Space Materials, in, University of Washington, Ann Arbor, 2011, pp. 294-n/a.

[22] Z. Kang, X. Gai, J. Li, Z. Wang, Influence of residual stress and surface morphology on fatigue properties of steel 60Mn, Acta Metallurgica Sinica Series A, Physical Metallurgy & Materials Science, 5 A (1992) 477-483.

[23] S.L. Lee, M.J. Glennon, A. Gabriele, Induced overload residual stresses in a multi-lug breech ring, in: American Society of Mechanical Engineers, Pressure Vessels and Piping Division (Publication) PVP, 1995, pp. 37-45.

[24] E. Real, C. Rodríguez, A.F. Canteli, F.J. Belzunce, Influence of the shot peening process on the fatigue behaviour of duplex stainless steel reinforcing bars, in: Materials Science Forum, 2007, pp. 4981-4986.

[25] V.V. Ivanov, I.R. Paine, P.J. Revnyuk, Study of thermal fatigue of H13 die steel with various surface treatments, High Temperature Materials and Processes, 21 (2002) 65-78.

[26] J. Arakawa, M. Kakuta, Y. Hayashi, R. Tanegashima, H. Akebono, M. Kato, A. Sugeta, Effect of ultrasonic shot peening on the fatigue strength of stainless cast steel ASTM CA6NM for hydraulic turbine runner, in: Advanced Materials Research, 2014, pp. 649-655.

[27] A. Malik, X. Lai, K. Langer, Residual stress and wave reflectivity when laser peening thin curved sections, in: ASME 2011 International Mechanical Engineering Congress and Exposition, IMECE 2011, 2011, pp. 91-99.

[28] R. Fathallah, H. Sidhom, C. Braham, L. Castex, Effect of surface properties on high cycle fatigue behaviour of shot peened ductile steel, Materials Science and Technology, 19 (2003) 1050-1056.

[29] C. Bouraoui, R. Ben Sghaier, R. Fathallah, An engineering predictive design approach of high cycle fatigue reliability of shot peened metallic parts, Materials and Design, 30 (2009) 475-486.

[30] S. Chakravarty, J.P. Dyer, J.C. Conway Jr, A.E. Segall, P.C. Patnaik, Influence of surface treatments on fretting fatigue of Ti-6242 at elevated temperatures, in: ASTM Special Technical Publication, 2000, pp. 491-505.

[31] M. Umemoto, Y. Todaka, K. Tsuchiya, Formation of nanocrystalline structure in steels by air blast shot peening, Materials Transactions, 44 (2003) 1488-1493.

[32] C.H. Chen, R.M. Ren, X.J. Zhao, Y.J. Zhang, Surface nanostructures in commercial pure Ti induced by high energy shot peening, Transactions of Nonferrous Metals Society of China (English Edition), 14 (2004) 215-218.

[33] M. Umemoto, Y. Todaka, K. Tsuchiya, Nanocrystallization of Steels by Various Severe Plastic Deformation, in: Processing and Properties of Structural Nanomaterial: Proceedings of Symposia held at the Materials Science and Technology 2003 Meeting, 2003, pp. 125-132.

[34] Y. Todaka, M. Umemoto, S. Tanaka, K. Tsuchiya, Formation of nanocrystalline structure at the surface of drill hole in steel, Materials Transactions, 45 (2004) 2209-2213.

[35] M. Umemoto, Y. Todaka, A. Ohno, M. Suzuki, K. Tsuchiya, Deformation and dissolution of cementite by severe plastic deformation, Journal of Metastable and Nanocrystalline Materials, 24-25 (2005) 157-160.

[36] Shot peening applications, in, Metal Improvement Company Inc, 2001.

[37] D. Kirk, Shot peening, Aircraft Engineering and Aerospace Technology, 71 (1999) 349-361.

[38] M. Avrami, Kinetics of phase change. i general theory, J. Chem. Phys., 7 (12) (1939) 1103-1112.

[39] G.S. Schajer, Practical residual stress measurement methods, Chichester, West Sussex, United Kingdom : Wiley, ISBN 9781118402832, 2013.

[40] V.M. Faires, Design of machine elements, in, MacMillan, New York, 1965.

[41] N.S. Rossini, M. Dassisti, K.Y. Benyounis, A.G. Olabi, Methods of measuring residual stresses in components, Materials & Design, 35 (2012) 572-588.

[42] ISO 25178-2:2012: Geometrical Product Specifications (GPS) - Surface Texture: Areal -- Part 2: Terms, Definitions and Surface Texture Parameters, (2012).

[43] R. Leach, Characterisation of Areal Surface Texture, Berlin, Heidelberg : Springer Berlin Heidelberg : Imprint: Springer. ISBN 9783642364587, 2013.

[44] K. Stout, Development of methods for the characterisation of roughness in three dimensions, London : Penton Press, c2000. ISBN 1857180232, 2000.

[45] T. Hong, J.Y. Ooi, B. Shaw, A numerical simulation to relate the shot peening parameters to the induced residual stresses, Engineering Failure Analysis, 15 (2008) 1097-1110.

[46] B. Bhuvaraghan, S.M. Srinivasan, B. Maffeo, Numerical simulation of Almen strip response due to random impacts with strain-rate effects, International Journal of Mechanical Sciences, 53 (2011) 417-424.

[47] M.S. Eltobgy, E. Ng, M.A. Elbestawi, Three-dimensional elastoplastic finite element model for residual stresses in the shot peening process, Proceedings of the Institution of Mechanical Engineers, Part B: Journal of Engineering Manufacture, 218 (2004) 1471-1481.

[48] G.H. Majzoobi, R. Azizi, A. Alavi Nia, A three-dimensional simulation of shot peening process using multiple shot impacts, Journal of Materials Processing Technology, 164-165 (2005) 1226-1234.

[49] H.Y. Miao, S. Larose, C. Perron, M. Lévesque, On the potential applications of a 3D random finite element model for the simulation of shot peening, Advances in Engineering Software, 40 (2009) 1023-1038.

[50] S. Bagherifard, R. Ghelichi, M. Guagliano, A numerical model of severe shot peening (SSP) to predict the generation of a nanostructured surface layer of material, Surface and Coatings Technology, 204 (2010) 4081-4090.

[51] LY-DYNA, in, User's manual. Ver. 5471, Livermore, California: Livermore Software Technology Corporation, 2014.

[52] O. Unal, R. Varol, Almen intensity effect on microstructure and mechanical properties of low carbon steel subjected to severe shot peening, Applied Surface Science, 290 (2014) 40-47.

[53] L. Trško, O. Bokůvka, F. Nový, M. Guagliano, Effect of severe shot peening on ultra-high-cycle fatigue of a low-alloy steel, Materials and Design, 57 (2014) 103-113.

[54] S. Bagherifard, I. Fernandez-Pariente, R. Ghelichi, M. Guagliano, Effect of severe shot peening on microstructure and fatigue strength of cast iron, International Journal of Fatigue, 65 (2014) 64-70.

[55] S. Bagherifard, I. Fernandez-Pariente, R. Ghelichi, M. Guagliano, Fatigue behavior of notched steel specimens with nanocrystallized surface obtained by severe shot peening, Materials and Design, 45 (2013) 497-503.

[56] K.T. Cho, K. Song, S.H. Oh, Y.K. Lee, K.M. Lim, W.B. Lee, Surface hardening of aluminum alloy by shot peening treatment with Zn based ball, Materials Science and Engineering A, 543 (2012) 44-49.

[57] S.M. Hassani-Gangaraj, A. Moridi, M. Guagliano, A. Ghidini, Nitriding duration reduction without sacrificing mechanical characteristics and fatigue behavior: The beneficial effect of surface nano-crystallization by prior severe shot peening, Materials and Design, 55 (2014) 492-498.

[58] S. Bagherifard, M. Guagliano, Fatigue behavior of a low-alloy steel with nanostructured surface obtained by severe shot peening, Engineering Fracture Mechanics, 81 (2012) 56-68.

[59] S.M. Hassani-Gangaraj, A. Moridi, M. Guagliano, A. Ghidini, M. Boniardi, The effect of nitriding, severe shot peening and their combination on the fatigue behavior and micro-structure of a low-alloy steel, International Journal of Fatigue, 62 (2014) 67-76.

[60] M. Palacios, I. Fernández Pariente, S. Bagherifard, M. Guagliano, Wear behavior of an aluminium alloy subjected to conventional and severe shot peening, in: Engineering Against Failure - Proceedings of the 3rd International Conference of Engineering Against Failure, ICEAF 2013, 2013, pp. 204-213.

[61] S.H. Yeh, L.H. Chiu, T.L. Chuang, C.Y. Wu, Thermal fatigue behavior evaluation of shot-peened JIS SKD61 hot-work mold steel, Materials Transactions, 54 (2013) 1053-1056.

[62] T. Wang, J. Yu, B. Dong, Surface nanocrystallization induced by shot peening and its effect on corrosion resistance of 1Cr18Ni9Ti stainless steel, Surface and Coatings Technology, 200 (2006) 4777-4781.

[63] S. Bagherifard, I. Fernández Pariente, R. Ghelichi, M. Guagliano, Fatigue properties of nanocrystallized surfaces obtained by high energy shot peening, Procedia Engineering, 2 (2010) 1683-1690.

[64] K. Miková, S. Bagherifard, O. Bokuvka, M. Guagliano, L. Trško, Fatigue behavior of X70 microalloyed steel after severe shot peening, International Journal of Fatigue, 55 (2013) 33-42.

[65] K. Schiffner, C. Droste Gen. Helling, Simulation of residual stresses by shot peening, Computers and Structures, 72 (1999) 329-340.

[66] M. Klemenz, V. Schulze, I. Rohr, D. Löhe, Application of the FEM for the prediction of the surface layer characteristics after shot peening, Journal of Materials Processing Technology, 209 (2009) 4093-4102.

[67] X. Kang, T. Wang, J. Platts, Multiple impact modelling for shot peening and peen forming, Proceedings of the Institution of Mechanical Engineers, Part B: Journal of Engineering Manufacture, 224 (2010) 689-697.

[68] T. Kim, J.H. Lee, H. Lee, S.k. Cheong, An area-average approach to peening residual stress under multi-impacts using a three-dimensional symmetry-cell finite element model with plastic shots, Materials and Design, 31 (2010) 50-59.

[69] M. Klemenz, T. Hochrainer, L. Delonnoy, V. Schulze, Similarity Rules for the Shot Peening Process Based on Finite Element Simulations, Proceedings of the 9th International Conference on Shot Peening: Paris: 6-9 September 2005, 94-99.

[70] S. Bagherifard, R. Ghelichi, M. Guagliano, On the shot peening surface coverage and its assessment by means of finite element simulation: A critical review and some original developments, Applied Surface Science, 259 (2012) 186-194.

[71] A.T. Vielma, V. Llaneza, F.J. Belzunce, Effect of coverage and double peening treatments on the fatigue life of a quenched and tempered structural steel, Surface and Coatings Technology, 249 (2014) 75-83.

[72] B.G. Scuracchio, N.B. de Lima, C.G. Schön, Role of residual stresses induced by double peening on fatigue durability of automotive leaf springs, Materials and Design, 47 (2013) 672-676.

[73] S. Bagherifard, R. Ghelichi, M. Guagliano, Mesh sensitivity assessment of shot peening finite element simulation aimed at surface grain refinement, Surface and Coatings Technology, 243 (2014) 58-64.

[74] H.J.C. Voorwald, M.P. Silva, M.Y.P. Costa, M.O.H. Cioffi, Improvement in the fatigue strength of chromium electroplated AISI 4340 steel by shot peening, Fatigue & Fracture of Engineering Materials & Structures, 32 (2009) 97-104.

[75] N. Kawagoishi, T. Nagano, M. Moriyama, E. Kondo, Improvement of fatigue strength of maraging steel by shot peening, Materials and Manufacturing Processes, 24 (2009) 1431-1435.

[76] N.W. Khun, P.Q. Trung, D.L. Butler, Mechanical and tribological properties of shot peened SAE 1070 steel, Tribology Transactions, (2016).

[77] M. Umemoto, Y. Todaka, J. Li, Change in microstructure and mechanical properties of steel components surface layer by severe plastic deformation, Tetsu-To-Hagane/Journal of the Iron and Steel Institute of Japan, 94 (2008) 616-628.

[78] P. Peyre, R. Fabbro, P. Merrien, H.P. Lieurade, Laser shock processing of aluminium alloys. Application to high cycle fatigue behaviour, Materials Science and Engineering A, 210 (1996) 102-113.

[79] R.A. Brockman, W.R. Braisted, S.E. Olson, R.D. Tenaglia, A.H. Clauer, K. Langer, M.J. Shepard, Prediction and characterization of residual stresses from laser shock peening, International Journal of Fatigue, 36 (2012) 96-108.

[80] H. Leitner, H.P. Gänser, W. Eichlseder, Surface treatment by shot peening and deep rolling - Mechanisms, modelling, methods, Materialpruefung/Materials Testing, 49 (2007) 408-413.

[81] Y. Nakamura, M. Nakajima, H. Masuda, T. Kakiuchi, Y. Uematsu, Improvement of fatigue properties in a cast aluminum alloy by roller burnishing and friction stir processing, in: Advanced Materials Research, 2014, pp. 662-667.

[82] L.L. Shaw, J.-W. Tian, A.L. Ortiz, K. Dai, J.C. Villegas, P.K. Liaw, R. Ren, D.L. Klarstrom, A direct comparison in the fatigue resistance enhanced by surface severe plastic deformation and shot peening in a C-2000 superalloy, Materials Science and Engineering: A, 527 (2010) 986-994.

[83] F. Gharbi, S. Sghaier, K.J. Al-Fadhalah, T. Benameur, Effect of ball burnishing process on the surface quality and microstructure properties of aisi 1010 steel plates, Journal of Materials Engineering and Performance, 20 (2011) 903-910.

[84] N.W. Khun, G.S. Frankel, M. Sumption, Effects of Normal Load, Sliding Speed, and Surface Roughness on Tribological Properties of Niobium under Dry and Wet Conditions, Tribology Transactions, 57 (2014) 944-954.

[85] N.W. Khun, P.Y. Loong, E. Liu, L. Li, Enhancing electrical and tribological properties of poly(methyl methacrylate) matrix nanocomposite films by co-incorporation of multiwalled carbon nanotubes and silicon dioxide microparticles, Journal of Polymer Engineering, 36 (2016) 23-30.

[86] N.W. Khun, D.W. Sun, M.X. Huang, J.L. Yang, C.Y. Yue, Wear resistant epoxy composites with diisocyanate-based self-healing functionality, Wear, 313 (2014) 19-28.

[87] N.W. Khun, A.W.Y. Tan, K.J.W. Bi, E. Liu, Effects of working gas on wear and corrosion resistances of cold sprayed Ti-6Al-4V coatings, Surface and Coatings Technology, 302 (2016) 1-12.

[88] D. Singh, D.P. Mondal, Effect of quenching and tempering processes and shot peening intensity on wear behaviour of SAE-6150 steel, Indian Journal of Engineering and Materials Sciences, 21 (2014) 168-178.

[89] S. Mitrovic, D. Adamovic, F. Zivic, D. Dzunic, M. Pantic, Friction and wear behavior of shot peened surfaces of 36CrNiMo4 and 36NiCrMo16 alloyed steels under dry and lubricated contact conditions, Applied Surface Science, 290 (2014) 223-232.

[90] M. Matsui, H. Kakishima, Improvement of tribological performance of steel by solid lubricant shot-peening in dry rolling/sliding contact wear tests, Wear, 260 (2006) 669-673.

[91] O. Unal, R. Varol, A. Erdogan, M.S. Gok, Wear behaviour of low carbon steel after severe shot peening, Materials Research Innovations, 17 (2013) 519-523.

[92] W.F. Hosford, Mechanical Behavior of Materials, Cambridge : Cambridge University Press, 2009, 2009.

[93] H. Berns, W. Theisen, Ferrous Materials : Steel and Cast Iron, Berlin, Heidelberg : Springer-Verlag, 2008., 2008.

[94] T.S. Barrett, G.W. Stachowiak, A.W. Batchelor, Effect of roughness and sliding speed on the wear and friction of ultra-high molecular weight polyethylene, Wear, 153 (1992) 331-350.

[95] F. Svahn, Å. Kassman-Rudolphi, E. Wallén, The influence of surface roughness on friction and wear of machine element coatings, Wear, 254 (2003) 1092-1098.

[96] I. Schmidt, Sliding wear of shot-peened austenitic manganese steels, Journal of Materials Science Letters, 5 (1986) 475-477.

[97] K. Murugaratnam, S. Utili, N. Petrinic, A combined DEM-FEM numerical method for Shot Peening parameter optimisation, Advances in Engineering Software, 79 (2015) 13-26.

[98] A. Ghasemi, S.M. Hassani-Gangaraj, A.H. Mahmoudi, G.H. Farrahi, M. Guagliano, Shot peening coverage effect on residual stress profile by FE random impact analysis, Surface Engineering, (2016) 1-10.

[99] D. Kirk, M.Y. Abyaneh, Theoretical basis of shot peening coverage control, The Shot Peener, 9(2) (1995) 5-7.

[100] M.A.S. Torres, H.J.C. Voorwald, An evaluation of shot peening, residual stress and stress relaxation on the fatigue life of AISI 4340 steel, International Journal of Fatigue, 24 (2002) 877-886.

[101] P.S. Prevéy, J.T. Cammett, E. Wallén, The Effect of Shot Peening Coverage on Residual Stress, Cold Work and Fatigue in a Ni-Cr-Mo Low Alloy Steel, Proceedings International Conference on Shot Peening, 254 (2002).

[102] S.A. Meguid, F. Yang, C. Zhuo, M. Guagliano, 3D FE analysis of shot peening of strain-rate sensitive materials accounting for multiple and repeated impingement, in: 13th International Conference on Fracture 2013, ICF 2013, 2013, pp. 4201-4208.

[103] J. Schijve, Fatigue of Structures and Materials., Dordrecht : Springer Netherlands, ISBN 9781402068089, 2009.

[104] C. Bathias, A. Pineau, Fatigue of materials and structures : fundamentals, London : ISTE ; Hoboken, NJ : John Wiley., ISBN 9781848210516, 2010.

[105] P.Q. Trung, N.W. Khun, D.L. Butler, Effects of shot peening pressure, media type and double shot peening on the microstructure, mechanical and tribological properties of low-alloy steel, Surface Topography: Metrology and Properties, 4 (2016) 045001.

[106] P.Q. Trung, N.W. Khun, D.L. Butler, Three-dimensional dynamic finite element modelling of shot peening process: New approach to estimate level of the coverage parameter, in: XXX International conference on surface modification technologies (SMT30), Milan, Italy., 2016.

[107] P. Trung, N.W. Khun, D. Butler, New Approach to Estimate Coverage Parameter in 3D FEM Shot Peening Simulation, Surface Engineering, (2017).

[108] C. Bathias, A. Pineau, Fatigue of Materials and Structures : Applications to Design and Damage, ISBN 9781118616994, London : Wiley., 2013.

[109] D. Závodská, M. Guagliano, O. Bokuvka, L. Trško, Effect of Shot Peening on the Fatigue Properties of 40NiCrMo7 steel, Manufacturing Technology, 16 (2016) 295-299.

[110] ASTM E466-07, Standard Practice for Conducting Force Controlled Constant Amplitude Axial Fatigue Tests of Metallic Materials, ASTM International, West Conshohocken, PA, 2007.

[111] N.W. Khun, P.Q. Trung, D.L. Butler, Mechanical and Tribological Properties of Shot-Peened SAE 1070 Steel, Tribology Transactions, 59 (2016) 932-943.